INFORMATION TO USERS

This manuscript has been reproduced from the microfilm master. UMI films the text directly from the original or copy submitted. Thus, some thesis and dissertation copies are in typewriter face, while others may be from any type of computer printer.

The quality of this reproduction is dependent upon the quality of the copy submitted. Broken or indistinct print, colored or poor quality illustrations and photographs, print bleedthrough, substandard margins, and improper alignment can adversely affect reproduction.

In the unlikely event that the author did not send UMI a complete manuscript and there are missing pages, these will be noted. Also, if unauthorized copyright material had to be removed, a note will indicate the deletion.

Oversize materials (e.g., maps, drawings, charts) are reproduced by sectioning the original, beginning at the upper left-hand corner and continuing from left to right in equal sections with small overlaps.

ProQuest Information and Learning
300 North Zeeb Road, Ann Arbor, MI 48106-1346 USA
800-521-0600

Modelling of Anisotropic Etching of Silicon in Tetra-Methyl Ammonium Hydroxide: Anomalies due to Facet Boundary Effects

Moulay-Ziyad Elalamy

A Thesis

in

The Department

of

Electrical and Computer Engineering

Presented in Partial Fulfillment of the Requirements
for the Degree of Master of Applied Science at
Concordia University
Montreal, Quebec, Canada

September 2002

Abstract

Modelling of Anisotropic Etching of Silicon in Tetra-Methyl Ammonium Hydroxide: Anomalies due to Facet Boundary Effects

Moulay-Ziyad Elalamy

Anisotropic etching of silicon is one of the fundamental techniques for the fabrication of micromachined structures such as microsensors and microactuators. Although the technique is used extensively in industry, the fundamentals of the atomic etching mechanism are still not well understood.

This work addresses the modelling aspect of anisotropic etching of silicon and begins with an idealized model in which the etch behaviour depends only on the crystal features presented to the etchant. New experiments on Si{110} and Si{100} at 25wt.% and 19wt.% TMAH using wagon-wheel etching masks, specially designed for the scope of this thesis, enable the extension of the idealized model by addressing certain anomalies observed in the variation of the resulting structures as a function of etch time :

- As anomalies, it is found that same crystal planes in the same etchant often exhibit different etch rates. Moreover, for certain specific mask-edge positions, these etch rates are found to vary substantially with time, modifying under-etch profiles and surface roughness.
- As to explain these anomalies, models of interactions at the boundaries between adjacent facets are developed.

Acknowledgments

Any accomplishment, so small it could be, is made possible with the effort and collaboration of an incredible number of people. I am conscious that in the case of this work, the above statement fully applies. I wish all parties involved in this work could be recognized and rewarded in their future being.

This work is my modest participation to the world of research, and it was a great fun being involved. In this incredible experience, the main values that I have been introduced to, are humility and sense of accomplishment.

This work is dedicated to my dear parents, Nicole and Moulay-Mehdi Elalamy, who always encouraged me in having the right attitude and in making my ambitions come true.

I would like to express my deep and sincere gratitude to my thesis supervisor, Dr. Leslie M. Landsberger, for his sustained help, effective guidance and unlimited encouragement during the course of this work. The hours of discussion and consultation with him taught me the importance of real effort in accomplishing a task. I am very grateful to Dr. Mojtaba Kahrizi for his important contribution to this thesis, for the valuable advice and guidance during the whole period of my M.A.Sc studies. Special thanks to Anand Pandy for his precious experimental work that served as a strong base for the advancement of this research work. Special thanks to my colleague Irina Stateikina for sharing visions, for bringing great ideas, and for her help in the lab. I would like to express my appreciation to ELEC6251 students for their dedicated effort and contribution to the thesis.

Special thanks to all the colleagues in the lab for sharing visions in a good and balanced ambiance of work. Special thanks to my numerous roommates during these two years for providing a healthy astmosphere, and for having borne with me and listened to my crazy theories of interaction between planes. Special thanks to my relatives who always encourage me in my decisions.

A very special thanks to my dear Sophie Belaube for motivating me advancing in the research work with continuous support and incredible patience.

Table of Contents

List of Figures

List of Tables

1 Introduction

Wet anisotropic etching of silicon is a widespread micro-fabrication technology that results in 3D geometric shapes formed in the bulk of crystalline silicon. The need for etched structures in silicon has seen great increase since the emergence and growth of MicroElectroMechanical Systems (MEMS), and microsystems technology (MST). Even though many more recently developed technologies also participate in the fabrication of MEMS/Microsystems, anisotropic etching is still one of the fundamental fabrication steps.

The technique of anisotropic etching emerged in the 1960's at the Bell Laboratories [1]. Since then, various research groups have tried to better understand etching phenomena and atomic mechanisms, experimentally develop ever more efficient etchants (for example to achieve "perfectly" smooth surfaces), predict etch profiles by CAD tools, and study new ways of using the etching technique as part of a fabrication process.

Whereas anisotropic etching is still an active research field, its industrial use is most often limited to simple structures bounded by {111} planes. This limited use of anisotropic etching is explained by a lack of control of the etched structures or surfaces. This is quickly quantified when comparing simulated structures of the latest CAD etching tools with the real structures obtained through experiments. The simulation limits of the software represent our understanding and control of etching. In other words, all deviations from simulated results constitute the next challenges to overcome. The task is difficult because it involves the fundamentals of the etching mechanisms that are still not completely understood.

1.1 Defining "Bulk wet anisotropic etching of silicon"

To better explain all the advantages of using wet anisotropic etching of silicon, let us compare it to other techniques.

First, the technique is "wet" as opposed to dry etching techniques such as plasma etching, reactive ion etching, or sputtering. For some applications where all these techniques may be candidates, the wet alternative using only a temperature controlled bath may be chosen

due to its low process cost, smoother achieved surfaces, higher selectivity of masking material, and lower environmental pollution [2]. On the other hand, in achieving high aspect ratio microstructures, dry etching techniques such as deep reactive ion etching may be more suitable. Figure 1-1 illustrates cross-sections of some typical achieved shapes using various etching techniques. Inclined sidewalls as in Figure 1-1-(1) is an example of features not suitable for dry etching techniques Figure 1-1-(2).

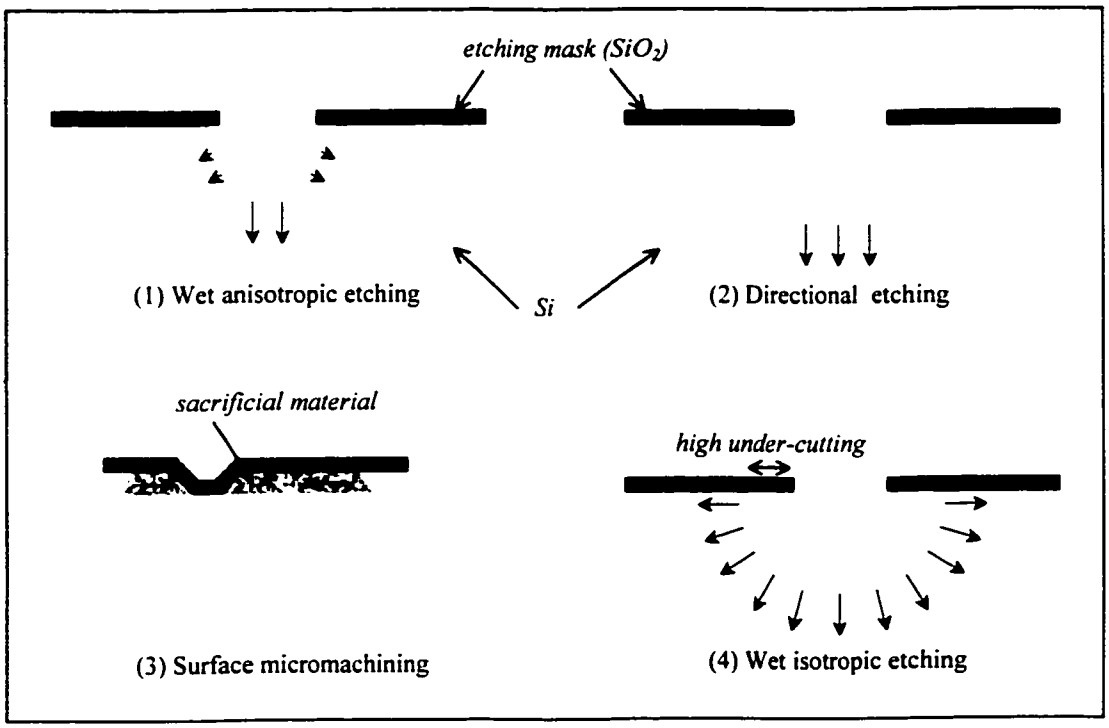

Figure 1-1 : Comparison of wet anisotropic etching with other common etching techniques.

Second, anisotropic etching is referred as a "bulk" technique, meaning that the body of silicon is etched, as opposed to surface micromachining where structures are formed after the etching of a sacrificial material (shown on Figure 1-1-(3)).

Third, "anisotropic" wet etching is suitable for achieving flat surfaces as opposed to "isotropic" wet etching that uses other etchants and which results in etched pits in the form of half spheres as shown on Figure 1-1-(4). The main advantage of anisotropic etching over isotropic etching is the ability to minimize undercutting and to use the crystal structure to guide the formation of a wider range of possible shapes.

1.2 TMAH and other anisotropic etchants

A wide variety of anisotropic etchants have been used for silicon etching. Among the alkaline aqueous solutions we find KOH, NaOH, LiOH, CsOH, NH_4OH, and quaternary ammonium hydroxides. These etchants are composed of hydroxyde ions (OH^-) and cations (K+, Na+,etc). Hydroxide ions play the major role in etching silicon but because each alkaline solution gives different etching results, cations are believed to influence etching as well. Alkaline organics such as EDP and hydrazine are used as well. KOH, which is very common, is very corrosive (avoid eye contact), have low selectivity with respect to silicon dioxide, and is not compatible with CMOS processes (alkali ion contamination). EDP and hydrazine are poisonous and dangerous chemicals (hydrazine is explosive). TMAH, a relatively new anisotropic etchant (compared to KOH and EDP), is presented here and is the subject of this thesis research, thanks to its good etching characteristics.

TMAH, having the molecular formula $(CH_3)_4NOH$, is a kind of quaternary ammonium hydroxide (QAH) solution proposed by Asano *et al* in 1976 [3] as an etching and cleaning solution for silicon and silicon dioxide surfaces. Detailed characteristics of QAH as a silicon anisotropic etchant had not been reported until 1990. The characteristics of TMAH were reported by Schnakenberg *et al* [4] and Tabata *et al* [5] in 1991. Besides the fact that TMAH can be easily obtained, because it has been used in large-scale integrated microelectronics processes, as developer for positive photoresist, TMAH has become popular due to the following characteristics:

- High compatibility with CMOS process.
- Ease of handling and low toxicity.
- High etching rates of silicon.
- Suitable anisotropy : e.g etch rate ratio {100}/{111} = up to 50.
- Smooth etched surfaces.
- Excellent selectivity to masking material (very low etch rates of SiO_2 and Si_3N_4).

1.3 Issues of interest

Industrial use of anisotropic etching of silicon is mostly limited to achieving grooves or cavities, for example for the release of active membranes. These simply etched geometries are bounded by {111} planes and do not need much control of the etching process. Obtaining more complex structures is possible, but less convenient due to the lack of control of the etch results, affecting reproducibility reproducibility of etched structures. Presently available etch simulation software packages usually bear some substantial inaccuracies.

The need for increased control over etching has led to intensive research for more than 30 years with a priority given to a better understanding of the etching phenomena, eventual control anticipated to be a direct consequence of that understanding. Initially, most research focused only on measuring etch rates of specific crystal directions such as {100}, {110}, or {111} planes. But recent publications of Sato *et al* [6,7] addressed all etch rates of all possible crystal directions. Its experiments rely on the etching of a single-crystalline half-sphere polished silicon piece. It should be noted, however, that Sato's experiment etching spheres measure of etch rates on a convex shape (distorted half-sphere after etching) where each plane on the surface is locally considered as infinite, which is different from the main use of anisotropic etching, where concave structures of limited size are formed in the bulk of silicon.

Etching using wagon-wheel mask patterns is an important experimental mode because it uses concave etched geometries (grooves) for the measure of plane's etch rate. However the range of planes appearing during these experiments is limited compared to Sato's experiments.

A recent study based on wagon-wheel experiments, performed by A. Pandy in a Master's thesis at Concordia University [8], enabled the construction of a model in which most under-etched surfaces appearing are identified and grouped into two families of crystal features. This model suggests that finding the etch rates of the two families should be very important in understanding the etching of concave structures. The prevalence of these two families of crystal features confirmed the relevance of the model, but it also demonstrated that real experimental results contain many substantial deviations from

"ideal" etch rates predicted by the model (based on steps on a {111} plane). By comparison of experiment with the model, it was found that surfaces presenting the same crystal feature to the etchant could etch at different speeds (in the same etchant bath at the same time!).

Interestingly, these variations of etch rate for common crystal features constitute a clear source of difficulty in controlling the etch process and suggest a clear direction for further study of the atomic mechanisms.

1.4 Scope of this thesis

Thus this thesis begins based previous work by A. Pandy using wagon-wheel under-etch experiments on silicon in TMAH [8,9]. The previous work led to the construction of simple model based on steps on {111} planes. to describe under-etch profiles. Several aspects of that model deserve to be examined and extended. Accordingly, this thesis adopts the following approach:

(a) extend the step-based model to predict entire under-etch curves, and predict more-rich detail of the under-etch profiles, so that deviations from it can be seen in more detail;

(b) use the more detailed version of the model to represent the (too-simplistic) hypothesis that the same crystal features should etch at the same rate in a given etchant, in order o provide a backdrop for insight into the nature of the deviations;

(c) extend the step-based model to account for the possibility of interactions between (usually adjacent) facets;

(d) perform wagon-wheel under-etch experiments for various etching times to further develop evidence of deviations from the model;

(e) analyze the experimental results with a view to elaborating a theory of interaction between facets of an under-etch profile, to explain some of the cases where the same crystal features may etch at different speeds.

The thesis is organized as follows:

In the next chapter (Chapter 2), is presented a review of the current research, experimental and modelling, available in the literature on anisotropic etching of silicon

(with focus on TMAH). Chapter 3 begins by explaining general characteristics of silicon etching and introduces the wagon-wheel method. Then the etching model based on identification of two types of planes is detailed. In Chapter 4, certain aspects of the model are developed (orientation and interaction of chains of atoms), and etching simulations (of chains and inverted planes) are presented to serve as foundation and tools for understanding mechanisms of interaction between facets. In Chapter 5, the experimental procedures necessary to perform wagon-wheel under-etch experiments are presented. Chapter 6 presents the experimental results of etching wagon-wheel patterns in 25wt% and 19wt% TMAH for various etching times. Cross-sections at strategic positions on the wagon-wheel are characterized by scanning electron microscopy (SEM) to visualize time effects on the under-etching profiles. Chapter 7 analyzes the experimental results of Chapter 6 using the information developed in Chapter 4. Finally, Chapter 8 concludes, summarizes the contributions, and suggests directions for future work.

2 Review of current research

Developed mainly by trial and error [1], wet anisotropic etching of silicon is a technique resulting from the assembly of a large number of experimental studies. Initially, most publications were concerned by the effect of some parameters on the etching profiles or rates and were composed of measurements and/or descriptions. Nowadays there is great concern on developing etching models for the achievement of better control, however a full understanding of the complexity of the phenomena is still far off.

2.1 Experimental studies

Most experimental work in the field of wet anisotropic etching was almost exclusively devoted to etching dependencies of silicon in KOH. As TMAH is becoming more and more important, a great number of recent papers are addressing the same questions for the case of TMAH. Since this thesis focuses on issues about silicon etching in TMAH, below is a review of recent findings relating mainly to TMAH solutions.

In their experimental work, researchers have (roughly) a choice among three different methods to measure etching rates:

(1) Obtaining silicon wafers whose surface is of the desired orientation, then patterning windows in a masking material (oxide or nitride), then etching the opened windows and measuring the etch depth in comparison with non-etched areas.

(2) The wagon-wheel method described further in detail in the next Chapter 3. In comparison to the first method, the wagon-wheel method consists of measuring under-etch rates and inclination angles of the sidewalls of trenches etched in the silicon wafer, and calculating the etch rates of those side-walls. In this way, more planes are consequently measurable than in method #1 above.

(3) The third method is almost exclusively used by Shikida et *al* [6]. It uses a solid hemispherical specimen of single-crystal silicon as shown in Figure 2-1. The radius of the hemisphere is few centimetres with a sphericity less than 10μm. As a result, all crystallographic orientations appear on the hemispherical surface. The etch rate

measurements are carried out by comparing distances before and after etching using a probing machine that sweeps along a predefined network of points on the hemisphere.

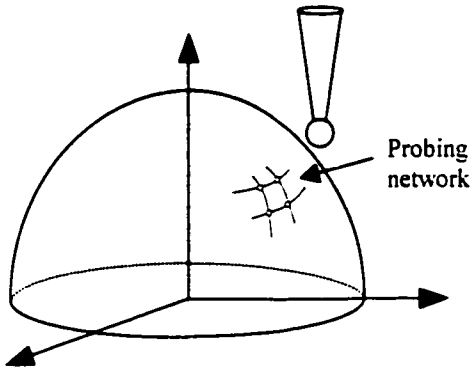

Figure 2-1 : Etching rate measurement using a hemispherical specimen of single-crystal silicon [6].

2.1.1 Temperature and concentration dependence

Etchant concentration and temperature are by far the most important parameters that affect silicon etching rates and surface roughness for all orientations. Two research teams. Sato et *al* [6] and Tabata et *al* [2], studied these effects in depth.

Figure 2-2 shows the dependence of the etching rates of various Si orientations on TMAH concentration varying from 10wt% to 25wt% [6]. Most orientations show similar trends with a maximum etch rate around 20wt%, except for the very important {100} orientation. The {100} etch rate increases with decreasing TMAH concentration. to a maximum around 2-5wt% [2]. However, on Si{100}, pyramidal hillocks are observed for concentrations less than 15wt%. For concentrations less that 5wt%, the high density of hillocks decrease dramatically the {100} surface etch rate and increase substantially its surface roughness. Therefore {100} surfaces exhibit a maximum etch rate around 2-5wt% TMAH [2].

Concerning the effects of temperature, Arrhenius plots for {100} and {110} planes are shown in Figure 2-3 for a concentration of 25wt% TMAH. Temperature conditions for the plots are 70°C, 80°C and 90°C. The figure shows that with increasing temperature etching rates increase considerably, as an example {100} planes etch approximately at 30um/hr at 80°C compared to 45um/hr at 90°C. For this reason, temperature should be precisely controlled for good repeatability.

Tabata et *al* [2] measured the dependence of silicon etch rate with respect to both temperature and concentration for {100} and {111} planes. These are plotted in Figure 2-4. The etching rate of Si{111} is about 0.02 – 0.05 times smaller than that of {100} and the {100}/{111} etch rate ratio decreases with decreasing temperature and increasing concentration. This ratio change has also been reported by Schnakenberg et *al* [26].

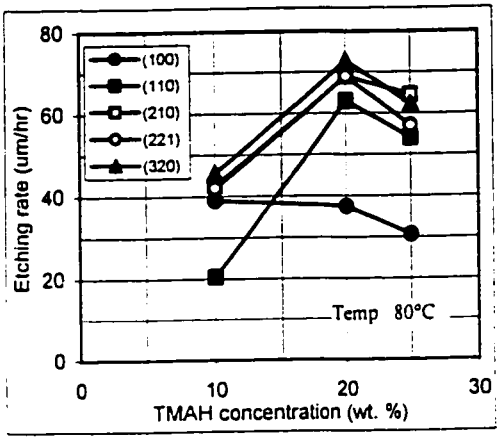

Figure 2-2 : Dependence of the etching rates on TMAH concentration for various crystallographic orientations [6].

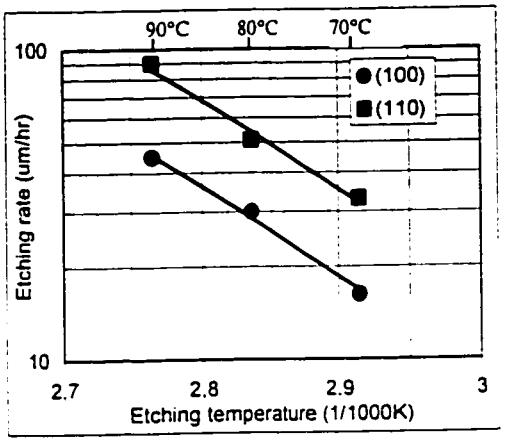

Figure 2-3 : Dependence of the etching rates on TMAH temperature for {100} and {110} planes [6].

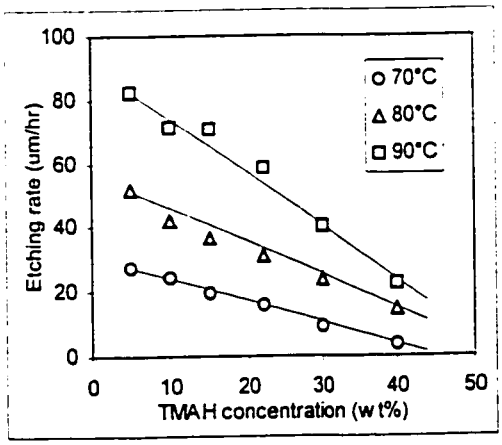

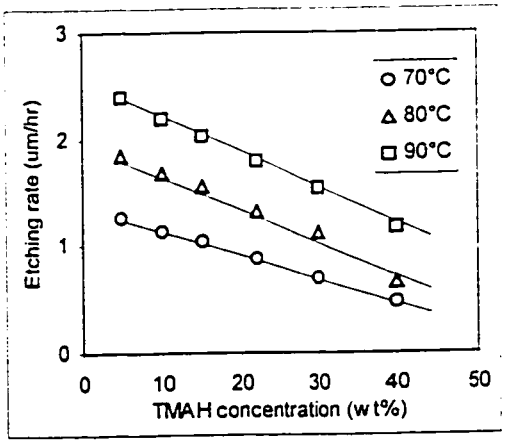

Figure 2-4 : Dependencies of {100} and {111} etching rate on temperature and concentration [2].

Uniformity

Sato et *al* [6] observed unequal etching rates for the four {110} planes positioned at 30° latitude on a single-crystal silicon hemisphere. This scattering shown in Figure 2-5 is particular to TMAH and has not been observed for KOH solutions. It was also found that

increasing both temperature and concentration as shown on Figure 2-5 (comparing left graph to right graph) decreases this non-uniformity.

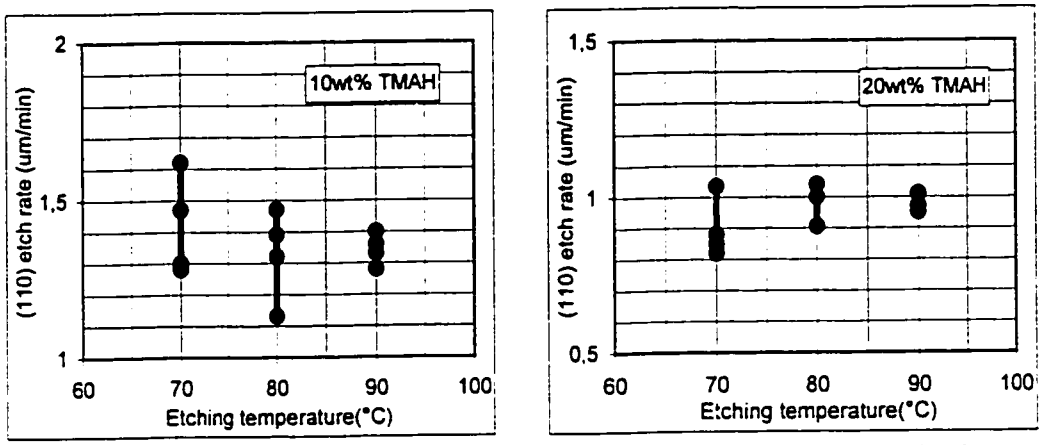

Figure 2-5 : Variation range in etching rates among four equivalent {110} planes [6]. The plots are normalized by the {110} at the top of the hemisphere.

2.1.2 SiO_2 and Si_3N_4

Silicon dioxide (SiO_2) as well as silicon nitride (Si_3N_4 or SiN_x) are often used in microfabrication as masking layers, isolators, or structural materials. They also serve as masks against etching due to their very slow etching rates. As an example, the etch rate of SiO_2 in TMAH is almost four orders of magnitude lower (a few Å/min) than that of Si{100} [2]. This is one of the advantages of TMAH when compared to KOH, which etches SiO_2 only two orders of magnitude slower than Si{100}. The activation energy of etching SiO_2 in TMAH was measured to be approximately 0.9eV [2]. This implies that selectivity of SiO_2 over Si increases with decreasing temperature. Potassium ions addition in the TMAH solution strongly affects the etching rate of SiO_2 (see section 2.1.3.1 below). LPCVD nitride is even more resistant to TMAH etching, to the point that its etch rate was too low to be measured. As a result, SiO_2 and Si_3N_4 are ideal masks against etching. Moreover, due to their good mechanical properties, they are often used as structural membranes such as cantilevers or overhanging membranes released after the creation of a cavity by TMAH etching.

2.1.3 Additives

Many additives may modify TMAH etching characteristics. The first intention is to modify the anisotropy property of TMAH as for example to limit undercutting or to achieve under-etch sidewalls composed by only one facet. The second intention is to achieve better surface roughness, especially for low TMAH concentrations.

2.1.3.1 Effects of potassium ions

TMAH and KOH have different anisotropy profiles and different SiO_2 etching selectivity, meaning that cations should also play a role besides hydroxide ions in the anisotropic etching mechanism. Therefore, researchers had the idea of adding potassium ions in TMAH using K_2CO_3. The experiments held by Tabata et *al* [10.11] confirmed that adding K_2CO_3 has a strong effect on the anisotropy profile as well as on the selectivity of SiO_2. Using a hemispherical specimen of single-crystal silicon (similar to that used by Sato et *al*), the authors measured the etch rate distribution over all orientations after an addition of K_2CO_3 in 20wt% TMAH at 80°C. The amount of added K_2CO_3 is 0.5 g/L. which was tested to cause the strongest change at the concentration used.

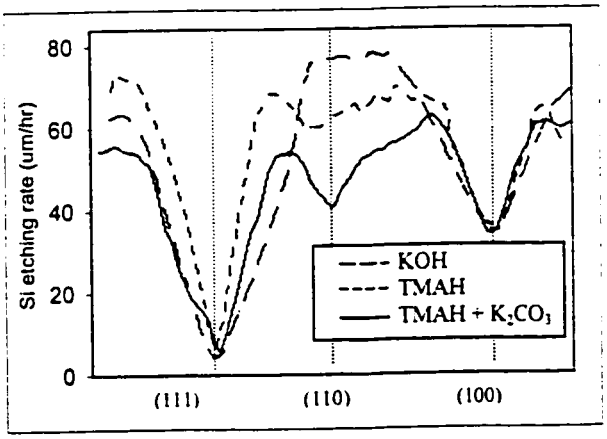

Figure 2-6 : Etching rate distribution along a line from the (111) to (110) and from (110) to the (100) plane, showing the effects of adding 0.5g/L K_2CO_3 in TMAH 20wt.% 80°C [2].

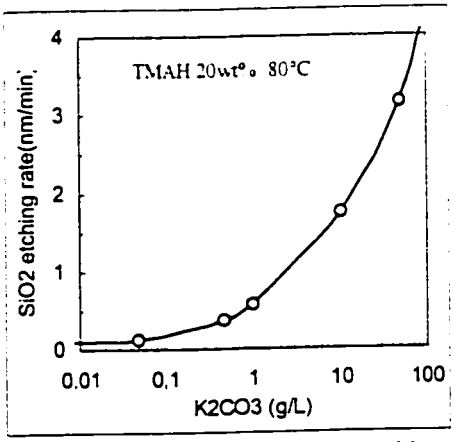

Figure 2-7 : Dependence of SiO_2 etching rate in TMAH on the amount of dissolved K_2CO_3 [10].

Figure 2-6 shows the etch rate distribution measured on the hemispherical specimen along a line from the {111} to {110} and from {110} to the {100} plane. The most

noticed effect is the dramatic etch rate decrease of the {110} plane. Interestingly, the characteristics of TMAH with potassium ions are not similar to those of KOH.

The addition of K_2CO_3 in TMAH [10] has also an effect on SiO_2 selectivity. Figure 2-7 shows the increase of silicon oxide etching rate for various amounts of dissolved K_2CO_3. This increase is actually not surprising since SiO_2 etching rate in KOH is roughly ten times oxide etching rate in TMAH.

2.1.3.2 Effects of surfactant NCW-601A

The influence of surfactant addition in TMAH for the three main planes {100}, {110}, and {111} was measured by Sekimura et *al* [12]. The added surfactant is named NCW-601A and it contains 30 wt% polyoxyethylene alkyl phenyl ether. Figure 2-8 shows the etching results in the case of TMAH 25wt% at 80°C. Among all crystal orientations, the {110} plane commands most of the attention since its etch rate decreases abruptly by an order of magnitude with only 2wt% surfactant addition. Moreover the author reports a significant improvement of surface roughness and a disappearance of the column-like texture commonly observed on {110} planes.

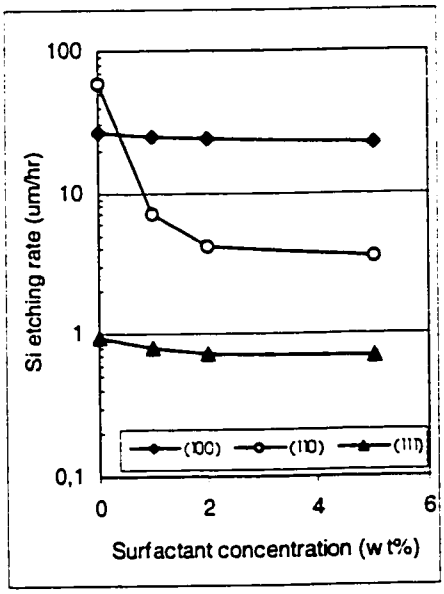

Figure 2-8 : Effects of the surfactant on the etching rate of the three principal orientations [12].

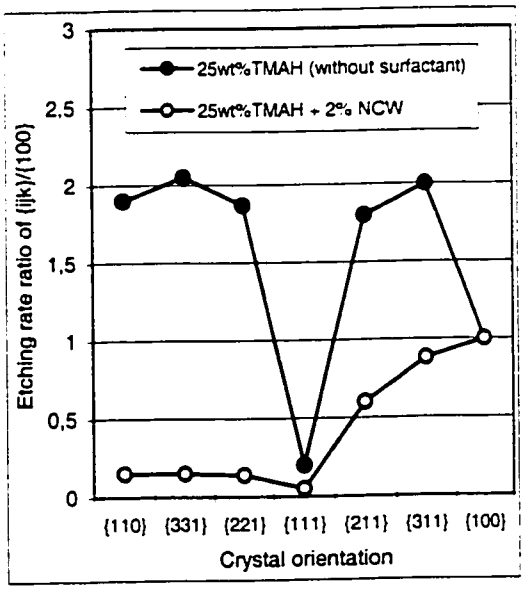

Figure 2-9 : Change in etching rate for different orientations after the addition of the surfactant [7].

Extending Sekimura's work, Sato et *al* [7] used a hemispherical single-crystal silicon specimen to evaluate the effect of adding the same surfactant in TMAH for all

crystallographic orientations. They discovered that it is actually the orientations having Miller indices of the form {hhl}, where h is greater than 1, that show considerably lower etching rates following the addition of the surfactant. This is shown in Figure 2-9. As a result, the etch rate ratio ER(110)/ER(100) decreases from 2 to 0.18 following the addition of the surfactant. This reveals to be very useful for the reduction of convex corners undercut and for the fabrication of 45°-inclined single-faceted (110) planes suitable for optical reflectors [12]. Both Sekimura's and Sato's publications do not mention any effects on hillocks that would be induced by the addition of the surfactant NCW-601A in the solution. But because the surfactant lowers the etch rate ratio ER(110)/ER(100), it is believed that the addition of the surfactant does not act to reduce the hillocks. Indeed, as the ridges (made of PBCs , the crystal feature which makes up {110} surfaces) of the pyramidal shape are etching at a reduced speed, the {100} surface on which hillocks are formed etches at an increased rate.

2.1.3.3 Effects of surfactant isopropyl alcohol (IPA)

Isopropyl alcohol can be mixed into TMAH solutions having concentrations of 5 to 40% without any restrictions, independent of TMAH concentration [13]. In general, the more IPA is introduced, the more the etch rate of silicon decreases. The authors [13] report that the decrease is relatively independent of concentration for TMAH, as shown on Figure 2-10.

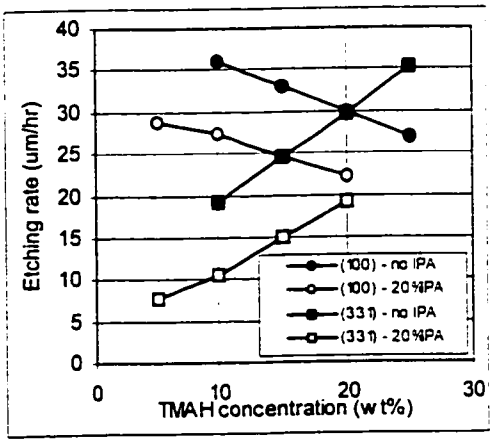

Figure 2-10 : {100} and {331} planes etching rate decrease following the addition of IPA in TMAH [13].

The main motivation for doping TMAH with IPA is for reducing undercutting, as studied by Merlos et *al* [14]. For example, mesa structures on Si{100} aligned with the wafer flat need less corner compensation structures when IPA is added to TMAH. It was also found that the addition of IPA slightly improves the surface quality of etched surfaces. No precise mention about effects on hillocks stability was clearly stated.

2.1.4 Additives for Aluminum protection

Undoped TMAH etches aluminum at a rate equal to, if not greater than, the rate that it attacks silicon. This means that integrated circuits where aluminum is the interconnect metal will be damaged if immersed in TMAH. Since the onset of MEMS fabricated by a TMAH post-process step added at the end of a standard CMOS processes, researchers have begun to investigate using additives to modify TMAH etching properties regarding aluminum.

Silicon dissolution in TMAH or simply the addition of silicic acid ($Si(OH)_4$) in the solution are alternatives for aluminum protection [15,16,17]. As shown on Figure 2-11, by increasing the amount of dissolved silicon, the etch rate of aluminum decreases slightly at first and then abruptly [2]. According to Tabata et *al* [2], 3.2 mol/L of silicon are required to be dissolved in 22wt% TMAH in order to lower aluminum etch rate to less than 0.01um/min.

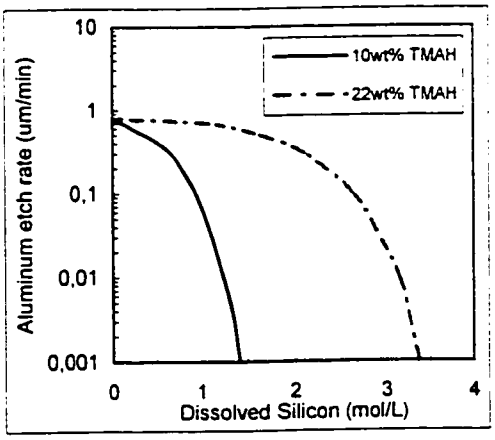

Figure 2-11 : Dependence of aluminum etching rate on the amount of dissolved silicon [2].

To explain this protection effect, Raman spectroscopy revealed that the aluminum surface is resistant to TMAH after the formation of a silicate polymer passivation layer [18]. Furthermore, besides the need for silicon to form the silicate, it was shown that a low pH value is a necessary condition to form the passivation layer. Adding acids to the TMAH solution such as $(NH_4)_2CO_3$ and $(NH_4)HPO_4$ helps in decreasing the aluminum etch rate by decreasing the pH of the solution [16].

These acids used to stop aluminum etching also affect the silicon etch rate and anisotropy in an undesired manner. Indeed, the subsequent decrease of the pH after the addition of acids encourages the formation of hillocks. Typically, these pyramidal protrusions form at pH values less than 13 and cause the silicon etch rate to drop drastically. Very often, oxidizing agents such as Ammonium Peroxodisulfate $(NH_4)_2S_2O_8$ are added to the solution [15,17,19] to eliminate hillocks formation and restore a satisfying surface smoothness and etch rate, specially for the case of {100} surface.

2.1.5 Electrochemical etch stop

"Etch-stop" techniques based are used to stop silicon etching when a certain cavity depth or a certain membrane thickness is reached [1]. There are several modes of etch stop based on electrochemical mechanisms. Some techniques involve the use of electrodes and applied potentials. Another, simpler, technique is accomplished by heavy p-type (boron) doping.

An electrochemical reaction is a reaction involving the transfer of charges as a part of a chemical reaction. Indeed, it is believed that electrons are injected into the conduction band during silicon etching by hydroxide ions. Accordingly, the electrochemical model of Seidel et *al.* [20] using band diagrams is outlined later in this chapter.

2.1.5.1 Heavy Boron doping etch stop

The boron etch-stop effect was first observed during etching in EDP (1969) and KOH for doping levels greater than about $10^{19}/cm^3$ [1]. The same study was performed later for TMAH solutions revealing that the effect also takes place but for slightly higher boron doping concentration [21]. Figure 2-12 shows the silicon etch rate versus the boron doping level. It was found that extreme doping levels greater than $4.10^{20}cm^3$ are required to reduce the etch rate by a factor more than 40.

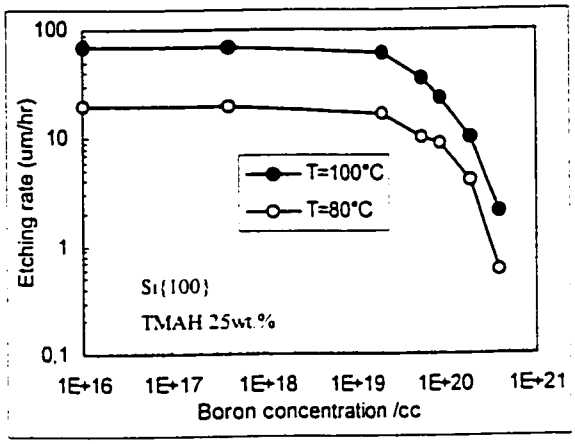

Figure 2-12 : Si{100} etching rate in TMAH 25wt.% vs. boron concentration [21].

The model published by Seidel et *al* [20] and discussed below, provides an elegant explanation for the etch stop technique. At a high p-type doping concentration, the Fermi level drops into the valence band. The electrons resulting from the silicon dissolution are injected into the valence band, and recombine rapidly with the many holes in the valence band. Consequently these electrons are not available for the subsequent reaction with water molecules (in the overall reaction $4H_2O + 4e^- \rightarrow 4OH^- + 2H_2$), the reduction of which is necessary for providing new hydroxide ions in close proximity to the negatively charged silicon surface.

A major drawback of this etch stop technique is that extremely high boron concentrations introduce slip planes and tensile stress. Moreover such high concentrations are not compatible with standard CMOS or bipolar-techniques, consequently this etch stop technique can typically only be used for microstructures without integrated electronics [1].

2.1.5.2 Etching under applied bias-voltage

The experimental setup for electrochemical etching is shown on Figure 2-13. A potentiostat and a wave generator control the potential of the silicon sample with respect to an Ag/AgCl reference electrode, while a platinum electrode acts as a counter electrode [2]. Figure 2-14 shows a typical voltammogram of silicon electrochemically etched in TMAH [22]. At the stable open circuit potential (OCP) the semiconductor dissolves chemically at a rate that depends only on the temperature and on the composition of the solution. At potentials more positive than the OCP, the current increases significantly and corresponds to the electrochemical dissolution of silicon in the solution. At the critical current (I_{pp}), corresponding to the passivation potential (V_{pp}), an oxide layer is formed on silicon, stopping the etch since the etchant no longer has access to the silicon surface bonds. On the return scan to negative potentials, the current remains low since oxide is etched back very slowly.

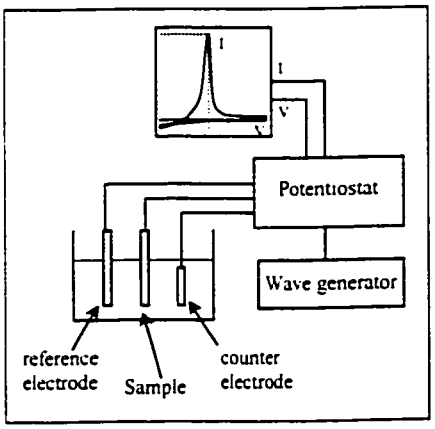

Figure 2-13 : Setup for electrochemical etching of silicon.

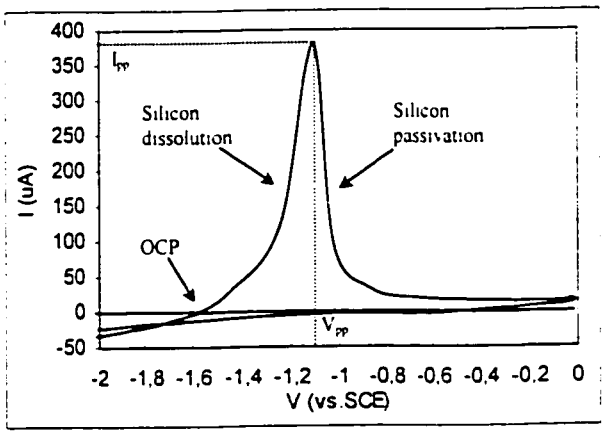

Figure 2-14 : A cyclic voltammogram of p-type Si in 25wt.% TMAH at 80°C, using an SCE as reference.

On the basis of this electrochemical theory, an etch-stop technique was first proposed in 1970 by Waggener [23]. Many researchers studied and improved this etch-stop technique. Globally, it consists of contacting an electrode to an N-type lightly-doped epi-Si layer grown on a P-type substrate. This PN junction forms a large diode such that there is a significant potential-drop at the junction. In this arrangement, the P-type substrate is selectively etched away (since its potential is less than V_{pp}). Etching then stops when the PN junction is reached (which has potential above V_{pp}).

2.1.5.3 Galvanic cell etching

The use of a galvanic cell to achieve an etch-stop in alkaline etchants was recently studied [22,24,25]. In this technique, gold [22,24] or alumium [25] is deposited on an N-type epi-layer on a P-type substrate forming a galvanic cell. In this configuration, the PN junction is reverse biased, and all the potential drops across the depletion zone. The P-type bulk floats at about the same potential as the etchant and etching proceeds until the depletion region is reached. Since the N-type silicon is positively biased with respect to the passivation voltage, it is passivated, i.e. etching stops. Figure 2-15 shows the etch rate in 25% TMAH for N-type and P type samples, with gold contact, as a function of temperature. An etching temperature lower than 90°C is required. Figure 2-16 shows an example of using the galvanic cell for achieving a N+ silicon membrane. The evaporated gold film should have a sufficent area exposed to the etchant so that the galvanic cell can provide enough current for the passivation. The current is created by the electrons injected into the n-Si conduction band, these electrons are consumed at the gold electrode to form hydroxyde ions from O_2

The advantage of this technique is that no externally applied bias is required to achieve the electrochemical etch stop. However practical issues must be adressed, in particular the area of metal required to generate sufficient current to passivate silicon.

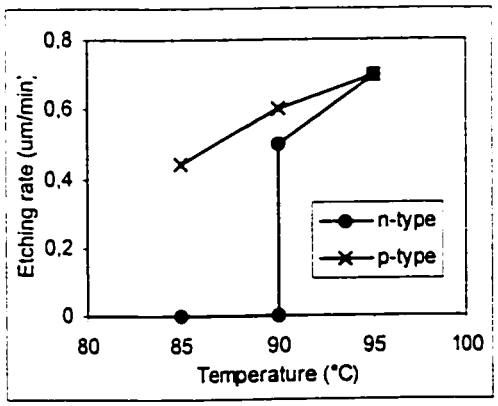

Figure 2-15 : Comparison of N-type and P-type etching rate after the formation of a galvanic cell [22].

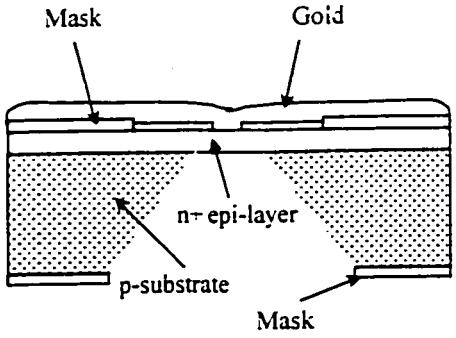

Figure 2-16 : Galvanic cell schematic

2.2 Towards a model of anisotropic etching

Since its emergence in the 1960s, anisotropic etching of silicon has been used and studied primarily experimentally. In the past decade, more researchers worked on both experiment and theoretical modelling simultaneously. Researchers considered two approaches in building models, i.e. microscopic and macroscopic.

2.2.1 Microscopic approach

In a microscopic approach, etching is viewed as the removal of units or individual atoms according to certain properties of their configuration (number of dangling bonds, potential difference with the solution, surface reconstruction, etc).

2.2.1.1 Band model and electrochemical etching

Seidel et *al* [20] developed a model based on band diagrams to explain etch stop phenomena and etch rate dependency versus etchant concentration. The model assumes that, after immersion in the etch bath, Fermi levels of both silicon and electrolyte are brought to the same level, as depicted on Figure 2-17. This results in a downward bending of the silicon bands, which provides a potential well for injected electrons released after the binding of OH^- ions with silicon dangling bonds.

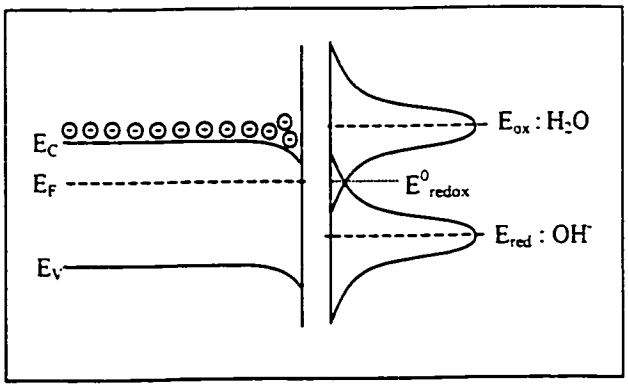

Figure 2-17 : Band model of N-type silicon / electrolyte interface for moderate doping concentrations

This band model involves electrochemistry since it assumes that four electrons are injected in the conduction band. Evidence of electron injection, rather than a mixed hole-and-electron mechanism, was first presented by Raley et *al* [27].

$$Si + 2OH^- \rightarrow Si(OH^-)_2^{2+} + 2e^- \quad (1)$$

$$Si(OH^-)_2^{2+} + 2OH^- \rightarrow Si(OH)_4 + 2\,e^- \quad (2)$$

The four injected electrons are highly "reducing " and react with water molecules.

$$4H_2O + 4e^- \rightarrow 4\,OH^- + H_2 \quad (3)$$

It is thought that etching proceeds by silicon dissolution involving the hydroxide ions formed in the vicinity of the silicon surface in reaction (3). Indeed, the hydroxide ions from the bulk are believed to be repelled by the negatively-charged surface due to the downward bending of the bands.

2.2.1.2 Step flow model

The etching rate of vicinal planes , i.e. crystallographic planes near atomically flat known planes (ex: {111}), may be described by the step flow model. The model assumes that vicinal planes are composed of flat terraces separated by steps, as illustrated in Figure 2-18. The height of steps is ideally equal to the width of a mono-atomic layer. Etching of vicinal planes is believed to occur almost exclusively at the atoms forming steps. As etching proceeds steps are simultaneously advancing in the same direction. Ideally, distances between steps is constant and unchanged during etching, but micrographs of etched surfaces often show merged steps that form macro-steps having heights and distances between steps orders of magnitude greater than ideal.

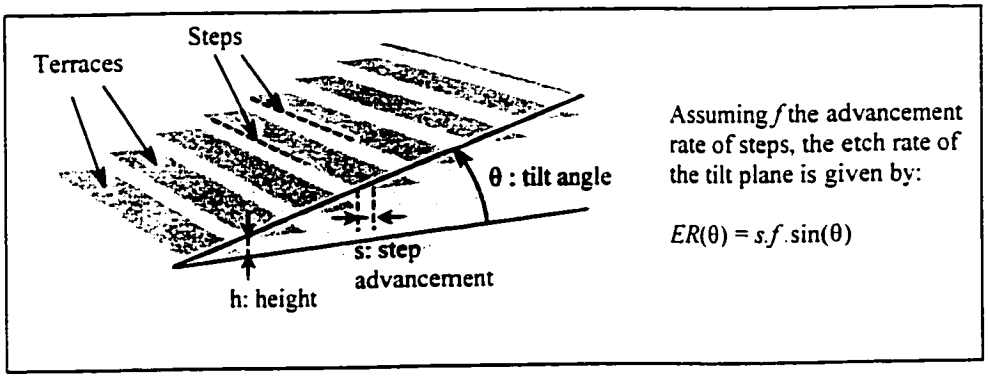

Figure 2-18 : Perspective view of simple steps on a flat plane.

The direct evidence of steps was performed by Allongue et *al.* [28] on vicinal-{111} planes tilted 0.7°. Using *in-situ* scanning tunnelling microscopy (STM) imaging on samples etched in NaOH at room temperature, they obtained micrographs of etched surfaces on which the steps are clearly visible with an average step spacing of 360Å.

2.2.1.3 Estimating removal probabilities of atoms

Hines and *al* [29] have demonstrated that combining STM experiments and kinetic Monte Carlo simulations could help understanding surface morphology after anisotropic etching. As they were trying to achieve "perfect" surfaces, the researchers studied the anisotropy of H-terminated vicinal-{111} silicon surfaces in NH_4F etching. The large-scale (10^6 atoms) chemically realistic simulations allowed them to directly compare STM experiments with theory and extract meaningful kinetic parameters. These parameters are the removal probability related to some specific configurations present on the silicon surface at the ledges between {111} terraces. Figure 2-19 illustrates the various possible atom configurations that differ according to the number of dangling bonds facing the etchant and the orientation of these dangling bonds. Indeed, it is believed that the more the silicon atom has dangling bonds, the easier it is to be etched. Moreover, dangling bonds are subject to further possible interactions as in the case of vertical dihydrides (on ledges) with vertical monohydrides (forming the {111} terraces).

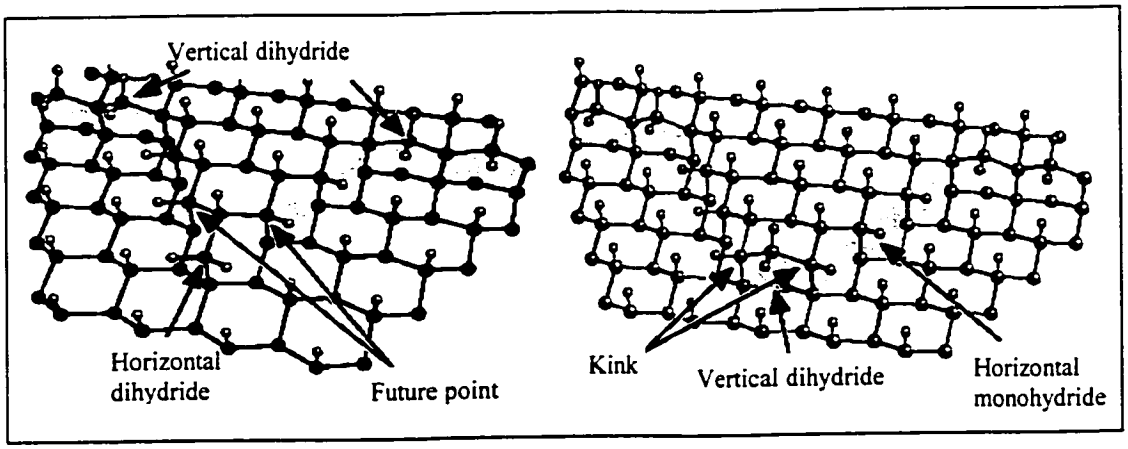

Figure 2-19 : Specific sites identified on H-terminated vicinal-{111} Si planes during an anisotropic etch [29].

Figure 2-20 compares the experimental morphologies with the best fit of Monte Carlo simulations for Vicinal-{111} planes cut at two directions $\langle 11\bar{2} \rangle$ and $\langle \bar{1}\,\bar{1}\,2 \rangle$.etched in IPA-doped NH_4F. The parameters set prior to simulation are the estimated relative removal probabilities of the different specific sites illustrated in Figure 2-19. The best fit presented in Figure 2-20 was achieved by applying the removal probabilities of Table 2-1. As a result, kinks are found to have a removal probability that is about 7 orders of magnitude greater than that of atoms in the terrace.

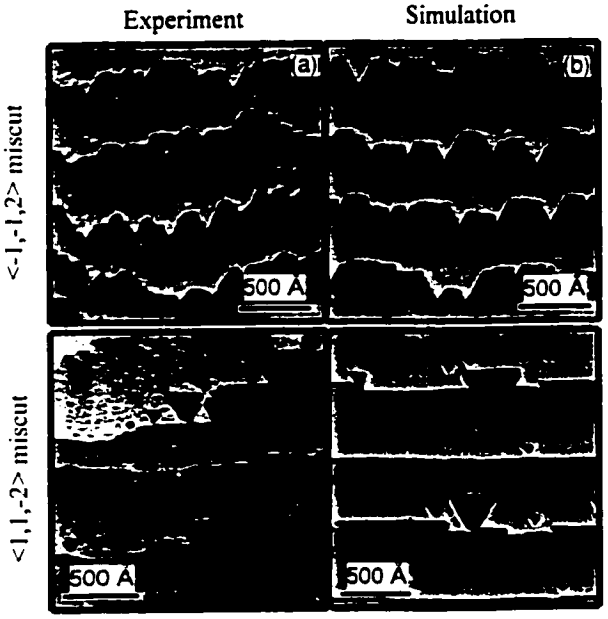

Figure 2-20 : Observed and simulated morphologies of Si{111} etched in 0.02% IPA-doped NH_4F [29].

Table 2-1 : Site-specific rates of NH_4F etching normalized to Kink etch probability [29].

Site	Removal probability
Kink	1
Point	0.1
Vertical Dihydride	0.01
Horizontal monohydride	0.005
Terrace	1.E-7

2.2.2 Macroscopic approach

While microscopic models help in understanding some etching phenomena such as etch rate variations and surface smoothness, they do not help directly in predicting etch profiles. As a result, macroscopic approaches are under development with an ultimate objective of being incorporated into etching software. The complexity of building a macroscopic model lies in developing a general model that would apply for all etching conditions while taking also account of many singularities observed during silicon etching.

2.2.2.1 The velocity source concept

The classical kinematic wave theory as introduced by Frank (1958) [30] and Chernov (1963) [31] describes the shape evolution of growing or dissolving crystals. The theory assumes that the evolution of the crystal surface depends only on its orientation. In a recent paper, Suchtelen and *al* [32] argue that the theory neglects boundary effects. These boundary effects could take place at contact lines: between two crystals, or between a crystal and a wall, or between a crystal and a mask. Boundary effects could also take place at contact points between interfaces and dislocations [33]. As a consequence, the traditional kinematic wave theory would be only relevant for "freely floating perfect single crystals". With boundary conditions added to the theory, the advance or dissolution rate at a junction is changed and the crystal around the junction is changed accordingly. It is then said that the junction acts as a "velocity source", as it acts as a source of kinematic wave trajectories.

As an example, Figure 2-21 illustrates the simplest possible case of velocity source : the contact line between a moving crystal interface and an immobile wall. Among the solutions of this case, we have shown 4 cases (various crystal orientations φ_∞ and growth rates) in which either a meniscus is created in close proximity to the interface or a macroscopic part of the interface is "nucleated" with a new orientation φ_0.

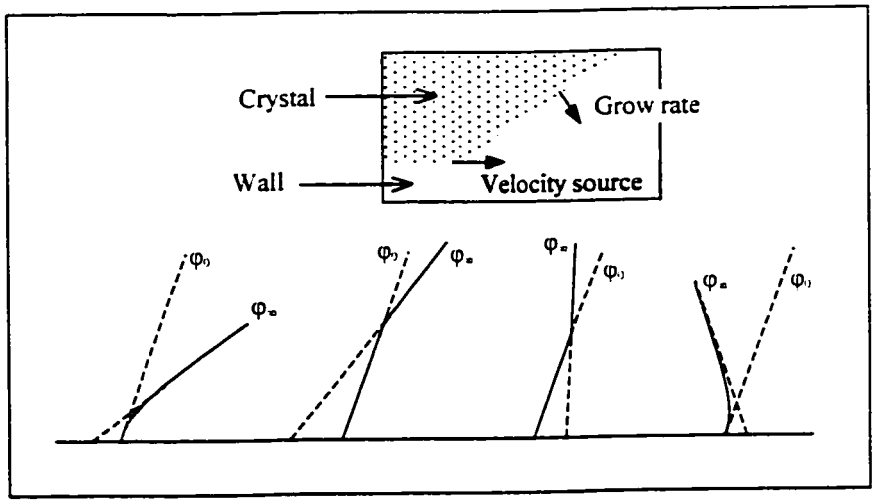

Figure 2-21 : Examples of shape evolution of a growing crystal in contact with a wall (could be the a growth vessel) φ_0 stands for the crystal orientation at the junction with the wall, while φ_∞ stands for the orientation at infinite distance from the wall [33].

2.2.2.2 Continuous description of the etch rate

A continuous description of crystal etching rather than the conventional atomistic description is needed for mathematical analysis and computer simulation. The objective is the construction of an orientation-dependent etch rate function R(**n**.*T*.*C*...) which would describe the etch rate of silicon for all orientations in space (4π steradians around a sphere). Suchtelen and *al* [32] succeeded in constructing such a function by assembling elementary functions through a non-linear network. R(**n**.*T*.C...) depends on the surface orientation **n** and on experimental variables such as temperature. concentration. etc...

The assembly of these functions is based on a complex mathematical toolbox that is not described here. however an electrical network analogy can be made: as in electrical circuits. two functions that describe etching phenomena that are supportive are assembled in a way comparable to parallel network. whereas in the case of competitive etching phenomena. the exponential assembling corresponds to a series network.

The building blocks of R(**n**,*T*,*C*,..) are elementary functions based on simpler models. specially the kink/step motion model. The kink/step motion model is an extension of the step flow model (described in paragraph 2.2.1.2). It also takes account of the birth-and-spread mechanism on smooth surfaces ({111} and {100}). Roughening parameters. microsteps velocities parameters. and some fitting constants also enter into the functions to give best simulation results. Figure 2-22 compares the experimental results (a) to two constructed etch rate functions (b) and (c). showing that the more parameters are included in the network of functions. the best the fit is.

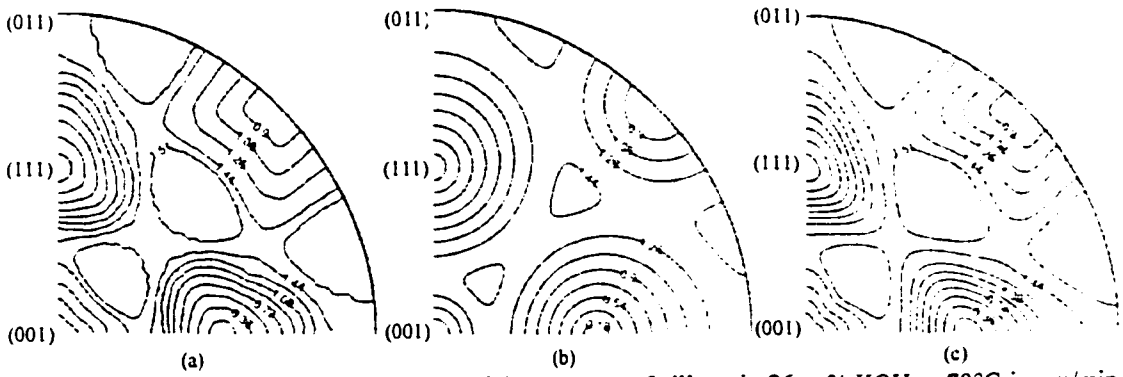

Figure 2-22 : Stereographic contour plots of the etch rate of silicon in 26 wt% KOH at 70°C in μm/min. [32] (a) Experimental results. (b) Fit for four parameter network etch rate function, assuming step velocities and roughness parameters of {111} and {100}. (c) Fit for the nine parameter etch rate function including anisotropy in the step velocity and representation of instabilities of the silicon surface.

3 Theory and Idealized Etching Model

This chapter begins with a review of basic theory about wet anisotropic etching of silicon. Then an idealized etching model is presented for the understanding of etched structures. By comparison of the idealized etching model with previous experimental data [8], anomalies are outlined as foundation for study in subsequent chapters 4,5,6,7.

3.1 Geometry of crystalline etched silicon

Silicon crystallography and geometry serve as foundation for understanding anisotropic etching. As etching proceeds in bulk silicon, three-dimensional structures with relatively flat surfaces are formed. The final shape may be simply bounded by {111} planes, or may be quite complicated, as occurs in most cases where the etching time is limited.
This section begins with a review of silicon geometry, then the wagon-wheel method is presented for the study of concave etching configurations.

3.1.1 Crystallographic properties of silicon

Silicon crystallizes in a diamond structure with lattice constant a=5.43Å. This structure is illustrated in Figure 3-1. Each silicon atom can be seen as being in the center of a tetrahedron made up of its four nearest neighbours (Figure 3-2). The four covalent bonds are built up from the four valence electrons of each silicon atom.

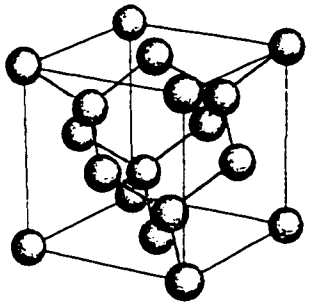

Figure 3-1: Silicon diamond structure

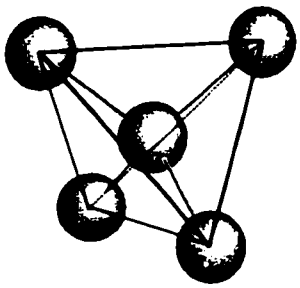

Figure 3-2 : Tetrahedron

During etching, the microscopic morphology of any face presented to the etchant is of great importance in determining etch behaviour. Atom and bond densities are particularly

important, at least from a global perspective. For example, a plane with many atoms but presenting few dangling bonds to the etchant is likely to etch more slowly, since more bonds bind each atom to the surface and more atoms need to be removed to have access to the next layer. Examples of planes with particularly noteworthy microscopic morphologies are the three plane families {100}, {110}, and {111}, oriented in the Si unit cell as shown in Figure 3-3. These planes are unanimously considered to be reference planes since their special microscopic morphologies lead to particular characteristics such as surface smoothness and etching rate minima.

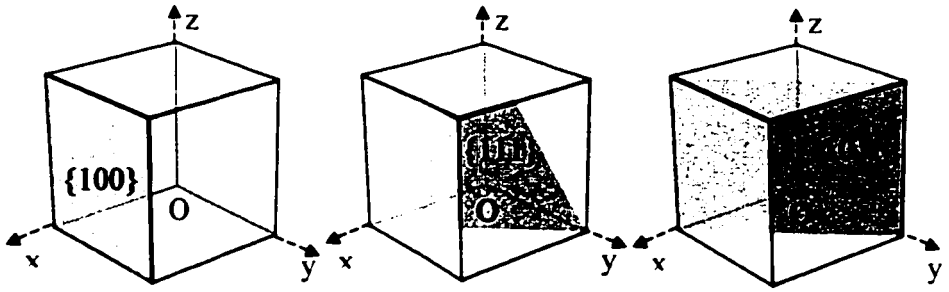

Figure 3-3: Orientation of {100}, {111}, and {110} planes in the simply-represented Si-unit cell (cube).

In this thesis, only {100} and {110} silicon wafers are studied, i.e. the horizontal silicon surface of the wafer is either a {100} or a {110} plane. Figure 3-4, aims to show the orientation of all planes belonging to the three families identified in Figure 3-3, for (a) Si{100} wafers, and for (b) Si{110} wafers.

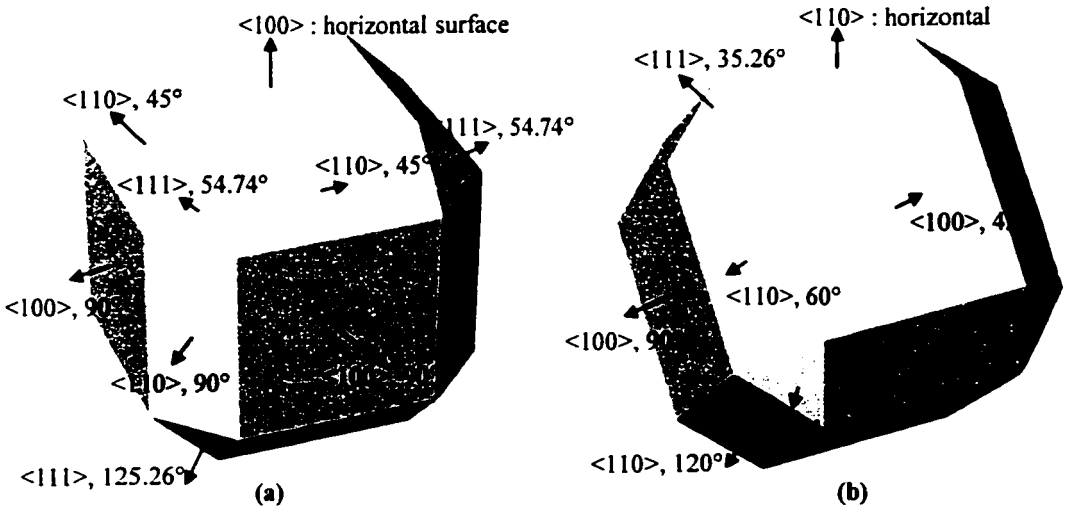

Figure 3-4 : Orientation of {100}, {110}, and {111} planes for: (a) Si{100}, (b) Si{110}. Angles specified are the inclination angles with respect to the horizontal surface.

3.1.2 Etching characteristics of silicon

Forming 3D structures in the bulk of silicon is performed by etching through opened windows, previously patterned in a masking material (ex: SiO_2 and Si_3N_4) on the surface of a silicon wafer. The silicon begins to dissolve in the areas exposed to the etchant liquid. As etching proceeds, other areas covered by the masking material and adjacent to an opened window are etched (referred to as "under-etching").

Limited etching times

Figure 3-5 shows an example of anisotropically etched silicon covered by a masking material for a limited etching time. The ring example was chosen because it is composed of both concave and convex edges. Convex corners lead to the appearance of fast-etch planes whereas concave corners lead to slow-etch planes.

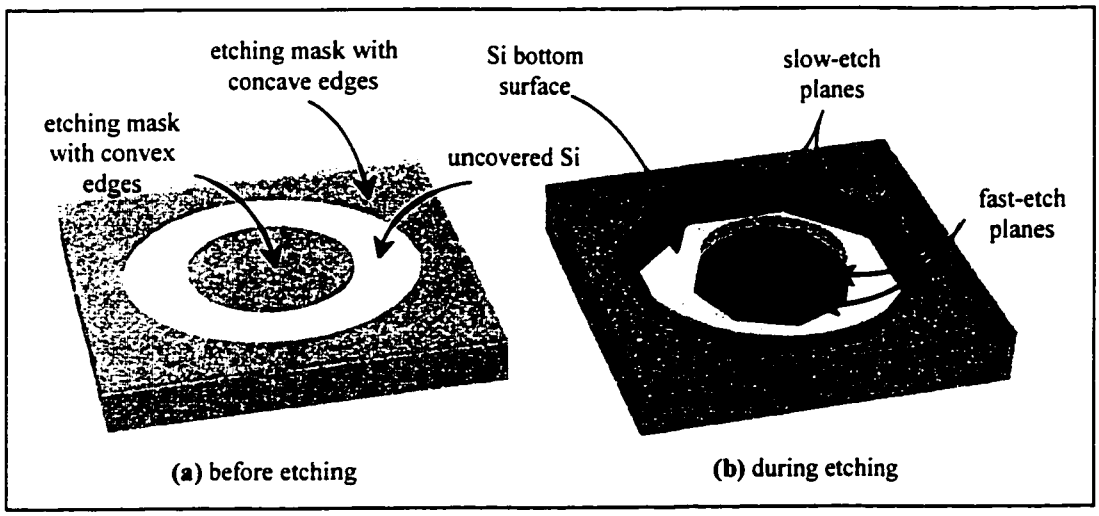

Figure 3-5 : Example of anisotropic etching through a ring window (uncovered Si area).

Long etching time

Shaping silicon by anisotropic etching is constrained by the fact that {111} family of planes confine the etching advancement since the etch rate of {111} planes is much lower than that of any other plane (e.g. the research of Tabata et *al* demonstrates that the etching rate of {111} plane in TMAH solutions is about 0.02-0.05 times smaller than that of {100} [2]). Consequently, after some time, and depending on the size of the opened window, the etched silicon shape does not evolve any longer, but it is composed of only

{111} planes. Figure 3-6 shows an example of anisotropically etched {100} silicon through an irregular window after a long etching time. "Under-etching" proceeds at all convex corners until {111} planes are reached, the {111} planes being tangent to *concave* corners. In Figure 3-6, further etching will affect only the {100} bottom surface, which tends to be etched away, leading to the formation of an inverse-pyramidal-like cavity.

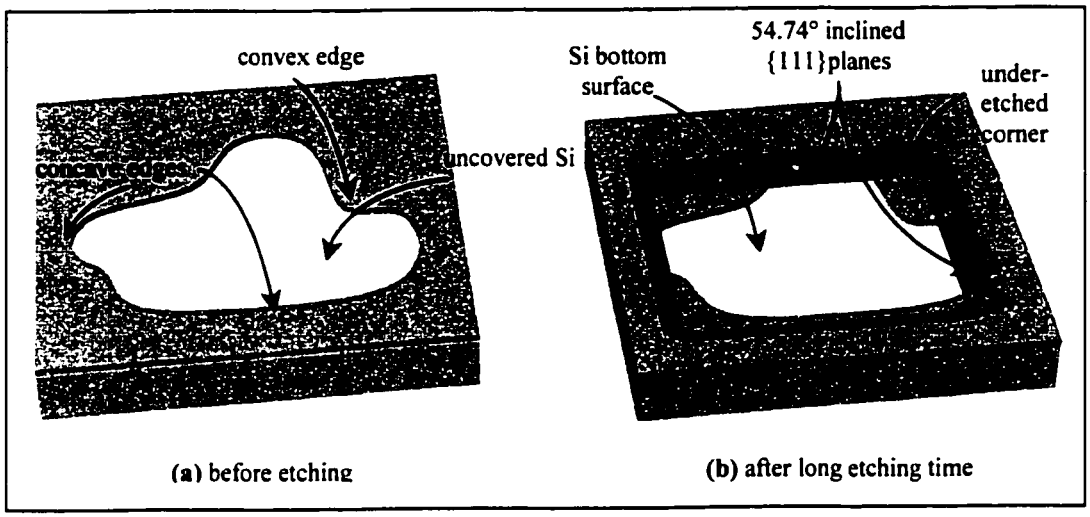

Figure 3-6: Long-time etching of Si{100} leading to {111} planes.

Anticipating the end shape in the bulk of silicon, starting with any opened window, is possible by identifying all {111} planes in Figure 3-4. More specifically, Si{100} wafers would lead to 54.74° inclined {111} planes forming a rectangular under-etched shape, whereas Si{110} wafers would lead to vertical (90°-) and 35.26°-inclined {111} planes forming a more complex structure.

3.1.3 Wagon-wheel method

The study of silicon etching, and more specifically the study of under-etching for all mask-edge angles, is facilitated by etching silicon through a wagon-wheel pattern shown in Figure 3-7. Dark areas represent the masking material that prevents the silicon from etching. White windows represent the areas in which silicon is etched away. The white areas are long isosceles triangles shaped as "spokes" of the "wagon-wheel" pattern. Spokes are often spaced every one degree, which is sufficient for studying the evolution of under-etched shapes. Assuming that silicon is being etched using such a mask,

(etching at the white windows), the dark areas are progressively reduced as shown in Figure 3-8. This lateral etching proceeds under the mask and induces a radial etching that is readily observed by the naked eye (Figure 3-9). Actually, radial etching is just an amplified measure of lateral etching but it is typically less precise.

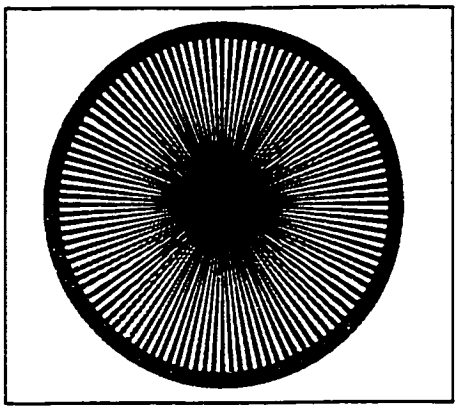

Figure 3-7 : Top view of typical wagon-wheel pattern. (dark = mask, white = uncovered Si).

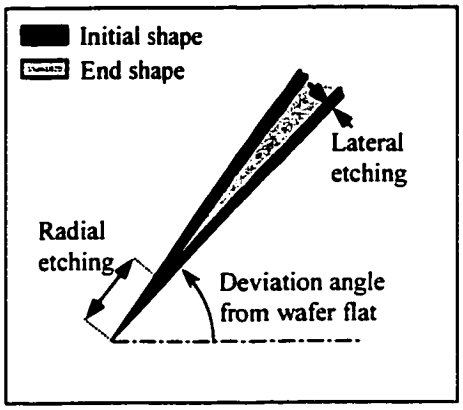

Figure 3-8 : Detail of mask-under-etching at a spoke of a wagon-wheel mask.

Examples of results of under-etching a wagon-wheel pattern for both Si{100} and Si{110} are presented in Figure 3-9. The emerging patterns at the centre of the samples are due to radial etching and may be converted to polar plots of the under-etching rate, i.e. no radial etching indicates the presence of {111} planes and maxima in radial etching correspond to fast-etch planes.

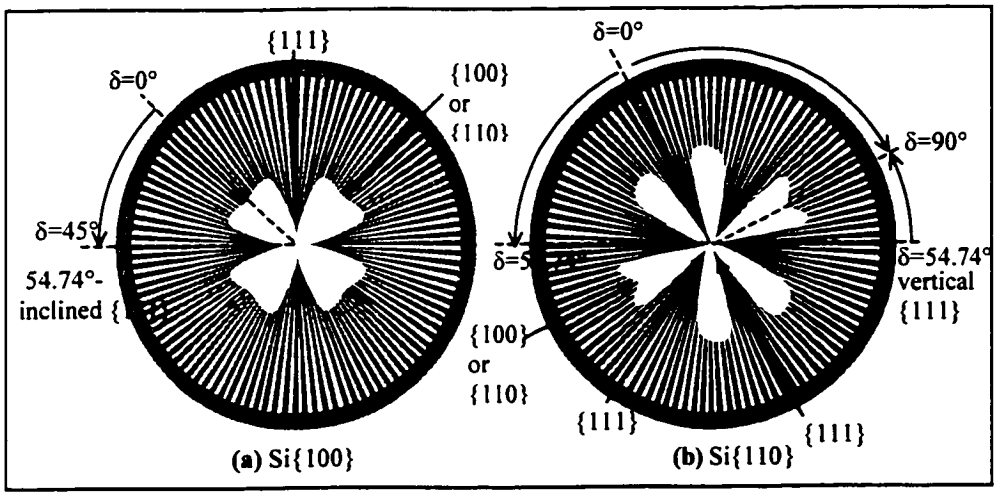

Figure 3-9 : Result of under-etching a wagon-wheel pattern on: (a) Si{100}, and (b) Si{110}. δ is referred to the deviation angle (see later in the text). Specified planes are side-wall planes of etched spokes.

Wagon-wheel etching profiles

Typical wagon-wheel experiments give rise to concave configurations, accordingly selecting slow-etch[1] planes. Among these planes, cavity having sidewalls of {111}, {100}, or {110} are most commonly desired in micromachined devices, and obtained by proper positioning (orientation) of the mask edge. Other mask edge orientations (measured by the angle (δ)), select other relatively slow-etch planes that generally form a multi-facet etch profile. Figure 3-10 depicts a segment of etched silicon using a wagon-wheel masked pattern. Each wagon-wheel "spoke" represents a different value of δ. The techniques of measurement of plane etch rates and inclination angles are detailed in Chapter 5.

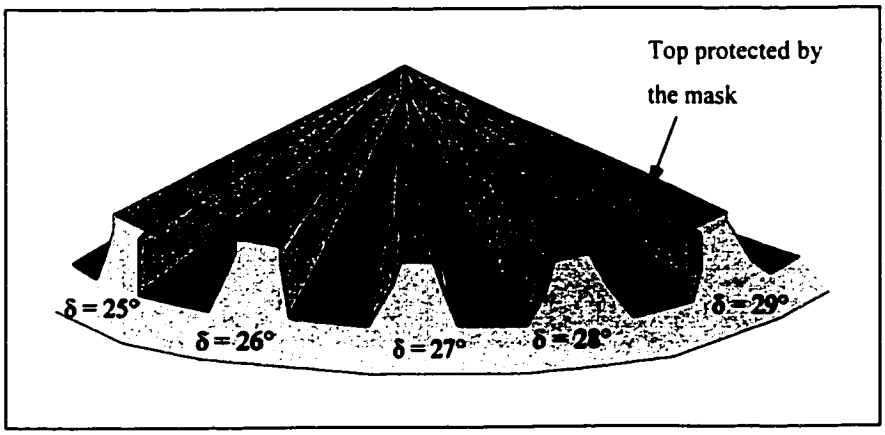

Figure 3-10 : Perspective view of a wagon-wheel segment

Figure 3-11 depicts a cross-sectional view of the general under-etch situation in a single "spoke", involving the possibility of several facets, each having different inclination angles with respect to the wafer surface. In this example, two facets, with inclination angles, α_1 and α_2, are depicted. Due to the concave configuration, each of these facets necessarily corresponds to a relative local minimum in etch rate, with respect to other directions very close to it. Under-etch rate (UER) as well as etch rates (ER) are measured from the mask edge since the sidewalls of the cavity emerge from the mask edge. An effective angle ($\alpha_{effective}$) has also been drawn in Figure 3-11. It represents the inclination

[1] In general, concave configurations select slow-etching planes. However, by careful design of the geometrical relationships between mask-edges and the crystal structure, relatively fast-etching planes can be forced to appear.

angle of the side wall which would be in effect if the under-etch profile were single-faceted.

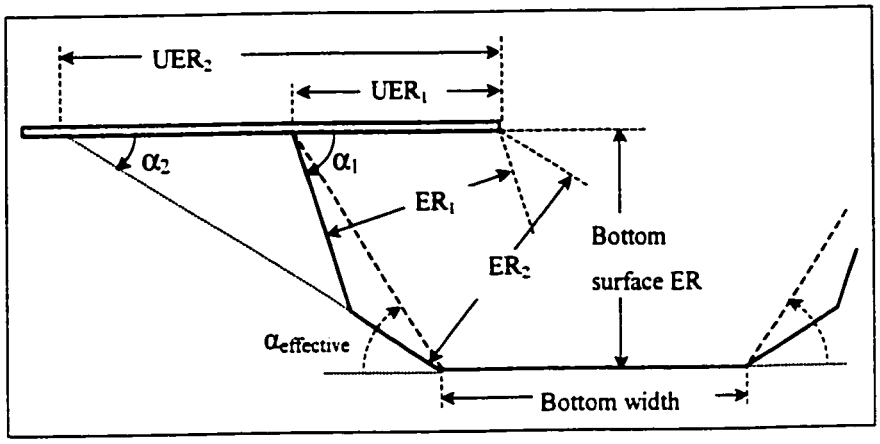

Figure 3-11 : Schematic cross-section of an under-etched masking oxide, showing main notations. "ER" stands for Etch Rate, "UER" stands for Under-Etch Rate.

3.2 Etching model

This section explains an etching model developed by study of wagon-wheel under-etch experiments on Si{110} and Si{100}, at 80°C in TMAH at concentrations ranging from 25wt% to 12wt% [8,9,34]. The model is based on identification of two different types of crystal features presented to the etchant: periodic bond chains (PBC's) and rows of kinks (k-rows) [8,9,35], from which exposed facets are generally composed. It is important to remember that this model only applies for concave configurations.

3.2.1 Angle definitions

At least three angles are needed for effective understanding of the under-etch phenomena.

Deviation angle: (δ)

Delta is defined to be the angle between the mask edge and a suitable reference direction on the wafer surface. For example, in the case of Si{100}, whose wafer flat is directed in a <110> direction, $\delta = (45° - \varphi)$, where φ is the angle between the mask edge (referred as *I* in Figure 3-12) and the wafer flat. As a more general definition for Si{100} wafers, (δ) is the angle between two lines, both on the wafer surface:

(1) the mask edge , and

(2) the nearest intersection line of a vertical {100}-family plane with the wafer surface.

Figure 3-12 clarifies the positioning of the reference directions for the measure of (δ).

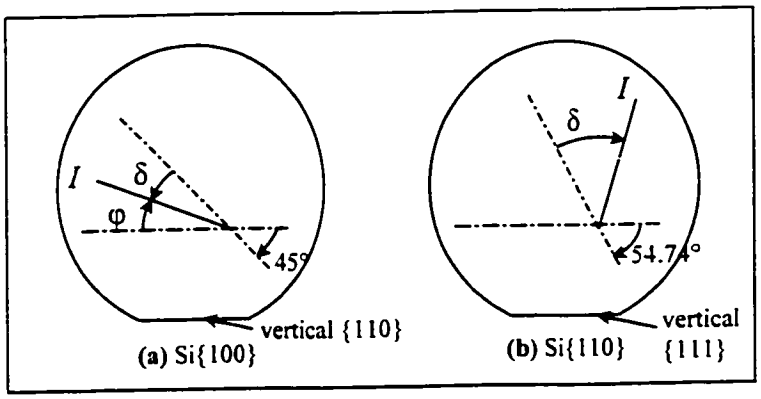

Figure 3-12 : Illustration of deviation angles (δ) for: (a) Si{100}, (b) Si{110}.

Inclination angle: (α)

Alpha is the inclination angle of a given plane with respect to the (horizontal) wafer surface (see Figure 3-11). Note that inclination angles greater than 90° correspond to planes which are inverted with respect to the wafer horizontal surface.

Rotation angle from a {111} plane: (θ)

Even though the above two angles give a complete description of the plane's orientation with respect to the wafer surface, a third angle, (θ), is defined specifically to emphasize the nature of P-based and K-based planes. For these planes, (θ) gives the angle of rotation of the plane away from a {111}-family plane, (the nearest {111}-family plane). If the plane in question is P-based or K-based (see next section for a detailed description), then the intersection between this plane and the nearest {111}-family plane will be a line oriented in a <110>-family direction. This line is its axis of rotation for the purposes of defining the angle θ. Figure 3-13 illustrates how P-based planes (or K-based planes) evolve by rotation θ_p (or θ_k), away from a {111}-family plane.

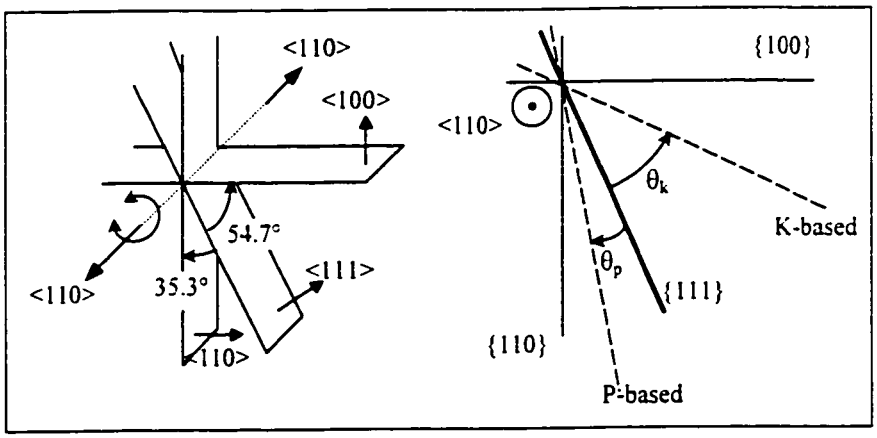

Figure 3-13 : Rotation angles from {111} : θ_p and θ_k.

3.2.2 P-based and K-based planes

The model is based on identification of two plane families that constitute under-etched emerging facets : P-based and K-based planes.

P-based planes have Miller Indices of the form {*h h l*}, where "*l* " indicates the lower of the two indices, and "*h* " indicates the higher, (examples: {221}, {552}, {331} families). These plane surfaces are defined by parallel periodic bond chains (PBCs). A PBC is a

zigzag chain of atoms, each having only one dangling bond, one backbond, and two bonds between atoms in the PBC itself (Figure 3-14). The etching of a PBC begins by removal of a single atom from the PBC, which "breaks" the connected chain, allowing rapid propagation of removal of atoms (like "zipping"). Thus PBCs are relatively stable until at least one atom is removed, after which they are etched more quickly.

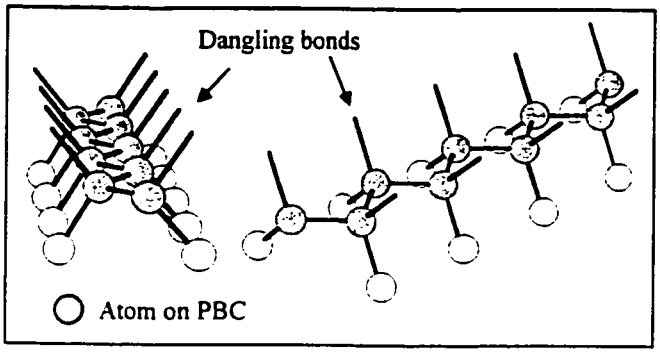

Figure 3-14 : Illustration of Periodic Bond Chains (PBCs).

On a P-based surface, depicted in Figure 3-15, idealized etching proceeds by movement of PBC-defined steps, along flat {111}-family planes (by removal of entire PBCs, exposing the next PBC). The etch rate of such P-based planes is (ideally) given by $ER(\theta_p) = s.f.\sin(\theta_p)$, where s is the step width and f is the removal frequency of a complete PBC. This equation matches experiment well enough for small θ_p below 15° [9.34].

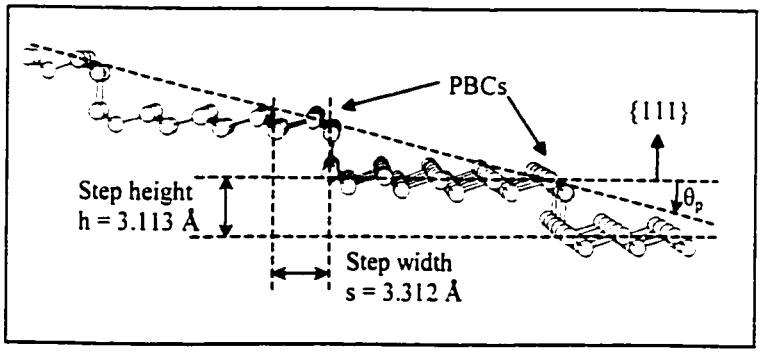

Figure 3-15 : Cross-view of typical vicinal-{111} P-based plane.

K-based planes have Miller Indices of the form {*h l l*}, (examples: {211}, {522}, {311} families). A kink is defined as an etch-front atom having two backbonds and two dangling bonds free to interact with the etchant. Rows of kinks (K-rows) compose {100}-family planes. The fact that etched {100} planes are flat suggests that K-rows are stable,

the stability being likely provided by surface reconstruction. Figure 3-16 shows the two possible forms of K-rows (differing only by the direction of the dangling bonds with respect to a fixed reference direction). The configuration in Figure 3-16 labelled "type-2" has been identified by Jakob *et al* [36] using infrared spectroscopy on H-terminated vicinal {111} planes after wet etching in solutions over a wide range of pH. Thus, in Figure 3-17 we depict a K-based plane as being composed of this "type-2" K-row. Etching of a K-row is assumed to proceed by a similar "zipping" procedure as described for PBCs. While this behaviour is not obvious, (since the atoms in a K-row are not formally bonded to each other), the fact that K-based facets are prevalent on under-etched surfaces, proves that in under-etch experiments, K-rows are removed as units, which must imply their relative stability and most likely their removal by a zipping process.

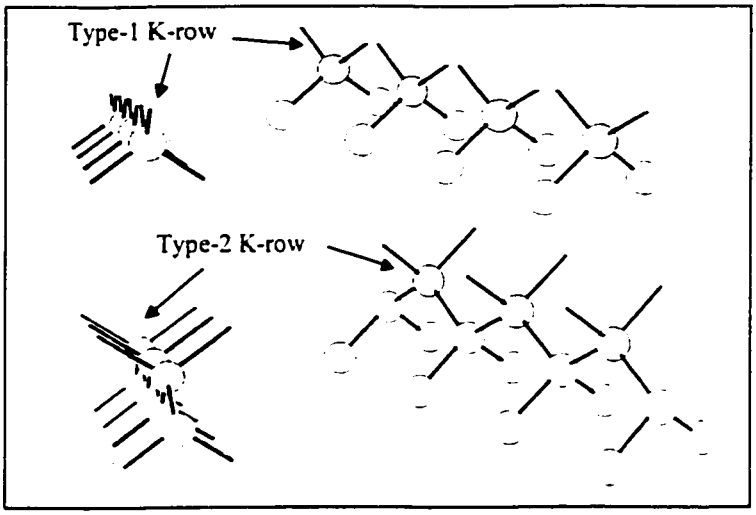

Figure 3-16 : Illustration of the two possible types of rows of Kinks (K-rows).

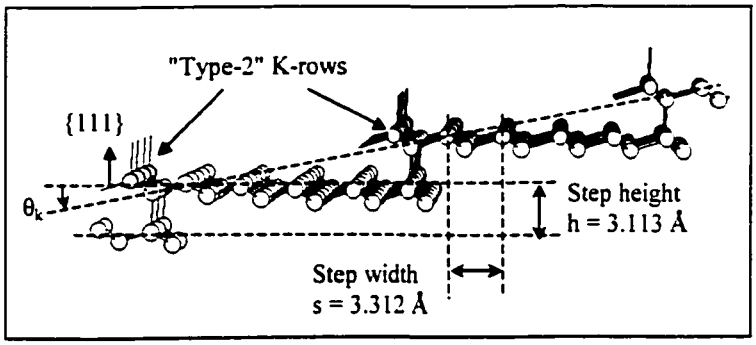

Figure 3-17 : Cross-sectional view of typical vicinal-{111} K-based plane composed of "type-2" K-rows.

3.2.3 Estimating the removal frequencies f_p and f_k

The crystal-feature-based model [8] assumes that, in a unit of time ($1/f$), the etching of stepped {111} planes propagates by one step-advancement width s. As a first approximation, the removal frequencies f_p and f_k represent the speed at which a newly-exposed step (Periodic-Bond-Chain (PBC) or row of Kinks (K-row)) is entirely removed by the etchant (which exposes the next step). By the successive removal of steps (PBCs or K-rows), stepped-{111} planes etch by successive advancements of a distance s along the {111} surface. The result of etching many steps can be translated into an effective etching rate of the near-{111} plane (which is rotated from the {111} plane by an angle θ_p or θ_k), using one of the following equations [8]:

$$ER(\theta_p) = s.f.\sin(\theta_p) \qquad (1)$$

$$ER(\theta_k) = s.f.\sin(\theta_k) \qquad (2), \qquad \text{where } s \text{ is equal to } 3.31\text{Å}.$$

By fitting the two above equations to the experimental under-etch data [8], it is possible to estimate the removal frequencies f_p and f_k. As an example Figures 3-18 and 3-19 present the experimental under-etch rate results on Si{110} etched for one hour in 25wt% and 19wt% unstirred-TMAH, respectively.

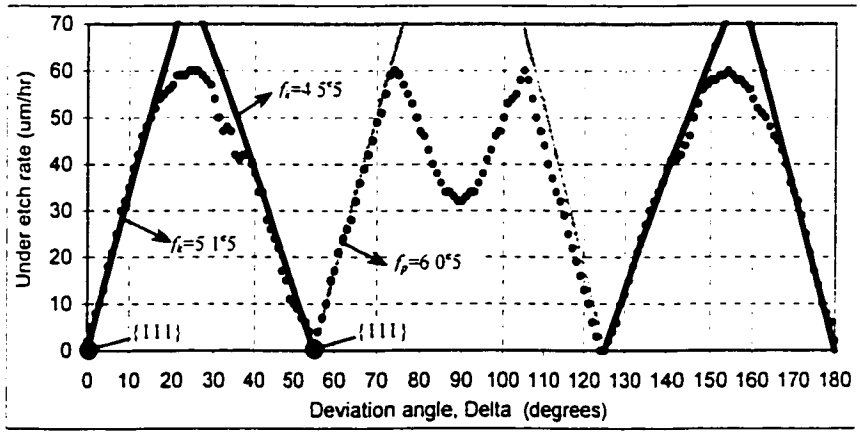

Figure 3-18 : Si(110) etched in 25wt% TMAH (redrawn from[8]).

In Figures 3-18 and 3-19, the *etch rate* functions with respect to θ angle (equations (1) and (2)) are transformed [8] into *under-etch rate* functions with respect to δ (solid lines in Figures 3-18 and 3-19), for fitting with the experimental under-etch rates near a {111} plane. It is observed in Figures 3-18 and 3-19 that the fitting results for the various

portions are in the same order of magnitude for P-based and K-based planes. When comparing results for the two concentrations, it is observed that the K-row removal frequencies f_k increase as the concentration goes from 25wt% to 19wt%, whereas the PBC removal frequency f_k is roughly unchanged [8].

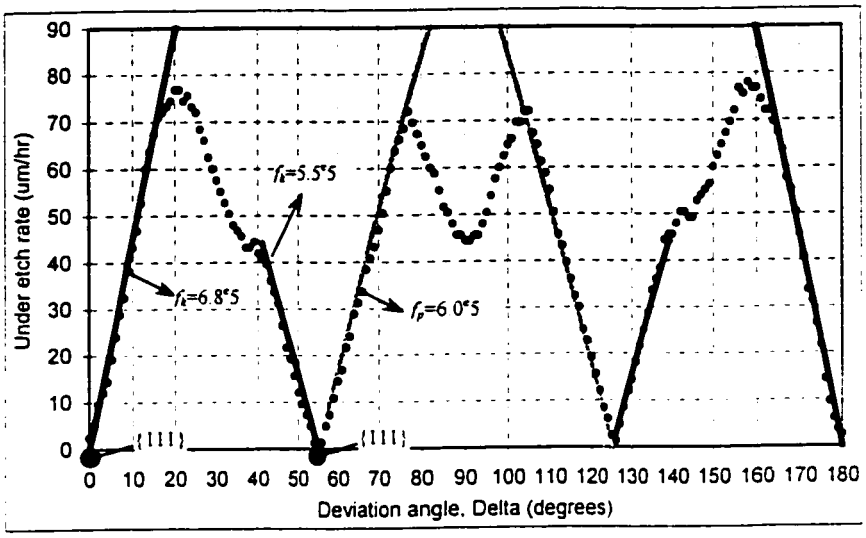

Figure 3-19 : Si(110) Etched in 19wt% TMAH (redrawn from[8])

3.2.4 Orientation of P-based and K-based planes

We define a P-based series (or K-based series) as the family of P-based planes (or K-based planes) obtained by angles of rotation θ_p (or θ_k) with respect to a given {111}-family plane. Due to the basic geometry and symmetry of the silicon crystal structure, there are many of such series, each oriented differently with respect to the wafer surface. They are readily identified by locating all {111}-family planes with respect to the wafer surface (Figure 3-4). Orientations of specific P-based and K-based planes is available in Appendix I.

Si{100}

Due to the symmetry of the Si lattice, Si{100} requires only a plot of δ from 0° to 45° to completely characterize under-etching features. However, a 90° span is plotted (from -45° to 45°) so that {100} and {110} planes are centered at δ=0°, more clearly showing a local minimum in such under-etch rate plots. Figure 3-20 summarizes the variation of θ_k (or θ_p) with respect to δ for the available K-based series (or P-based series) for Si{100}, using following equations (3) and (4).

- K-inclined: $$\theta_k = \text{atan}\left(\frac{1}{\tan(\delta)\sqrt{2}}\right) - 35.26° \qquad 0 \le \delta \le 45° \qquad (3)$$

- P-inclined: $$\theta_p = 35.26° - \text{atan}\left(\frac{\tan\delta}{\sqrt{2}}\right) \qquad 0 \le \delta \le 45° \qquad (4)$$

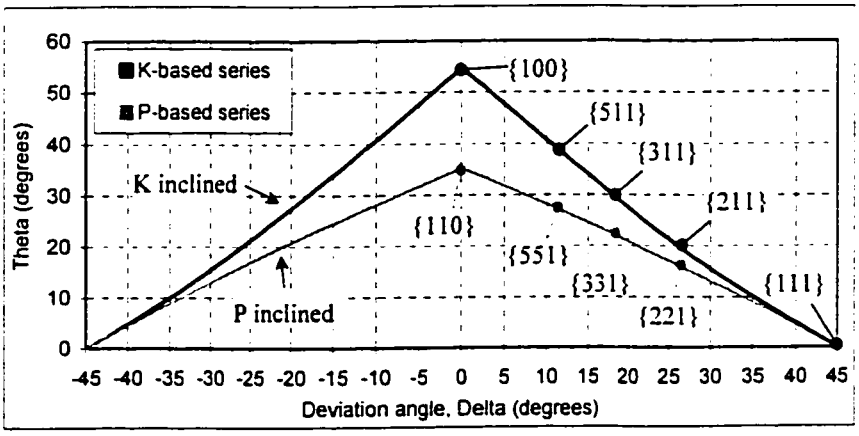

Figure 3-20 : Theoretical rotation angles (θ) versus mask edge deviation angle (δ) for Si{100}.

Figure 3-20 summarizes the Miller indices of the planes that may appear as a result of positioning the mask edge at a given deviation angle (δ). Note that the curves drawn in Figure 3-20 and referred as "inclined" planes, may also represent "inverted" planes that are symmetric (with respect to the horizontal surface) to the "inclined" planes. Figure 3-20 also demonstrates that on Si{100}, K-based planes and P-based planes having the same *h*-index (ex: 5 in {511} and {551}), are positioned at the same deviation angle (δ), which is not true for Si{110}.

Figure 3-21 summarizes the variation of α_k (or α_p) with δ for the various available K-based series (or P-based series) for Si{100}, using equations (5) and (6):

- K-inclined: $\alpha_k = \text{atan}\left(\frac{1}{\sin(\delta)}\right)$ $\quad 0° \le \delta \le 45°$ (5)

- P-inclined: $\alpha_p = \text{atan}\left(\frac{1}{\cos(\delta)}\right)$ $\quad 0° \le \delta \le 45°$ (6)

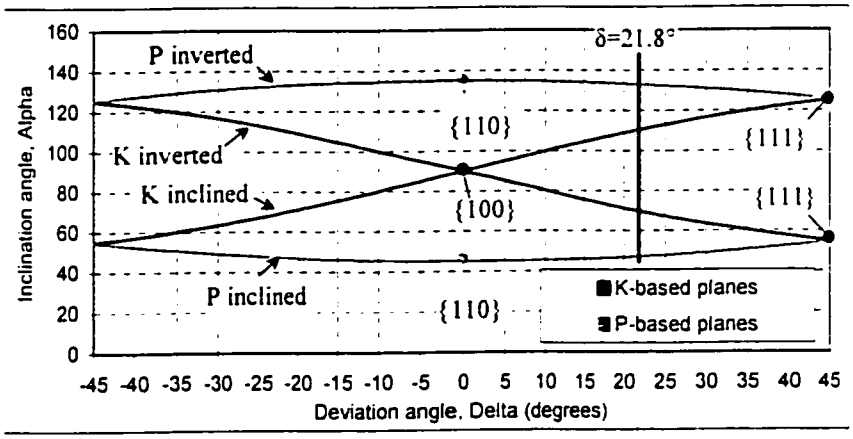

Figure 3-21 : Theoretical inclination angles (α) versus mask edge deviation angle (δ) for Si{100}.

Angles of α greater than 90° correspond to planes which are inverted with respect to the wafer surface. To illustrate the use of Figure 3-21, let us consider an example of an under-etching experiment on Si{100}, where the mask edge is positioned at 23.2° from the wafer flat, (i.e. δ = (45° - 23.2°) = 21.8°). At this δ, we find that four different planes (two P-based, two K-based)[2] may be involved in shaping the under-etch profile. The inclination angles of these planes are 47.12° and 132.88°, 69.63° and 110.37°, respectively. Actual experimental under-etched inclination angles are to be observed and

[2] *identified as* $(255), (25\bar{5}), (252), (25\bar{2})$.

compared with these theoretical angles. If they match, then one can conclude (forced by basic geometry of the silicon crystal structure) that the actual facets are P-based or K-based. The final under-etched profile (e.g. α_1 and α_2) should be constituted exclusively by some subset of these four planes, their relative sizes depending on their actual etch rates in the solution.

Si{110}

Due to the symmetry of the Si lattice, Si{110} requires a plot of δ from 0° to 90° to completely characterize under-etching features. However, a span of 180° is plotted so that {100} and {110} planes are centered at δ=90°, which leads to a local minimum in under-etch rate plots. Figure 3-22 summarizes the variation of θ_k (or θ_p) with δ for the available K-based series (or P-based series) for Si{110}, using equations (7) to (11):

K1-inclined: $$\theta_k = \text{atan}\left(\tan\delta - \frac{1}{\sqrt{2}}\right) - 35.26° \qquad 54.74° \le \delta \le 90° \qquad (7)$$

K2-inclined: $$\theta_k = \text{atan}\left(\frac{1}{\sqrt{2}} + \tan\delta\right) - 35.26° \qquad 0 \le \delta \le 90° \qquad (8)$$

K-vertical: $$\theta_k = 54.74° - \delta \qquad 0 \le \delta \le 54.74° \qquad (9)$$

P-inclined: $$\theta_p = 35.26° - \text{atan}\left(\left|\frac{1}{\sqrt{2}} - \tan\delta\right|\right) \qquad 0 \le \delta \le 54.74° \qquad (10)$$

P-vertical: $$\theta_p = \delta - 54.74° \qquad 54.74° \le \delta \le 90° \qquad (11)$$

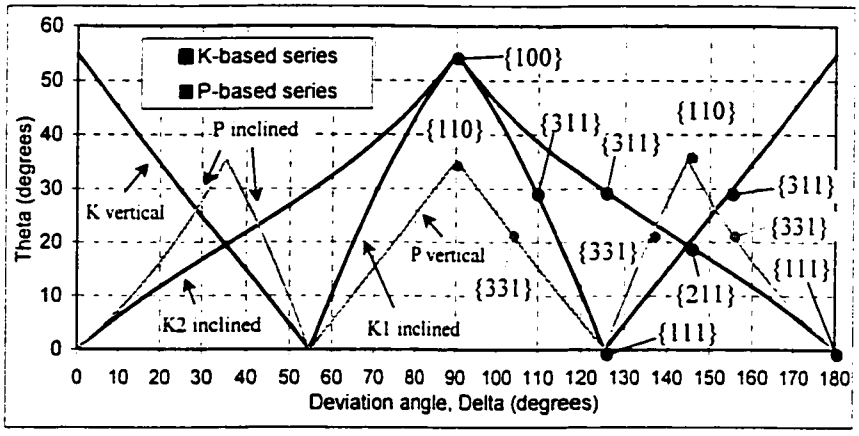

Figure 3-22 : Theoretical rotation angles (θ) versus mask edge deviation angle (δ) for Si{110}.

It can be see in Figure 3-22 that many series (vertical and inclined) are available on Si{110}. Horizontal lines cross K-based series (or P-based series) at planes having the same Miller indices. {111} planes are situated at θ=0° (corresponding to the horizontal (X) axis), {110} planes are situated at θ=35.26°, and {100} planes at θ=54.74°. To distinguish between the K-based inclined planes, "K1" refers to the K-based inclined series with $54.74° \le \delta \le 90°$, while "K2" refers to the K-based inclined series with $0 \le \delta \le 90°$. Actually, K1-inclined is the top-most facet (higher inclination angle than that of K2-inclined, as seen in Figure 3-23), and K2-inclined is the lower facet of an under-etch profile when both planes are competing at $54.74° \le \delta \le 90°$.

Figure 3-23 summarizes the variation of the inclination angle α_k (or α_p) with respect to the mask edge deviation angle (δ) for the various available K-based series (or P-based series) for Si{110}. Calculation of the inclination angle (α) for each series is performed using the following steps:

- Calculating θ_k (or θ_p) from δ using the appropriate equation from (7) to (11).
- Calculating the corresponding (hkl) Miller Indices.
- Calculating α using : $\alpha = \text{acos}\left(\frac{\langle hkl \rangle \cdot \langle 011 \rangle}{\|\langle hkl \rangle\| \cdot \sqrt{2}}\right)$

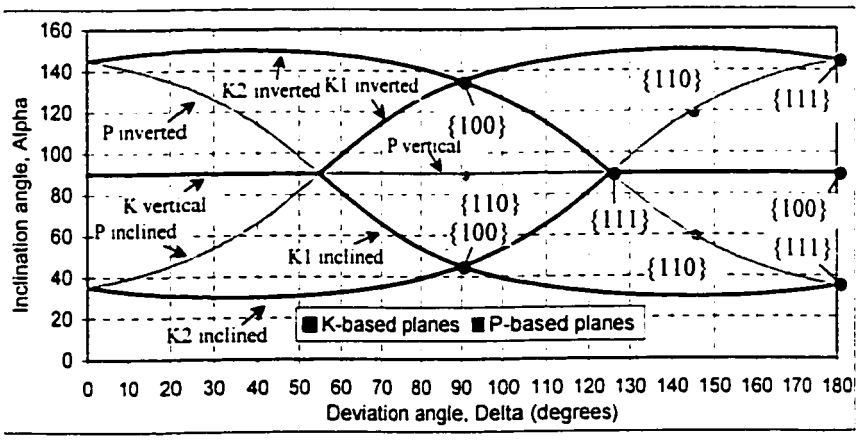

Figure 3-23 : Theoretical inclination angles (α) versus mask edge deviation angle (δ) for Si{110}.

3.3 Model fitting for 25wt% TMAH

In this section, we show how the etching model composed of K-based and P-based planes applies. Starting from experimental results on Si{110} and Si{100} etched in 25wt% TMAH, K-based and P-based series are extracted and their etch rates are compared. Canonical etch rates of these series are then estimated. Next, to confirm the use of the model, ideal under-etch rates curves are constructed as well as the under-etch profiles from the canonical etch rates of the P-based and K-based series. Finally, theoretical and experimental results are compared.

3.3.1 Experimental results

Figure 3-24 and Figure 3-25 show the experimental results of 1-hour under-etched Si{110} in 25wt% TMAH [8.34]. Figure 3-26 and Figure 3-27 show the corresponding experimental results for Si{100}. The designation of P-based and K-based planes has been made by comparing to Figure 3-23 for Si{110} and to Figure 3-21 for Si{100}. In all figures, black symbols or curves correspond to K-based planes, while grey symbols or curves correspond to P-based planes. Because the under-etch rate (Y-axis of Figure 3-25 and Figure 3-27) refers to the advancement distance under the mask (Figure 3-11), it is linked to the advancement of the top-most facet of an under-etch profile (named "1st facet" in Figure 3-24 and Figure 3-26). Portions of curves are numbered in Figure 3-25 and Figure 3-27. These portions are those exported to Figure 3-28 (see next section below).

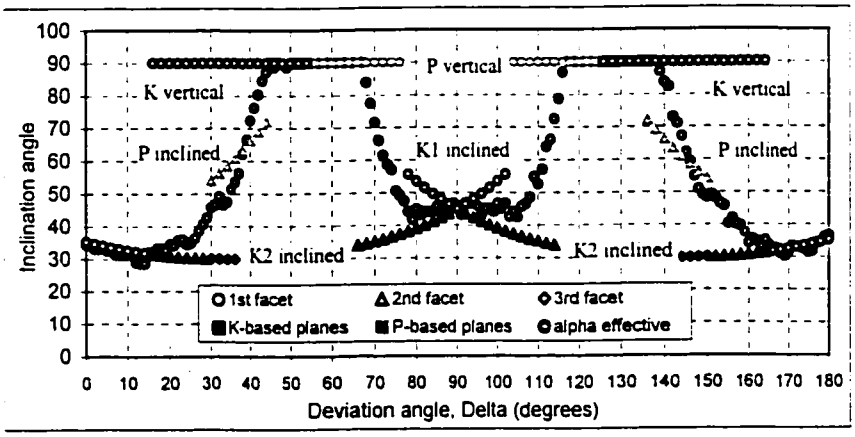

Figure 3-24 : Si{110} 25wt%TMAH - Facet details with respect to δ (measurements are within +/-2 degrees, and roughness of the surfaces vary widely, not reported here) [8].

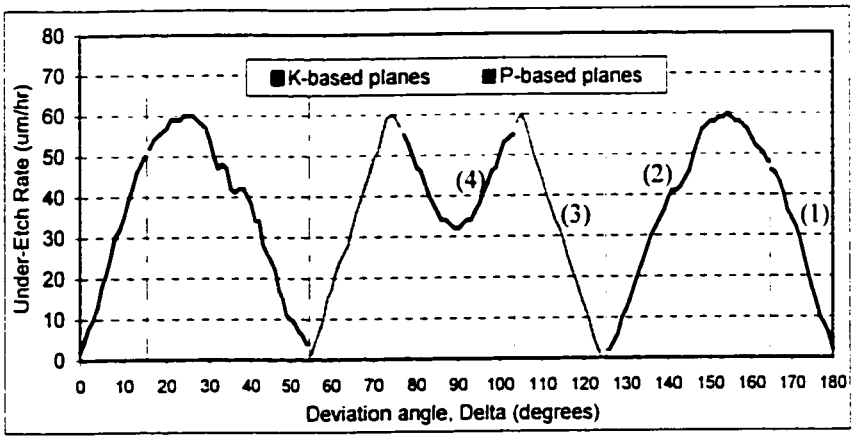

Figure 3-25 : Si{110} 25wt%TMAH - Experimental under-etch rate [8].

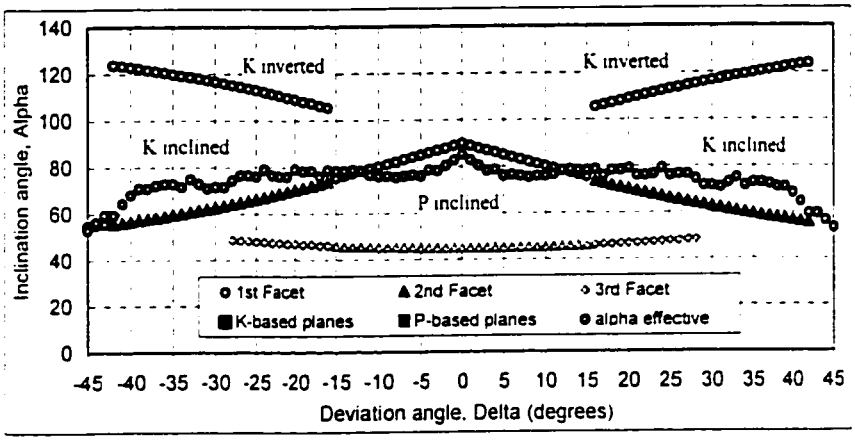

Figure 3-26 : Si{100} 25wt%TMAH - Facet details with respect to δ (measurements are within +/-2 degrees, and roughness of the surfaces vary widely, not reported here) [8].

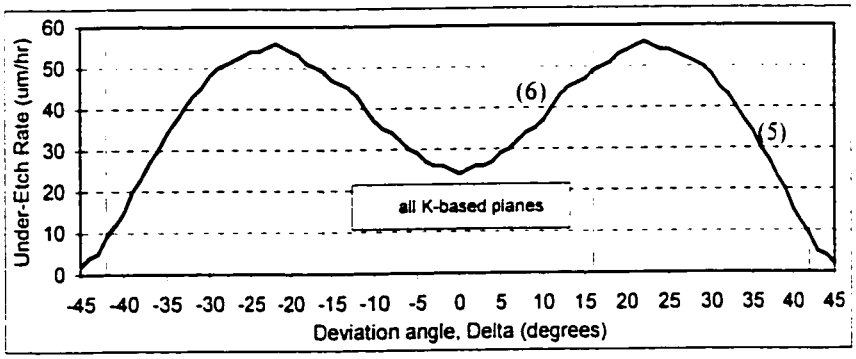

Figure 3-27 : Si{100} 25wt%TMAH - Experimental under-etch rate [8].

Measured experimental facet inclination angles were clearly very close to the ideal inclination angles. Therefore, specified inclination angle in Figure 3-24 and Figure 3-26, correspond to inclination angles of Figure 3-21 and Figure 3-23. The fact that

experimental and theoretical inclination are very close confirms that the planes are indeed defined by PBCs and K-rows.

3.3.2 K-based and P-based etch rate extraction

A more extended way to test the validity of the crystal-feature-based model is to compare etch rates of *all* appearing K-based series with each other (and all P-based series with each other). The crystal-feature-based model would predict that all K-based series should have exactly the same etch rates *provided that all surfaces are etching based only on crystallographic features presented to the etchant*. If this assumption applied, there would be a well-defined etch rate for each K-based plane as a function of the rotation angle θ_k (theta being the most suitable reference to compare K-based planes) . In other words, in the ideal case, the etch rate of a particular family of $\{h\,l\,l\}$ planes should be the same regardless of its actual inclination angle, or the behaviour of its neighbours. Obviously, the same analysis should apply to compare P-based planes $\{h\,h\,l\}$ to each other at given values of theta. To test this hypothesis, several portions of Figure 3-25 (curves (1) to (4) for δ>90°) and Figure 3-27 (curves (5) and (6)), are geometrically transformed and exported to Figure 3-28, (K-based on the right, P-based on the left), for comparison at common values of rotation angle θ. The transformation is achieved as follows: for each facet defined by the angles (δ, α), one calculates the values of θ_p or θ_k, with respect to the nearest {111} plane, using the equations (3), (4), and (7) to (9). One also calculates the etch rate (ER_1) of the top-most facet from the overall, measured under-etch rate (UER_1) and the inclination angle α_1, as depicted in Figure 3-11.

The resulting Figure 3-28 shows the etch rate (not under-etch rate), as a function of θ_p (left side) or θ_k (right side). Any particular value of θ_p or θ_k corresponds to a particular $\{h\,h\,l\}$ or $\{h\,l\,l\}$, respectively. In Figure 3-28, the obtained curves exhibit the same general trends, *but do not coincide exactly with each-other*. One concludes that facets are indeed P-based or K-based but that the crystal-feature-based model neglects some second-order effects. These effects are hypothesized later in Chapter 4 to be due to interactions between adjacent facets. Representative canonical P-based and K-based series curves (solid lines) have been drawn through the experimental data, roughly anticipating the

principles of interaction. The two canonical curves are intended to roughly represent the etch rate variations of infinite-sized P-based and K-based planes, which would be observed if there were no boundary effects.

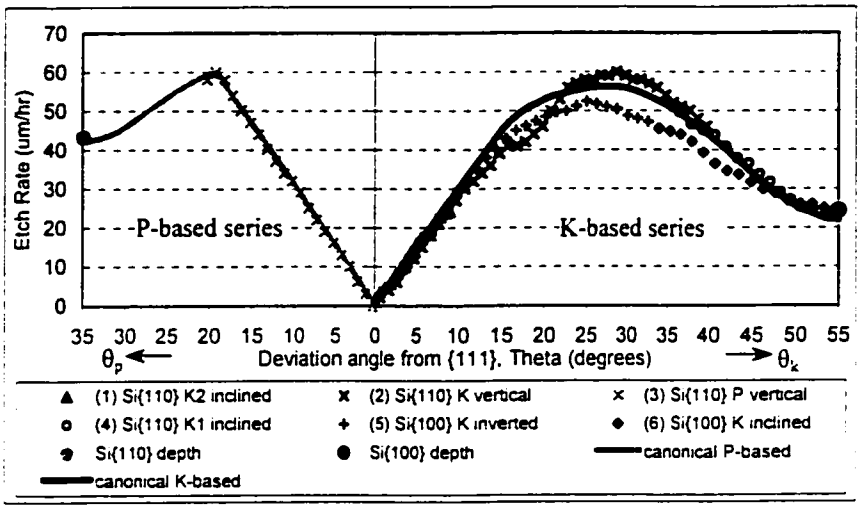

Figure 3-28 : Etch Rate Comparison of P-based and K-based Series in 25wt% TMAH. The drawn series are extracted from the numbered portions of Figure 3-25 and Figure 3-27.

3.3.3 Under-etch rate curve construction

Based on the representative canonical curves drawn in Figure 3-28, one can reverse-construct the under-etch rates which would correspond to the various P-based and K-based series variations as functions of δ. These constructions are made by the inverse geometric transformations of those used to obtain the data in Figure 3-28: from θ_p or θ_k, one calculates the $\{h\ h\ l\}$ or $\{h\ l\ l\}$ Miller Indices, then calculates the corresponding α and δ. The results of the under-etch construction are presented in Figure 3-29 for Si{110} and in Figure 3-30 for Si{100}.

Figure 3-29 and Figure 3-30 help in predicting the actual under-etch rate by following the curve *composed of the slowest under-etching portions*. It can be seen that the shape of the experimental data in Figure 3-25 roughly follows slowest-etching portions of Figure 3-29, while Figure 3-27 roughly follows the K-based series of Figure 3-30. The curves in Figure 3-25 and Figure 3-27 do vary slightly from the predicted under-etch rate in Figure 3-29 and Figure 3-30, respectively. Again the difference is hypothesized to be due to interactions between planes.

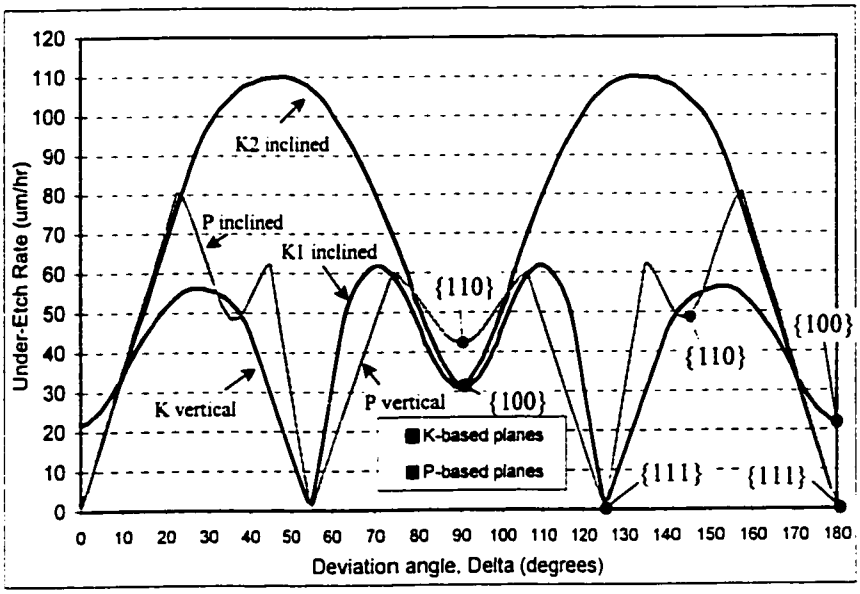

Figure 3-29 : Si{110} 25wt% TMAH : Ideal under-etch rates (construction from etch rate estimations drawn in Figure 3-26 for P-based and K-based planes).

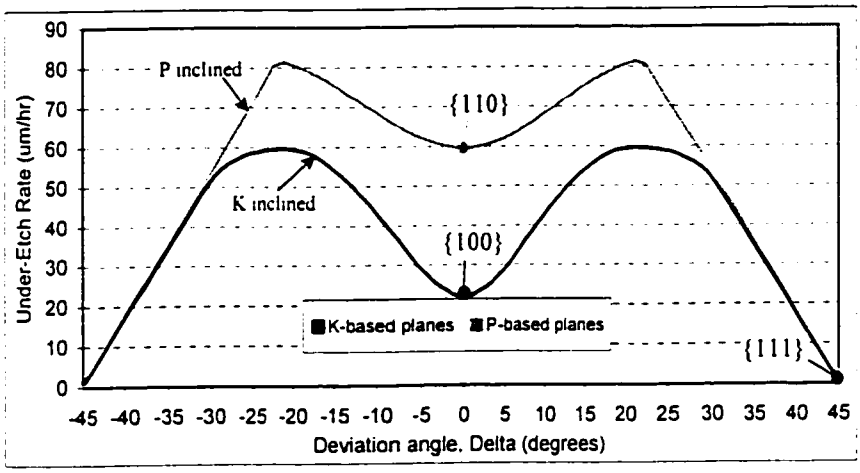

Figure 3-30 : Si{100} 25wt% TMAH : Ideal under-etch rates (construction from etch rate estimations drawn in Figure 3-26 for P-based and K-based planes).

3.3.4 Construction of cross-sectional under-etch profiles

Based on the representative K-based and P-based canonical curves drawn in Figure 3-28, one can calculate the number of facets and their relative sizes as function of the deviation angle δ. The ultimate objective is to predict the shape of an under-etch profile at any mask edge deviation angle.

The inputs required to calculate facet lengths at any deviation angle δ are the under-etch rates (imported from Figure 3-29 and Figure 3-30) and the inclination angles (imported

from Figure 3-21 and Figure 3-23), of all hypothetical K-based or P-based planes that may appear at that deviation angle δ. Note that at any δ in Figure 3-29, for Si{110}, three series are competing to compose the under-etch profile. Non-vertical series actually represent both inclined (α<90°) and inverted planes (α>90°). But, because the model predicts that symmetric inclined and inverted planes do have same etch rates, inverted planes *should not*[3] appear. For this reason, according to the etching model, only 3 inclined facets may constitute an ideal under-etch profile on Si{110}. The same concept applies for Si{100} in Figure 3-30, for which only 2 non-inverted facets (both inclined) may constitute any ideal under-etch profile. Table 3-1 summarizes the equations for the calculation of facet lengths of an under-etch profile. UER_i, α_i, and L_i, correspond respectively to the etch rate, the inclination angle and the length of the i-th facet. "d" refers to the etching depth and is found using Figure 3-28, i.e. for Si{100}, $d=ER(\theta_k=54.74°)$, and for Si{110}, $d=ER(\theta_p=35.26°)$.

Table 3-1 : Facet length calculation of an under-etch profile

	Case 1 one facet	Case 2 two facets	Case 3 two facets	Case 4 three facets
$L_1=$	$\frac{d}{\sin\alpha_1}$	$\frac{\sin\alpha_2\cdot(UER_2-UER_1)}{\sin(\alpha_1-\alpha_2)}$	$\frac{\sin\alpha_3\cdot(UER_3-UER_1)}{\sin(\alpha_1-\alpha_3)}$	$\frac{\sin\alpha_2\cdot(UER_2-UER_1)}{\sin(\alpha_1-\alpha_2)}$
$L_2=$	0	$\frac{d-L_1\cdot\sin\alpha_1}{\sin\alpha_2}$	0	$\frac{\sin\alpha_3\cdot(UER_3-UER_2)}{\sin(\alpha_2-\alpha_3)}$
$L_3=$	0	0	$\frac{d-L_1\cdot\sin\alpha_1}{\sin\alpha_3}$	$\frac{d-L_1\cdot\sin\alpha_1-L_2\cdot\sin\alpha_2}{\sin\alpha_3}$

Once the lengths and inclination angles of each facet is known at any deviation angle δ, under-etching profiles may be easily drawn (as XY plots). The results are presented in Figure 3-31 and Figure 3-33, showing the evolution of the under-etching profiles for Si{110}and Si{100}, respectively, as a function of mask edge deviation. For more clarity, Figure 3-29-(a) shows an example of a cross-section of a single spoke involving

[3] In reality they do appear, (see section 6.1.2.c later in this thesis), but ideally they should not, so there are only three relevant facets for these *ideal* under-etch profiles.

two facets. All cross-sections are drawn with a scale of 10um/division (vertically or horizontally).

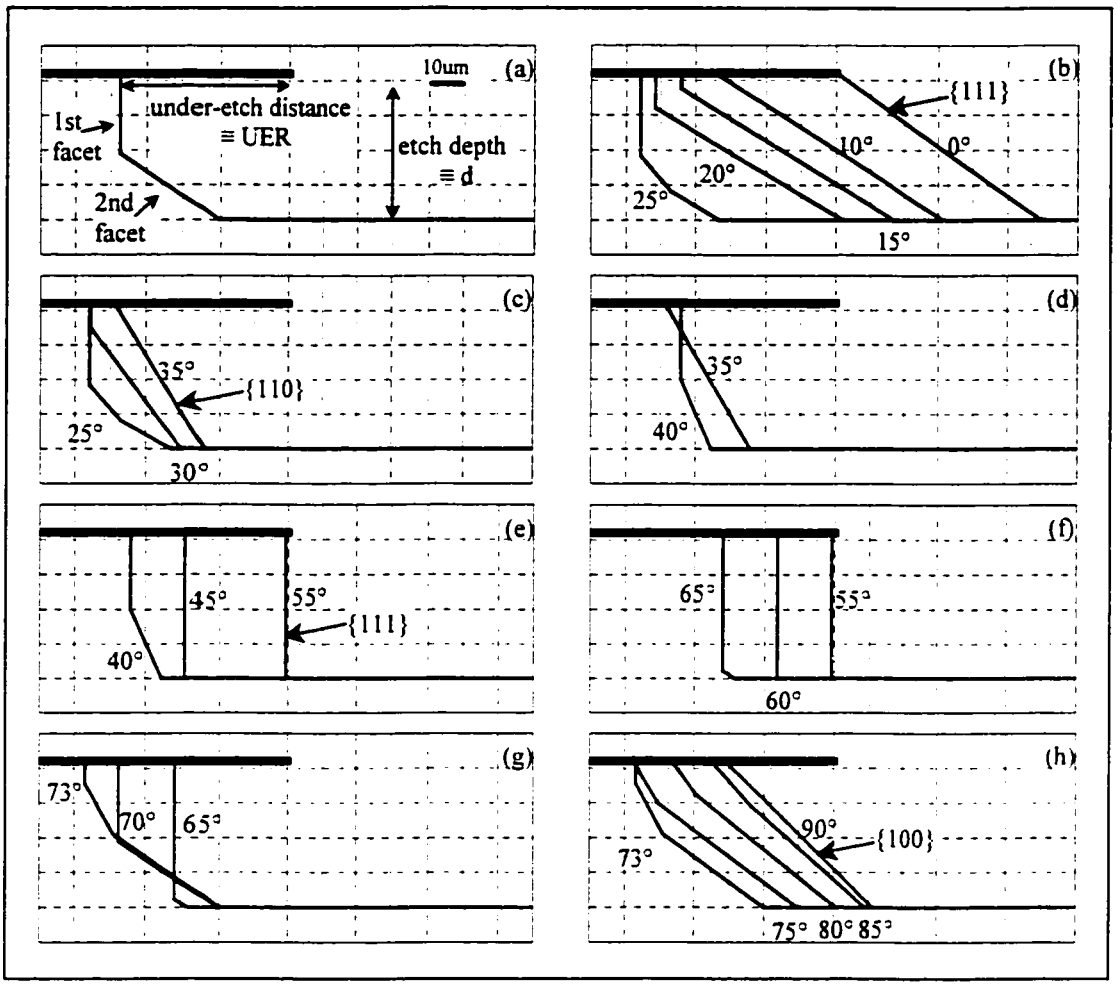

Figure 3-31 : Evolution of under-etching profiles on Si{110} for deviation angles ranging from δ=0° to δ=90°: (a) example of under-etch profile construction showing main notations and etch distances. (b) to (h) superimposed under-etch profiles for chosen deviation angles δ emphasizing important variations such as inclination angles variations or emergence of planes.

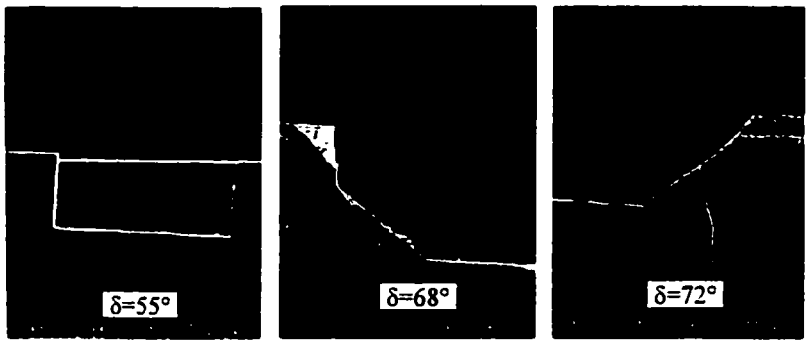

Figure 3-32 : Si{110} 25wt% TMAH : SEM pictures of cross-sections at deviation angles of δ=55°, δ=68°, and δ=72° (left to right) [8].

Figures 3-29 (b) to (h) and Figure 3-33 show the superposition of ideally reconstructed cross-sections of single spokes at particular deviation angles δ. These profiles predicted by the model may then be compared with experiment. Figure 3-32 shows SEM pictures of cross-sections at deviation angles of δ=55°, δ=68°, and δ=72° [8]. Comparison of Figure 3-32 with corresponding profiles in Figure 3-31 shows good agreement of the model at these particular deviation angles. However, on Si{100}, comparing experimental profiles of Figure 3-34 with corresponding ideal profiles in Figure 3-33 reveals important anomalies of the model, such as the absence of inclined P-based series for deviation angles from δ=0° to δ=20°.

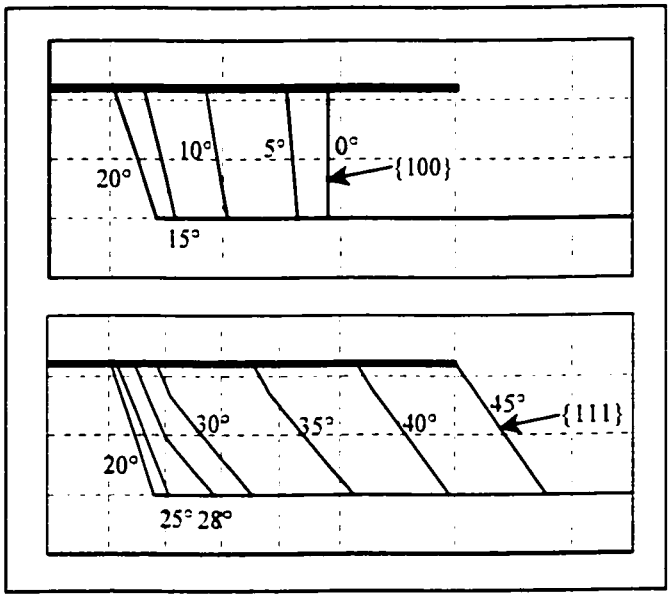

Figure 3-33 : Under-etching profiles evolution on Si{100} for deviation angles ranging from δ=0° to δ=20° on (a) and from δ=20° to δ=45° on (b).

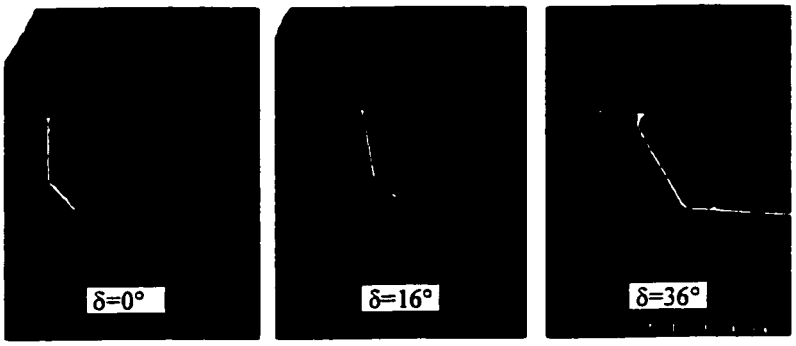

Figure 3-34 : Si{100} 25wt% TMAH : SEM pictures of cross-sections at deviation angles of δ=0°, δ=16°, and δ=36° (left to right) [8].

3.4 Model applicability

A good model of anisotropic under-etching should not only identify facets after measurement of their relative inclination angles, but it should also predict most characteristics of an under-etch profile such as the number of appearing facets, the inclination angle of each facet, and the size of facets.

The crystal-feature-based model detailed in the previous section approaches the second, more powerful type of model. Below is a summary of the main advantages and anomalies of the model.

Advantages of the model

1) Under-etching complexity in concave configurations is simplified to the study of K-based and P-based planes, (i.e. the study of general {hkl} planes etch rates is shown to be less important or not necessary for the under-etch situation).
2) For any given mask-edge deviation angle, inclination angles of the facets that may appear are identified using Figure 3-21 for Si{100}, and Figure 3-23 for Si{110}.
3) Under-etch rate curves and cross-sectional profiles are explained and may be approximately predicted.

Anomalies of the model

1) Inverted planes are not supported by the model.
2) Roughness issues are not covered.
3) There are still some important discrepancies of the model when comparing ideal reconstructions of under-etch curves and cross-sectional profiles with experiment.

3.5 Contributions

Building on the foundation of previous work by A. Pandy et al [8], where the step-based model was introduced and the theoretical dependence of the rotation angle θ on the deviation angle δ was developed, for P-based and K-based planes for both Si{100} and Si{110}, Chapter 3 further develops and presents the crystal-feature-based model,

particularly tailored to support and assist the experimental study of Si{100} and Si{110}. *in combination*:

- A method is developed to analyze typical under-etch data (under-etch rate and detailed facet inclination angles), to estimate a canonical crystal-feature-based curve for a given etchant at a given concentration.
- Based on the canonical curve, a model is developed to predict the details of the under-etch profile (relative sizes of the facet sizes), as a function of mask-edge deviation angle.

4 Boundary Effects : Model Development and simulations

The etching model of P-based and K-based planes presented in Chapter 3 is unable to explain variations in under-etch rate for surfaces having identical crystal features. This chapter presents further analysis, to serve as foundation for the hypothesis of interaction between facets that would be responsible for the anomalous etch rate variations. The analysis is organized as follows:

- in Section 4.1, the silicon crystal geometry is studied with a focus on how steps on adjacent facets could interact at the junction between the facets.
- in Sections 4.2 and 4.3, results of etch simulations are presented to support the interaction hypothesis. The etching simulations are the fruit of a collaboration with graduate students in the form of projects to fulfill the requirements for the course ELEC 6251, in the Department of Electrical and Computer Engineering at Concordia University [37].

4.1 PBCs and K-rows Orientation and Interaction

Let us assume that two facets of an under-etched surface can interact at the boundary between them. If the etching of each (independent) facet were governed by zipping of PBCs or K-rows, then the orientation of these chains would be of fundamental importance. In this section are presented some geometric parameters that may affect the interaction between chains at facet junctions: the orientation of chains on facets (denoted γ), the direction of movement of steps on facets, and the angle of interaction between chains (denoted ψ).

4.1.1 Orientation of chains on facets: (γ)

Figure 4-1 shows an example of two adjacent facets on which steps (zipping chains) are drawn. The angle γ of a facet is defined to be the angle that its chains make with a reference line (which is perpendicular to the junction between the two facets). For

vertical P-based and K-based facets that appear on Si{110}, PBCs or K-rows are also vertical, so γ is equal to zero: $\gamma_{Si\{110\}\_vertical\_plane} = 0$.

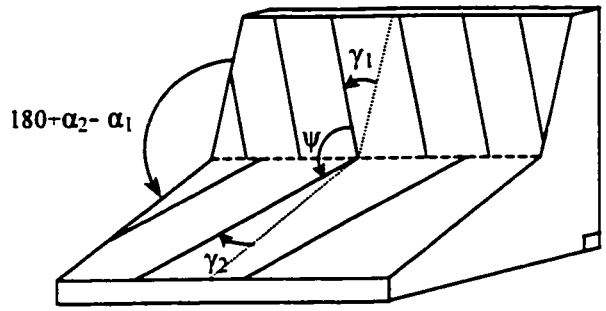

Figure 4-1 : Various angles defining the orientation of PBCs and K-rows.

Actually, all PBCs or K-rows are aligned with a <110> direction, and <110> is also the axis of rotation for variations in θ (see Section 3.2.3 in the previous Chapter). For the calculation of γ as described in Appendix II, one must know the exact vector of the <110>-family with which the chains of a given plane are aligned.

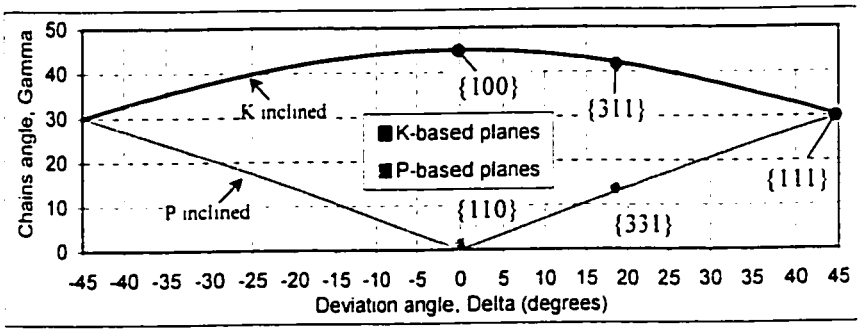

Figure 4-2 : Chains angle (γ) versus mask edge deviation angle (δ) for Si{100}.

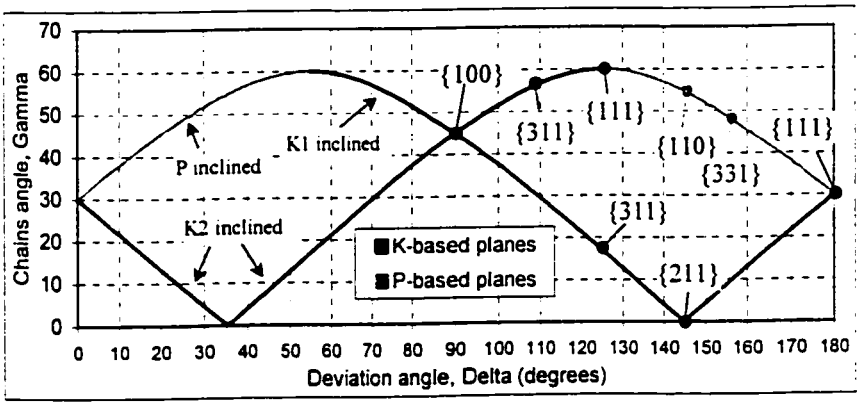

Figure 4-3 : Chains angle (γ) versus mask edge deviation angle (δ) for non vertical planes on Si{110}.

Figure 4-2 and Figure 4-3 summarize the variation of the angle γ with respect to the mask edge deviation angle δ, on Si{100} and Si{110} respectively, for the various P-based and K-based planes. Vertical planes on Si{110} are not shown since $\gamma_{Si\{110\}\_vertical\_plane} = 0$.

Notice the interesting case (illustrated in Figure 4-4) on Si{110} at δ=35.26° (or δ=144.74°) where the K-vertical plane as well as the K2-inclined planes are both in the {211}-family with vertically-aligned K-rows (γ=0°). A more detailed crystallographic reconstruction of this interesting situation is presented later in this Chapter in Figure 4-13. At 25wt%TMAH, the middle (101) in Figure 4-4 facet does appear, but by changing concentration (or perhaps also by using additives) it is believed that its etch rate is increased and therefore made not to appear. In that case, then the K-vertical and the K2-incline facet would be contiguous, and might be expected to strongly interact (since they have the same crystal features, and same step spacing).

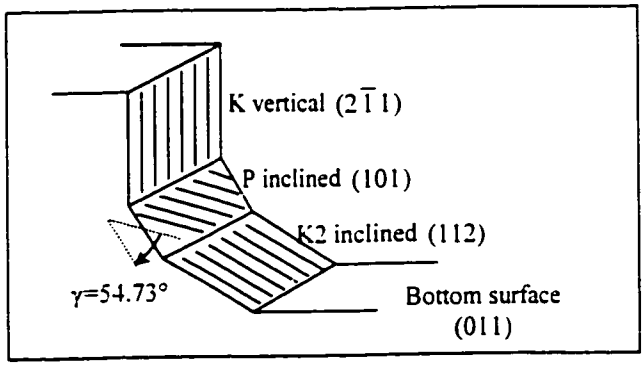

Figure 4-4 : Chains orientation on Si{110} at δ=35.26°.

4.1.2 Direction of movement of steps on facets

P-based planes, as well as K-based planes in close vicinity to {111} planes (small θ angle), are microscopically composed of steps propagating along flat terraces (see Section 2.2.1.2). For other higher rotation angles θ, distinct steps are very difficult to observe and are replaced by roughness features or faceting. However, the fact that P-based and K-based planes are formed during etching suggests that steps are still very likely to play a role. It is thus assumed in this section that all P-based and K-based planes are formed by steps that propagate along flat {111} terraces. It is intended here to record and summarize the direction of propagation of steps on the facets, as illustrated in Figure 4-5.

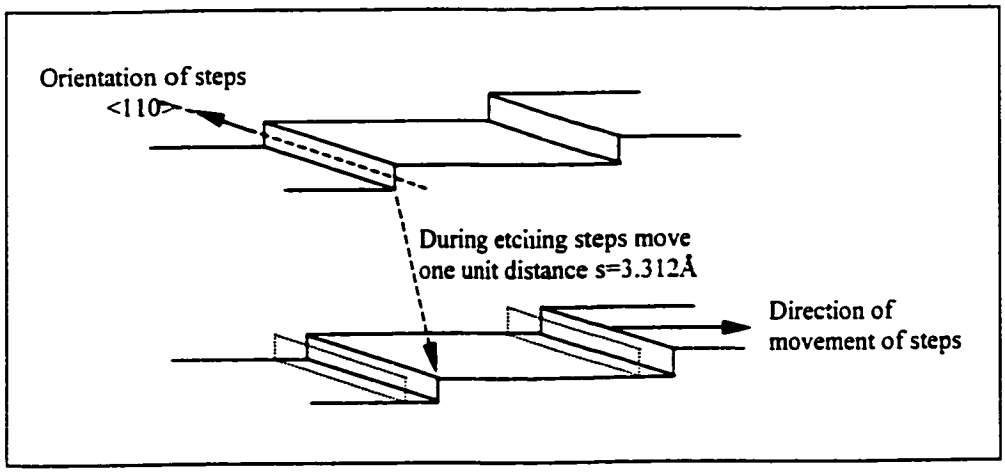

Figure 4-5 : Direction of movement of steps propagating along ideal {111} flat terraces.

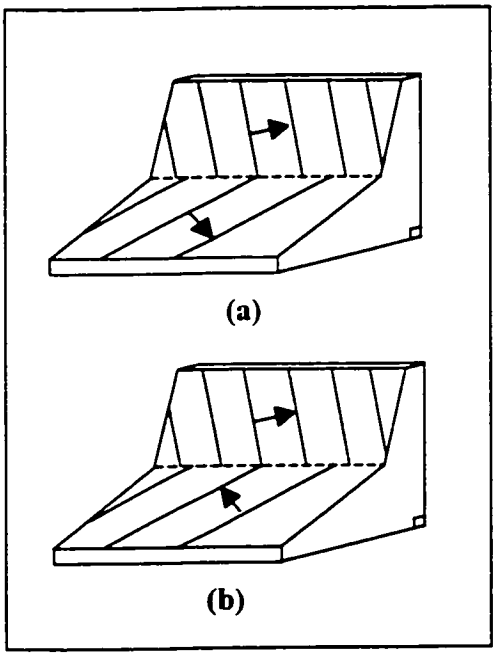

Figure 4-6 : Illustration of step movement on two adjacent facets: (a) movement in the same direction, (b) movement in opposite directions.

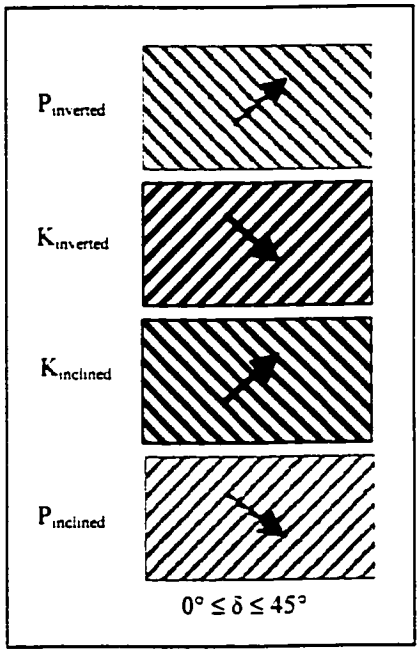

Figure 4-7 : Orientation and direction of propagation of PBCs or K-rows steps on Si{100}.

Consider two adjacent facets having different inclination angles, as illustrated in Figure 4-1. The angle (γ) describes the orientation of steps on each facet. Note that one also needs the direction of propagation of steps since steps may propagate in the same direction (case (a) in Figure 4-6) or propagate in opposite directions (case (b) in Figure 4-6). Indeed it is hypothesized in this work that interactions between adjacent facets would be of different nature for the two possible cases (a) and (b).

Using a Miller cube (represented in Figure 3-4), the direction of propagation of steps for P-based and K-based planes can be studied. The results are presented in Figure 4-7 for Si{100} and in Figure 4-8 for Si{110}. The side of inclination of the lines symbolizes the orientation of the steps (i.e. leaning to the left or leaning to the right) as viewed from the front of the facet. An examination of the step orientation and direction of step propagation for the two types of silicon wafers leads to several general observations:

- Steps on inclined and inverted planes (symmetric with respect to a horizontal surface, ex: P-inclined and P-inverted) always propagate in the same direction.
- For Si{100}, all P-based or K-based planes propagate in the same direction.
- For Si{110}, for $54.74° \leq \delta \leq 90°$, all planes propagate in the same direction.
- On Si{110}, as δ varies from ($\delta \leq 35.26°$) to ($\delta \geq 35.26°$), the direction of propagation of P-based planes is reversed, while the orientation of K2 planes goes from a angle γ inclined to the right to an angle γ inclined to the left.

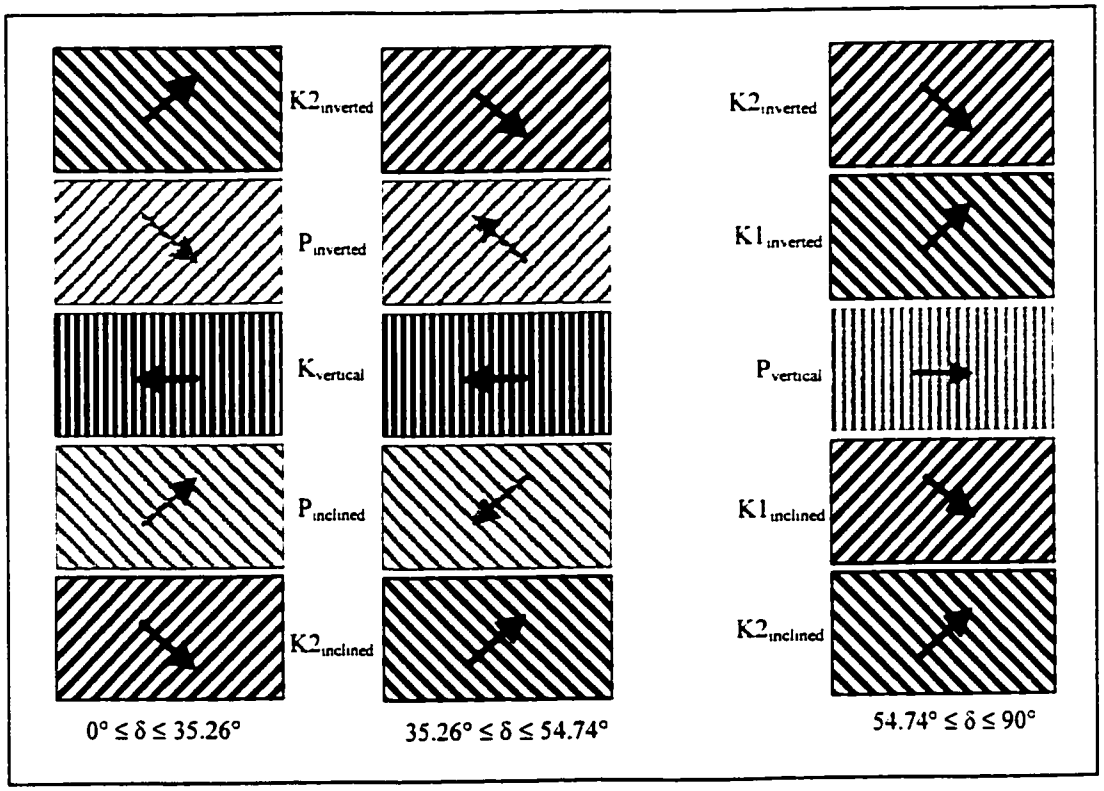

Figure 4-8 : Orientation and direction of propagation of PBCs or K-rows steps on Si{110}.

4.1.3 Angle of interaction between chains: (ψ)

We define the angle (ψ) as a measure of the angle between interacting chains of adjacent facets. (ψ) is shown in Figure 4-1 and is not to be confused with the angle between the two facets which is $(180+\alpha_2-\alpha_1)$, where α_1 and α_2 are the inclination angles of the first and second facet, respectively. Table 4-1 and Table 4-2 summarize the interaction angles (ψ) for Si{100} and Si{110}, respectively. Because chains are aligned with a <110>-family direction, the angles of interaction (ψ) between chains must all be 60°, 90°, or 120°.

Table 4-1: Angles of interaction (ψ) between chains for Si{100}. $0 \le \delta \le 45°$

	K bottom		
P inclined	120/120	P inclined	
K inclined	120/60	120	K inclined
K inverted	-	120	90
P inverted	-	90	120

Notice that for Si{100}, the bottom surface (chosen for this example to be the (001) specific plane) is composed of K-rows aligned along the $[1\,\bar{1}\,0]$ direction for the first atomic mono-layer, and by K-rows aligned along the [110] direction (perpendicular to the $[1\,\bar{1}\,0]$), for the next layer of atoms, as illustrated in Figure 4-9. Consequently the angles of interaction (ψ) between the (001) bottom surface and the K-inclined series (Figure 4-9-(a)) alternate between the values ψ=60° and ψ=120°, as etching of atomic layers proceeds. However, in Figure 4-9-(b)), one sees that if the inclined plane is P-inclined instead of K-inclined, both angles of interaction are 120° (ψ=120° for both orientations of the bottom (001) surface.) The two cells in Table 4-1 denoted (120/60) and (120/120) reflect this singularity.

Table 4-2 : Angles of interaction (ψ) between chains for Si{110}.

	P bottom			
K2 inclined	120	K2 inclined		
P inclined	60	120	P inclined	
K vertical	90	120	120	K vertical
P inverted	-	90	60	120
K2 inverted	-	60	90	120

$0 \le \delta \le 54.74°$

	P bottom			
K2 inclined	120	K2 inclined		
K1 inclined	120	90	K1 inclined	
P vertical	90	120	120	P vertical
K1 inverted	-	120	60	120
K2 inverted	-	60	120	120

$54.74° \le \delta \le 90°$

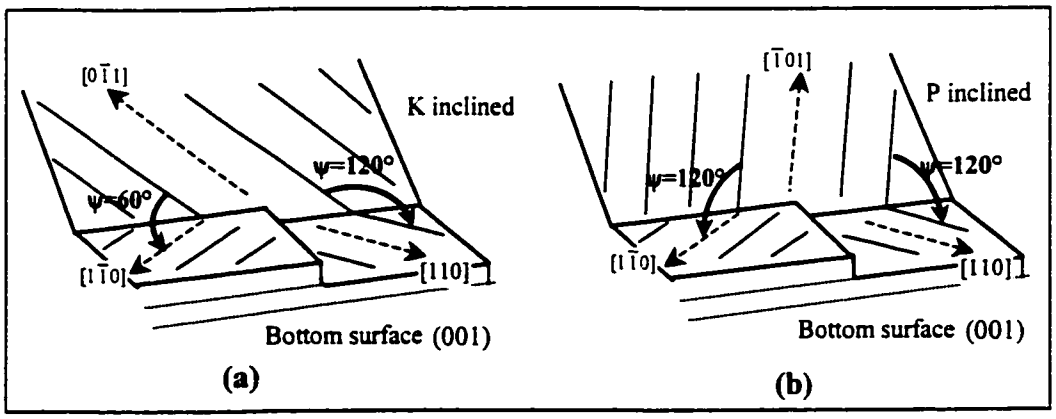

Figure 4-9 : Si{100} interaction angles ψ between the bottom surface and: (a) the $K_{inclined}$, , (b) the $P_{inclined}$. The various ψ angles are due to the fact that K-rows on the bottom surface of Si{100} are alternatively oriented in the [1$\bar{1}$0] direction and in the [110] direction, as atomic mono-layers are etched.

An examination of Table 4-1 and Table 4-2 reveals that:

- On Si{100}, inclined planes and their symmetrically inverted planes interact through chains having an angle ψ =90°, while on Si{110} the chains have an angle ψ =60°.
- All inclined or vertical planes intersect by chains making an angle ψ=120°, except for K1-inclined and K2-inclined on Si{110}for 54.74°≤δ≤ 90° whose chains intersect with an angle ψ =90°.
- There are no cases of ψ =120° for the intersection of two P-based planes.
- The interaction angle between a P-based plane and a K-based plane is never ψ=60°.

Since under-etched facets are composed of zipping chains (steps), it is assumed that each facet may interact with its adjacent facets by means of zipping propagation of PBCs or K-rows across the junctions between facets. As a result, the study of interaction between facets should include the study of the connections between zipping chains, that is between two PBCs (denoted P-P), between two K-rows (denoted K-K), and between a PBC and a K-row (denoted P-K or K-P).

Angles of interaction ψ are limited to 60°, 90°, or 120°. Consequently there are 9 possible connections between chains (3 possible angles (ψ) times 3 types of connections (P-P, K-K, P-K)). The study of orientation of chains for Si{100} (Table 4-1) and for Si{110} (Table 4-2) demonstrated that the connection P-P with ψ =120° and the connection P-K with ψ=60° do not occur for these two silicon wafer orientations . Therefore there are 7

types of connections which can occur between chains: between two K-based planes (K-K-60°, K-K-90°, and K-K-120°), between two P-based planes (P-P-60°, P-P-90°), and between a P-based plane and a K-based plane (P-K-90°, P-K-120). Figure 4-10 shows how the chains are connected for these seven possibilities.

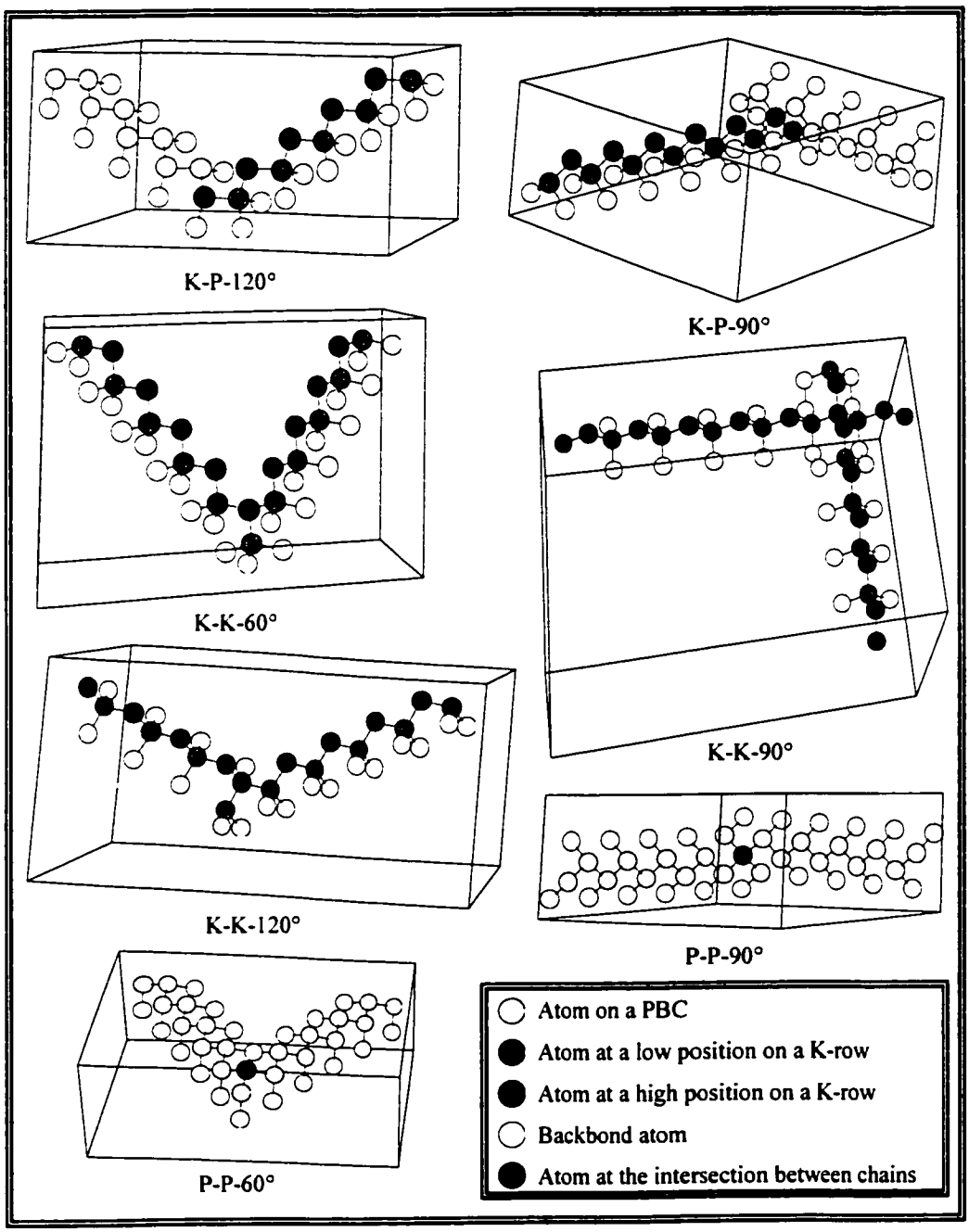

Figure 4-10 :The seven possible connections between Chains (PBCs or K-rows).

4.1.4 Examples of crystallographic reconstruction of interacting facets

The following crystallographic reconstructions (made using Carine Crytallography software) help visualizing microscopic morphologies of under-etch facets. Surface atoms are highlighted for more clarity of plane crystal features (bulk atoms are not shown). Side views are presented to illustrate inclination angles of facets whereas front views give more information on the orientation of chains (PBCs or K-rows). The four examples that were chosen show the K-K-90° and the K-P-120° connections because these are the connections that are found to be interesting after analysis of experimental data (see Chapter 7). PBCs and K-rows are represented using the legend of Figure 4-10. The orientation of the chains on facets as well as the type of connection is clarified on the right side of the figures.

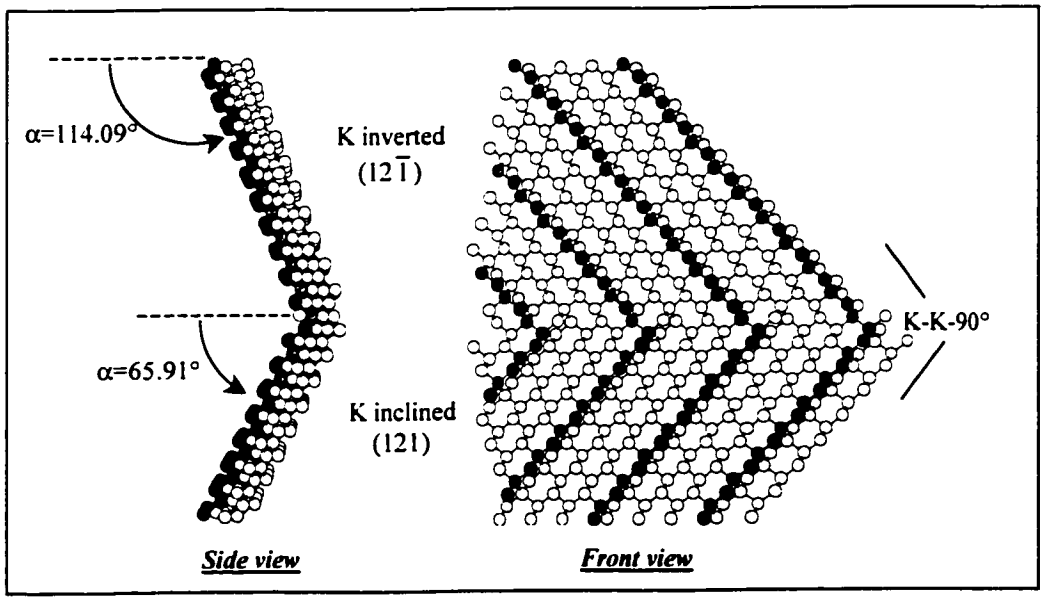

Figure 4-11 : Si{100}, δ=26.57°, ψ=90°

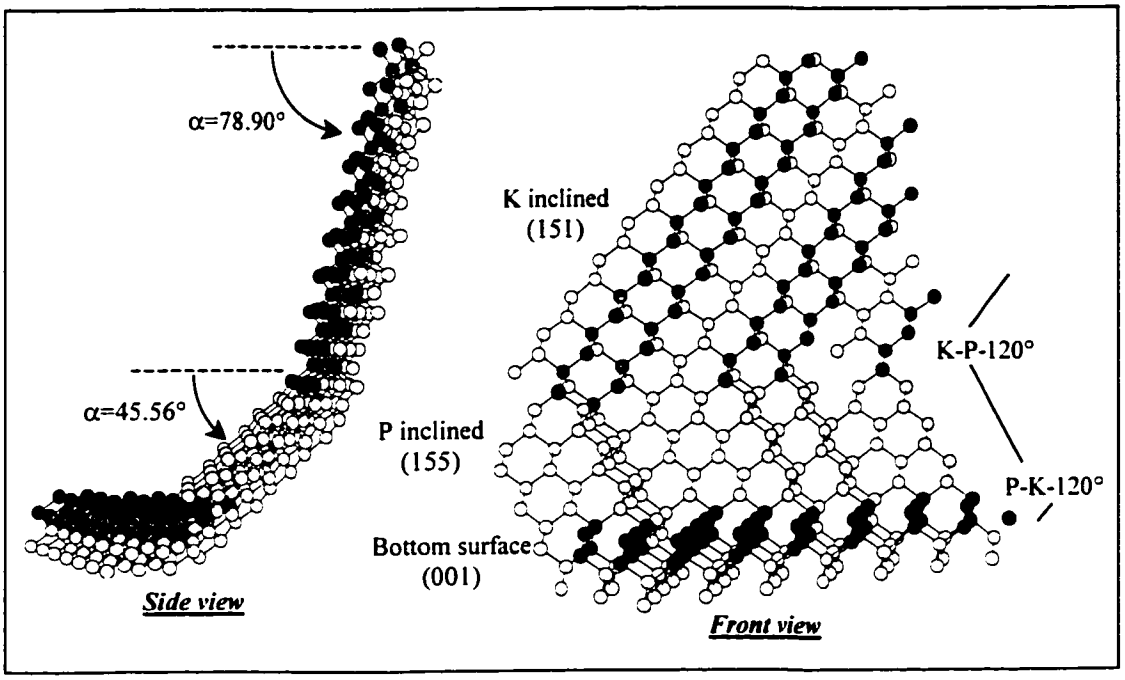

Figure 4-12 : Si{100}, δ=11.31°, ψ=120°

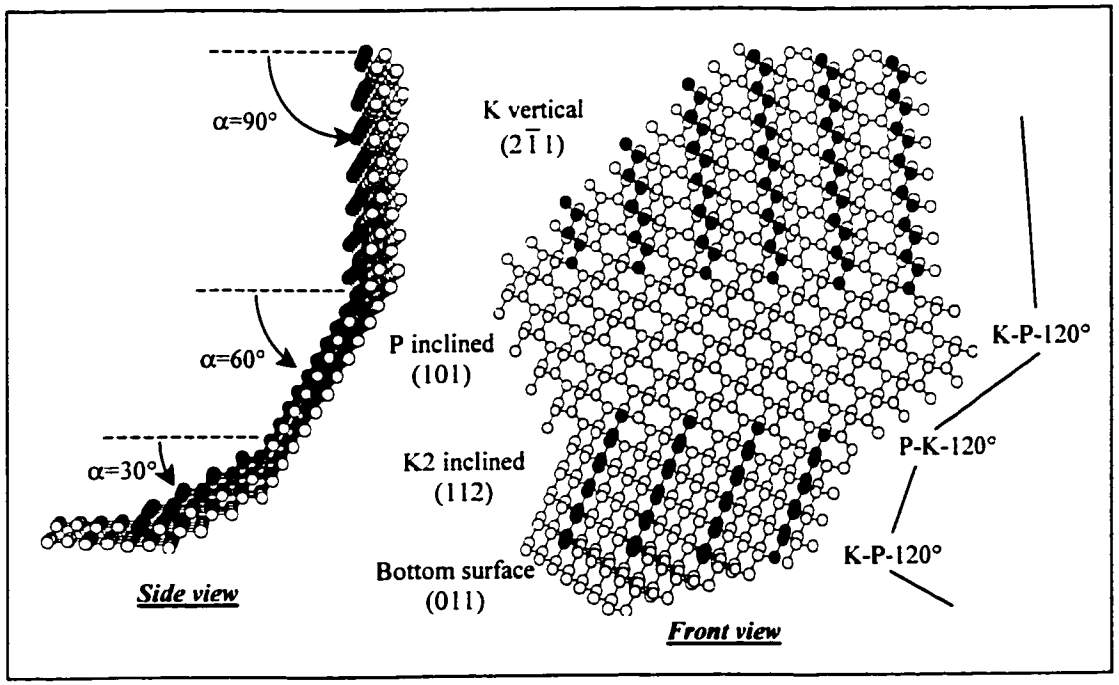

Figure 4-13 : Si{110}, δ=35.26°, ψ=120°

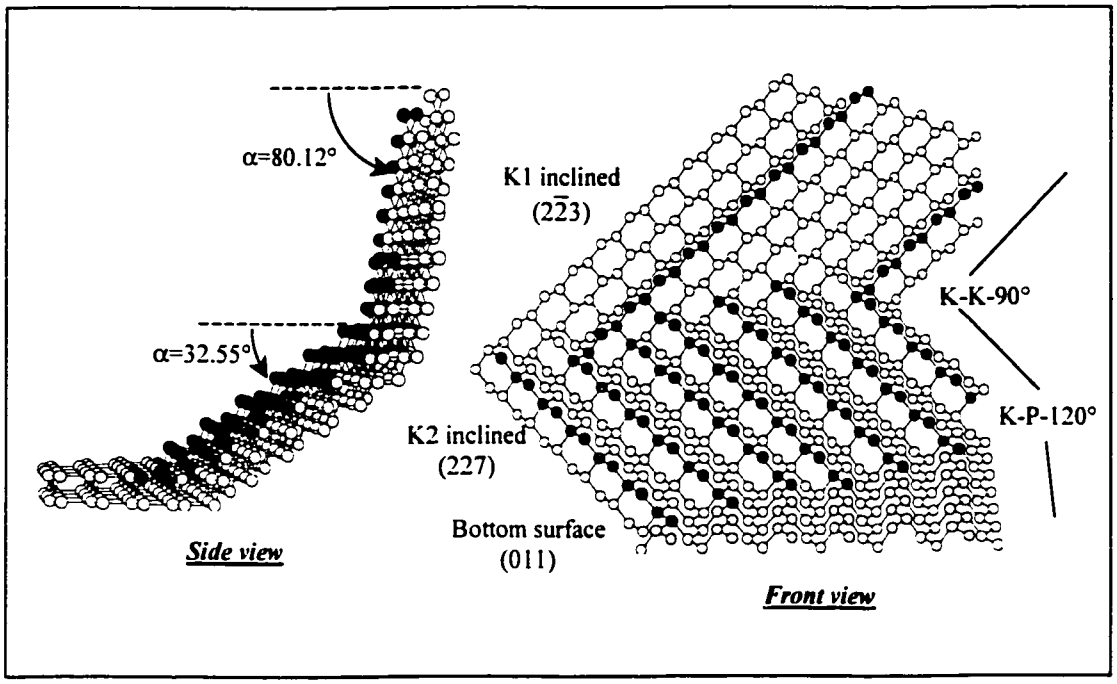

Figure 4-14 : Si{110}, δ=60.51°

4.2 PBC etch simulation

The following simulation[4] is designed to estimate the impact of boundary conditions on the etching rate of facets. For purposes of simplicity, rather than simulating the etching of a whole facet, a single Periodic Bond Chain (PBC), illustrated in Figure 3-16, is considered. It is believed that the simulated results of etching of a single PBC, and how it is affected by boundary effects, can be extrapolated to help to interpret variations in etch rates of facets.

4.2.1 Simulation principles

Figure 4-15 illustrates the etching mechanism of a single finite-sized PBC. The identified parameters that affect the etching time of a single PBC are: the length of the chain (L), the removal probability of the central atoms (P_n), and the removal probability of the atoms at boundaries (P_b).

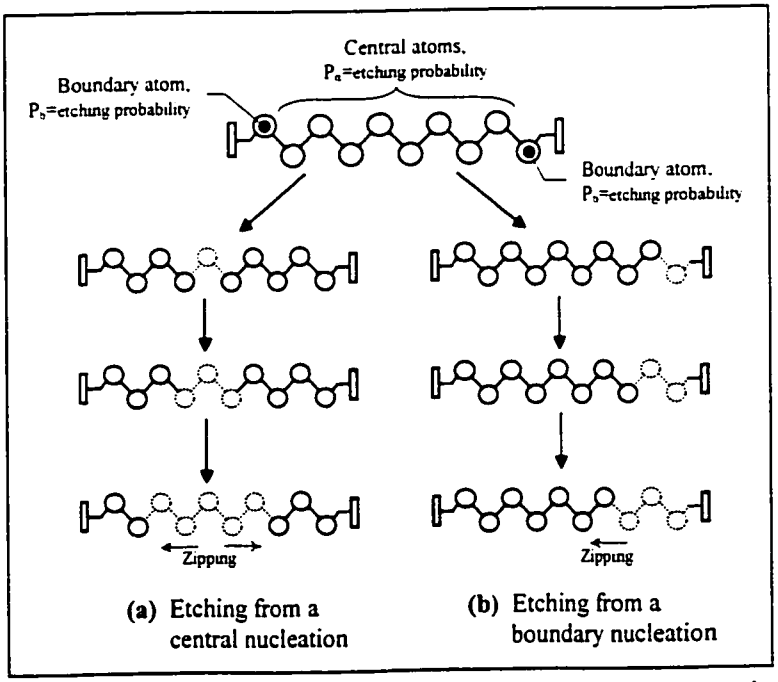

Figure 4-15 : Illustration of the etching mechanism of a finite size PBC (top view).

[4] The results of these simulations were verified in part by a course project in ELEC6251, in May 2001.

The zipping process is simulated by applying a removal probability that is certain, $P_z=1$, for any atoms whose neighbor has just been etched in the previous time step in the simulation. The left part (a) of Figure 4-15 illustrates an etching propagation originated from a nucleation of a central atom, while the right part (b) shows an etching spread from a boundary. Actually, a combination of both processes is the most likely probable.

A Matlab simulation was carried out to study the effects of the parameters (L), (P_n), and (P_b) on the etching time of a single PBC. Table 4-3 summarizes, for each case (a) to (g), the values that were set prior to simulation for the removal probabilities of the atoms on the PBC. These values were inspired from the Monte-Carlo simulation study of Hines et *al* [29] presented on Table 2-1.

Table 4-3 : Removal probabilities for the simulations. $P_z=1$.

	(a)	(b)	(c)	(d)	(e)	(f)	(g)
Pn	0,001	0,005	0,0005	0,001	0,001	0,001	0,001
Pb	0,1	0,1	0,1	0	0,005	0,01	1

4.2.2 Simulation results

The question of whether boundaries conditions affect the etching rate of a single PBC (and consequently affect the etching rate of a facet) was studied. Figure 4-16 shows the necessary time to completely etch a single PBC depending on its starting length (L). The graph is obtained for case (a) of Table 4-3, which corresponds to easily etched atoms at boundaries. The etching time of the PBC is found to vary dramatically for short PBC lengths on the order of few tens of microns.

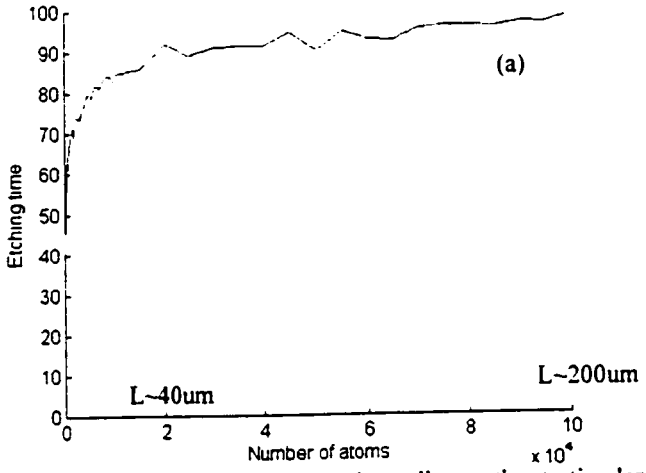

Figure 4-16 : Single PBC etching time of case (a) depending on the starting length (L) of the chain.

The effects of modifying the nucleation probability of central atoms was studied, the results are plotted on Figure 4-17 for the three cases (a), (b) and (c) of Table 4-3. It is observed that the etching time is increased when decreasing the nucleation probability P_n. More attention is to be paid to the fact that boundary conditions have more effects on chains having lower nucleation probabilities (i.e. on (c) rather than on (b) on Figure 4-17). Indeed, this is readily seen by comparing the gradient of the three curves for the same number of atoms (on the X-axis): high gradient means that the etching time of the PBC is very influenced by boundary conditions.

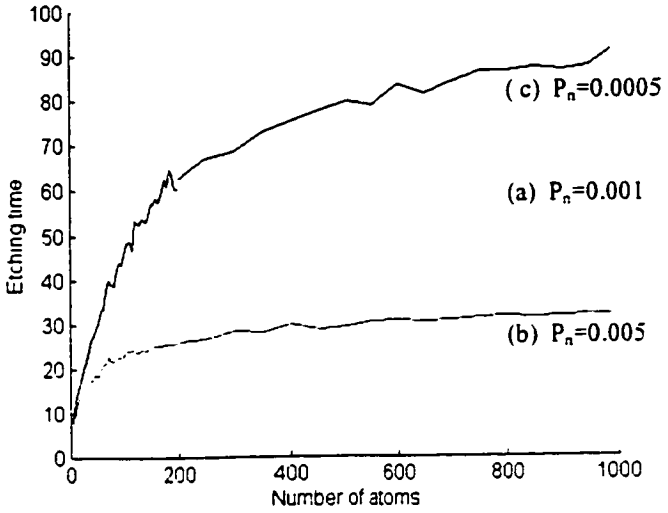

Figure 4-17 : Effects of the nucleation probability (P_n) of center atoms on the etching time of a single PBC.

The results concerning the effects of the removal probability (P_b) of atoms at boundaries on the etching time of a single PBC are presented in Figure 4-18. All curves become coincident for long PBCs (L>10um, not shown here). Figure 4-18 focuses on the differences that appear for short chains (small L). It is found that all simulation possibilities are confined between curves (d) for which P_b=0 and (g) for which P_b=1. Stable atoms at boundaries (example of (d) or (e)) may decrease dramatically the etching rate of a PBC (equivalent to increasing the time).

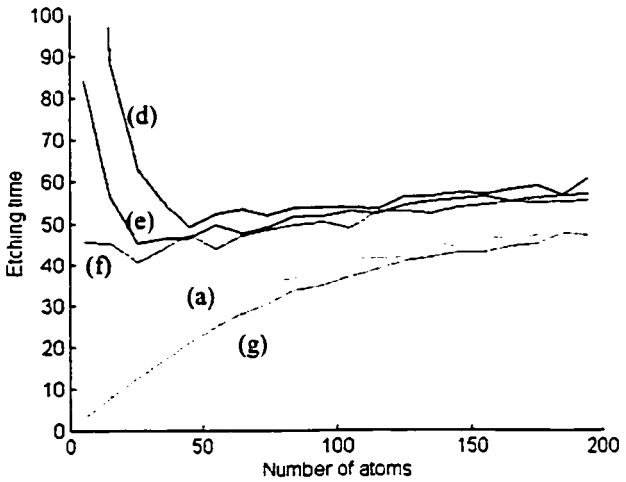

Figure 4-18 : Effects of the nucleation probability (Pb) of the atoms at boundaries on the etching time of a single PBC.

4.2.3 Summary of the etching simulation of a single PBC

- For long PBCs (portion 1 on Figure 4-19), the etching rate does not depend on the chain length (L), but depends only on the probability of nucleation of central atoms.
- For shorter PBCs (few tens of microns), boundary effects are noticeable and increase the etching rate, whatever is the probability of removal of the atoms at boundaries (portion 2 on Figure 4-19).
- For lengths less than a certain critical length (portion 3 on Figure 4-19), boundary conditions may dramatically either accelerate the etching speed of a PBC (easily remove atoms at boundaries) or decrease it (stable atoms at boundaries).

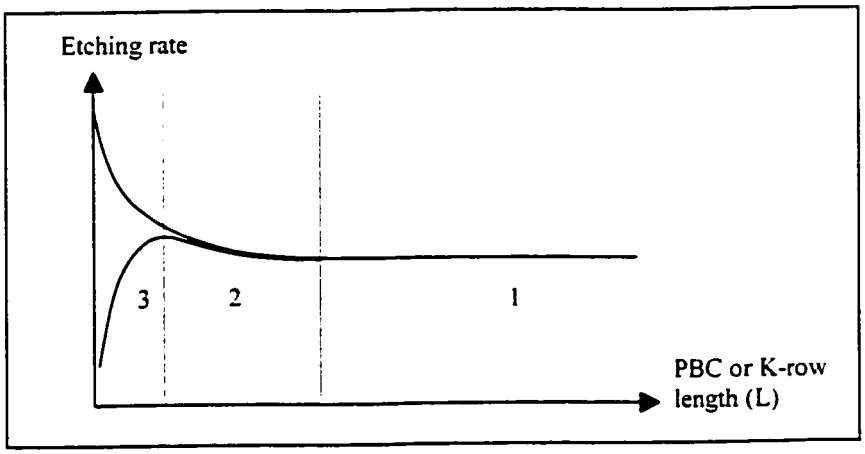

Figure 4-19 : Variation of etching rate versus PBC/K-row length.

Limitations

The simulation of a single PBC (or K-row) was used here to explore the effects of boundary conditions on the etch rate of a P-based (or K-based) facet. We believe that general trends of Figure 4-19 related to the etching rate of a single PBC can also apply for the etching of an entire under-etched facet. However, the positioning of each portion (1, 2, and 3 on Figure 4-19) for the etching of a single PBC may not apply when addressing an entire facet. The main limitation being the fact that during the zipping of a PBC, nucleations of newly exposed atoms are very probable on an underlying PBC. As a result, the overall etch rate of a P-based or K-based facet is not proportional to the speed at which an entire PBC is etched.

4.3 Inverted planes simulation

An inverted plane is defined as having an inclination angle (α_{inv}) greater than 90°. Such a plane can only be the first (top-most) facet of an under-etched surface. In most of these cases, the second facet is found to be a symmetrically-inclined ($\alpha = 180 - \alpha_{inv}$) facet of the same Miller Index family. In this section, we present observations and simulation results[5] to support a theory based on boundaries effects to explain the emergence of inverted facets.

4.3.1 Etch rate of inverted planes

Figure 4-20 depicts a wagon-wheel cross-section showing an inclined facet and its inverted symmetric facet. Etch rates are measured from the mask edge since all planes initially emerge at this position when silicon starts dissolving in TMAH. The analysis in Figure 4-20 demonstrates that inverted planes (providing that they have appeared), etch more slowly than inclined ones. The existence of inverted facets along with their non-inverted inclined partner, clearly shows that the same crystal features, in close proximity to each-other, are etching at different rates. This contradicts the crystal-feature-based etching model (in which the same crystal features are modelled to etch at the same rate).

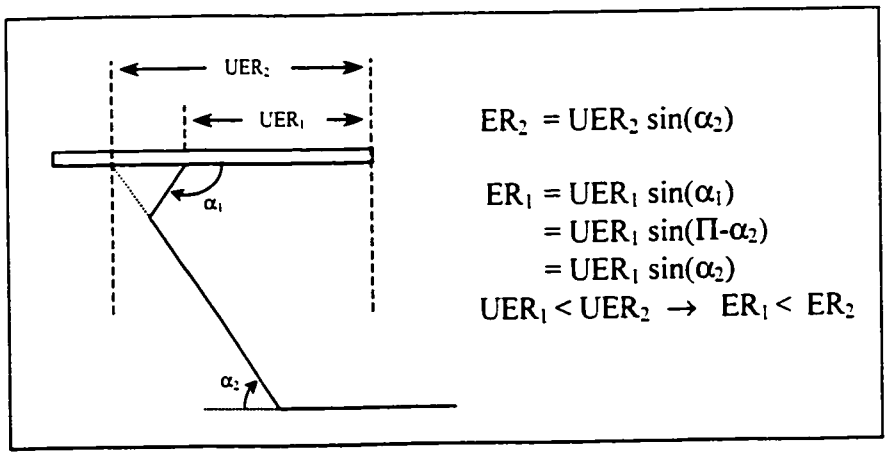

Figure 4-20 : Etch rate comparison between an inverted facet and its symmetrically inclined facet.

[5] The simulations were the fruit of collaboration with two ELEC6251 students who executed the simulations .... [36]

Occasionnaly, SEM micrographs of cross-sections where inverted facets are involved (example of Figure 4-21-(a)) show many small structures at the junction between the top (inverted) facet and the lower (inclined, non-inverted) facet. These small structures illustrated on Figure 4-21-(b) are horizontally roughly symmetric, being made up of pairs of symmetric vertical or near-vertical sub-facets. The presence of such structures may indicate that these are involved in the interaction between adjacent facets.

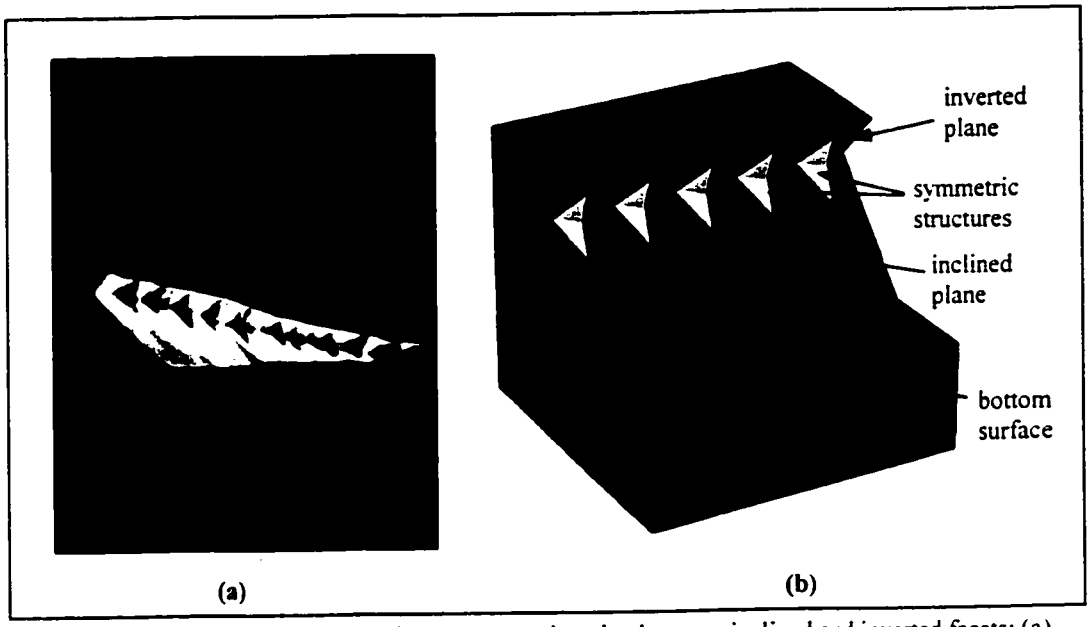

Figure 4-21 : Presence of symmetric structures at junction between inclined and inverted facets: (a) SEM of Si{110} 15wt% δ=25°; (b) typical geometry of structures at junction between facets.

4.3.2 Simulation of inverted facets

C^{++} simulations were carried out to check if boundary effects may be responsible for the appearance of inverted facets, particularly whether atoms at the junction of the inclined and the inverted facets are stopping the propagation of zipping of chains from one facet to the next.

The objective of the simulation is to study the emergence and stability of inverted facets depending on the relative nucleation and zipping probability. Figure 4-22 shows an evolution with time of an under-etch profile involving the growth of an inverted facet. The relative size of the inverted facet compared to the inclined facet is simulated using a column vector or matrix that represents a horizontal projection of both the inclined and the inverted facet (see vector/matrix on Figure 4-22). Actually, if the inclined and the

inverted facets were not perfectly symmetric, the projection solution would not be tolerated. The zipping process (Figure 4-15) as described for the etching simulation of PBCs is applied. But rather than etching a single PBC, inverted planes as well as inclined planes are viewed as superpositions of PBCs. Therefore, during zipping of atoms of the PBC in contact with the etchant, exposed atoms of the next PBC may start nucleate and zip.

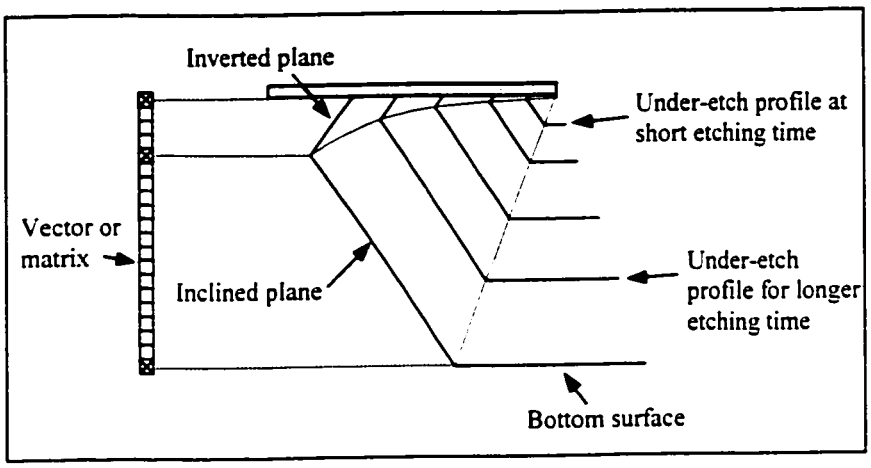

Figure 4-22 : Implementation of the simulation of the emergence and stability of inverted facets.

Figure 4-23 shows an example of an initialized matrix set prior to the etching simulation of the inverted and inclined plane couple. All "1"s in the occupancy matrix symbolize central atoms that are present. When the simulation is launched, which is equivalent to an ongoing etching, "1"s are gradually replaced by zeros. Etching of these atoms starts from random nucleation and proceeds by zipping (described in Figure 4-15).

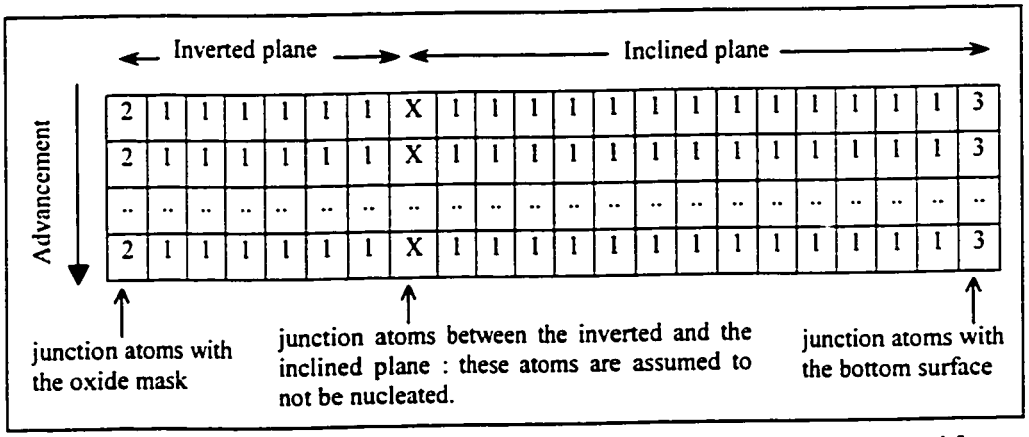

Figure 4-23 : Example of initialized matrix prior to the etching simulation of an inverted facet. "1"s symbolize the presence of a central atom. During etching "1"s are replaced by zeros.

Atoms at junctions are treated specially and are set with independent removal probabilities: P_{b2} for atoms at the junction of the inverted plane with the mask (denoted "2" in Figure 4-23), P_{b3} for atoms at the junction of the inclined plane with the bottom surface (denoted "3"), and P_X for atoms at the junction of the two symmetric facets (denoted "X"). Actually, P_X is set to zero to simulate a blocked boundary that would be responsible for the growth of the inverted facet.

Appendix-III gives more details on how an initialized matrix similar to that of Figure 4-23 is modified during simulation, but the main principles are outlined below:

- A zipping chain that reaches the junction between an inverted facet and the inclined facet stops (blocked boundary). But subsequently, the facet in which chain was zipping is reduced in size, whereas the other facet gets bigger. This is similar to the fact that faster (respectively slower) facets are getting smaller (respectively larger).
- To simulate the etching of the bottom surface, the size of the inclined facet should always become larger after a certain time. This is simulated by adding at each time step an appropriate number of columns at the right side of the matrix of Figure 4-23.

4.3.3 Simulation results

Figure 4-24 shows an example of stabilization of the size ratio (inverted facet / inclined facet) at 0.1 after 450,000 computer time steps (which represents the etching time). In other words, it shows that after some etching time the cross-sectional profile involving the two facets increases in all dimensions but does not change in shape: the inverted facet stabilizes at a size 10 times smaller than the inclined facet.

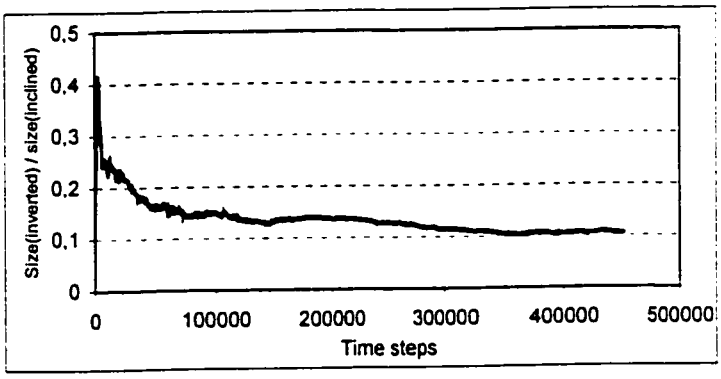

Figure 4-24 : Stablization of the relative size of the inverted facet over the inclined facet. Settings: P_n=0.01, P_{b2}=P_{b3}=0.001, ER(inc)=46um/hr, ER(bottom)=22um/hr.

This supports the following assumption : providing that the two facets (inverted and inclined) are etching independently with atoms at their junction stopping the propagation of chains from one side to the next, inverted facets may grow and reach a constant etch rate that is slower than the etch rate of the inclined facet partners.

The effects of modifying the nucleation probability P_n on the size ratio (inverted plane / inclined plane) was studied. The results are plotted on Figure 4-25. It is observed that the inverted facet relative size increases with decreasing the nucleation probability P_n. Notice that the curve with P_n=0.01 is actually a zoom of Figure 4-24 plotted for time steps up to 40,000. The other curves (P_n=0.001 and P_n=0.0001) in Figure 4-25 are believed to have the same trend as Figure 4-24 that is for long etching time.

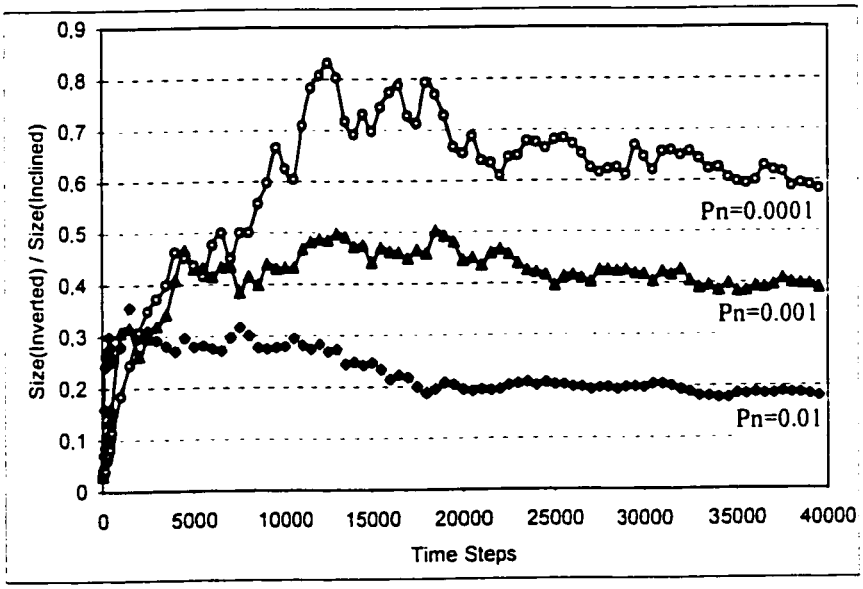

Figure 4-25 : Effects of changing the nucleation probability (P_n) (similar to modifying the etchant concentration). Settings : P_{b2}=P_{b3}=0.001, ER(inc)=46um/hr, ER(bottom)=22um/hr.

A relationship between nucleation probability and etchant concentration is likely to hold. As shown in Figure 2-2, [6], 20wt% TMAH etches faster than 25wt% for most orientations. One then hypothesizes that in the range of 20-25 wt% TMAH, the nucleation probability increases with decreasing TMAH concentration. Accordingly, Figure 4-25 may be considered to simulate the effects of concentration on the appearance

of inverted facets, perhaps suggesting that inverted facets reach bigger sizes for 25wt% than for 20wt%.

Figure 4-26 shows the simulation results for various etch rates of the inclined facet. We are interested here in the size evolution of the inverted facet as the edge of the mask is deviated (angle δ). It is found that the size ratio (inverted plane / inclined plane) decreases when the inclined plane etch rate is decreased. In other words, when the mask edge gets closer to the {111} planes, the inverted facet size decreases.

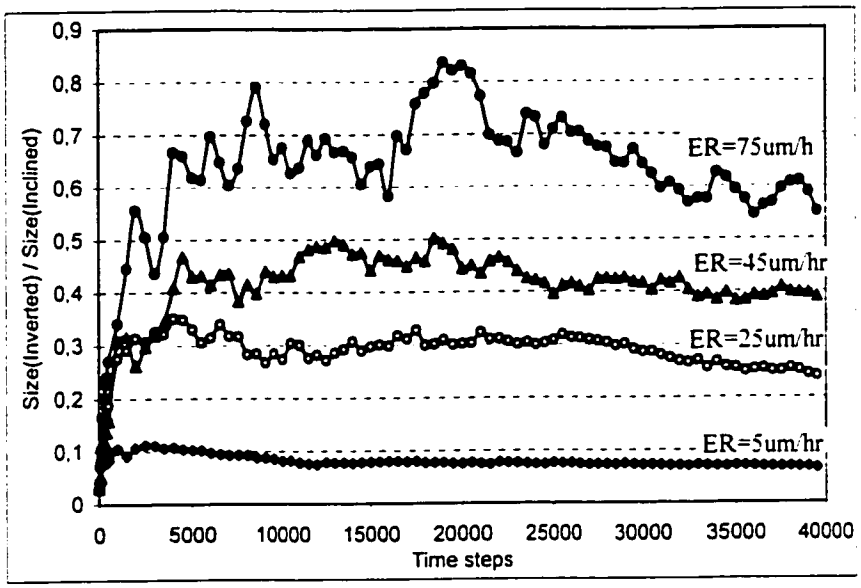

Figure 4-26 : Effects of changing the inclined plane etch rate (similar to changing the positioning of the mask edge). Settings: Pn=Pb=0.001, ER(bottom)=22um/hr.

The effects of atoms nucleation at the junction between the mask and the inverted plane were also studied and plotted in Figure 4-27. The size of the inverted facet is initialized at 250 whereas the size of the inclined facet is initialized at 2500. We observe that the inverted facet disappears with time if the nucleation probability of the atoms at the junction (labelled "2" on Figure 4-23) is bigger than a certain critical P_{b2}. In the plot, that is for P_n= 0.001, the critical P_{b2} seems to be 0.01.

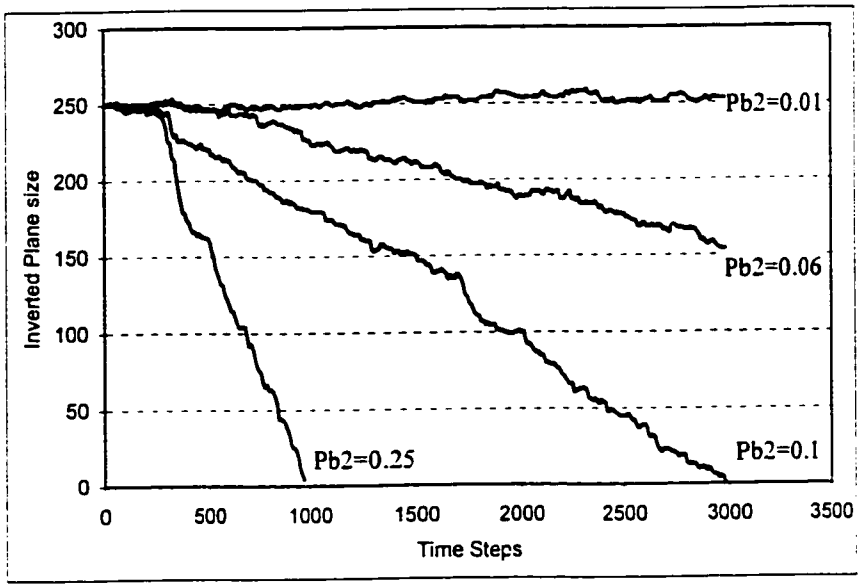

Figure 4-27 : Effects of increasing the removal probability of atoms at the junction between the mask and the inverted. Settings : Initial inverted facet size = 250, Initial inclined facet size = 2500, Pn=Pb3=0.001, ER(inc)=46um/hr, ER(bottom)=22um/hr.

4.3.4 Further analysis

It was demonstrated that the assumption of blocking atoms at the junction between the inverted and the inclined plane is a tangible explanation for the appearance of inverted facets. It was also shown that nucleations originating at the junction between the mask and the inverted plane may prevent the inverted facet from appearing.

Assuming that the two previous conditions (blocked atoms between inclined and inverted plane, and few nucleations from the mask) are satisfied, then an inverted facet should grow and evolve with time. Figure 4-28 illustrates different modes of stability describing the evolution with time of the size of the inverted facet. The first mode is the growth of the inverted facet until its etch rate stabilizes at a constant value, which is the second mode. In the second mode the relative size of the inverted facet compared to the inclined facet is constant. Finally, once the inverted facet reaches a size at which boundary effects are no longer affecting it, its etch rate should start increasing to reach the nominal etch rate corresponding to its Miller index. Once the etch rate of the inverted plane reaches the etch rate of the inclined plane, then the junction between both facet is advancing horizontally as depicted in Figure 4-28. This is the third mode and is identified by the

constant size of the inverted facet, whereas the inclined facet keeps on growing due to the etching of the bottom surface.

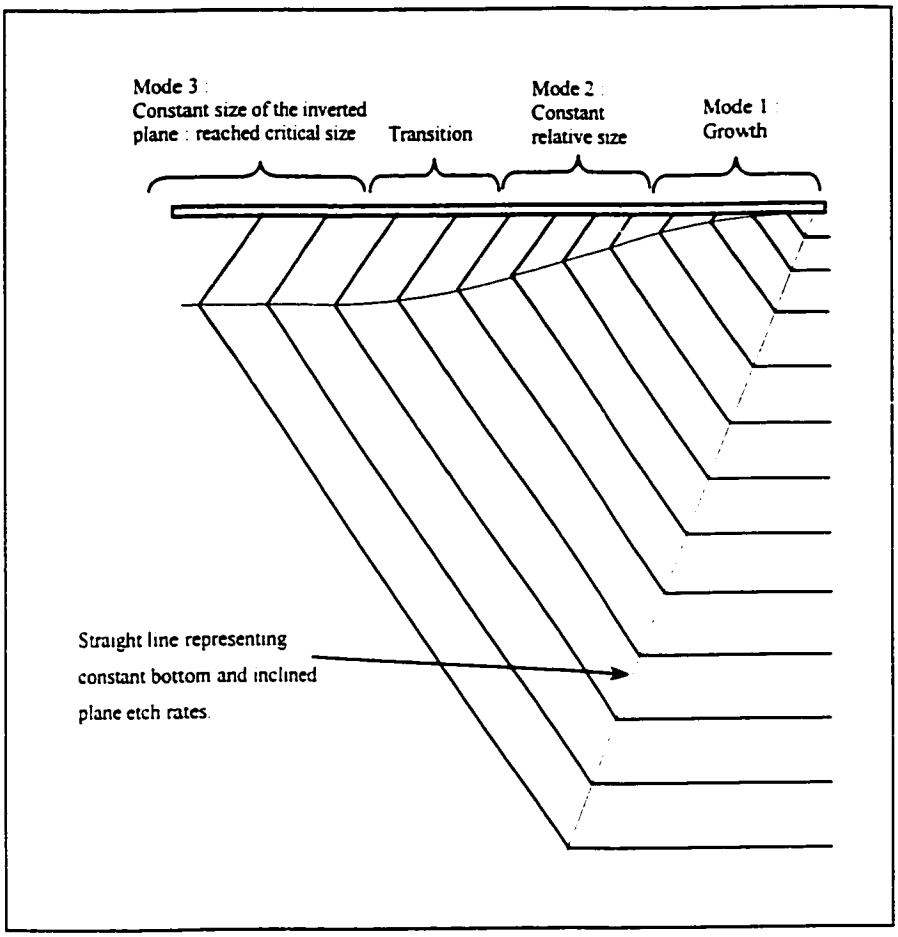

Figure 4-28 : Stability modes for inverted facets.

4.4 Contributions

Chapter 4 further develops crystal-based theoretical concepts to support the hypothesis of interactions between planes. These developments consist of a compendium of possible facet interactions during under-etch experiments on {100} and {110} silicon:

- The angle of orientation (γ) of steps on P-based and K-based facets is defined and visualized.
- The direction of propagation of steps for P-based and K-based facets is studied and schematically presented.

- The angle of interaction (ψ) between chains on adjacent facets is studied and summarized.
- The seven (7) possible connections between chains on adjacent facets are identified and visually diagrammed for Si{100} and Si{110}.
- A Matlab simulation tests the effects of boundaries on the etching of a single chain (PBC or K-row) depending on boundary conditions.
- A rudimentary simulation of inverted planes is developed. The C^{++} implementation of this simulation program is developed by graduate students in partial fulfillment for the course ELEC6251 [37], in collaboration with this author.

5 Experimental procedures

This chapter addresses the practical issues necessary to perform silicon wagon-wheel under-etching experiments. Obtaining reliable and repeatable results is the main focus. The chapter starts by describing two mask layouts designed especially for this thesis research. Then an overview of sample preparation methods and TMAH etching technique is detailed. Finally, the methods of measurement of the features of the resulting structures are described.

5.1 Mask design

Typical wagon-wheel layouts consist of spokes regularly spaced (by one degree per spoke), as was previously illustrated in Figure 3-7. Narrow spacing allows precise measurement of etching variations versus mask-edge deviation angle. However, the relatively close positioning of the spokes limits etching times to about one hour. Reaching higher etching times requires the design of new masks with spokes being more widely spaced.

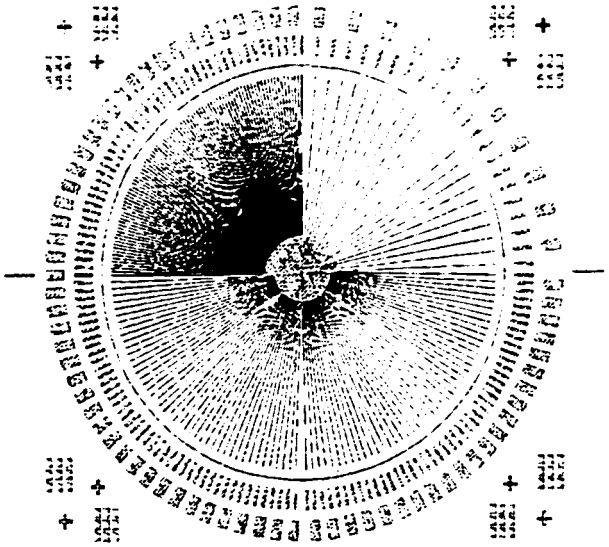

Figure 5-1 : Wagon-wheel mask layout designed for Si{100} etching

Figure 5-1 shows a wagon-wheel mask layout designed especially for etching experiments of Si{100}. The upper left quadrant of the mask consists of one-degree

regularly spaced spokes enabling etching times up to 1 hour. The right upper quadrant is designed for etching experiments lasting up to 6 hours of etching, the spokes being spaced every four degrees.

The bottom part of the Si{100} mask layout in Figure 5-1 is made of two-degrees spaced spokes for etching experiments that could last between one hour and 3 hours. These long radial spokes are 100um wide at their outermost extremity. However, in order to examine the effects of spoke size on under-etching profiles, short rectangular spokes with a width of 300um or 1000um were also designed at the periphery of the mask.

Figure 5-2 shows a wagon-wheel mask layout designed especially for etching experiments on Si{110}. The previously-described areas (on the Si{100} mask layout) dedicated to different etching times were rearranged for the design of the Si{110} mask layout. Indeed, the numbering and partitioning of the spokes was required to match with the pattern of deviation angles (δ) described previously in Figure 3-12. The zero reference is positioned 54.74°-deviated from vertical {111} planes (planes at which Si{110} wafers break).

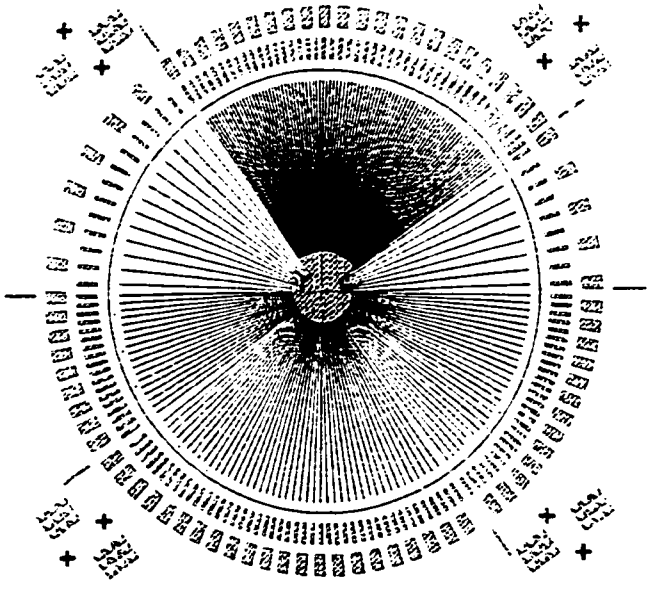

Figure 5-2 : Wagon-wheel mask layout designed for Si{110} etching.

An alignment pattern was also designed on the two mask layouts to verify the rotation alignment of the zero reference of the spokes with the inclined {111} planes in the silicon crystal. Copies of this pattern, shown in Figure 5-3, are situated at the four corners of each of the two masks. Misalignments up to two degrees are measurable with a precision better than half degree. The alignment pattern consists of nine identical elements differing by a half-degree of rotation. Etching occurs at the two symmetrical triangles of each element. Figure 5-4 shows (simulated using the Anise software), top views of a single element of the alignment pattern being etched for 5h. Any misalignment is amplified at the fast-etch planes. As an example, two-degree misalignments were set before the simulation; this misalignment is readily observed by rapid comparison of the symmetric fast-etch planes. Determining the degree of misalignment of the mask with the silicon crystal is made by identifying the most symmetrical etched pattern (at fast etch-planes) of the nine elements.

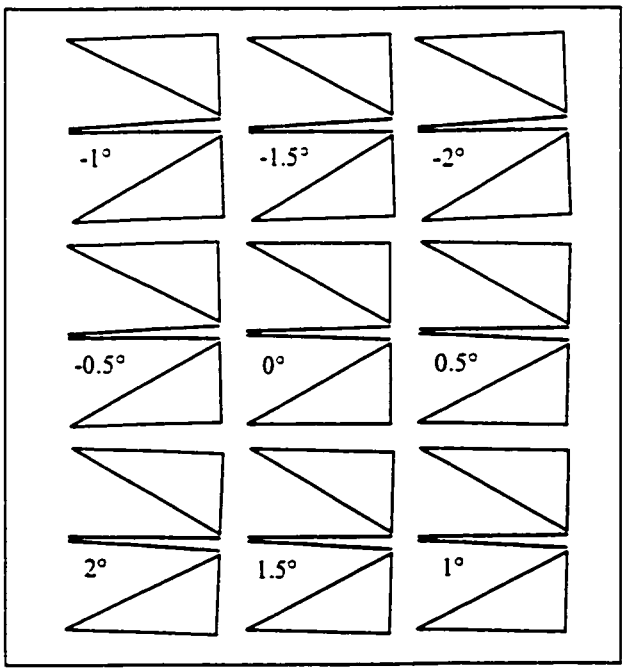

Figure 5-3 : Alignment pattern.

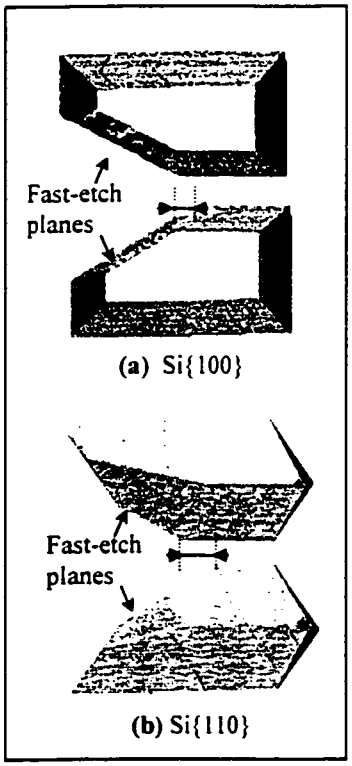

Figure 5-4 : Two degrees misalignment etching simulation (using Anise software from Intellisense Inc.) of a single pattern of Figure 4-3for: (a) Si{100} and (b) Si{110}.

5.2 Laboratory work

Performing wagon-wheel under-etch experiments requires the preparation of silicon samples covered with patterned oxide having the layout of one of the two masks of Figure 5-1 and Figure 5-2. The preparation steps are described in this section, as well as etch settings.

5.2.1 Sample preparation

A clean-room environment is necessary to achieve defect-free samples ready to be etched in TMAH. Figure 5-5 gives an overview of the process steps required for wagon-wheel under-etch experiments.

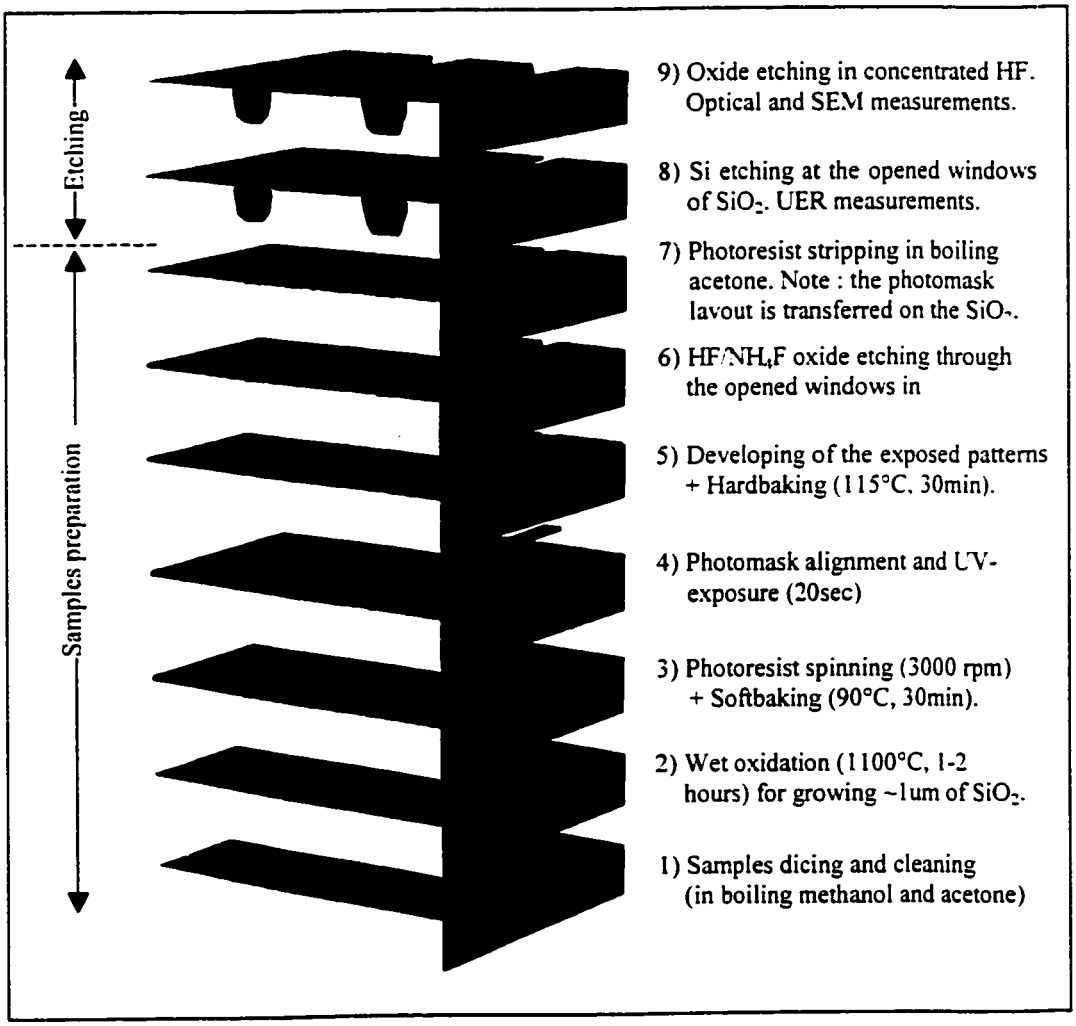

Figure 5-5 : Illustration of the sample state through the process steps .

Four-inch wafers of both types Si{100} and Si{110} are first diced with geometries shown in Figure 5-6. The wagon-wheel schematic is overlaid to illustrate the fact that mask layouts are aligned with the {111} planes at which the Si crystal easily cleaves. Actually Si{100} cleaves at the 54.74° inclined {111} planes whereas Si{110} cleaves at the vertical {111} planes as shown in Figure 5-6.

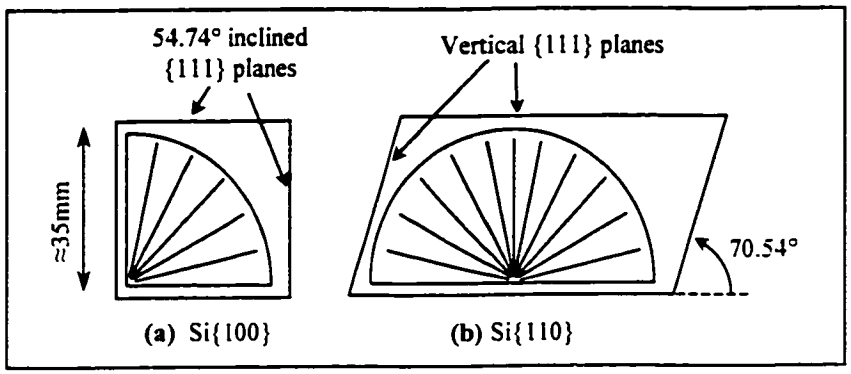

Figure 5-6 : Si{100} (a) and Si{110} (b) dicing for wagon-wheel sections positioning.

After being cleaned in heated acetone and methanol, the samples are oxidized in a tube furnace at 1100°C. Wet oxidation was performed for one hour or two hours according to the planned TMAH etching time. Indeed, the thicker is the oxide layer, the more it can resist to under-etching and not break before optical measurement. However, a thick oxide needs more etching time when immersed in HF (step 6 in Figure 5-5), this leads to a loss of precision due to the lateral component of the isotropic HF etching. As a compromise, 0.6um of oxide was thermally grown on the samples dedicated to TMAH etching times lower than 3 hours, while for other samples 1.2um of oxide was grown. After wet oxidation, photolithography (steps 3 to 7 in Figure 5-5) using masks shown on Figure 5-1 or Figure 5-2 is performed. The samples, having wagon-wheel openings in the oxide, are then verified under an optical microscope for selection. Unsatisfactory samples are rejected or used for pilot tests. The selection step is critical because 12 samples are etched simultaneously in TMAH, and all the samples have to be defect-free for reliable inter-sample comparison. Otherwise, the whole etching experiment is to be reset with 12 new samples.

5.2.2 Etching experiments

The objective of the experiments is to study the evolution of silicon under-etch profiles with respect to time in 25wt.% and 19wt.% TMAH. At each concentration, 12 samples (six (6) Si{100}, six (6) Si{110}) were simultaneously immersed in the TMAH bath. After time periods of 10min, 25min, 50min, 1h30min, 3h, and 5h (each time measured from the beginning of the experiment), one sample of each orientation was removed from the etching solution. The reason for etching many samples at the same time is to attain greater certainty for SEM comparison across silicon orientation.[6]

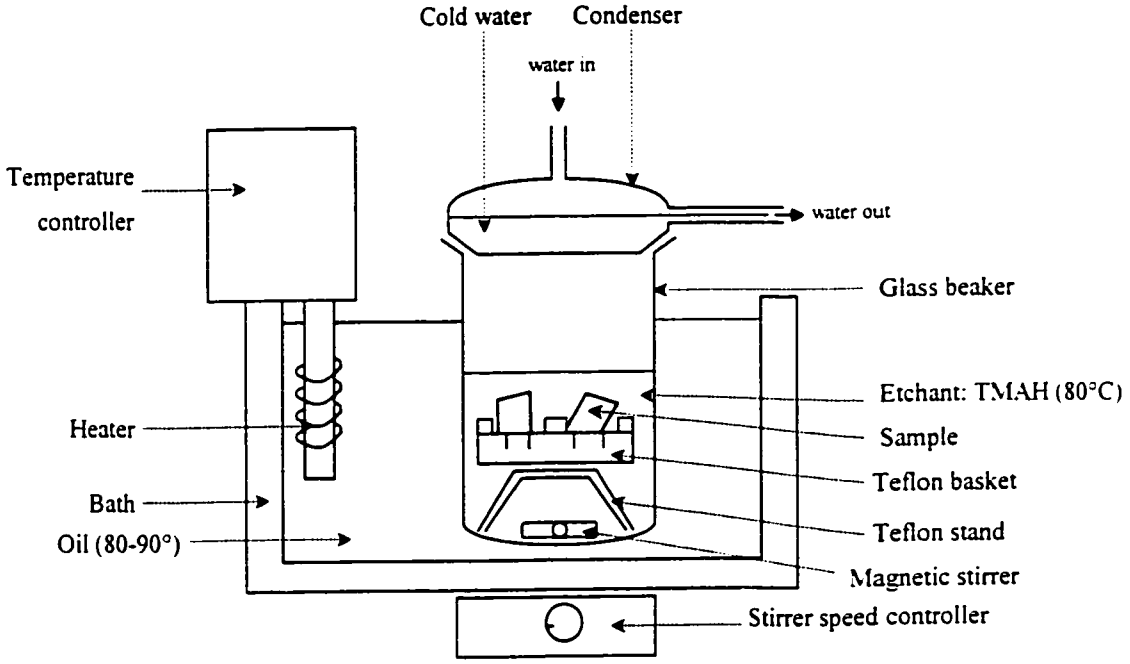

Figure 5-7: TMAH etching experimental set up.

Figure 5-7 shows the experimental set-up for TMAH etching. Samples are secured in a Teflon basket and immersed in a glass beaker containing TMAH. The etchant temperature is maintained at 80°C by an oil bath electrically heated and controlled with a

[6] Another method might have been to etch an individual sample for a short period of time, removing it from the etching solution, perform the necessary measurements, immersing the sample back to the TMAH solution for a another short period of time, removing it, performing measurements, and so on.... This method was not chosen, since the repeated removal and re-immersion actions could have invalidated the longer-time experiments. Moroever, it was important to be able to (later) simultaneously analyze and compare samples at all experimental times.

precision of 0.1°C. A reflux cap was used to condense the vapor of the etch solution in order to keep the TMAH concentration constant. A Teflon stand was used to hold the Teflon basket above a magnetic stirrer controlled externally.

TMAH solutions

The TMAH used in all experiments was bought from the same source (Moses Lake Industries) and has an initial concentration of 25wt.% in water. Fresh TMAH was used in every experiment. Lower concentrations were achieved by proper dilution with adding de-ionized water. As an example, the making of a solution of 20wt% TMAH is described:

→ Start with 1000 mL of 25wt.% TMAH. It contains 260g of pure TMAH and weighs a total of 1040g. Deionized (DI) water should be added so that the 260g makes 20wt.% of the total weight :

- Total weight = 260*100/20 = 1300g.
- DI water to be added = 1300g - 1040g = 260g = 260 mL.

TMAH temperature setting

Figure 5-8 shows measurements of both oil and TMAH temperatures vs. time. At t=0. the oil bath is switched on and set at a temperature of 84.5°C. The graph shows that the TMAH solution stabilizes at a temperature of 80°C and requires 1h30min for complete stabilization. The difference between the oil and TMAH temperatures is explained by the TMAH cooling due to reflux condenser.

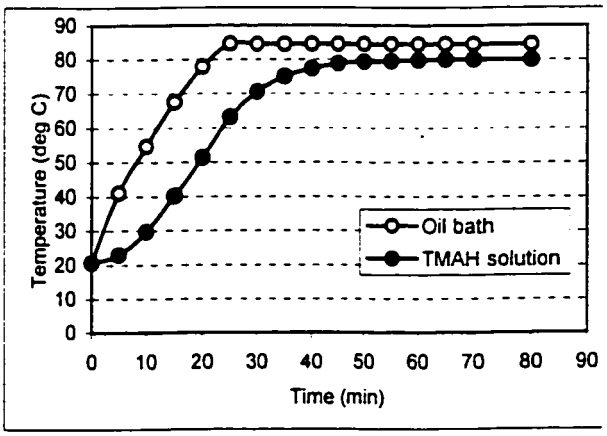

Figure 5-8 : TMAH bath temperature stabilization with time.

It was also noticed that the immersion of the holder carrying new samples causes a decrease in temperature of the TMAH solution of 1.5 degree. This disturbance was balanced by heating the solution to 86°, only beginning 30 seconds before the immersion. As soon as the samples were immersed, the heater was re-set at 84.5°.

5.2.3 Measurements

The under-etching distances need to be long enough for optical measurements to give reliable results. However this may become critical for samples etched for short times (10min and 25min). For accurate comparison between samples, measurements are performed at fixed locations (Figure 5-9) on the wagon-wheel.

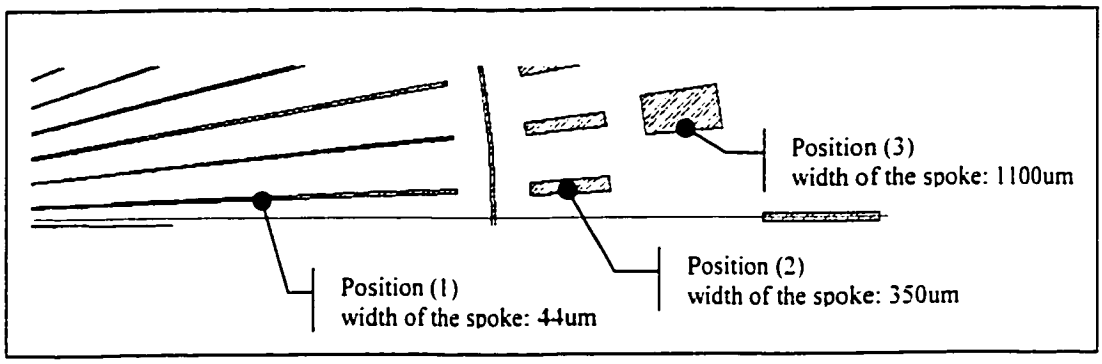

Figure 5-9 : Measurement locations on wagon-wheel spokes.

After etching in TMAH, etch distances, illustrated in Figure 5-10, are measured using an optical microscope. The under-etch rate (UER) is first determined by measuring the under-etch distance of the transparent overhanging thin oxide mask. Then, after dissolution of the covering oxide mask in HF solution, the bottom cavity width, the etched depth, and the spoke width after etching are measured. The etching depth is measured at both center and edge of the bottom surface, especially for deviation angles at which trenches are formed. Horizontal distances are measured using the transparent image of a graduated standard superposed onto the microscope image, whereas vertical distances are measured using the graduation on the knob controlling the vertical movement (focus) of the microscope table. Table 5-1 summarizes the precision of the measurements for both horizontal and vertical distances.

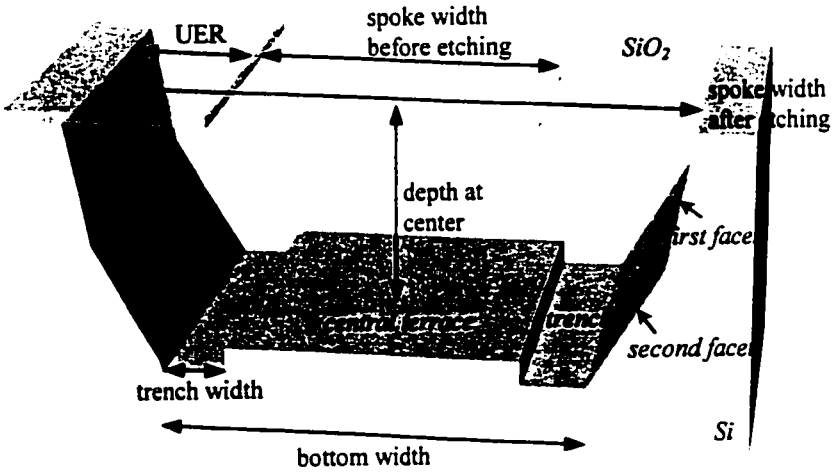

Figure 5-10 : Perspective view of a portion of an etched spoke.

Table 5-1 : Precision of the optical measurements.

	Magnification	Calibration	precision
Horizontal measurements	x5	20 um/div	±10um
	x10	10 um/div	±5um
	x20	5 um/div	±2.5um
	x50	2 um/div	±1um
Depth measurements	-	2 um/div	±1um

The inclination angle $\alpha_{effective}$ (see Figure 3-11) is easily derived from the measure of the spoke with after etching and the cavity bottom surface etching rate, using the equation :

$$\alpha_{eq} = \text{atan}\left[\frac{\text{Bottom suface ER/2}}{\text{spoke width after etching /2}}\right]$$

On the contrary, facets inclination angles (α_1 and α_2 on Figure 3-11) may only be measured after visualizing a cross-section of a single spoke under a scanning electron microscope (SEM).

To obtain SEM cross-section micrographs of a specific spoke at a desired deviation angle δ, each silicon sample was first carefully diced. Figure 5-11 shows an example of a

Si{100} sample dicing. A special care was given when inducing the {111} planes (at which the sample cleaves) so that the cleave plane propagates across the desired spokes at a reasonable distance from the center of the mask (avoiding the areas where spokes are completely under-etched). As shown n Figure 5-11, spokes on the sub-pieces of silicon are very often not perpendicular to the cleaved plane. As a result, to get precise measurements of the facets inclination angle (α) for a given spoke, the SEM micrographs were obtained after tilting the sample with an angle (τ) from the view perpendicular to the cross-section plane, as illustrated in Figure 5-11

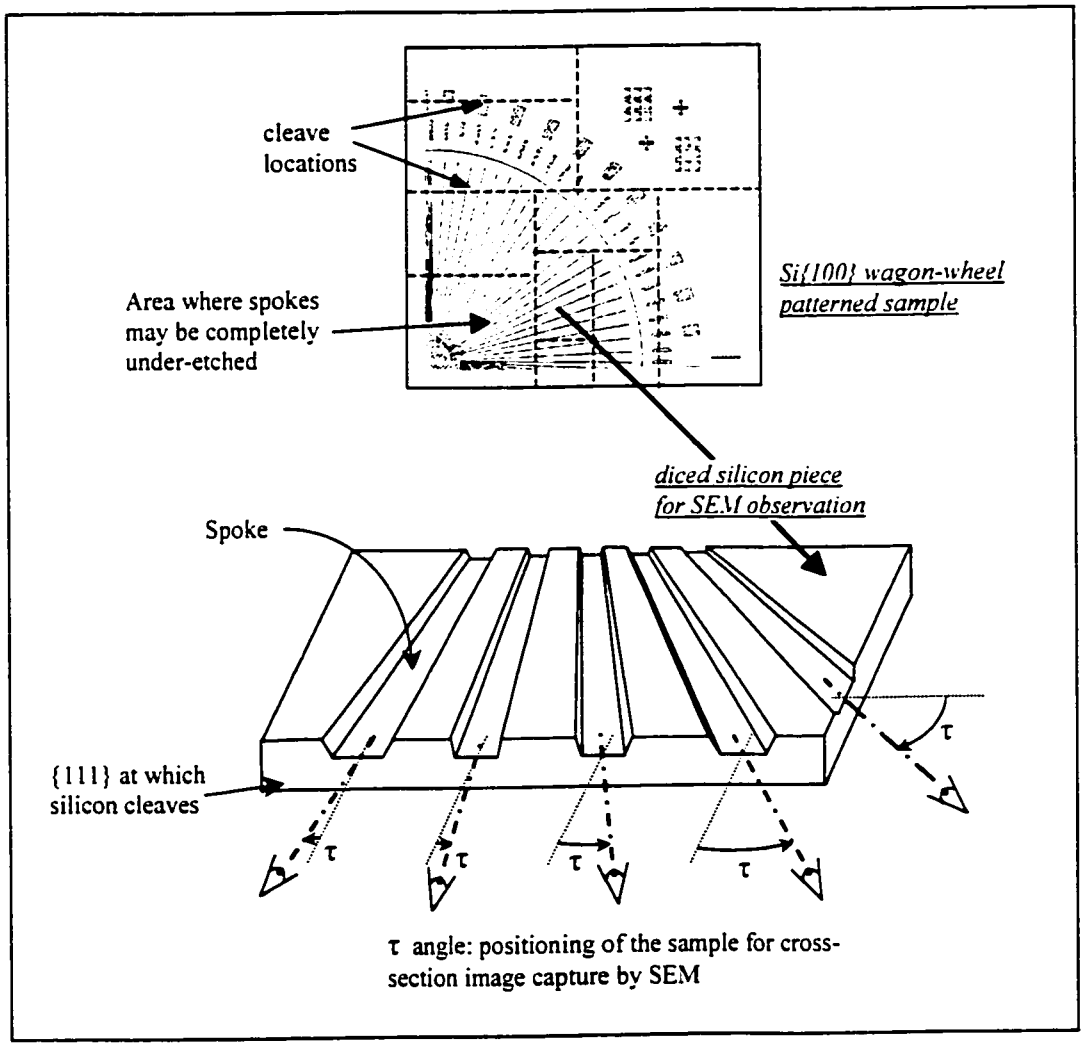

Figure 5-11 : Si{100} Samples dicing for spokes cross-section observation by SEM

5.3 Stirring effects

In literature, it is most often suggested [10,14], that stirring has little or no effect on etching. Because most researchers perform their experiments without stirring, preliminary experiments for this thesis were performed without any stirring. However, measurements and observations of etched samples revealed some undesired effects and difficulty with reproducibility, which was all the more annoying since this thesis aims to identify and explain very small deviations from the crystal-feature-based etching model. Figure 5-12 shows the results of wagon-wheel under-etch rate measurements on Si{100} etched in *unstirred* TMAH. Notice that in this unstirred data there is an evolution with time of the under-etch rate (UER) curve whereas in the stirred data at same etchant conditions (Figure 6-1 in Chapter 6), the UER curve is much more constant with time. It is noteworthy that it does happens that the UER curve vary with time for other experiments on other silicon orientations or with other TMAH concentrations , but comparing Figure 5-12 with Figure 6-1 gives us confidence that the experimental situation with stirring. is stable.

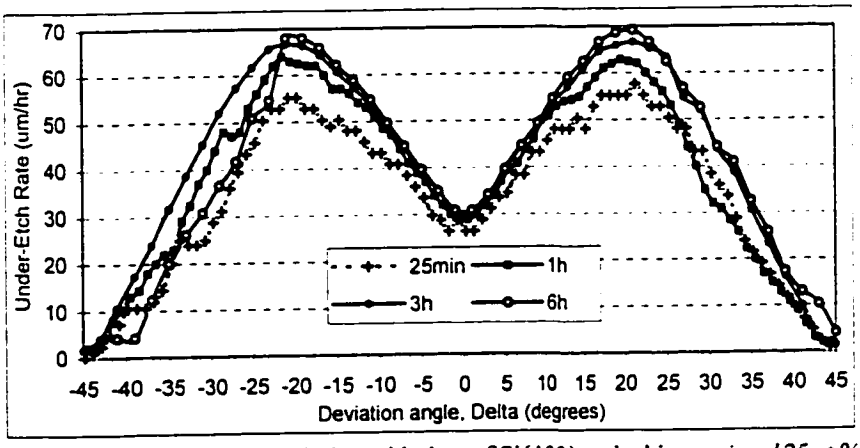

Figure 5-12 : Under-etch rate evolution with time of Si{100} etched in *unstirred* 25wt.% TMAH

Notice also in Figure 5-12 that the *unstirred* curves are globally symmetric around $\delta=0°$ (which is normal due to the symmetry of Si{100}), but upon closer inspection one sees that the curves are irregular and asymmetric. For better clarity, curves from the two sides of Figure 5-12 (the 25min and 6h data) are folded horizontally around $\delta=0°$ and presented in Figure 5-13. Dotted lines in Figure 5-13 correspond to measurements on spokes at

deviation angles $-45° \leq \delta \leq 0°$ (the left side of Fig. 5.11), symmetrically transposed for comparison with solid lines that correspond to measurements at $0° \leq \delta \leq 45°$ (the right side of Fig. 5.11). The fact that in Figure 5-13 solid lines and dotted lines do not coincide demonstrates that the corresponding curves in Figure 5-12 are actually not symmetric. In contrast, Figure 5-14 shows folded under-etch rate curves (Figure 6.1) obtained from vigorously *stirred* experiments using a 6cm magnetic stirrer at about 500rpm. Solid lines and dotted lines coincide satisfyingly, which suggests that vigorous stirring is effective against the anomalies observed without stirring.

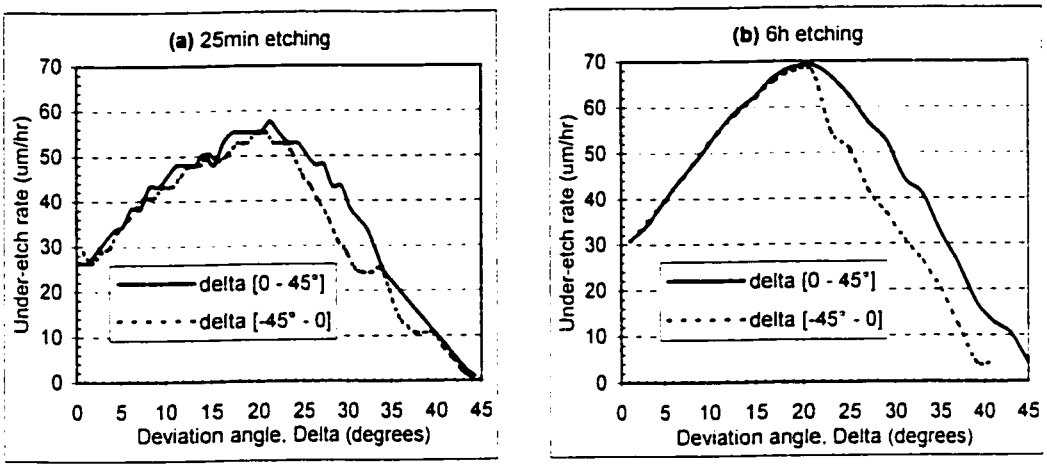

Figure 5-13 : Examples of irregular and poorly symmetric curves on *unstirred* Si{100} 25wt%TMAH. This curves are the 25min (a) and 6h (b) data imported from Figure 5-11 and folded over around δ=0°.

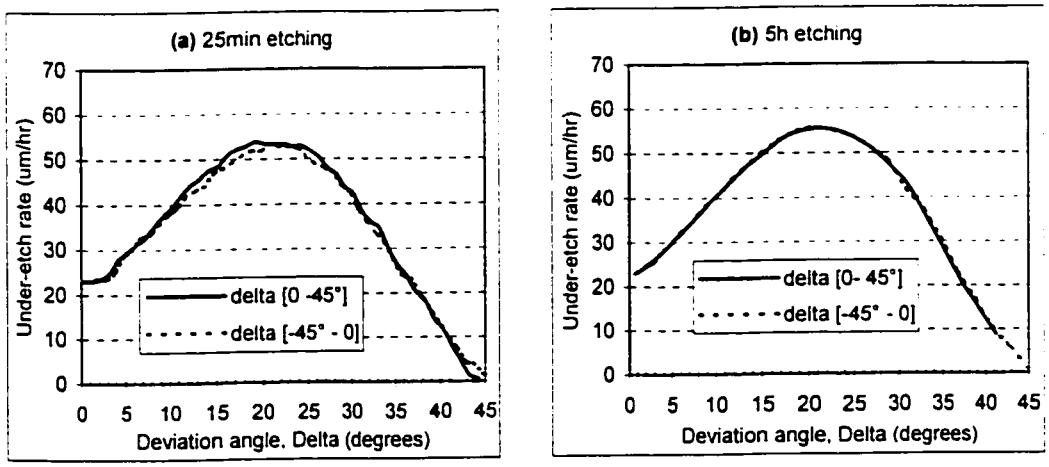

Figure 5-14 : Examples of regular and symmetric curves on *stirred* Si{100} 25wt%TMAH. This curves are the 25min (a) and 5h (b) data imported from Figure 6-1 and folded over around δ=0°.

For unstirred experiments, it is thought that positioning of the spokes during etching might be involved since measurements on Si{100} at $45° \leq \delta \leq 90°$ were found to always be lower than that of $0° \leq \delta \leq 45°$. Figure 5-15 shows the positioning of the spokes during etching. Because the samples are etched in a vertical position, some spokes are aligned vertically whereas others are aligned horizontally. Etching of silicon in TMAH releases hydrogen bubbles (H_2) which spread towards the surface of the solution. It is suspected that some of these bubbles may be trapped in horizontal spokes and affect their etching rate.

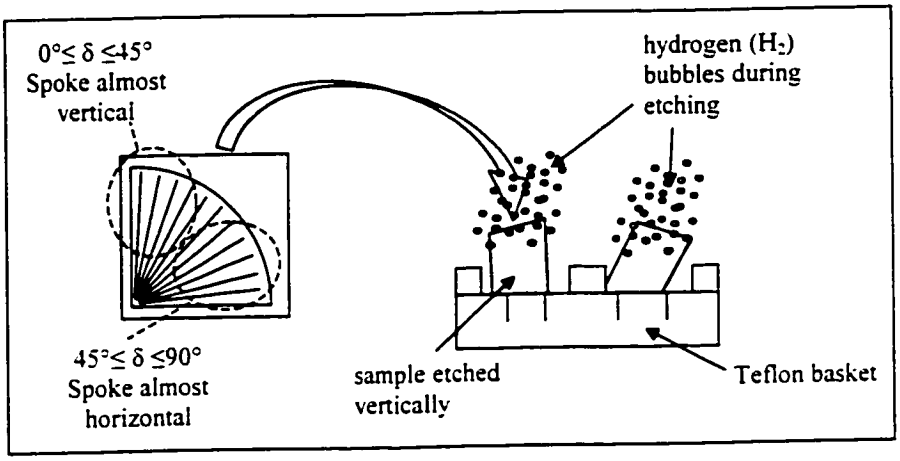

Figure 5-15 : Spokes position during etching and emanation of hydrogen bubbles.

To minimise the non-uniformity (suspected to be caused by hydrogen bubbles), etching experiments were vigorously agitated using a 2-inch magnetic stirrer. It was found that the stronger is the stirring, the more reproducible is the etching. This observation is in agreement with prior research literature which found that hydrogen bubbles affect the silicon etch surface on which they are attached [38]. Also, prior research found that with an increased mixing by ultrasonic agitation, silicon etches faster with more uniform and smoother surfaces [39].

5.4 Contributions

In Chapter 5, the experimental procedures for etching wagon-wheel patterned silicon samples are presented. Besides routine sample preparation and etching experiments, there are two particular contributions.:

- Two etching masks were designed to enable wagon-wheel etching experiments on Si{100} and Si{110} for up to six hours of etching, including patterns for measuring the misalignment of the mask within better than 0.5°.
- It is shown that stirring during anisotropic etching of silicon in TMAH gives much more reproducible results, both on a single sample, and over time.

6 Experimental results and observations

This chapter presents experimental results of wagon-wheel experiments on Si{110} and Si{100} samples, etched for various times in 25wt.% and 19wt.% TMAH concentrations. The experiments were vigorously stirred and the etch-bath temperature was 80°C.
In each of the four cases,

- Si{100} 25wt%
- Si{110} 25wt%
- Si{100} 19wt%
- Si{110} 19wt%

the analysis begins with a graphical summary of the optical measurements of under-etch rates, effective inclination angles and cavity-bottom etch rate, as a function of deviation angle. Each graph includes curves for all of the experimental times, thus summarizing the evolution with time of the three measurements.

As was pointed out in Chapter 3, the effective inclination angles do not show the full details of the facet inclination angles, so SEM's are required to obtain a sufficient view. It should be noted that an exhaustive recording and presentation of the details of the time-variations of the under-etched surfaces (number of facets, facet sizes, several parameters of roughness for each facet, at each δ) would be prohibitive. Therefore, an approach was taken to select areas of particular interest for more in-depth analysis, including SEM's. These were selected based on observations in the phase of optical measurements and in preliminary scans using SEM. It was found during these optical and SEM scans that there were many anomalies[7] from the crystal-feature-based model outlined in Chapter 3, for example:

- under-etch rates varying with etch time
- the presence of inverted facets
- facets appearing and/or disappearing with etch time

[7] In fact, some non-ideality could be found for the majority of the wagon-wheel spokes, in all four cases of concentration and wafer orientation.

- roughness changing substantially with etch time
- roughness changing dramatically from one δ to the next[8]

In light of this, the analysis is organized as follows. In this Chapter, for each of the four cases, several interesting and strategic locations are explored (3-4 per case), each demonstrating one or more of the types of anomalies listed above. Then, in Chapter 7, these types of anomalies are explored in more depth, including more SEM's of nearby or related locations, and hypothesizing them to be due to boundary effects occurring at facet junctions.

The presentation of the data begins with annotated graphs, showing the deviation angles at which SEM's will be presented.

6.1 Optical measurements

This section presents optical measurements of wagon-wheel experiments on Si{110} and Si{100} samples, etched for various times in 25wt.% and 19wt.% TMAH concentrations. In each of the four cases, the evolution with time of under-etch rates, effective inclination angles and cavity-bottom etch rate, as a function of deviation angle, are presented.

6.1.1 Si{100} 25wt% TMAH

The results of the optical measurements on wagon-wheel etching experiments for six Si{100} samples etched in 25wt.% TMAH at 80°C with etching times ranging from 10min to 5h are presented in Figure 6-1, Figure 6-2, Figure 6-3. Note that these six Si{100} samples were etched simultaneously with other six Si{110} samples (the results of which are presented in the next section 6.1.2). This enables precise comparison between the two silicon orientations since the samples are etching in the identical etchant. Vertical lines in Figure 6-1 identify the locations which are the subject of scanning electron microscopy (SEM) presented in Section 6.3.1. It is observed in Figure 6-1 that there is very little evolution with time of the under-etch rate curves (providing that the

[8] This aspect is explored only in Chapter 7.

very noisy 10min curve is ignored). It can be stated that, at least after the first 10 minutes, the top-most facet of the under-etched surface is etching at a constant rate.

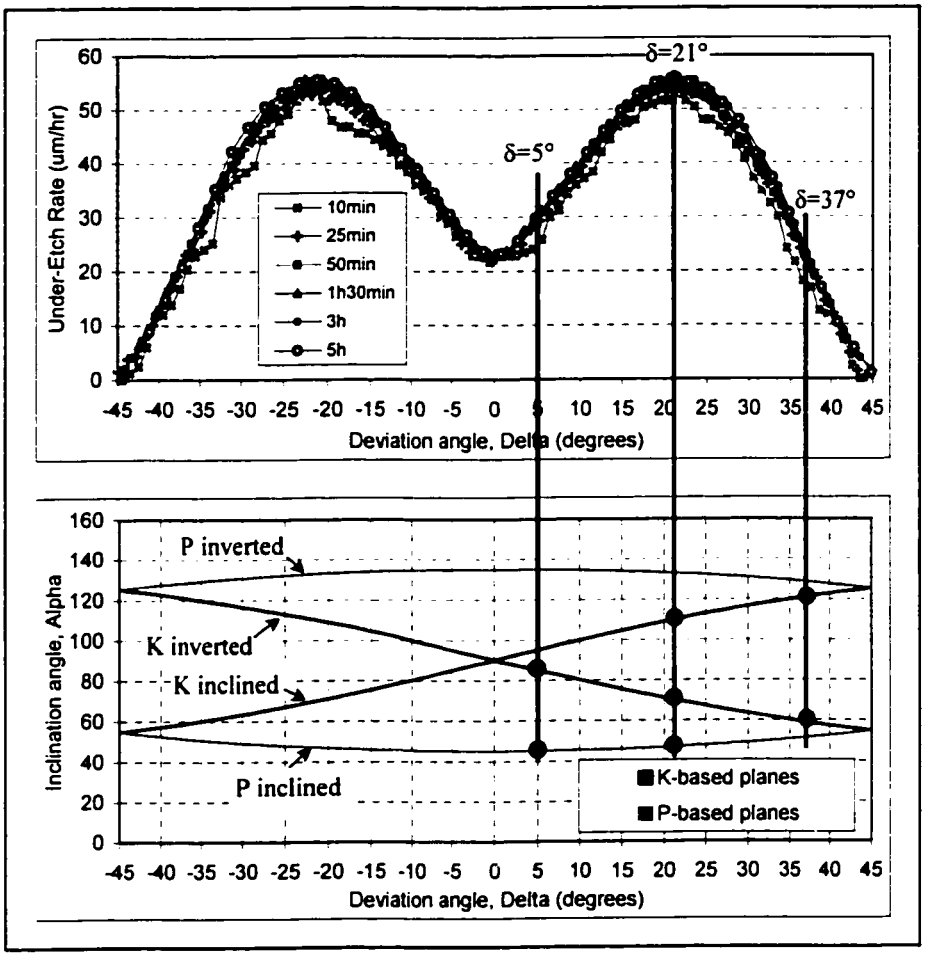

Figure 6-1 : Si{100} 25wt.% TMAH: Under-etch rate curve evolution with time.

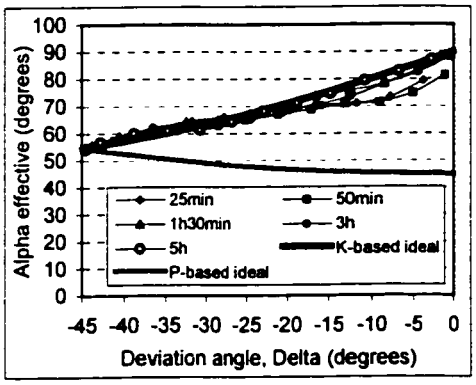

Figure 6-2 : Si{100} 25wt.% TMAH: Evolution with time of the effective inclination angle $\alpha_{effective}$.

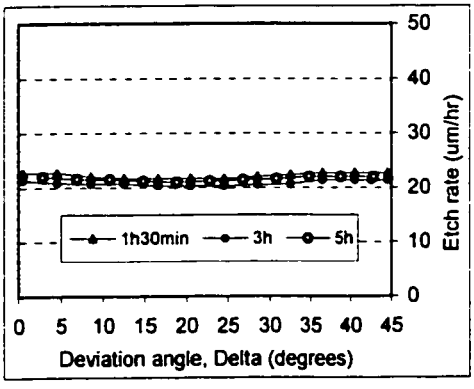

Figure 6-3 : Si{100} 25wt.% TMAH: Bottom surface etch rate evolution with time.

In Figure 6-2, the fact that the effective inclination angles ($\alpha_{effective}$) follow (as the mask edge is rotated) close to the K-based ideal inclination angles demonstrates that the etch profile is largely composed of the K-based inclined series. However, upon closer inspection, it is seen that at deviation angles in the vicinity of δ=0°, the measured effective inclination angles deviate from the ideal K-based inclined line, suggesting the appearance of another less-steeply inclined facet, at the foot of the top-most facet, which is revealed by SEM (Figure 6-28) to be a P-based inclined series.

Figure 6-3 shows that the etch rate of the bottom surface remains largely constant with time. The dependence of the bottom surface etch rate with respect to the deviation angle is very subtle. In summary, the {100} bottom surface is etching in 25wt.% at a roughly constant rate of 22um/hr, without being affected by boundaries. The rate of 22um/hr is in agreement with the local minimum of Figure 6-1, which is also the measure of a {100} etch rate.

6.1.2 Si{110} 25wt% TMAH

The results of the optical measurements on wagon-wheel etching experiments for six Si{110} samples etched in 25wt% TMAH at 80°C with etching times ranging from 10min to 5h are presented in Figure 6-4, Figure 6-5, Figure 6-6, and Figure 6-7. Note that these six Si{110} samples were etched simultaneously with other six Si{100} samples (the results of which are presented in the previous section 6.1.1).

Vertical lines in Figure 6-4 identify the locations which are the subject of scanning electron microscopy (SEM) presented in Section 6.3.2. It is observed in Figure 6-4 that there is very little evolution with time of the under-etch rate curves. However at deviation angles around δ=39.5° and δ=70°, most under-etch rate curves show anomalous shape (clarified below in Sections 6.3.2 (b) and (c)).

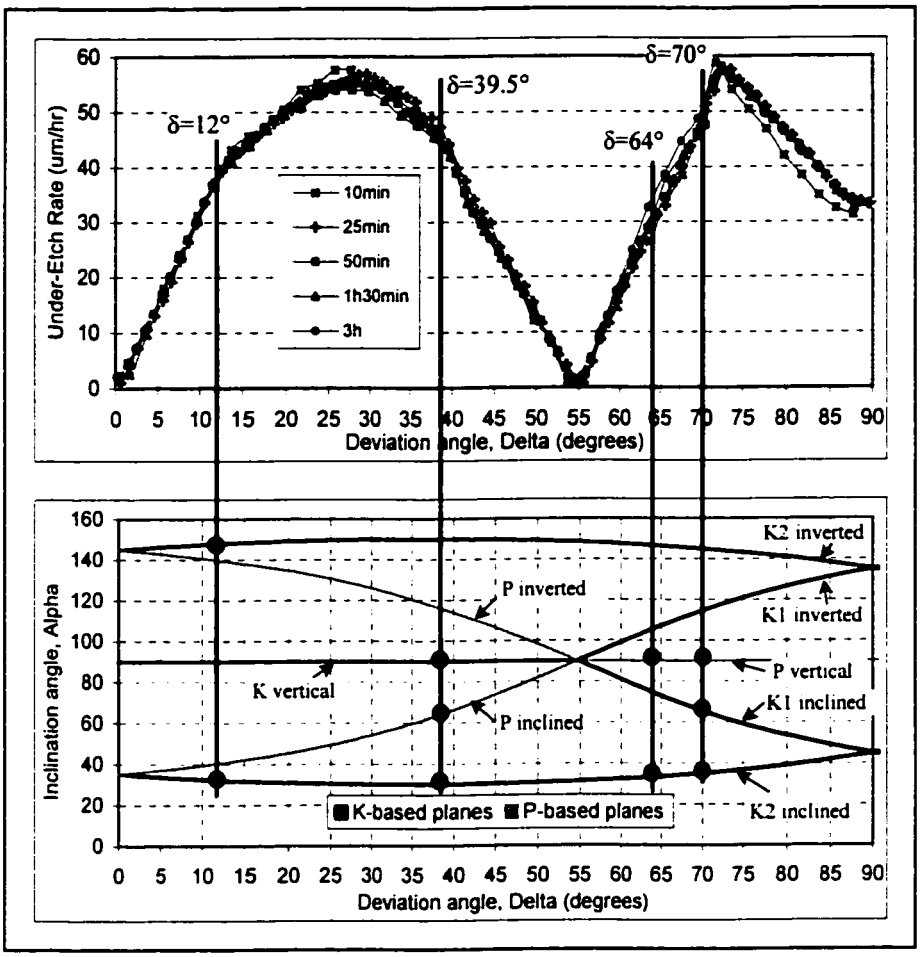

Figure 6-4 : Si{110} 25wt.% TMAH: Under-etch rate curve evolution with time.

The evolution with time of the effective inclination angle $\alpha_{effective}$ is presented in Figure 6-5 for etching times from 10min to 1h30min and in Figure 6-6 for etching times from 1h30min to 5h. It is observed in both figures that the effective inclination angles do vary with time for deviation angles ranging from $\delta \approx 27°$ to $\delta \approx 72°$: in Figure 6-5 (short etch times), $\alpha_{effective}$ increases with time, whereas in Figure 6-6 (long etch times), it decreases with time. In this range of δ, two particular facets are prevalent: the top-most facet is either a $K_{vertical}$ (δ <54.74°) or a $P_{vertical}$ (δ >54.74°), and the lowest facet is a $K2_{inclined}$ (Section 6.3.2 (c)). Since the top-most planes can not explain the anomalous variations of $\alpha_{effective}$ in Figure 6-5 and Figure 6-6 (the UER variations with time in Figure 6-4 are too small), the variations of $\alpha_{effective}$ are likely to be related to the etch rate variations (and corresponding size variations) of the lowest facet $K2_{inclined}$.

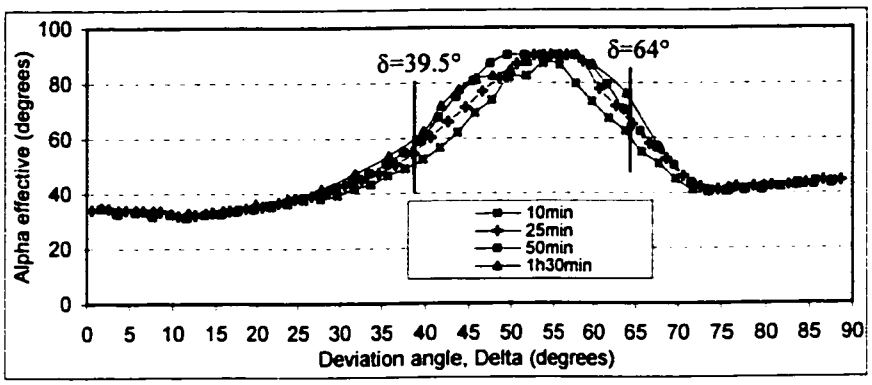

Figure 6-5 : Si{110} 25wt.% TMAH: Evolution with time of the effective inclination angle $\alpha_{effective}$ for etching times from 10min to 1h30min.

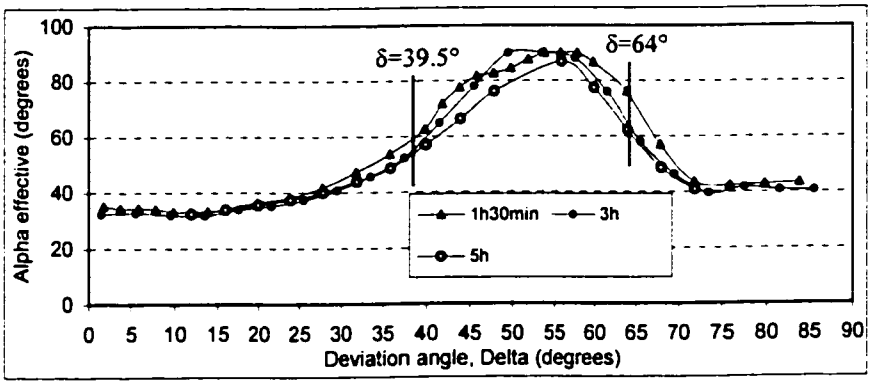

Figure 6-6 : Si{110} 25wt.% TMAH: Evolution with time of the effective inclination angle $\alpha_{effective}$ for etching times from 1h30min to 5h.

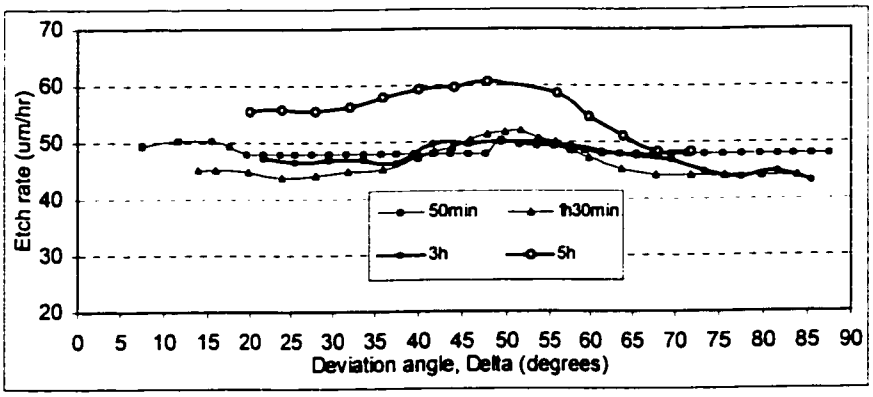

Figure 6-7 : Si{110} 25wt.% TMAH: Bottom surface etch rate evolution with time.

Figure 6-7 shows the bottom surface etch rate with respect to the mask deviation angle δ. Figure 6-7 shows evolution with time which is not simple. However, most curves in Figure 6-7 have a local maximum around δ=50°. This acceleration of the Si{110} bottom

surface around δ=50° may be related[9] to interactions between the {110} bottom surface and the $K2_{inclined}$ facet, since the $K2_{inclined}$ facet is present for δ <50° and absent for δ>50°. The 5h etching curve in Figure 6-7 is different from the others, and this may be related to a change in the surface roughness (Figure 6-8-(5h)).

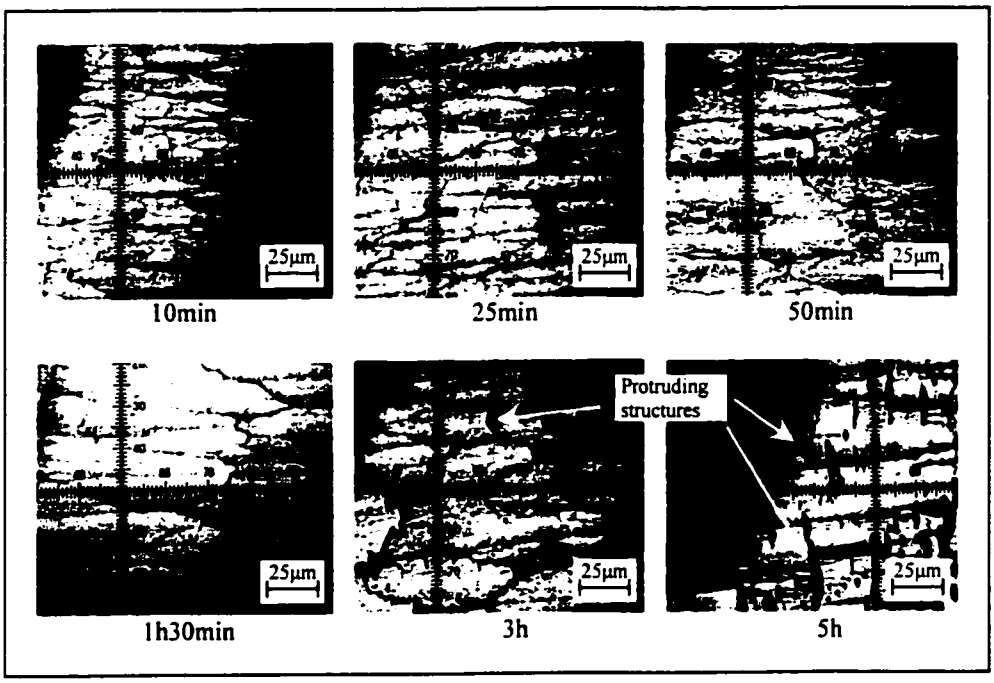

Figure 6-8 : Evolution with time of the Si{110} surface roughness in 25wt.% TMAH.

Figure 6-8 shows the evolution with time of the Si{110} surface roughness in 25wt.% TMAH. The X-axis in all pictures is aligned with the orientation of PBCs on the etched surface. The features (depressions) observed in Figure 6-8 seem to increase in size as etching proceeds from 10min to 3h etching. At 3h etching, protruding structures are observed. At 5h etching, the number and size of the protruding structures have increased. As mentioned earlier, the Si{110} roughness change beginning at 3h etching may be responsible for or correlated with the etch rate acceleration of the 5h curve observed in Figure 6-3.

Figure 6-9 shows the Si{110} surface evolution with time at the bottom surface of a spoke cavity positioned at deviation angle δ=70°. Very similar depressions as in Figure 6-8 are observed at 10min etching. As etching proceeds, however, the depressions

[9] See Section 7.2.2.(f) for more analysis.

increase in size and start interacting with the edges of the cavity. The roughness of the cavity-bottom is then modified from depressions into more directional lines aligned parallel to PBCs (aligned to cross the trenches obliquely).

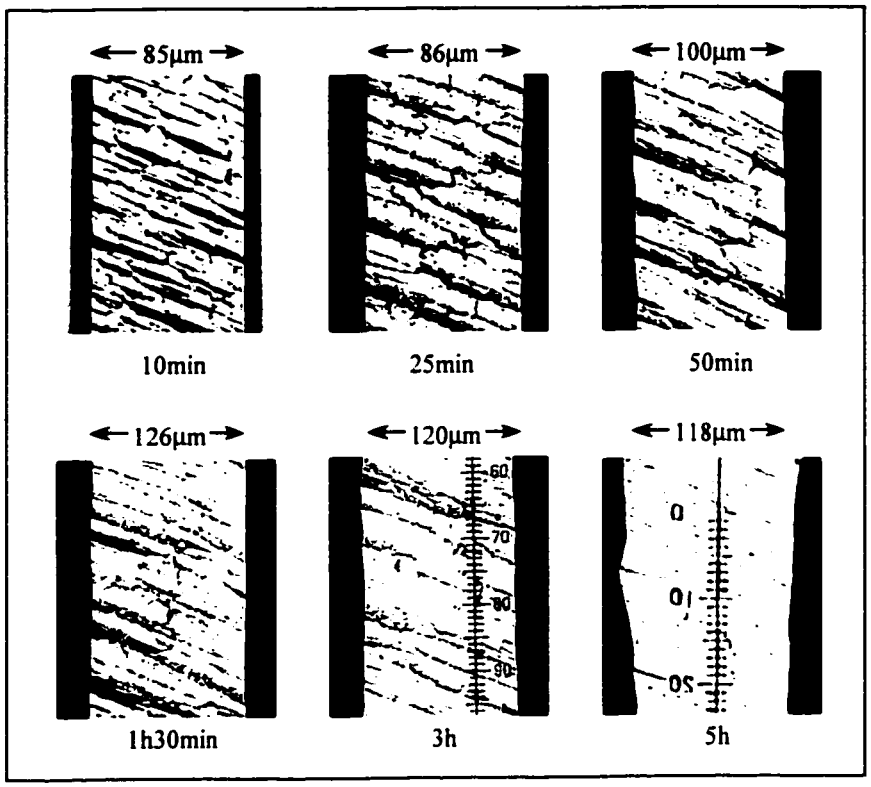

Figure 6-9 : Evolution with time of the Si{110} surface roughness at the bottom cavity at δ=70°.

6.1.3 Si{100} 19wt% TMAH

The results of the optical measurements on wagon-wheel etching experiments for five Si{100} samples etched in 19wt% TMAH at 80°C with etching times ranging from 25min to 5h, are presented in Figure 6-10, Figure 6-11, and Figure 6-12. Note that these five Si{100} samples and another Si{100} sample (etched for 10min, the optical measurements of which are not included because too noisy) were etched simultaneously with other Si{110} samples (the results of which are presented in the next section 6.1.4). Vertical lines in Figure 6-10 identify the locations which are the subject of scanning electron microscopy (SEM) and presented in Section 6.3.3. It is observed in Figure 6-10 that the under-etch rate curves (corresponding to different etching times) do not coincide for the range of deviation angle $13° \leq \delta \leq 30°$. The etching curve for 25min (the shortest

time), is much lower than the other curves, which may be due to a transient state. Among the 50min, 1h30min, and 3h etching curves in Figure 6-10, the under-etch rate decreases with time and coincides with the growth of a very rough near-vertical facet (see below in Section 6.3.2.(b)). Notice also among these three curves the evolution of the UER from the sharp tooth shape around δ=18° for the 50min etching curve to a more uniform UER (over a wider range of δ) for the 3h etching curve.

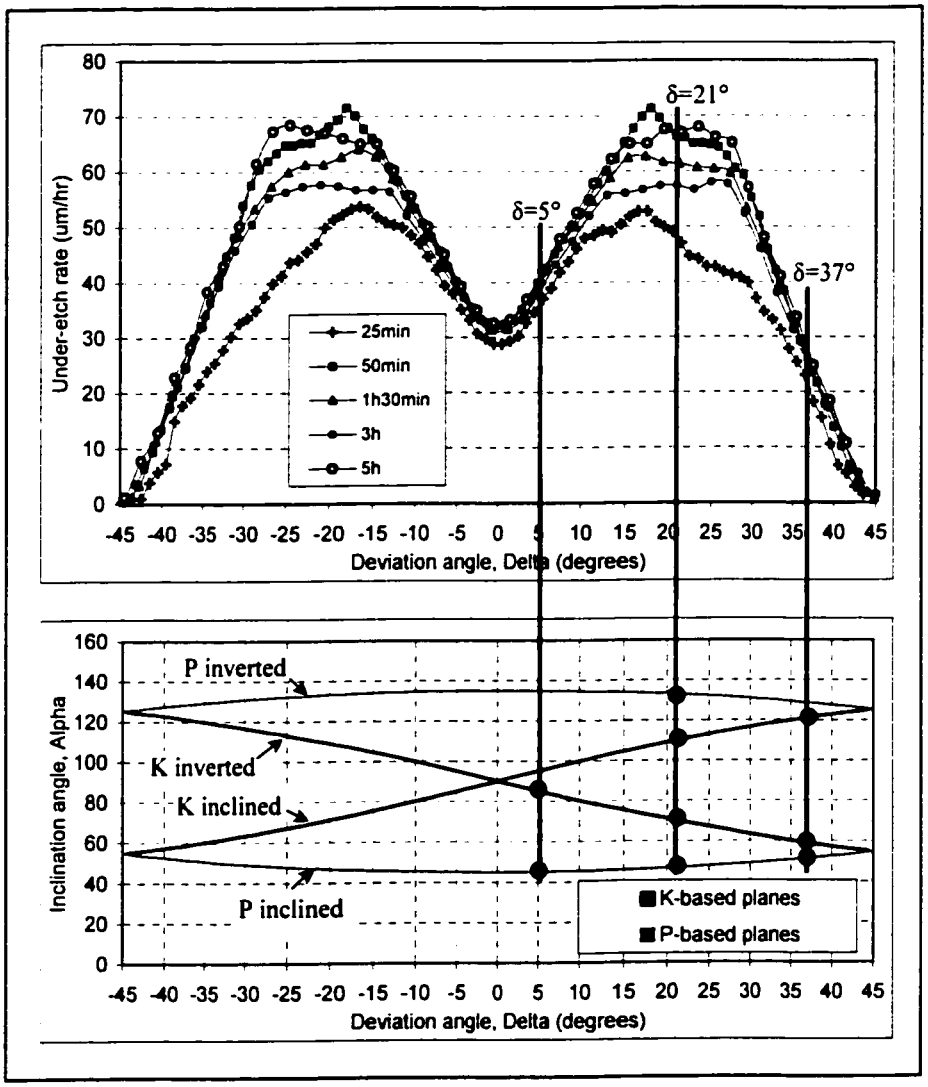

Figure 6-10 : Si{100} 19wt.% TMAH: Under-etch rate curve evolution with time.

It is observed in Figure 6-10 that, similarly to the 3h etching curve, the maximum of the 5h etching curve is relatively stable over a wide range of δ. However the maximum of the 5h etching curve is well above the maximum of the 3h etching curve (a 10um/hr

difference). SEM micrographs of the 5h etching curve at δ=21° (see Figure 6-47-(5h)) show the emergence of a new facet that is likely to be related to the dramatic increase of the under-etch rate between 3h and 5h.

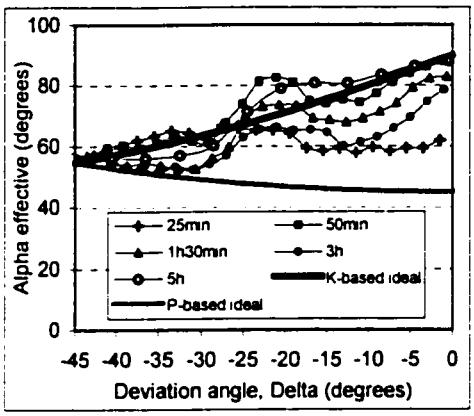

Figure 6-11 : Si{100} 19wt.% TMAH: Evolution with time of the effective inclination angle.

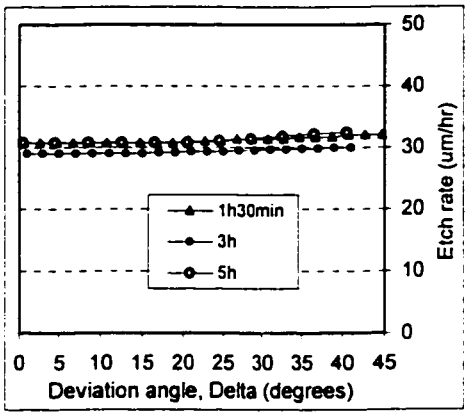

Figure 6-12 : Si{100} 19wt.% TMAH: Bottom surface etch rate evolution with time.

Figure 6-11 shows complex evolution with time of the effective inclination angle ($\alpha_{effective}$). Three ranges of δ are separated for the study of $\alpha_{effective}$:

- In the first range $-45° \leq \delta \leq -30°$, the variations of $\alpha_{effective}$ coincide with changes in the relative size of the $K_{inclined}$ and the $P_{inclined}$ under-etched facets: the 25min and 50min samples are composed (in this range of δ) of mostly the $K_{inclined}$ facet (in Figure 6-11 $\alpha_{effective}$ is closer to the K-based ideal inclination angle curve), whereas the 1h30min, 3h, and 5h samples are mostly composed of the $P_{inclined}$ facet (see section 6.3.3-(c)).
- In the second range $-30° \leq \delta \leq -15°$, the substantial increase of all effective inclination angles curves (for all etching times) coincides with the presence of the very rough near-vertical facet (see Figure 6-47).
- In the third range $-15° \leq \delta \leq 0°$, the variations of $\alpha_{effective}$ also coincide with changes in the relative size of the $K_{inclined}$ and the $P_{inclined}$ under-etch surfaces. The relative size of each of the two facets is clearly seen in Figure 6-45. Notice that in this range of delta ($-15° \leq \delta \leq 0°$), the $\alpha_{effective}$ curve corresponding to 25min is closer to the P-based ideal inclination angle curve, as opposed to the range $-45° \leq \delta \leq -30°$ where it is closer to the K-based ideal inclination angle curve.

Figure 6-12 shows that there is almost no evolution with time of the bottom surface etching rate. There is almost no dependence with respect to the deviation angle. The {100} bottom surface is etching in 19wt.% at a constant rate of 32um/hr without being strongly affected by boundaries. The 32um/hr is in agreement with the local minimum of Figure 6-10, which is also the measure of an {100} etch rate.

6.1.4 Si{110} 19wt% TMAH

The results of the optical measurements on wagon-wheel etching experiments for five Si{110} samples etched in 19wt% TMAH at 80°C with etching times ranging from 25min to 5h, are presented in Figure 6-13, Figure 6-14, and Figure 6-15. Note that these five Si{110} samples and another Si{110} sample (etched for 10min, the optical measurements of which are not included because too noisy) were etched simultaneously with the other six Si{100} samples (the results of which are presented in the previous Section 6.1.3). Vertical lines in Figure 6-13 identify the locations which are the subject of scanning electron microscopy (SEM) presented in Section 6.3.4. It is observed in Figure 6-13 that there is a substantial increase with time of the under-etch rate in the range $30° \leq \delta \leq 40°$. In the range of $\delta \geq 72°$, it is observed that the under-etch rate is constant with time up to 1h30min etching, then it accelerates for the 3h and 5h etching curves. For $55° \leq \delta \leq 72°$, the acceleration is clear for the 5h curve only, while the 3h curve seems to be in transition in the range $68° \leq \delta \leq 72°$.

The evolution with time of the effective inclination angle $\alpha_{effective}$ is presented in Figure 6-14 for etching times from 25min to 5h. It is observed in Figure 6-14 that the effective inclination angle curve decreases with time for deviation angles ranging from $\delta \approx 38°$ to $\delta \approx 70°$. In this range of δ, mostly two facets are involved. The top-most facet is either a $K_{vertical}$ ($\delta < 54.74°$) or a $P_{vertical}$ ($\delta > 54.74°$), and the lowest facet is a $K2_{inclined}$. The decrease of $\alpha_{effective}$ is suggested to be due to a probable simultaneous variation of the etch rates of sidewall facets and the cavity bottom surface: the top most vertical facet accelerates (at least for the 5h etching sample, measured in Figure 6-13, $\delta > 54.74°$), the $K2_{inclined}$ facet may slow down (as was suggested for the 25wt% experiments on Si{110}, Section 6.1.1), and the cavity bottom surface accelerates with time (measured in Figure 6-15)

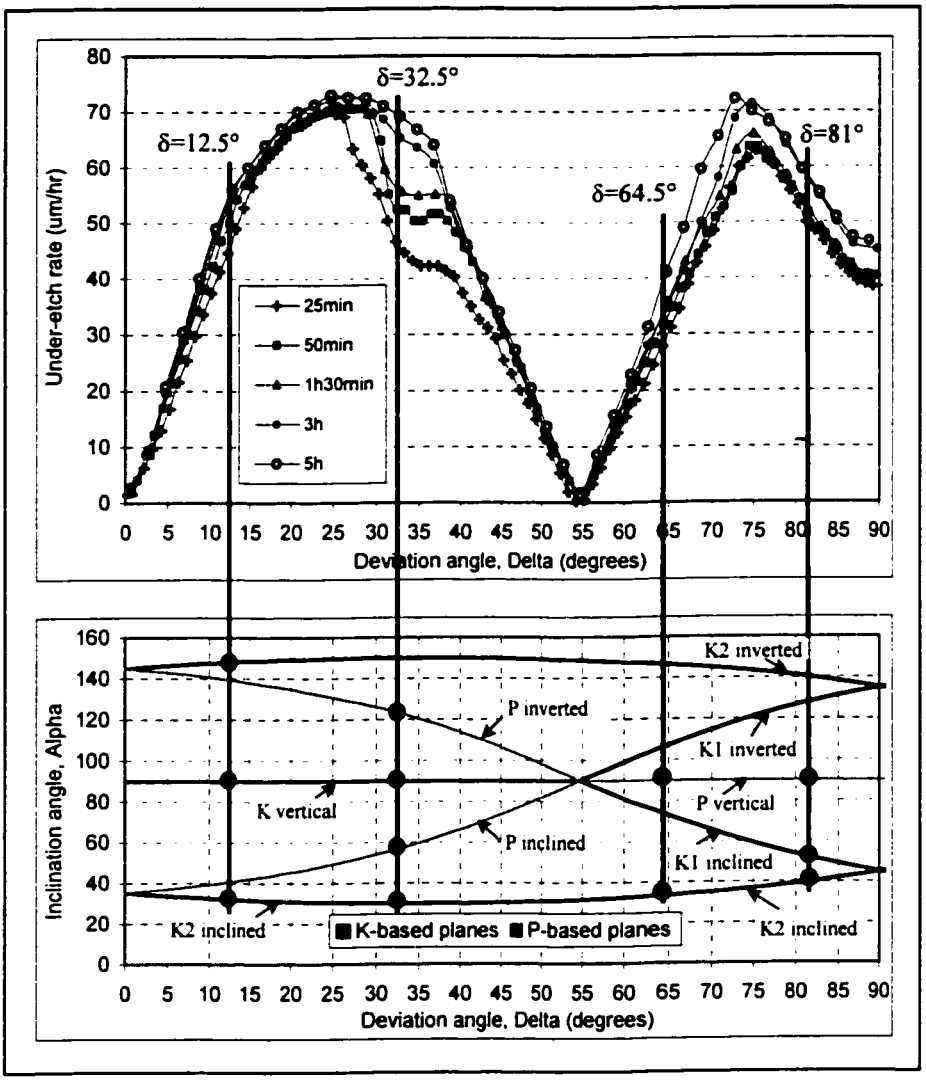

Figure 6-13 : Si{110} 19wt.% TMAH: Under-etch rate curve evolution with time.

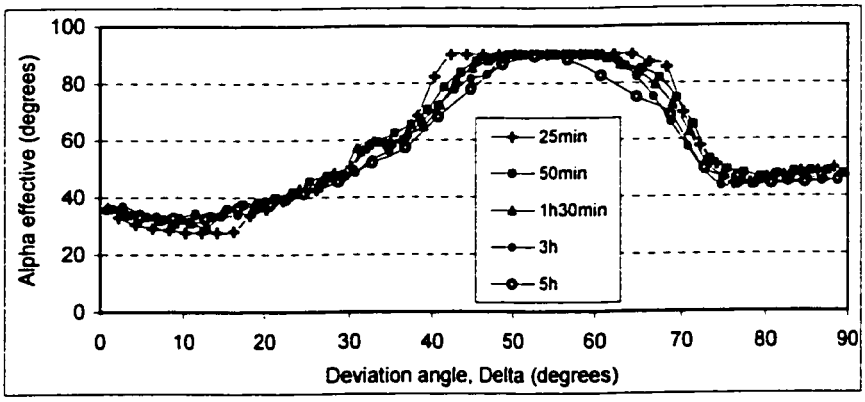

Figure 6-14 : Si{110} 19wt.% TMAH: Evolution with time of the effective inclination angle $\alpha_{effective}$.

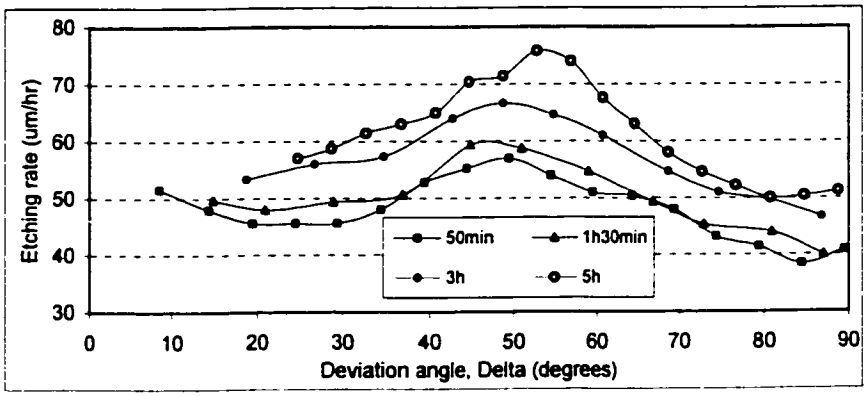

Figure 6-15 : Si{110} 19wt.% TMAH: Bottom surface etch rate evolution with time.

Figure 6-15 shows the etch rate of the bottom surface (measured at the edges of the bottom surface) with respect to the mask deviation angle δ, for etching times from 50min to 5h (other shorter time measurements are not included because they are too noisy). It is observed in Figure 6-15 that the various bottom surface etching rate curves have similar variation with δ, but the etch rates have gradually increased with time. The various curves in Figure 6-15 have a common local maximum around δ=48°, except for the 5h etching curve whose maximum is shifted to δ=52°.The acceleration of the Si{110} bottom surface around δ=48° may be related[10] to interactions between the {110} bottom surface and the $K2_{inclined}$ facet, since the $K2_{inclined}$ facet is present for δ <50° and absent for δ>50°. Figure 6-17 shows the small $K2_{inclined}$ facet which may be responsible for accelerating the {110} bottom etch. The general increase with time of the bottom surface etch rate is suggested to be related to an evolution with time of the Si{110} surface morphology and roughness (Figure 6-16).

Figure 6-16 shows the evolution with time of the Si{110} surface morphology and roughness in 19wt.% TMAH. The X-axis in all pictures is aligned parallel to the orientation of PBCs. The features observed in Figure 6-16 for 10min and 25min etching are depressions that increase in size with time. At 50min etching, protruding structures extending perpendicularly to the direction of PBCs are observed. For longer etching times, the size of the protruding structures have increased. Figure 6-18 schematically illustrates the surface morphology involving the protruding structures. As mentioned earlier, the Si{110} morphology and roughness change, beginning at 50min etching may

[10] See Section 7.2.2.(f) for more analysis.

be related to, or responsible for, the global etch rate acceleration of the Si{110} etch rate curve observed in Figure 6-15.

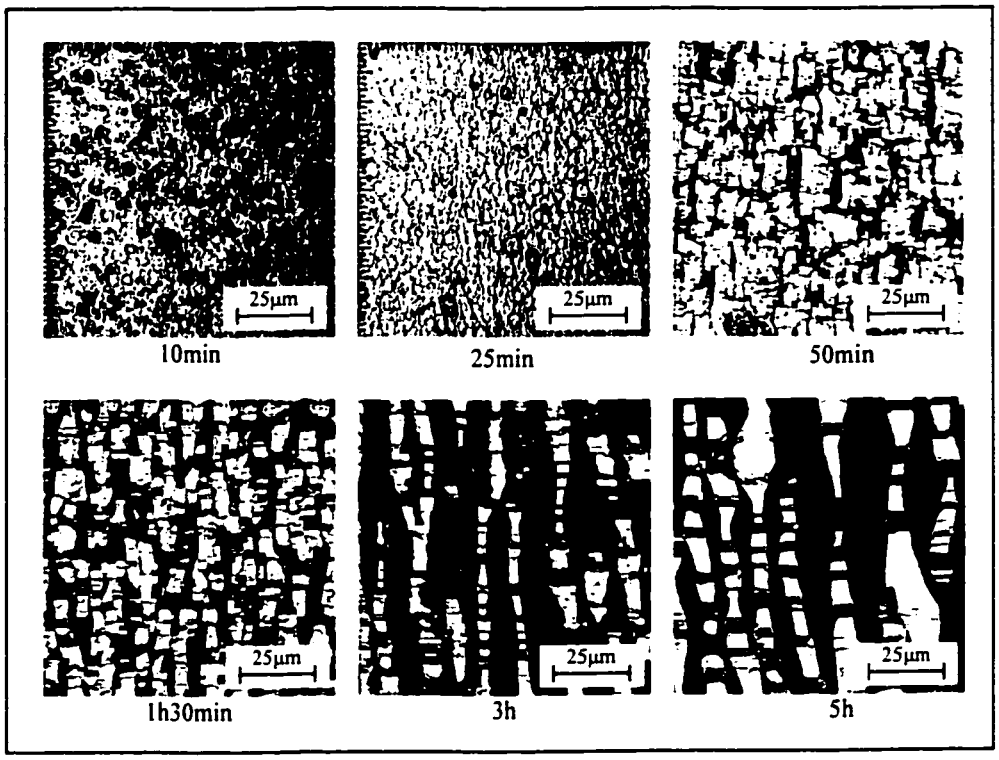

Figure 6-16 : Evolution with time of the Si{110} surface roughness in 19wt.% TMAH.

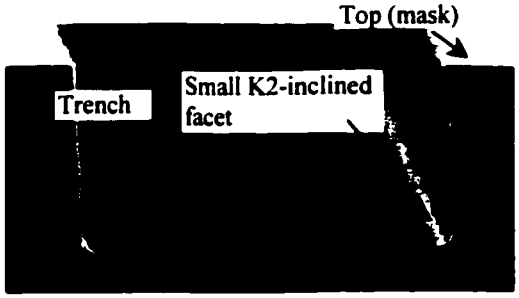

Figure 6-17 : SEM cross-section micrograph of the spoke at δ=46°, showing the small K2-inclined facet which may be responsible for accelerating the {110} bottom etch.

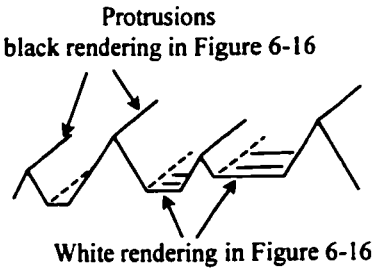

Figure 6-18 : Schematic cross-section of the {110} surface profile.

Figure 6-19 shows the evolution of the Si{110} surface with time at the bottom of a spoke cavity positioned at deviation angle δ=70°. It is observed in Figure 6-19 the presence of trenches on the {110} bottom surface. These trenches grow in width over time, and eventually meet (between 3h and 5h) in the center of the cavity. The roughness

visible in the trenches is aligned parallel to the direction of PBCs on the {110} surfaces (aligned to cross the trenches obliquely). The fact that trenches have met for the 3h and 5h samples may be related to, or responsible for, the acceleration of the corresponding under-etch rate curves in Figure 6-13 for $\delta > 54.74°$.

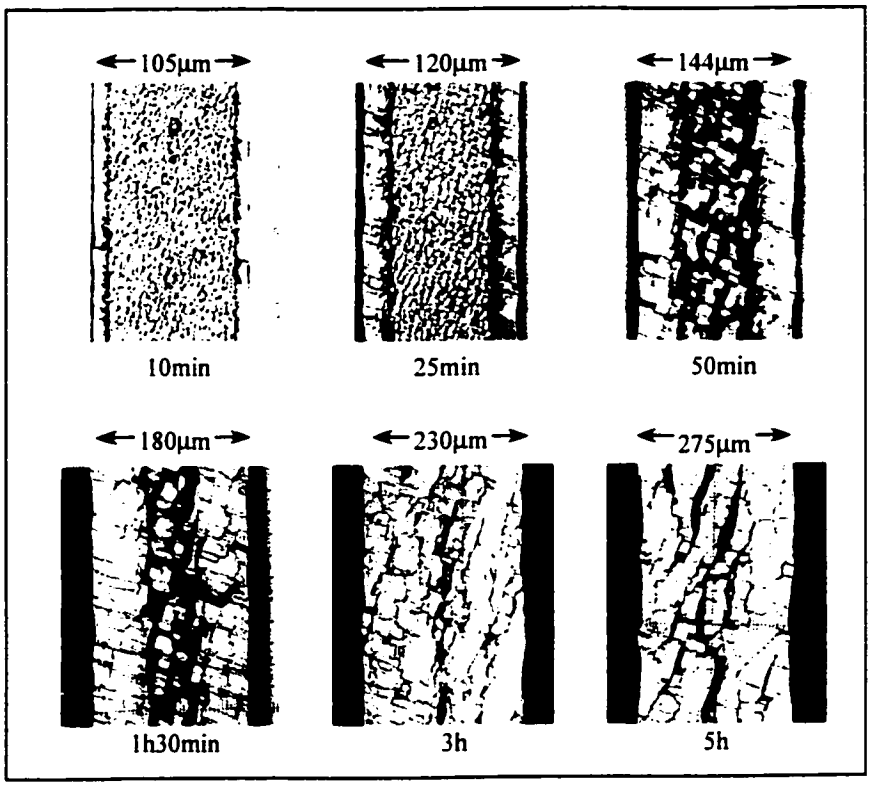

Figure 6-19 : Evolution with time of the Si{110} surface roughness at the bottom cavity at δ=70°.

6.2 Extraction of P-based and K-based canonical curves

The objective of this section is to apply the etching model of Chapter 3, Section 3.3, to the experimental results presented in the previous Section 6.1. The 1h30min etching samples, for both orientations, are chosen to construct the canonical P-based and K-based etch rate curves (for 25wt% and 19wt% TMAH). To do so, the experimental under-etch rate curves of the samples etched for 1h30min in 25wt% and 19wt% TMAH are first drawn and compared. Then, portions of these experimental under-etch rate curves are exported and compared at common values of rotation angle θ for the estimation of the canonical P-based and K-based curves.

The results of these transformations and constructions (the canonical curves) are used in the next Section 6.3.1: from these P-based and K-based canonical curves, "ideal" under-etch profiles are constructed in Section 6.3.1 for comparison with corresponding experimental SEM pictures.

6.2.1 Concentration comparison of under-etch rate curves

Figure 6-20 shows a comparison (between 25wt.% and 19wt.%) of the experimental under-etch rates for the Si{100} samples etched for 1h30min. The 25wt.% curve is imported from Figure 6-1, whereas the 19wt.% curve is imported from Figure 6-10.

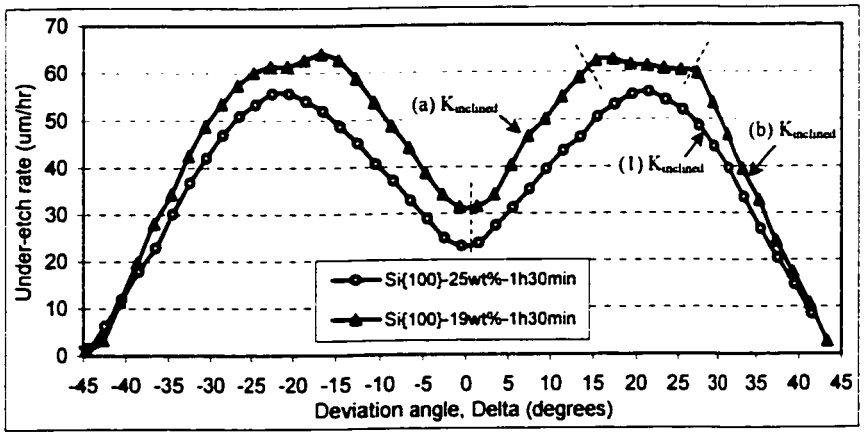

Figure 6-20 : Under-etch rate comparison between Si{100} samples etched 1h30min in 25wt% and 19wt.% TMAH.

It is observed in Figure 6-20 that the 19wt.% curve is above the 25wt.% curve, suggesting that the etching rate of K-based planes increases with decreasing TMAH concentration from 25wt.% to 19wt.%, consistent with the findings of other researchers, as outlined in Chapter 2 regarding Sato *et al* [6]. Notice the lettered and numbered portions in Figure 6-20: these are exported to Figure 6-22 (curve numbered (1)) or Figure 6-23 (curves lettered (a) and (b)) for comparison with other K-based series. The portion of the 19wt.% curve for δ from 17° to 27° is not exported to Figure 6-23 (too large a difference from the crystal-feature-based model).

Figure 6-21 shows a comparison (between 25% and 19wt%) of the experimental under-etch rates for the Si{110} samples etched for 1h30min. The 25wt.% curve is imported from Figure 6-4, whereas the 19wt.% curve is imported from Figure 6-13. It is observed in Figure 6-21 that the portion (f) of the 19wt.% curve is close to the portion (4) of the 25wt.% curve, suggesting that the etching rate of P-based planes is maintained roughly constant over this decrease in TMAH concentration, whereas all other portions of the 19wt.% corresponding to K-based planes are well above the 25wt.% curve.

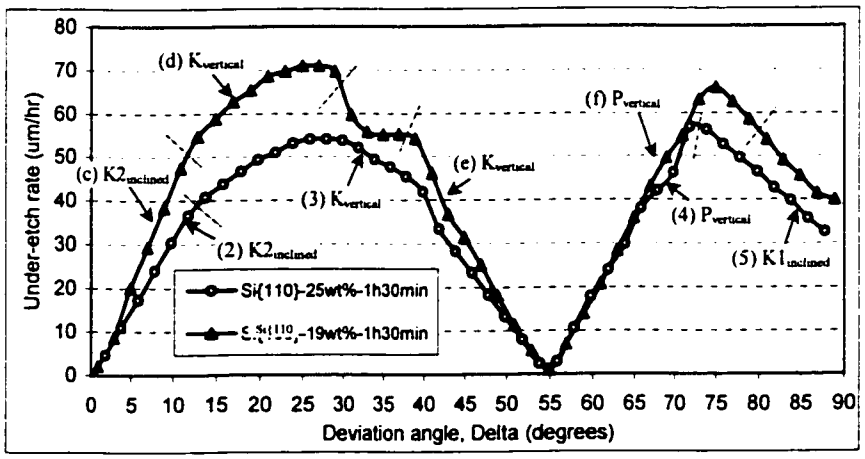

Figure 6-21 : Under-etch rate comparison between Si{110} samples etched 1h30min in 25wt% and 19wt.% TMAH.

6.2.2 P-based and K-based etch rate extraction

Using the methodology detailed in Section3.3.2, the numbered portions (lettered portions, respectively) of Figure 6-20 and Figure 6-21 are geometrically transformed and exported to Figure 6-22 (Figure 6-23 respectively), (P-based on the left. K-based on the right), for

comparison at common values of rotation angle θ. The {100} surface etching rate measured from the etched depth measurements on Si{100} are also included in Figure 6-22 and Figure 6-23 and correspond to the etching rate of the K-based series at θ_k=54.74°. In the case of {110} surfaces, no clear etching rate was identified to correspond to the etching rate of the P-based series at θ_p=35.26°. As a result, in Figure 6-22 and Figure 6-23, several values of {110} etching rate are included from many sources:

- because the Si{110} bottom surface etching rate varies with the mask edge deviation angle δ (see in Figure 6-7 and Figure 6-15), the maximum, minimum and average values are included in Figure 6-22 and Figure 6-23.
- In Figure 6-23, the measure of the {110} etching rate at a wide open area in the mask (representing an area having a large, nominally infinite size) is also included.

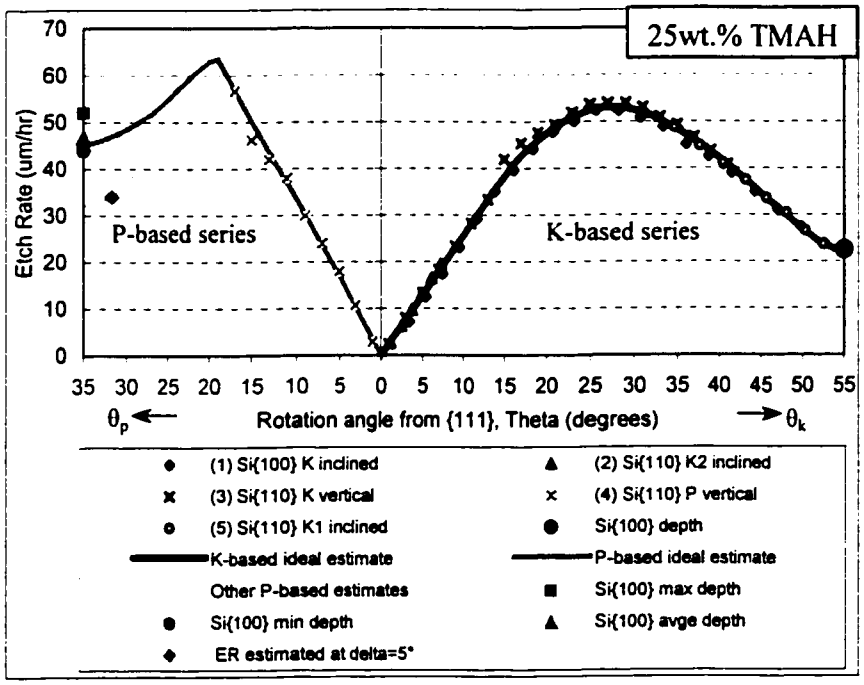

Figure 6-22 : Estimates of the canonical etch rate of P-based series and K-based series in 25wt.% TMAH (the estimations are drawn by comparison of imported portions (numbered) of Figure 6-20 and Figure 6-21).

- A near-{110} etching rate was also estimated from the size of the P-based inclined facet at δ=5°. Figure 6-24 and Figure 6-25 show the SEM micrographs corresponding to Si{100} etched for 1h30min in 25wt.% and 19wt.%, respectively. At δ=5°, the P-

based inclined facet is close to a {110} that is δ=0°. Using Figure 6-24 and Figure 6-25, one can estimate, by reconstructing the profile of the under-etch, the etching rate of the P-based inclined facet (at δ=5°). The rotation angle (needed for plotting the $P_{inclined}$ etch rate in Figure 6-24 and Figure 6-25) corresponding to the P-based inclined facet is θ_p=31.7°.

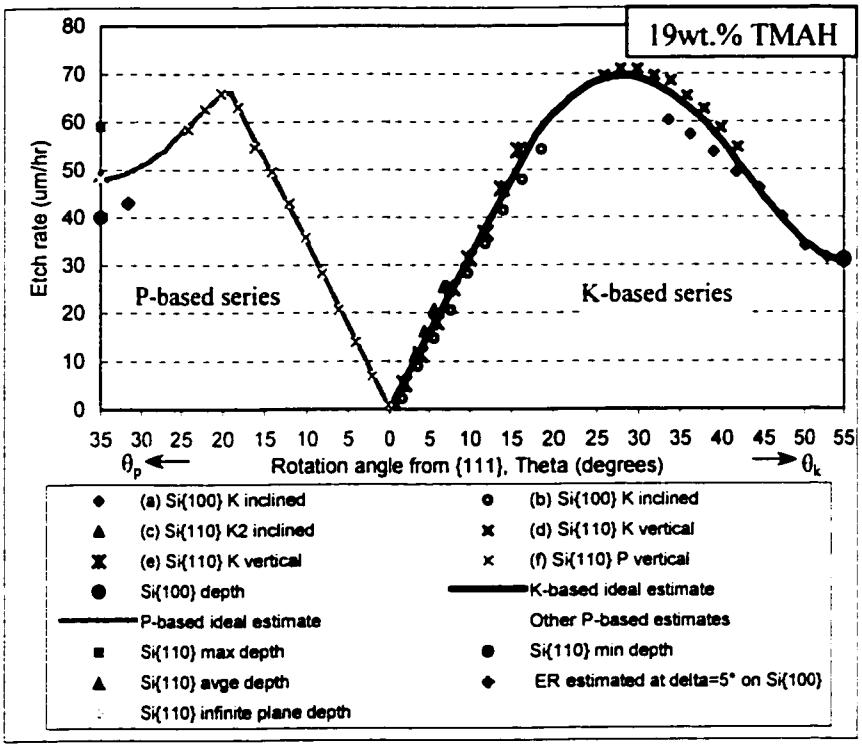

Figure 6-23 : Estimates of the canonical etch rate of P-based series and K-based series in 19wt.% TMAH (the estimations are drawn by comparison of imported portions (lettered) of Figure 6-20 and Figure 6-21)

Including all these values of {110} surface etching rate in Figure 6-22 and Figure 6-23 is necessary because the P-based series that are exported from Figure 6-21 to Figure 6-22 and Figure 6-23 do not cover the range of θ close to θ_p=35°, and thus do not help enough in estimating the P-based canonical curve.

In Figure 6-22 and Figure 6-23, solid lines representing the *estimated canonical etch rate curves* of P-based and K-based series have been drawn through the experimental data. Light lines have also been drawn to show other estimates of the P-based canonical etch rate which would be in effect if the {110} etch rate was estimated from one of the other sources of {110}ER.

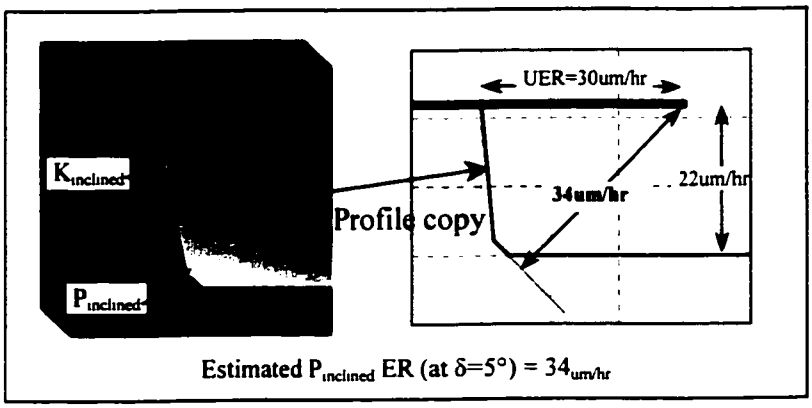

Figure 6-24 : 25wt.% estimation of a near-{110} etch rate from the size of the $P_{inclined}$ facet from a cross-section SEM taken on Si{100} at δ=5° for 25wt% ,1h30min etching.

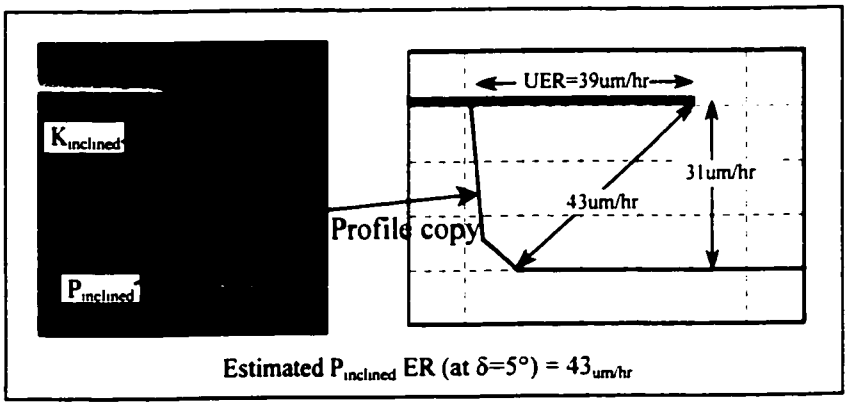

Figure 6-25: 19wt% estimation of a near {110} etch rate from the size of the $P_{inclined}$ facet from a cross-section SEM taken on Si{100} at δ=5° for 19wt% ,1h30min etching.

It is noteworthy to compare Figure 6-22, which corresponds to *stirred* experiments, to Figure 3-26 which corresponds to experiments at the same etchant concentration (25wt.%) but *unstirred:* the stirred experiments result in K-based series that coincide much better once exported for comparison at common values of θ.

6.2.3 Concentration comparison of canonical curves

The estimated canonical etch rate curves of P-based and K-based series of Figure 6-22 and Figure 6-23 are exported to Figure 6-26 for concentration comparison It is observed in Figure 6-26 that the etch rate of the K-based series substantially increases with

decreasing concentration from 25wt.% to 19wt.% whereas the etch rate of P-based series varies only slightly. This result explains the high variations of the under-etch profile when P-based and K-based planes are present at a given mask edge deviation angle.

From the canonical curves of Figure 6-26, ideal under-etch profiles are constructed for comparison with the SEM micrographs presented in Section below 6.3.

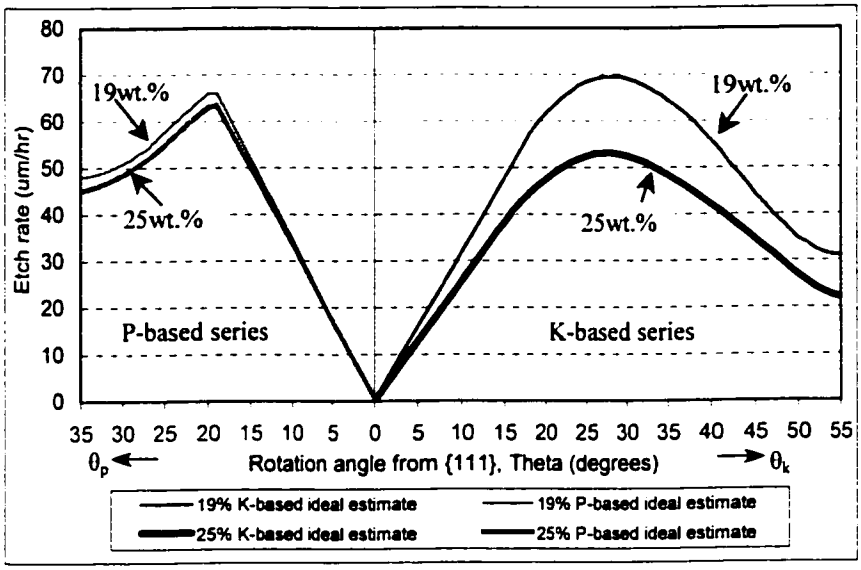

Figure 6-26 : Comparison of the canonical P-based series and K-based series estimates for 25wt.% and 19wt.% TMAH

6.3 Scanning Electron Micrographs

6.3.1 Si{100} 25wt.% TMAH

a) Si{100} 25wt.% TMAH, $\delta = 5°$

Figure 6-28 shows the evolution with time of the under-etch profile at deviation angle $\delta \approx 5°$. The under-etch profile (illustrated in Figure 6-27-(a)) is composed of two under-etch facets:

- The top-most facet is a near vertical K-based facet (belongs to an inclined K-based series) on which the K-rows are oriented $\gamma \approx 45°$ (in agreement with Figure 4-2). This K-based facet etches at a constant rate as discussed in Figure 6-1 (constant under-etch rate curve).
- The lower facet is a P-based inclined facet with an inclination angle $\alpha \approx 45°$.

Figure 6-27-(b) shows the ideal under-etch profile constructed from the canonical curve in Figure 6-26. Note that this crystal-feature-based model predicts that the $P_{inclined}$ facet should etch too fast to appear at all on the under-etched surface. Figure 6-27-(b) represents this by the location of the line labelled P_{inc}.

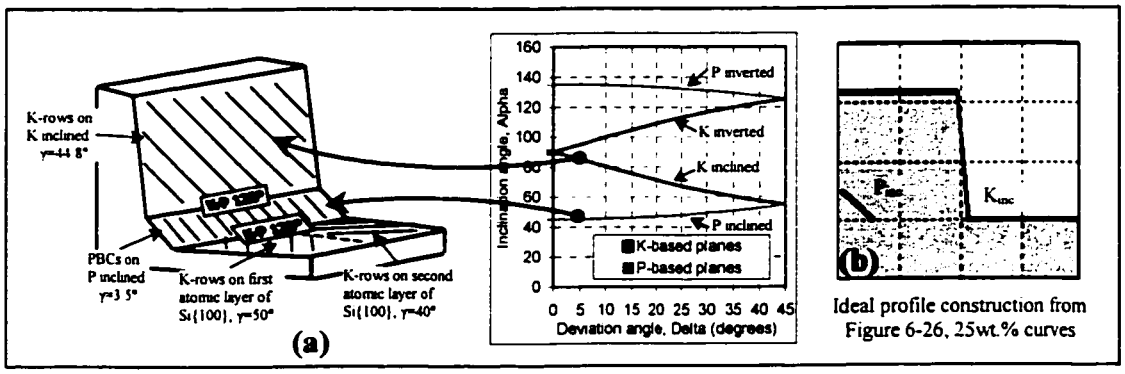

Figure 6-27 : (a) Correspondence between under-etched facets at $\delta = 5°$ and ideal inclination angles; (b) Ideal profile construction.

It is observed in Figure 6-28 that the P-based facet increases in size for etching times from 10min to 50min then decreases in size and almost disappears for etching times from 50min to 5h. The surface roughness of the P-based facet is aligned with the orientation of

PBCs. Noteworthy structures aligned with PBCs appear (see 3h and 5h etches) as the P-inclined facet tends toward disappearance.

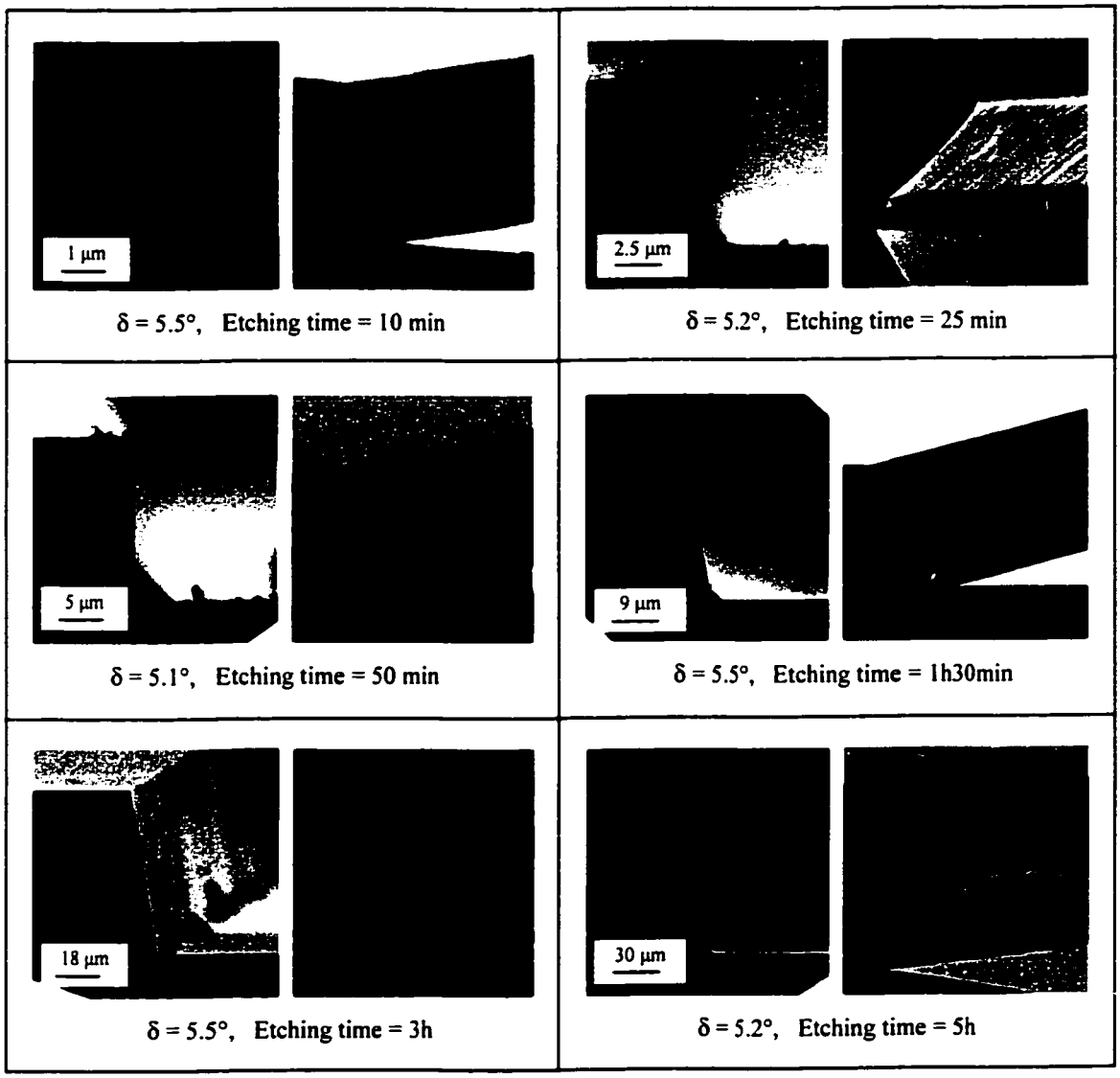

Figure 6-28 : Evolution with time of the under-etch profile at deviation angle δ≈5° in Si{100} 25wt%

Because the etch rate of the K-based facet is evidently constant after the first 10 minutes (seen in Figure 6-1) , the evolution with time of the relative size of the K-based and the P-based facets seen in Figure 6-28, is attributed to an anomalous variation of the etch rate

specifically of the P-based inclined facet[11]. This anomalous variation is all the more important since the crystal-feature-based model in 25wt% TMAH (Figure 6-27-(b) and Figure 3-31) predicts that the P-based inclined facet *should not appear at all*. Thus, by comparison with the crystal-feature-based model, the etch rate of the P-based facet appears to be dramatically reduced, for etching times up to 50 min. Then it accelerates and tends to toward the ideal model.

The anomalous etch rate variation of the P-based facet may be hypothesized to be due to effects[12] taking place at one or both of the two junctions ($K_{inclined}$-$P_{inclined}$) and ($P_{inclined}$ - {100} bottom surface).

b) Si{100} 25wt.% TMAH, $\delta = 21°$

Figure 6-30 shows the evolution with time of the under-etch profile at deviation angle $\delta \approx 21°$, corresponding to the deviation angle at which the under-etch curve in Figure 6-1 is at a maximum. The under-etch profile (illustrated in Figure 6-29-(a)) is composed of the same K-based and P-based inclined series as in the previous sub-section (a). Figure 6-29-(b) shows the ideal under-etch profile constructed from the canonical curve in Figure 6-26. Note again that the crystal-feature-based model predicts that the $P_{inclined}$ facet should etch too fast to appear as part of the under-etched surface.

Notice in Figure 6-30 the presence of a very small inverted facet at the top of the under-etch profile. It is observed in Figure 6-30 that the P-based inclined facet increases in size for etching times from 10min to 50min, then decreases in size and completely disappears for etching times from 50min to 5h. Similarly to the previous section (δ=5°), boundary effects at the two junctions ($K_{inclined}$-$P_{inclined}$) and ($P_{inclined}$ -{100} bottom surface) are hypothesized to be responsible for the etching rate variation with time of the $P_{inclined}$ facet.

---

[11] While the etch rate of the P-based facet has not been directly measured in this work, there can be no doubt that it is varying with etch time, since the large near-vertical facet and the cavity-bottom are maintaining constant etch rates (from 25min on).

[12] See Section 7.2.2.(a) for more analysis.

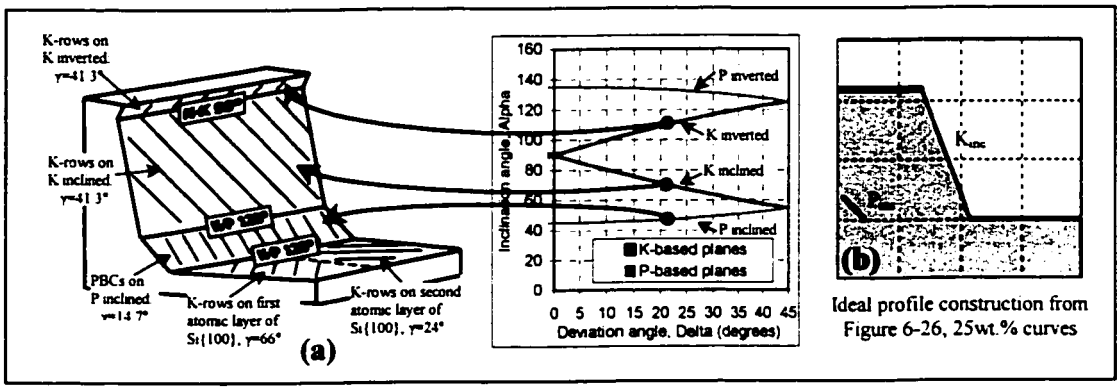

Ideal profile construction from Figure 6-26, 25wt.% curves

Figure 6-29 : (a) Correspondence between under-etched facets at δ=21° and ideal inclination angles; (b) Ideal profile construction.

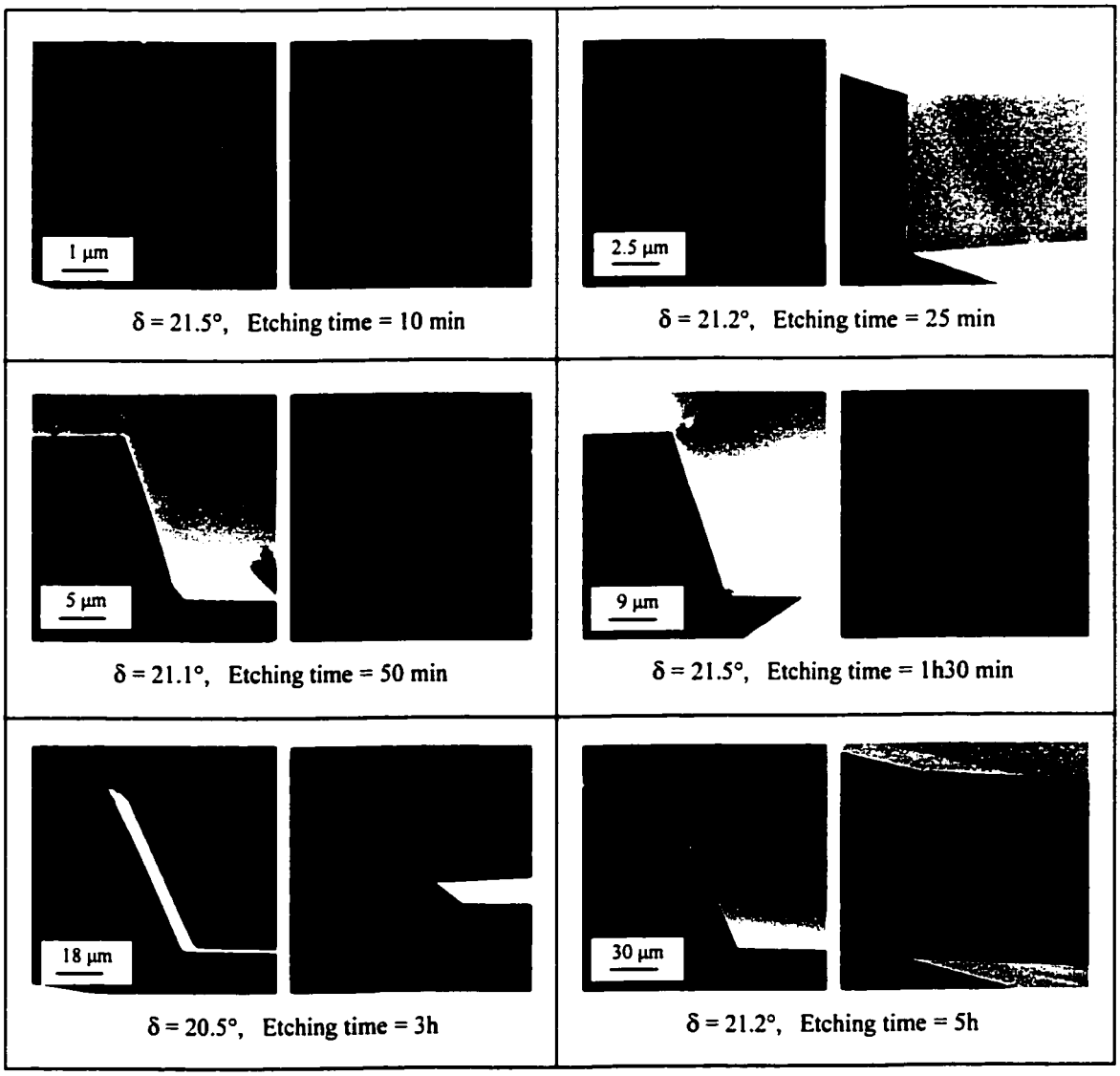

Figure 6-30 : Evolution with time of the under-etch profile at deviation angle δ≈21° in Si{100} 25wt%.

c) Si{100} 25wt.% TMAH, $\delta = 37°$

Figure 6-32 shows the evolution with time of the under-etch profile at deviation angle $\delta \approx 37°$. The under-etch profile (illustrated in Figure 6-31-(a)) is composed of a K-based inclined facet and its symmetrically (with respect to the horizontal surface) K-based inverted facet. Note again that the crystal-feature-based model predicts that the $P_{inclined}$ facet should etch too fast to appear as part of the under-etched surface. However, the relative etch rates are much closer, such that the appearance of the $P_{inclined}$ facet in Figure 6-32-(50min) is not dramatically non-ideal. Figure 6-31-(b) shows the ideal under-etch profile constructed from the canonical curve in Figure 6-26.

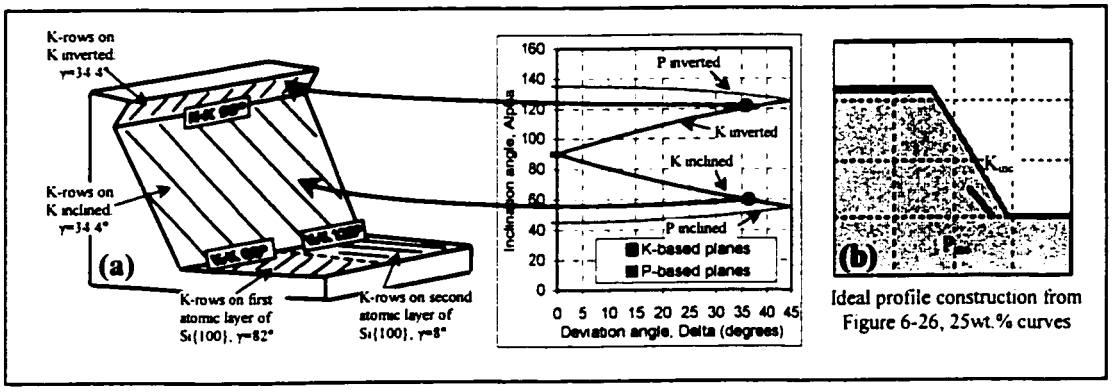

Figure 6-31: (a) Correspondence between under-etched facets at $\delta=37°$ and ideal inclination angles; (b) Ideal profile construction.

It is observed in Figure 6-32 that in the range of 10min to 5h etching time, the inverted facet has a *constant relative size* compared to the size of the inclined facet. Consequently the inverted plane etching rate is constant at a value lower than the constant etch rate of the K-based inclined plane.

The fact that the inverted planes etch more slowly than inclined planes is demonstrated in Section 4.3.1. (Figure 4.18) and is hypothesized to be due to the fact that the junction between the pair of planes blocks the zipping of chains from one facet to the next (Section 4.3.2. explores in more detail this hypothesis through etching simulations).

Notice also that the roughness of the two under-etched K-based planes in Figure 6-32 is different. Each plane is faceted with the appearance of macrosteps (with several microns

height, thus several thousand atoms) propagating along {111} planes. The spacing of steps on the inverted facet is in all cases wider than on the main (inclined) facet (Figure 6-32-(3h)).

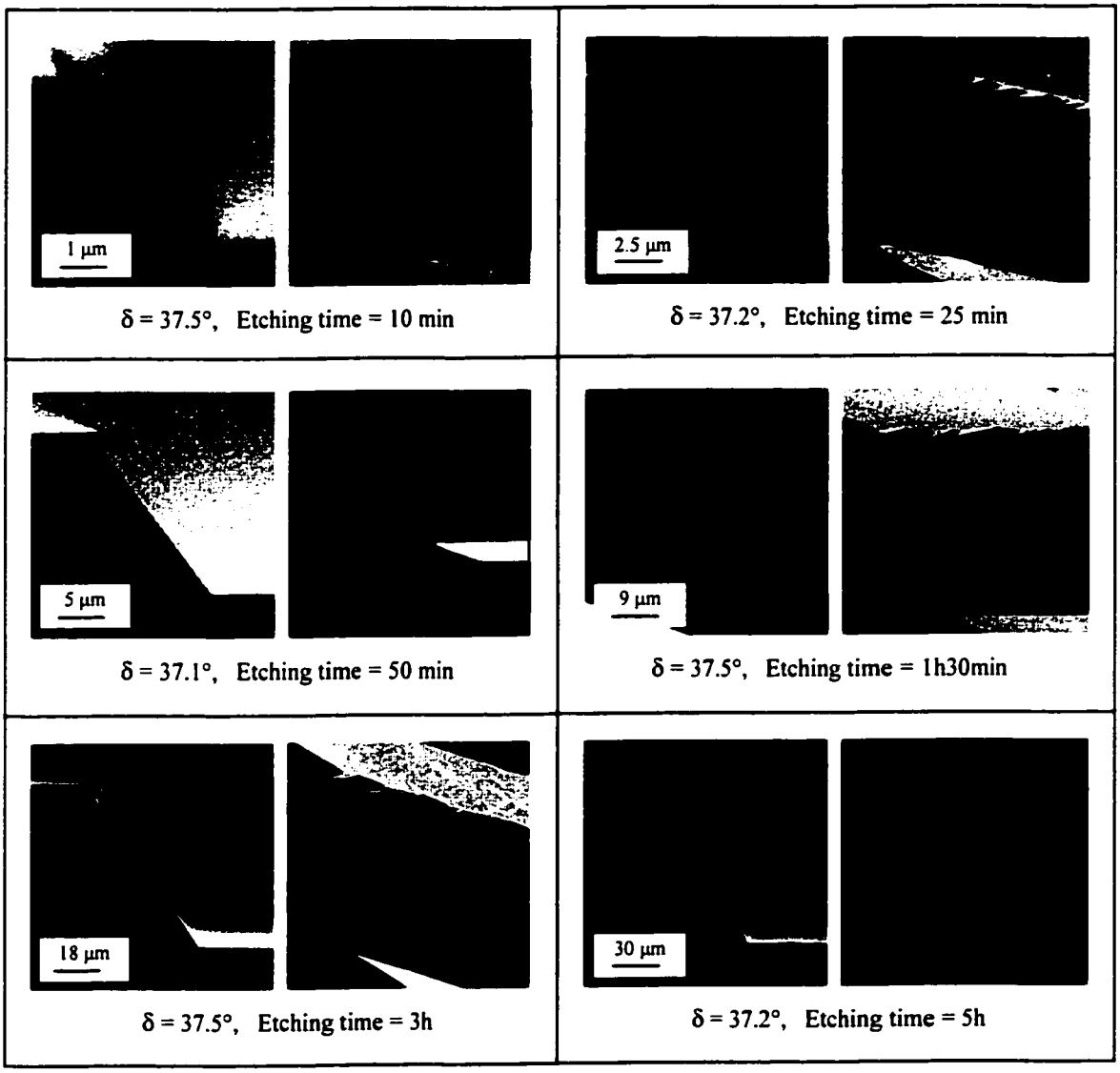

Figure 6-32 : Evolution with time of the under-etch profile at deviation angle δ≈37° in Si{100} 25wt%

6.3.2 Si{110} 25wt.% TMAH

a) Si{110} 25wt.% TMAH, $\delta = 12°$

Figure 6-34 and Figure 6-35 show the evolution with time of the under-etch profile at deviation angle $\delta \approx 12°$. The under-etch profile (illustrated in Figure 6-33-(a)) is composed of a large K-based inclined facet ($K2_{inclined}$) and its very small inverted partner ($K2_{inverted}$), expect for the 5h etching sample where a small vertical K-based plane ($K_{vertical}$) appears as a top facet. Figure 6-33-(b) shows the ideal under-etch profile constructed from the canonical curve in Figure 6-26. Note that the crystal-feature-based model predicts that the $K_{vertical}$ facet should etch too fast to appear as part of the under-etched surface. However, the relative etch rates are much closer, such that the appearance of the $K_{vertical}$ facet in Figure 6-34-(5h) is not dramatically non-ideal.

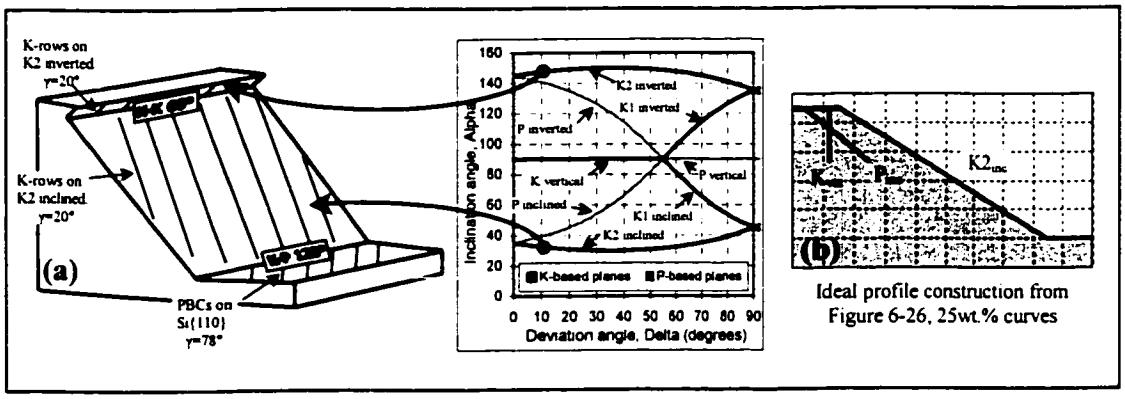

Figure 6-33 : (a) Correspondence between under-etched facets at δ=12° and ideal inclination angles; (b) Ideal profile construction.

It is observed in Figure 6-34 and Figure 6-35 for all SEM side-view micrographs (right side micrographs) that the directional lines (aligned with K-rows) on the $K2_{inclined}$ facets are more regular for the top-most 3/4 of the facet surface than they are for the remaining (lower) 1/4 of the facets. This surface roughness change close to the bottom edge of the facet is suggested to be due to interactions between the $K2_{inclined}$ facet and the bottom {110} surface (for 10min and 25 min samples) or between the $K2_{inclined}$ facet and the $K2_{inclined}$ facet of the other side of the spoke whenever the cavity bottom surface has disappeared (for 50 min 5h etching samples).

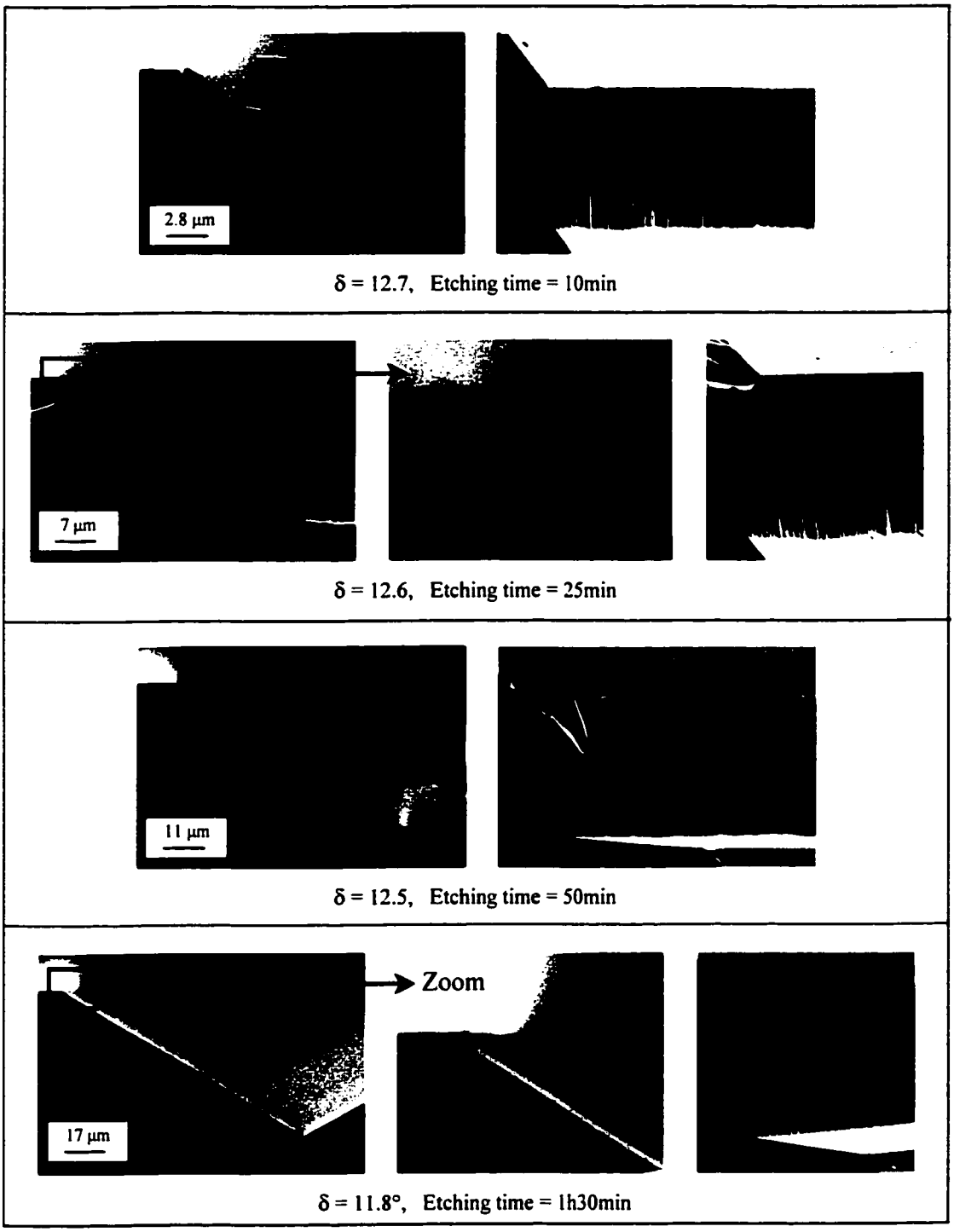

Figure 6-34 : Evolution with time (10min to 1h30min) of the under-etch profile at deviation angle δ≈12° in Si{110} 25wt%

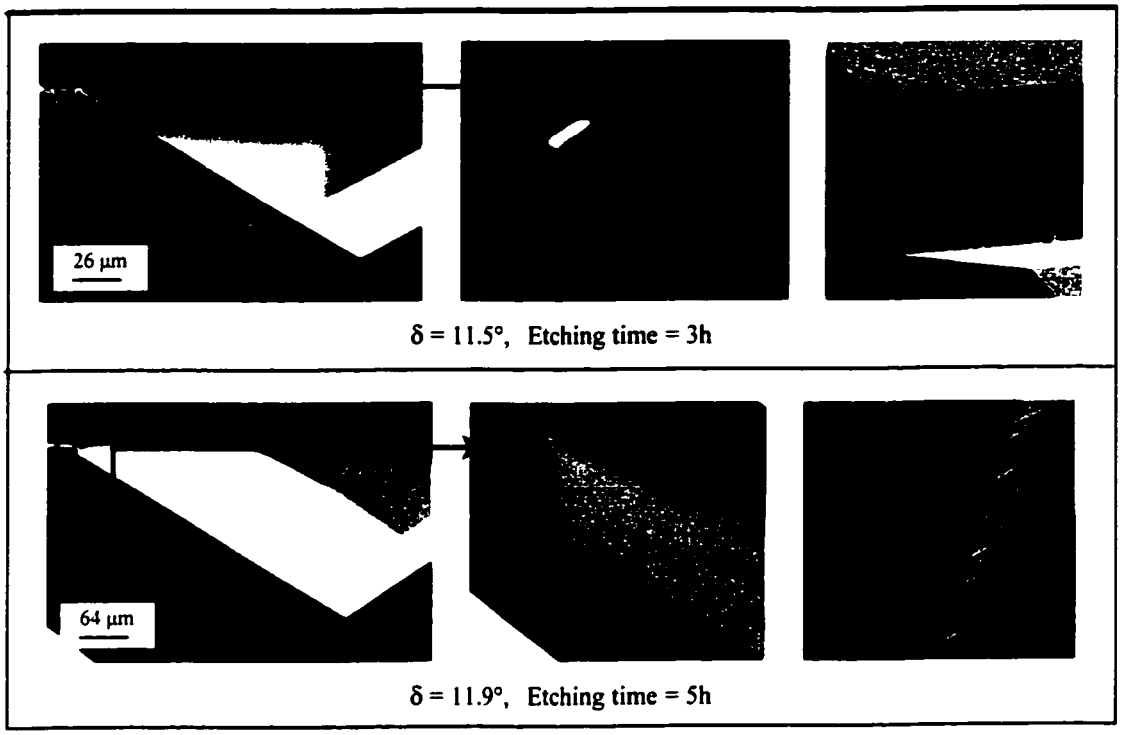

Figure 6-35 : Evolution with time (3h and 5h) of the under-etch profile at deviation angle δ≈12° in Si{110} 25wt%

b) Si{110} 25wt.% TMAH, δ = 39.5°

Figure 6-37 shows the evolution with time of the under-etch profile at deviation angle δ≈39.5°. The under-etch profile (illustrated in Figure 6-36-(a)) is composed of three facets: the top-most facet of the under-etch is a relatively large K-based vertical facet ($K_{vertical}$), the middle facet is a P-based inclined plane ($P_{inclined}$) and the lowest facet is a $K2_{inclined}$ plane. Figure 6-36-(b) shows the ideal under-etch profile constructed from the canonical curve in Figure 6-26. Note that this crystal-feature-based model predicts that the $P_{inclined}$ facet may appear but should remain small, which coincides with the experimental results of Figure 6-37.

Notice in Figure 6-37 that the $K_{vertical}$ facet appears to have a gentle smooth "waviness" except for the 5h etching sample where it is multifaceted (composed of more-clearly visible stepped {111} planes). Notice on the $K_{vertical}$ facet for the 10min and 25min etching the interesting features that seem to be a peeling process originating from the junction between the mask and the $K_{vertical}$ facet.

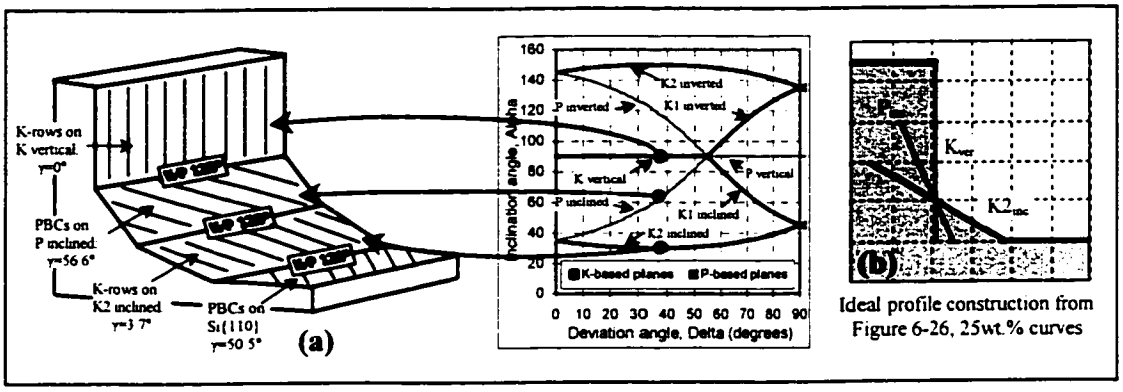

Figure 6-36 : (a) Correspondence between under-etched facets at δ=39.5° and ideal inclination angles; (b) Ideal profile construction.

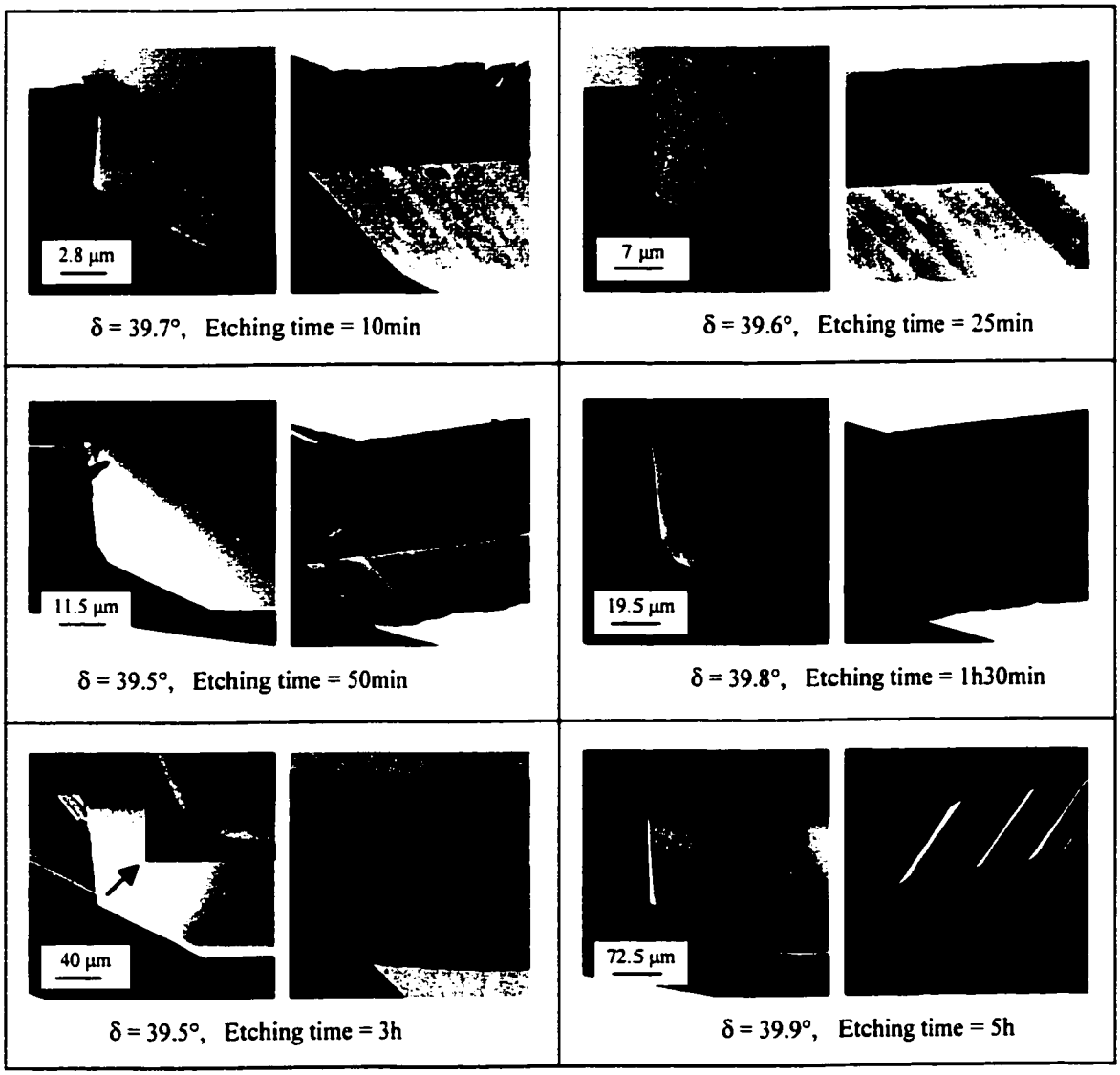

Figure 6-37 : Evolution with time of the under-etch profile at deviation angle δ≈39.5° in Si{110} 25wt%

The peeling process is hypothesized to be due to "nucleations from the mask", which are a possible explanation to the anomalous shape (above what the crystal-feature-based model would predict) of all under-etch rate curves in Figure 6-4 at δ=35°-42°. For better clarity, Figure 6-38 shows two curves of Figure 6-4 (1h30m and 3h) involving the anomalous increase in under-etch rate of the $K_{vertical}$ facet compared to the step flow model. Notice in Figure 6-37-(5h) that the $P_{inclined}$ facet has disappeared which may be related to the multifaceted aspect of the $K_{vertical}$ facet.

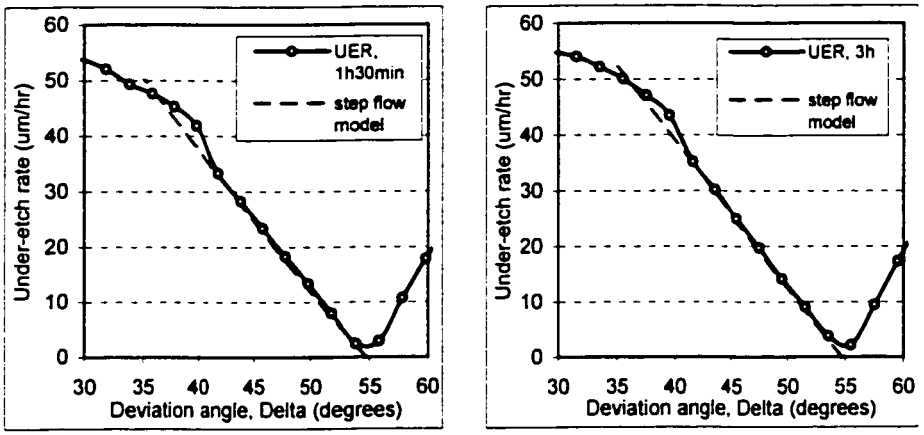

Figure 6-38 : Anomalous shape around δ=39.5° for two UER curves (1h30min and 3h) of Figure 6-4.

c) Si{110} 25wt.% TMAH, δ = 64°

Figure 6-40 shows the evolution with time of the under-etch profile at deviation angle δ≈64°. The under-etch profile (illustrated in Figure 6-39-(b)) is composed of a P-based vertical facet (top-most facet) $P_{vertical}$ and a K-based inclined facet $K2_{inclined}$ (lowest facet). Figure 6-39-(a) shows the ideal under-etch profile constructed from the canonical curve in Figure 6-26. Note that this crystal-feature-based model predicts that both $P_{vertical}$ and $K2_{inclined}$ facet should appear, which coincides with the experimental results of Figure 6-40. The crystal-feature-based model also predict that the $K1_{inclined}$ should etch too fast to appear as part of the under-etched surface. However, the relative etch rates are much closer, such that the appearance of the $K1_{inclined}$ facet as a sub-facet inserted between $P_{vertical}$ and $K2_{inclined}$ is not dramatically non-ideal.

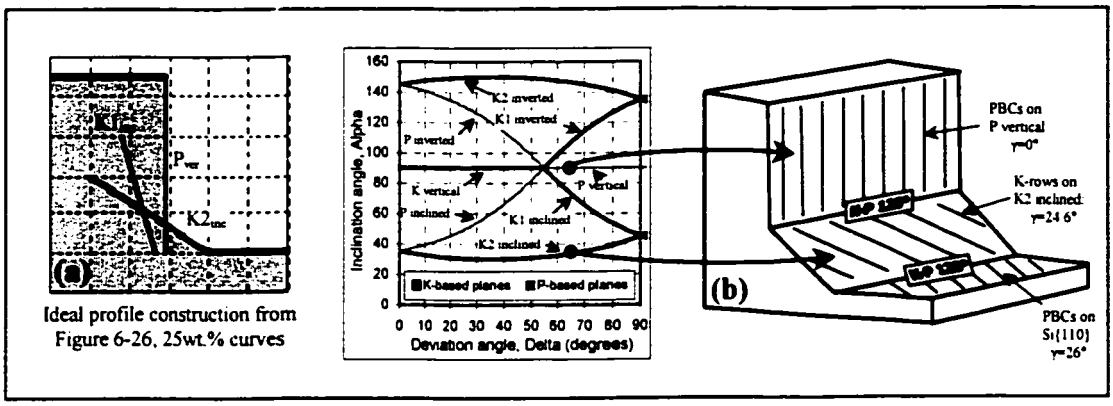

Figure 6-39 : (a) Ideal profile construction; (b) Correspondence between under-etched facets at δ=64° and ideal inclination angles.

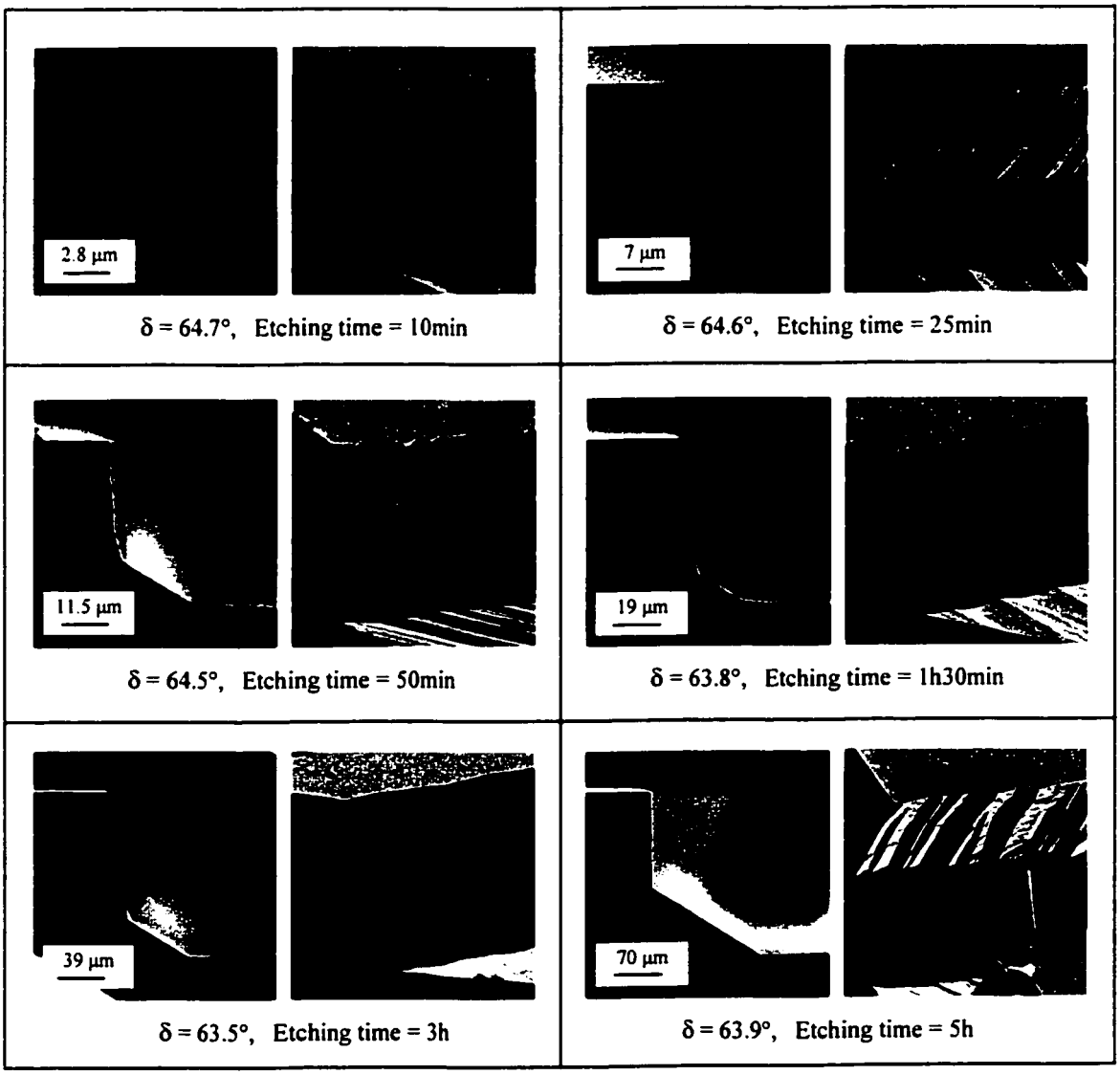

Figure 6-40 : Evolution with time of the under-etch profile at deviation angle δ≈64° in Si{110} 25wt%

It is observed in Figure 6-40 that the $P_{vertical}$ surface is multifaceted composed of alternations of the {111} plane and a fast-etch plane (to be more likely {331}). By viewing the $P_{vertical}$ surface stepped {111} planes, it is seen that the steps spacing as well as the steps height increase with time: the 3h side-view micrograph shows clear macroscopic steps and {111} plane terraces.

In Figure 6-40, the various cross-section micrographs show that the $K2_{inclined}$ facet decreases in size between 10min and 1h30min etching and increases in size between 1h30min and 5h etching. This size evolution of the $K2_{inclined}$ facet is consistent with the variations with time of the effective inclination angle $\alpha_{effective}$ in Figure 6-5 and Figure 6-6. Upon closer inspection of the junction between the $K2_{inclined}$ facet and the $P_{vertical}$, localized flat planes (at the low edge of the $P_{vertical}$ fast-etch sub-facet) are identified as $K1_{inclined}$ planes. It is suggested that the variations of the etch rate of the $K2_{inclined}$ facet may be due to the local growth of the $K1_{inclined}$ sub-facets between the $P_{vertical}$ and the $K2_{inclined}$.

d) Si{110} 25wt.% TMAH , $\delta = 70°$

Figure 6-42 shows the evolution with time of the under-etch profile at deviation angle $\delta \approx 70°$. The under-etch profile (illustrated in Figure 6-41-(b)) is composed of three facets. The top-most facet is a P-based vertical facet, the middle facet is a K-based inclined facet $K1_{inclined}$, and the lowest facet is a K-based inclined facet $K2_{inclined}$. Figure 6-41-(a) shows the ideal under-etch profile constructed from the canonical curve in Figure 6-26. Note that this crystal-feature-based model predicts that the three facets should appear, which coincides with the experimental results of Figure 6-42.

The $P_{vertical}$ facet is composed of small {111} planes and wider fast-etch surfaces. For the 25min, 50min, and 1h30min micrographs in Figure 6-42, the fast-etch surface (part of the $P_{vertical}$ facet) seems to peel from top to bottom as etching proceeds. The peeling process may be explained by a blocked boundary between the fast-etch plane and the lower adjacent facet ($K1_{inclined}$), compared to more probable nucleations at the junction between the fast etch plane and the mask (or a small inverted plane).

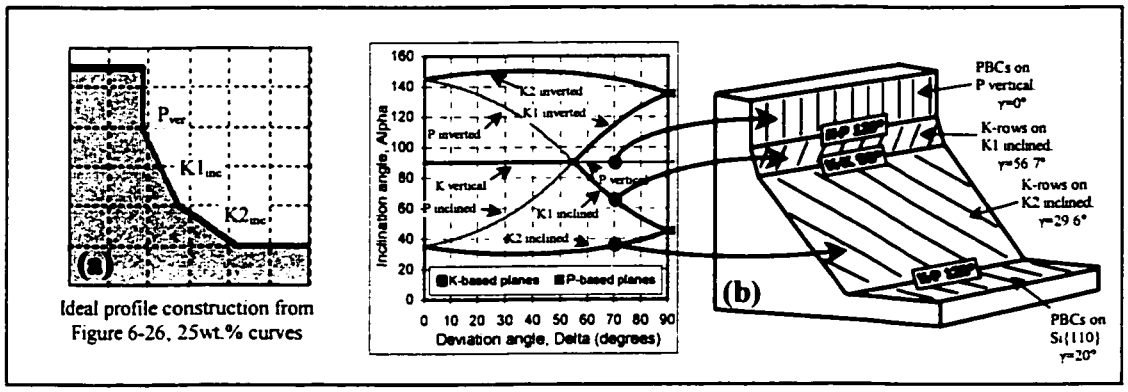

Figure 6-41 : (a) Ideal profile construction; (b) Correspondence between under-etched facets at δ=70° and ideal inclination angles.

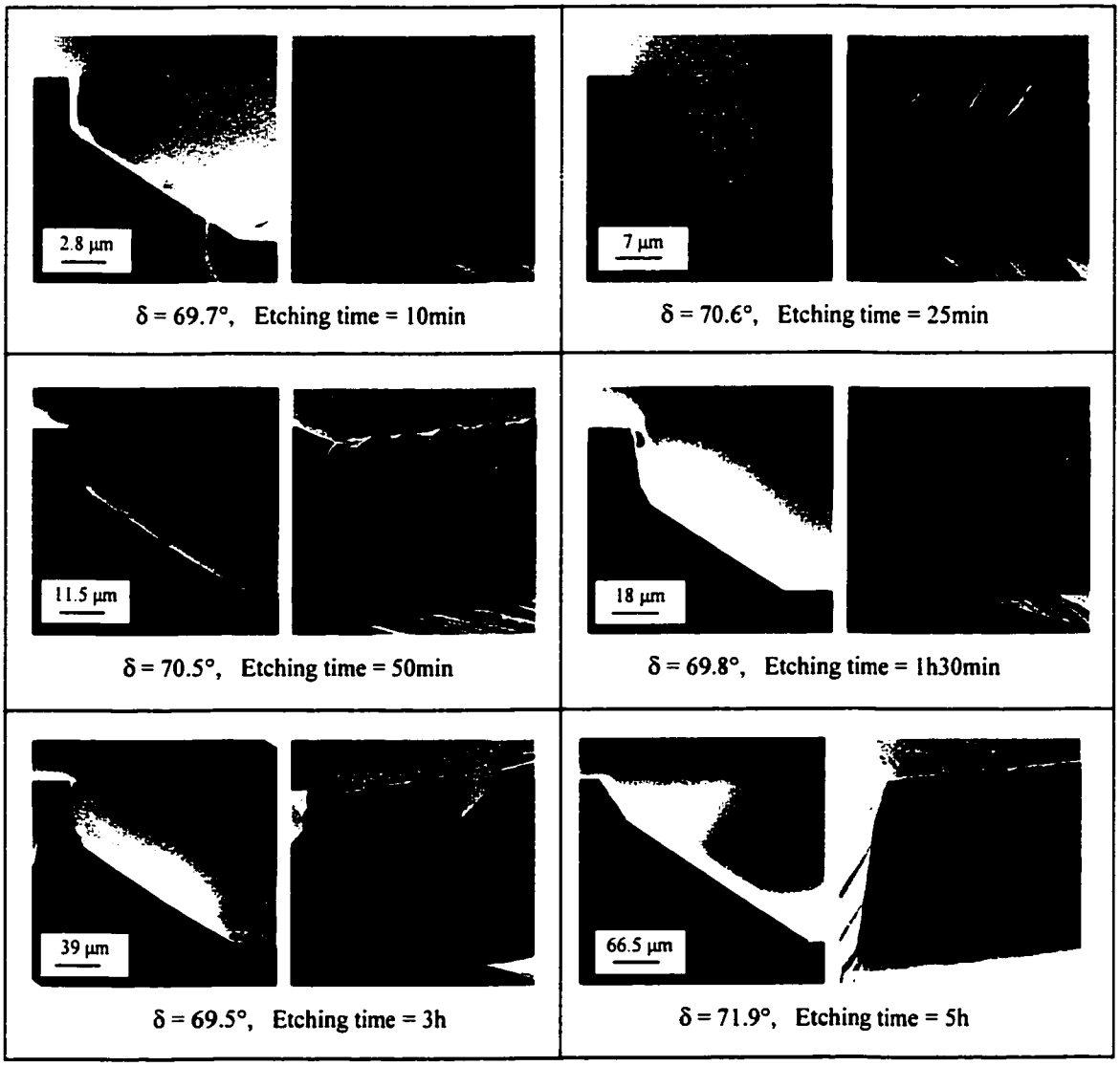

Figure 6-42 : Evolution with time of the under-etch profile at deviation angle δ≈70° in Si{110} 25wt%

Figure 6-43 focuses on the anomalous low under-etch rate around δ=70° observed for two curves (50 min and 1h30min) of Figure 6-4. As shown in Figure 6-43, the anomalous decrease of the etch rate of the $P_{vertical}$ facet is closely related to the presence of the $K1_{inclined}$ facet inserted between $P_{vertical}$ and $K2_{inclined}$ facets.

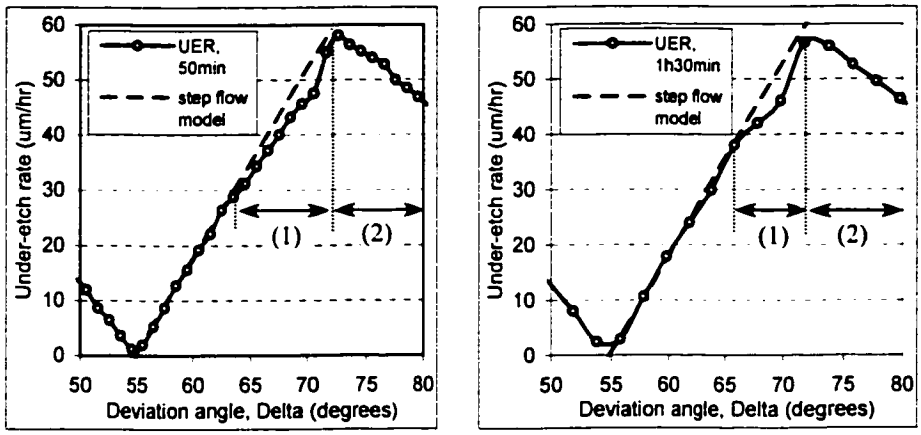

Figure 6-43 : Anomalous shape around δ=70° for two UER curves (50min and 1h30min) of Figure 6-4. (1): range of δ where $K1_{inclined}$ facet emerged as a middle facet between $P_{vertical}$ and $K2_{inclined}$facets. (2) range of δ where $K1_{inclined}$ is the top-most facet ($K2_{inclined}$ is the lowest).

6.3.3 Si{100} 19wt.% TMAH

a) Si{100} 19wt.% TMAH, δ = 5°

Figure 6-45 shows the evolution with time of the under-etch profile at deviation angle δ≈5°. The profile is composed (illustrated in Figure 6-44-(a)) of two under-etched facets: the top-most facet is a near-vertical K-based facet (which belongs to a $K_{inclined}$ series), the lower facet is a P-based inclined facet ($P_{inclined}$) with an inclination angle α≈45°. Figure 6-44-(b) shows the ideal under-etch profile constructed from the canonical curve in Figure 6-26. Note that this crystal-feature-based model predicts that $P_{inclined}$ facet should etch too fast to appear as part of the under-etched surface. However, the relative etch rates are much closer, such that the appearance of the $P_{inclined}$ facet in Figure 6-45 is not dramatically non-ideal. In Figure 6-10, all under-etch rate curves coincide at δ=5°, which demonstrates that the $K_{inclined}$ facet etches at a constant rate. However the etch rate of the $P_{inclined}$ facet is varying with time, indeed it is observed in Figure 6-45 that the size of the P-based plane is very unstable with time.

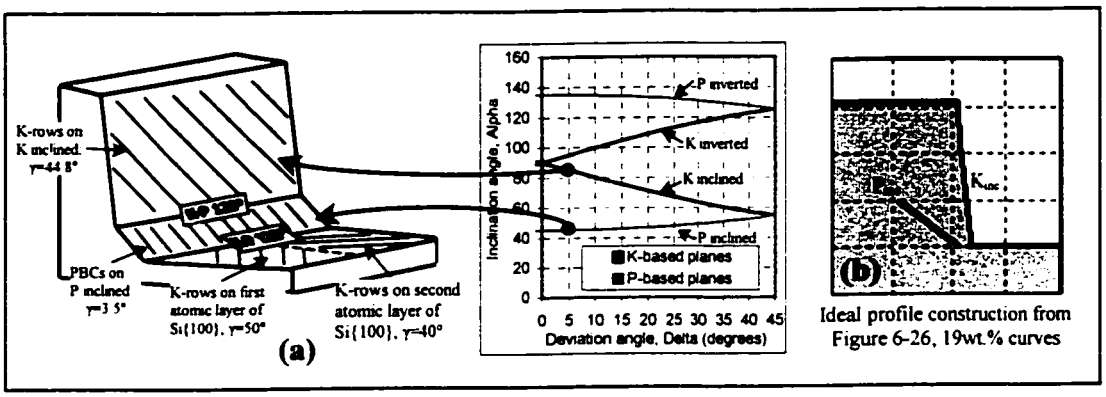

Figure 6-44 : (a) Correspondence between under-etched facets at δ=5° and ideal inclination angles; (b) Ideal profile construction.

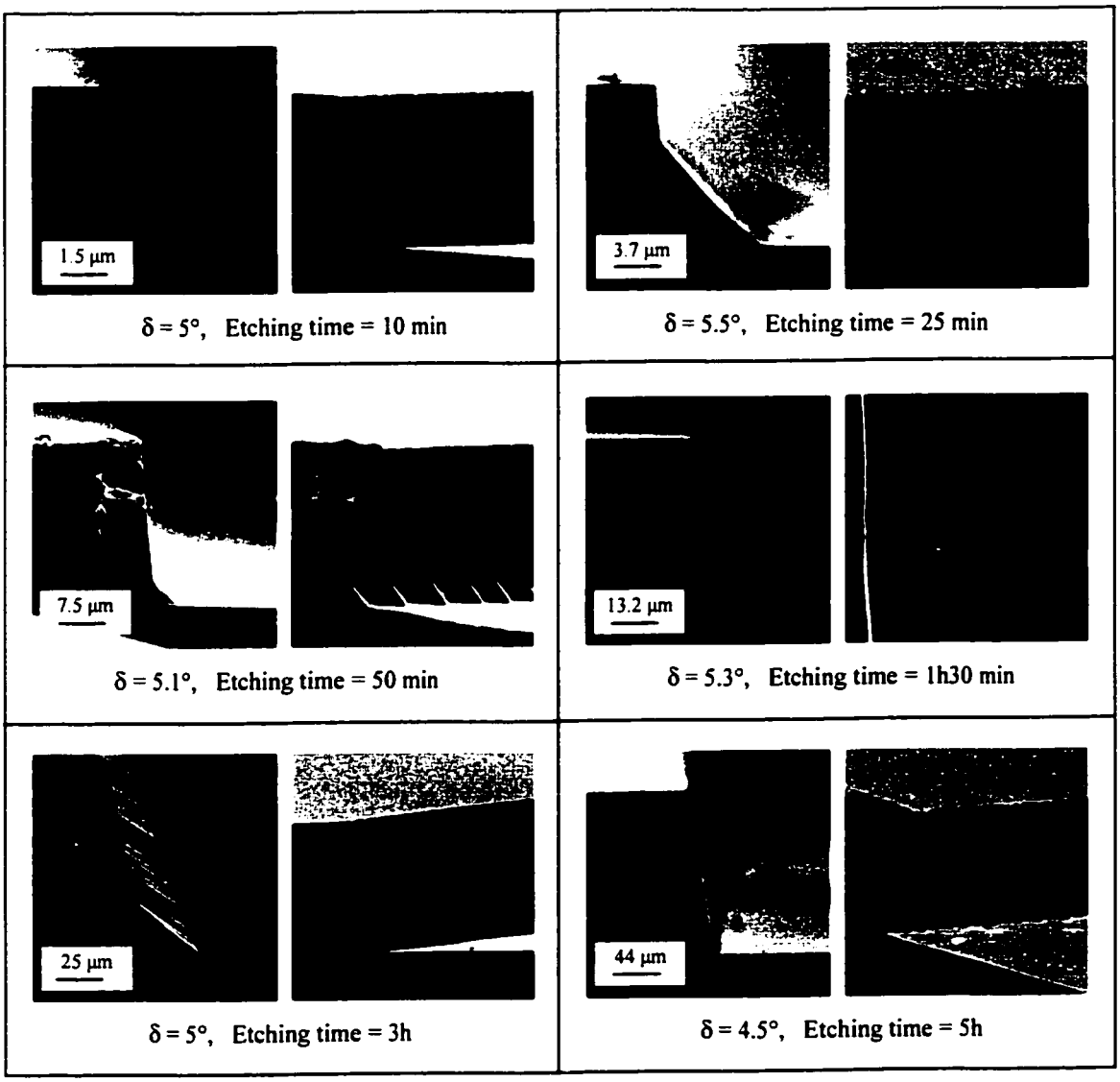

Figure 6-45 : Evolution with time of the under-etch profile at deviation angle δ≈5° in Si{100} 19wt%

On the side-view micrographs of Figure 6-45, it is observed that whenever the $P_{inclined}$ facet is large (10min, 25min, and 3h) its surface is rather smooth, and whenever the $P_{inclined}$ facet has a small or intermediate size (relative to the $K_{inclined}$ facet) there are interesting structures, aligned parallel to the PBCs.

Notice in Figure 6-45 that for the 50min, 1h30min and 3h etching samples, the relative size of the $P_{inclined}$ facet is increasing gradually, meaning that the relative etch rate of the $P_{inclined}$ facet is decreasing gradually with time. Figure 6-11 shows that the effective inclination angle is decreasing gradually for the 50min, 1h30min and 3h etching samples in a wide range of δ (not only at δ=5°). As a result, at δ=21° (studied in the next section 6.3.2-(b)), one can make the hypothesis that etch rate of the $P_{inclined}$ facet also decreases gradually for the 50min, 1h30min and 3h etching samples (this result will be used in the next section 6.3.2-(b)).

As in the case of 25wt.% TMAH, the anomalous etch rate variation of the P-based facet is hypothesized to be due to boundaries effects taking place at the two junctions ($K_{inclined}$-$P_{inclined}$) and ($P_{inclined}$-{100} bottom surface).

b) Si{100} 19wt.% TMAH, $\delta = 21°$

Figure 6-47 shows the evolution with time of the under-etch profile at deviation angle $\delta \approx 21°$. Depending on the etching time, the under-etch profile (illustrated in Figure 6-46-(a)) is composed of two or three facets. For all etching times, the lowest facet is identified to be a P-based inclined facet ($P_{inclined}$). Figure 6-46-(b) shows the ideal under-etch profile constructed from the canonical curve in Figure 6-26. Note that this crystal-feature-based model predicts that $P_{inclined}$ facet appears as part of the under-etched surface, which is consistent with the experimental results in Figure 6-47.

For 50min, 1h30min, and 5h etching samples, a very smooth K-based inclined facet ($K_{inclined}$) is also observed. In Figure 6-47, it is observed that the topmost facet is a near vertical facet which is itself multifaceted for most etching times. The sub-facets of this near-vertical facet are probably a $K_{inverted}$ fast-etch plane and the {111} plane.

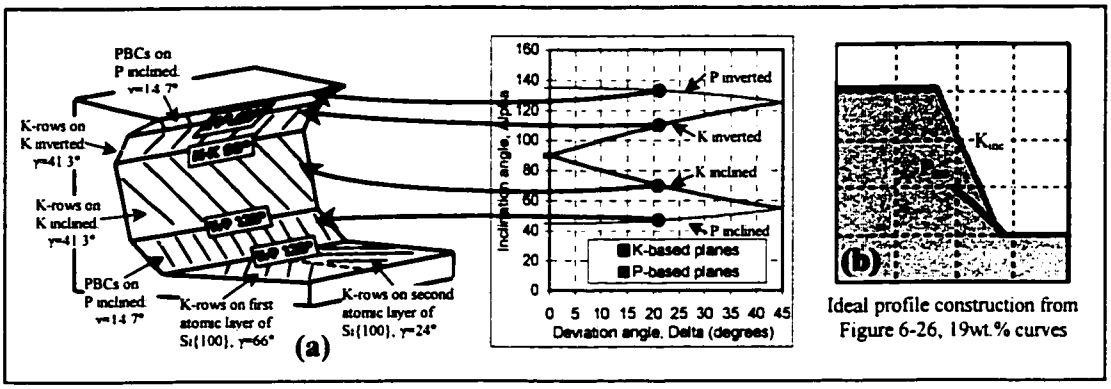

Figure 6-46 : (a) Correspondence between under-etched facets at δ=21° and ideal inclination angles; (b) Ideal profile construction.

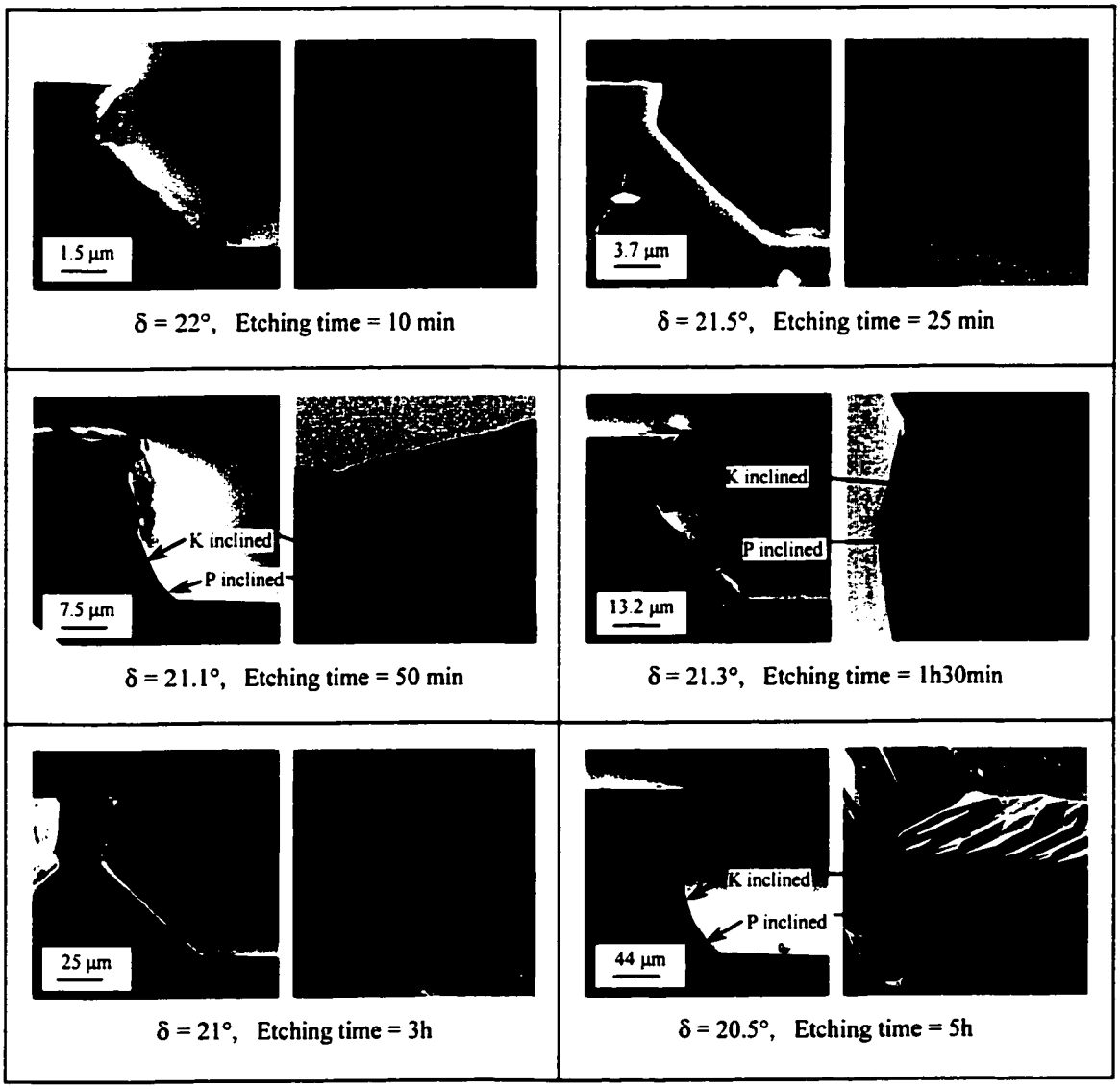

Figure 6-47 : Evolution with time of the under-etch profile at deviation angle δ≈21° in Si{100} 19wt%

For the 25min, 50min, 1h30min, and 3h etching samples, the ratio of the size of the top-most facet to the size of the rest (lower part of) of the under-etched surface is roughly constant with time, which is surprising because it contradicts the substantial variations of the under-etch rate curves during this time (Figure 6-10) at δ=21°. This must imply that the etch rates of the two facets are varying together. The following explanation may apply: the etch rate of the near-vertical top most facet may be strongly influenced (through interactions at boundaries) by the etch rate of the $P_{inclined}$ facet. It was shown in the previous Section 6.3.3-(a) (study at δ=5°) that the etch rate of the $P_{inclined}$ facet should decrease gradually for the 50min, 1h30min and 3h etching samples. At δ=21°, the P-inclined series is part of the same series as was studied at δ=5°. Thus it is not surprising that here at δ=21°, the same P-based series exhibits a gradual decrease of the under-etch rate curve (Figure 6-10) *at the same etching times*.

c) Si{100} 19wt.% TMAH, δ = 37°

Figure 6-49 shows the evolution with time of the under-etch profile at deviation angle $\delta \approx 37°$. The under-etch profile (illustrated in Figure 6-48-(a)) is composed of a stepped-{111} inclined facet and an inverted plane (likely $K_{inverted}$). Figure 6-48-(b) shows the ideal under-etch profile constructed from the canonical curve in Figure 6-26. Note that this crystal-feature-based model predicts that both $K_{inclined}$ and $P_{inclined}$ facets should appear.

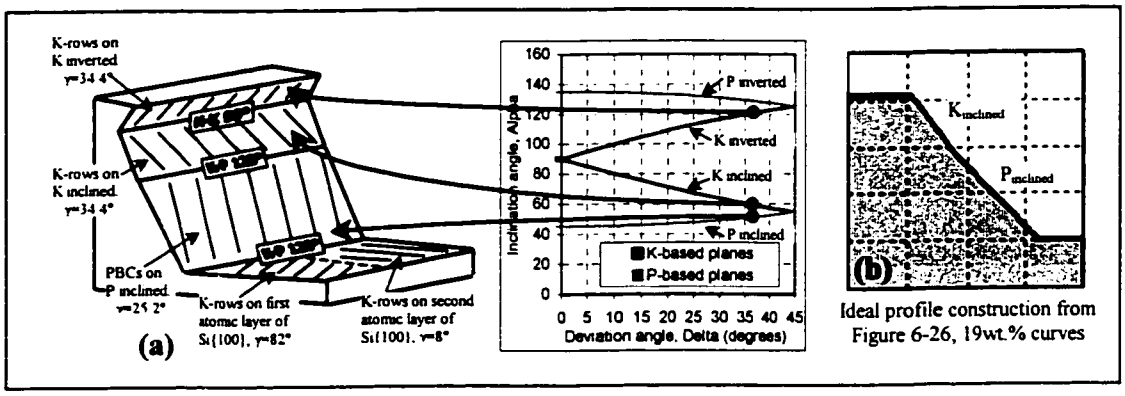

Figure 6-48 : (a) Correspondence between under-etch facets at δ=37° and ideal inclination angles; (b) Ideal profile construction.

With close inspection to the stepped-{111}inclined, one sees that it is actually composed of a K-based portion (top part of the facet) and a P-based portion (bottom of the facet), as illustrated in Figure 6-50. The size of each portion varies with time, which may explain why the various $\alpha_{effective}$ curves in Figure 6-11 do not coincide around δ=37°.

It is observed in Figure 6-49 that the relative size of the inverted plane (compared to the size of the inclined facet) decreases as the time goes from 10min to 1h30min etching time. After 1h30min etching, the ratio of sizes of the inverted facet to the inclined facet seems to be stabilized

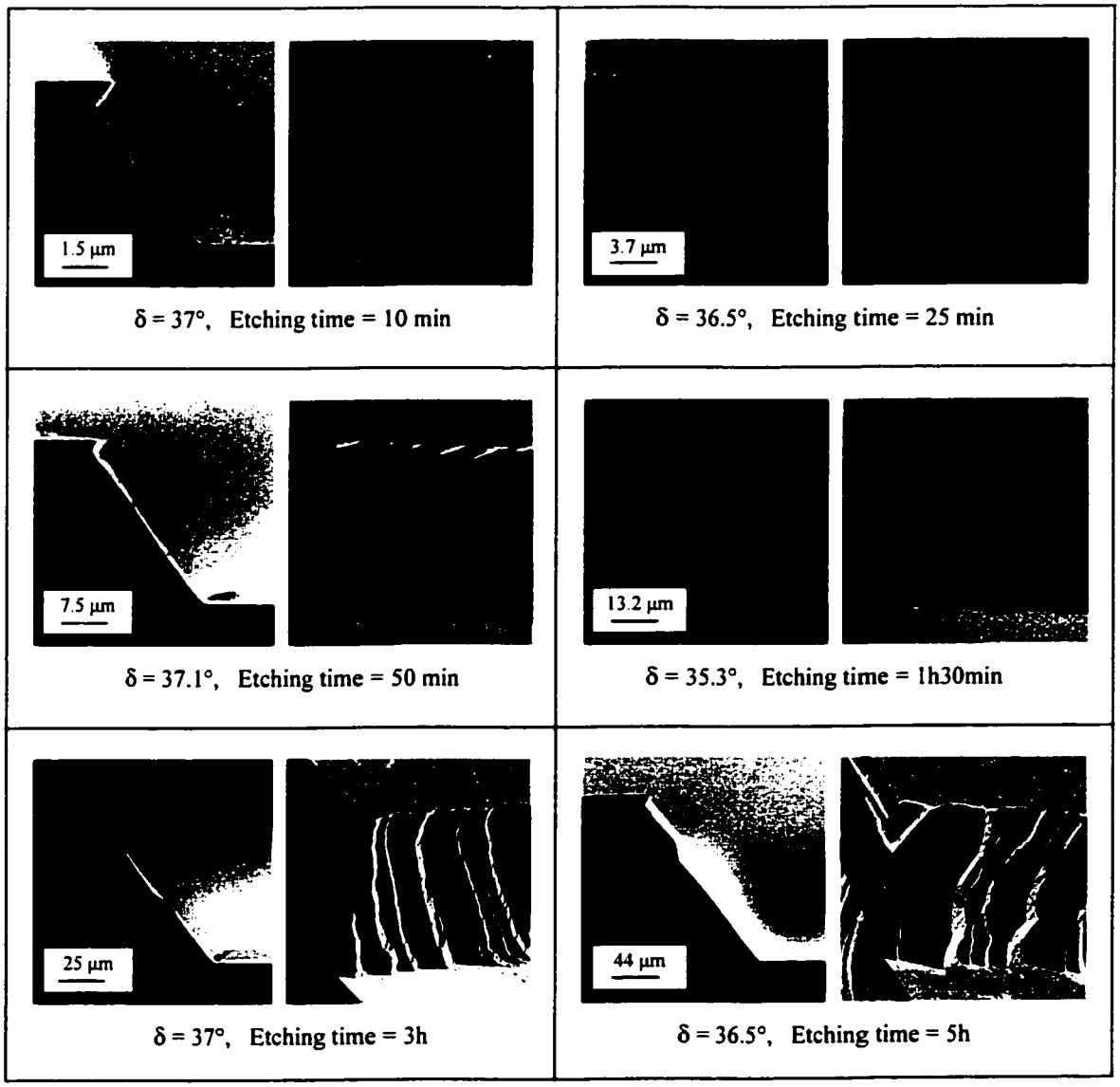

Figure 6-49 : Evolution with time of the under-etch profile at deviation angle $\delta \approx 37°$ in Si{100} 19wt%.

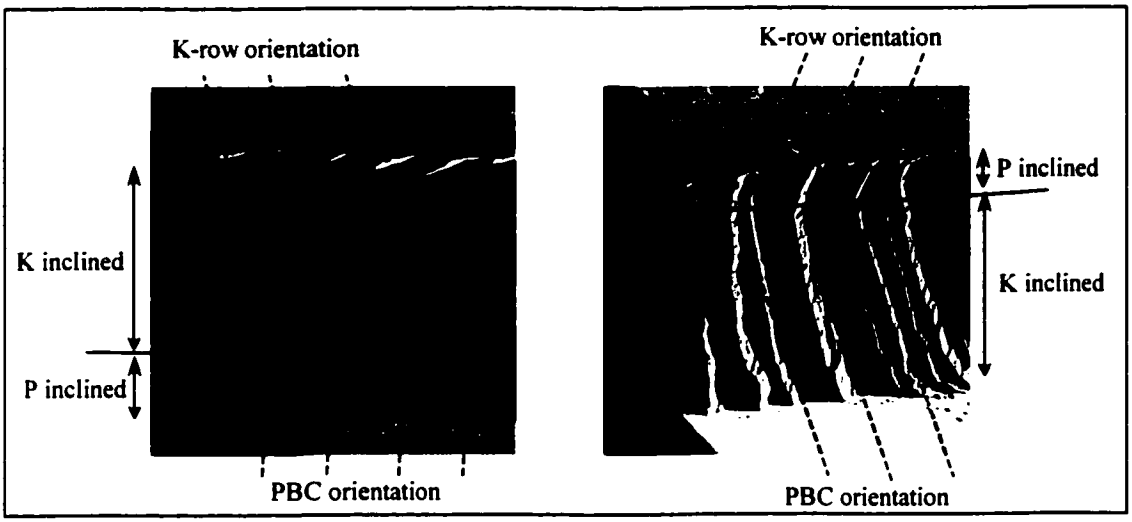

Figure 6-50 : Si{100} 19wt% δ≈37°: SEM side-view micrographs showing stepped-{111} inclined facets composed of both $K_{inclined}$ and $P_{inclined}$ portions.

6.3.4 Si{110} 19wt.% TMAH

a) Si{110} 19wt.% TMAH, δ = 12.5°

Figure 6-52 and Figure 6-53 show the evolution with time of the under-etch profile at mask deviation angle δ≈12.5°. The under-etch profile (illustrated in Figure 6-51-(a)) is composed of a large K-based inclined facet ($K2_{inclined}$) and a small top-most facet. A closer view revealed that the top-most facet is an inverted facet ($K2_{inverted}$) for the 25min and 50min etching samples, and a vertical K-based plane ($K_{vertical}$) for the 1h30min and 3h etching samples. Figure 6-51-(b) shows the ideal under-etch profile constructed from the canonical curve in Figure 6-26. Note that the crystal-feature-based model predicts that the $K_{vertical}$ facet should etch too fast to appear as part of the under-etched surface. However, the relative etch rates are much closer, such that the appearance of the $K_{vertical}$ facet in Figure 6-53-(1h30min and 3h) is not dramatically non-ideal.

It is observed in Figure 6-52 and Figure 6-53 that roughness features are superimposed on the larger directional lines (which are aligned with K-rows) on the lowest half-part of the $K2_{inclined}$ facets. These roughness features may be related to interactions between the K2inclined facet and the bottom {110} surface (for 25min and 50 min samples in Figure 6-53) or between the $K2_{inclined}$ facet and the $K2_{inclined}$ facet at the other side of the spoke,

when the bottom cavity has disappeared (for 1h30 min and 3h etching samples in Figure 6-53). The fact that the vertical K-based facet (the top-most plane in the 3h etching sample) emerges after some time may be related to the small acceleration with time of the $K2_{inclined}$ facet (close inspection in Figure 6-13 for $0° \leq \delta \leq 13°$, where only $K2_{inclined}$ emerges, reveals that the UER curve accelerates with time).

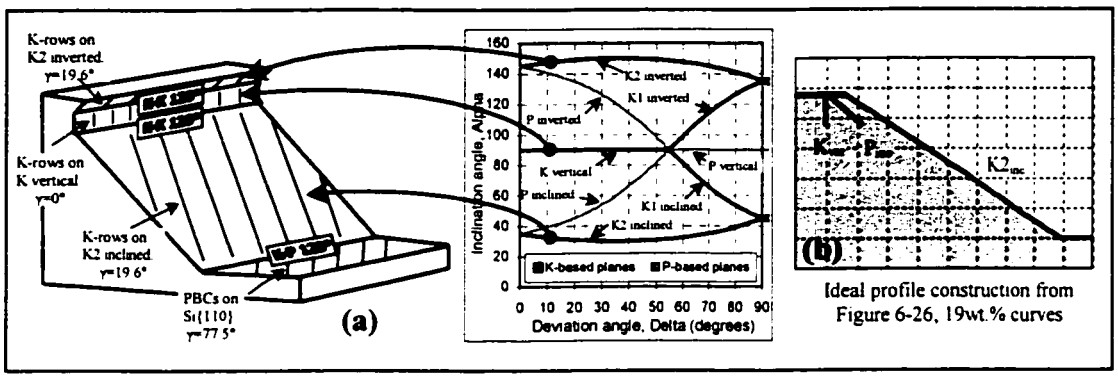

Figure 6-51 : (a) Correspondence between under-etch facets at δ=12.5° and ideal inclination angles; (b) Ideal profile construction.

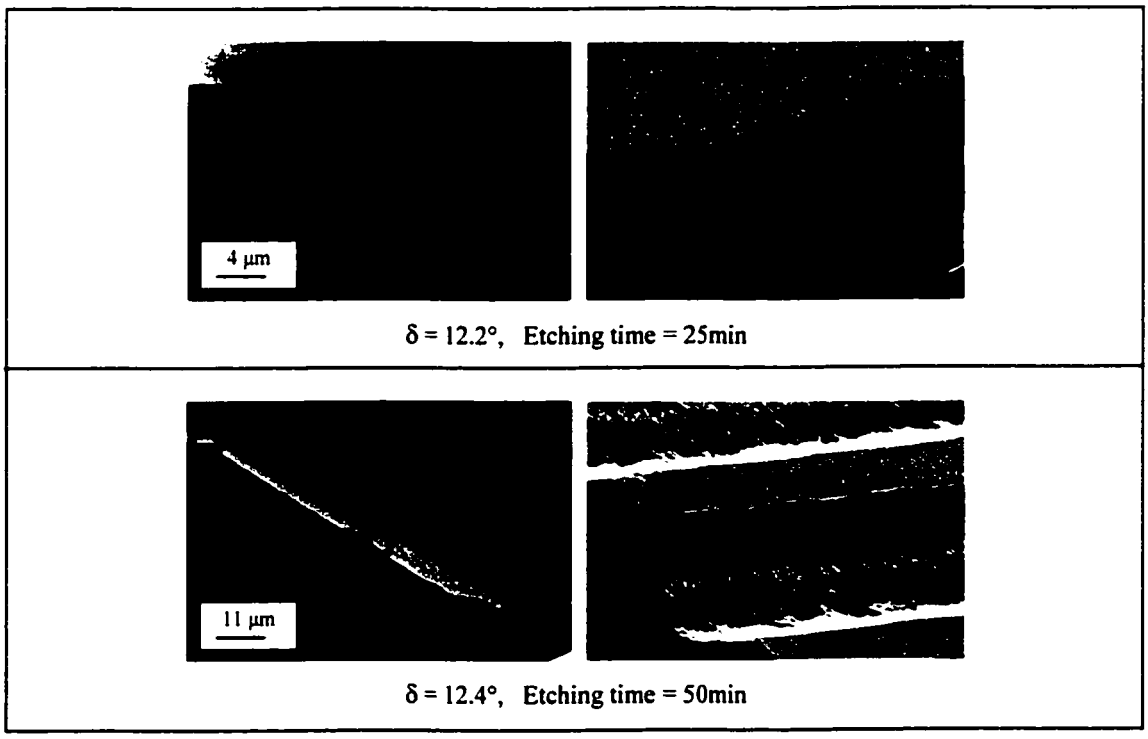

Figure 6-52 : Evolution with time (25min and 50min) of the under-etch profile at deviation angle $\delta \approx 12.5°$ in Si{110} 19wt%

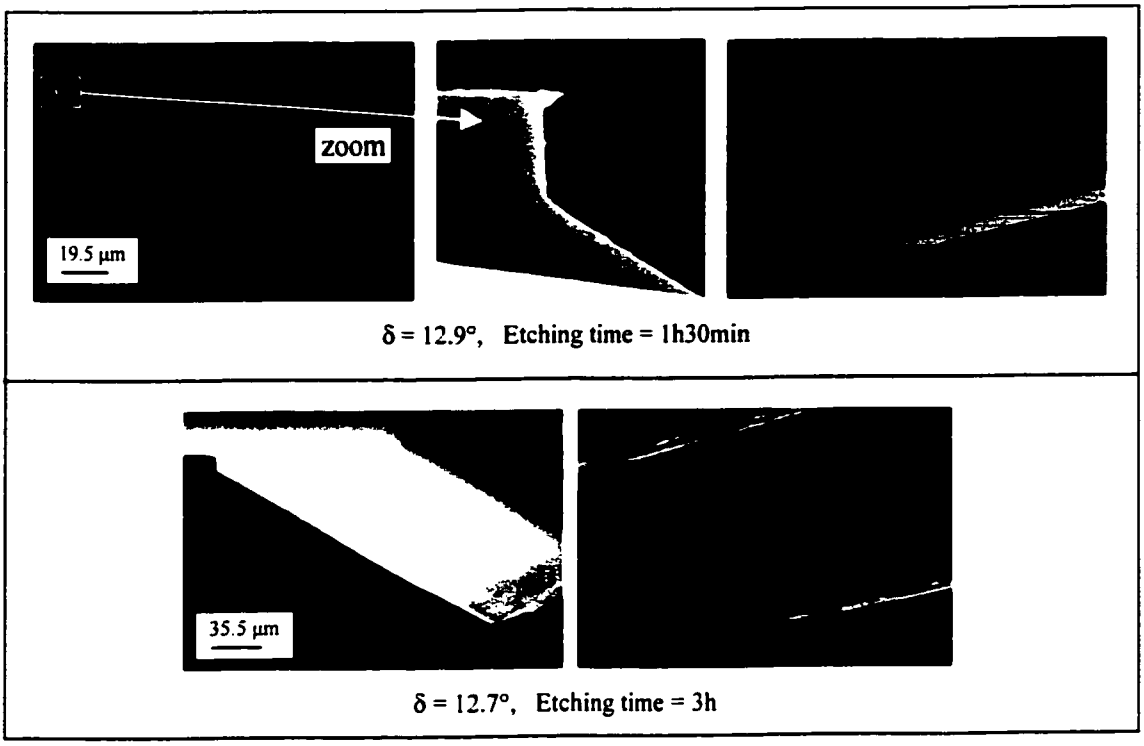

Figure 6-53 : Evolution with time (1h30min and 50min) of the under-etch profile at deviation angle δ≈12.5° in Si{110} 19wt%

b) Si{110} 19wt.% TMAH, δ = 32.5°

Figure 6-55 shows the evolution with time of the under-etch profile at deviation angle δ≈32.5°. It is observed in Figure 6-55 that the under-etched surfaces vary substantially with time. All facets involved are illustrated in Figure 6-54-(a). Figure 6-54-(b) shows the ideal under-etch profile constructed from the canonical curve in Figure 6-26. Note that the crystal-feature-based model predicts that only the $P_{inclined}$ facet should appear as part of the under-etched surface. However, the relative etch rates of the $K_{vertical}$ and $K2_{inclined}$ facets are close enough such that the appearance of the $K_{vertical}$ and $K2_{inclined}$ facets in Figure 6-55-is not dramatically non-ideal.

At 25min, only a pair of same-index P-based facets ($P_{inclined}$ and $P_{inverted}$) are present. This corresponds to a slow etch rate, perhaps consistent with the junction between the two facets being "blocked" (see Chapter 7). At 50min, a new facet, $K2_{inclined}$, emerges between the $P_{inclined}$ and the bottom surface, and simultaneously the other facets seem to accelerate.

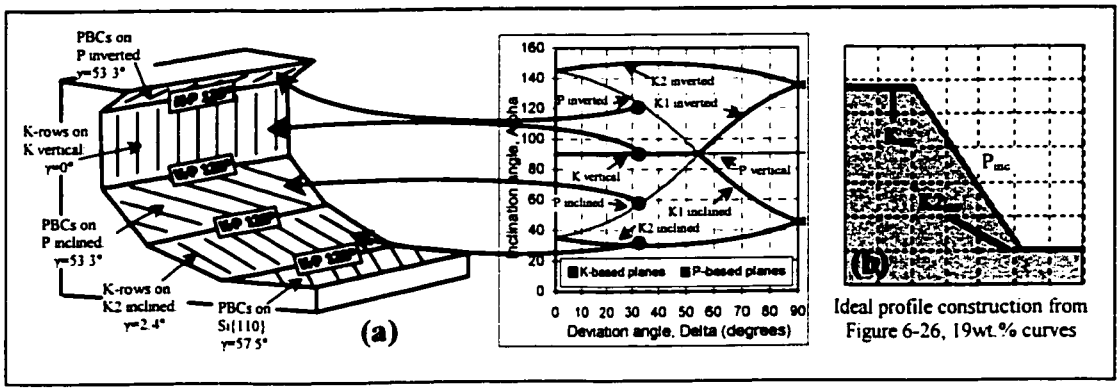

Figure 6-54 : (a) Correspondence between under-etch facets at δ=32.5° and ideal inclination angles; (b) Ideal profile construction

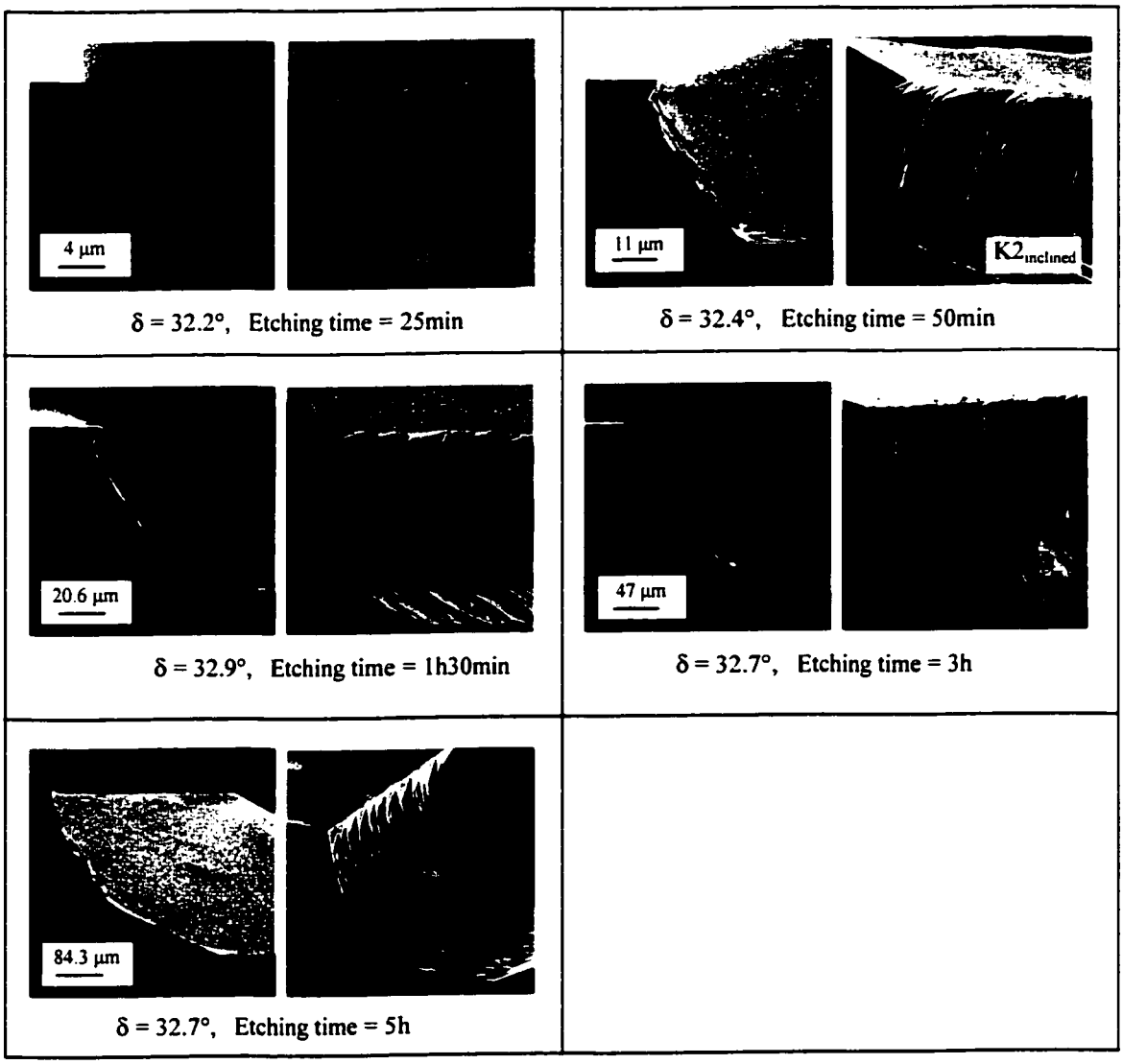

Figure 6-55 : Evolution with time of the under-etch profile at deviation angle δ≈32.5° in Si{110} 19wt%

It is observed in Figure 6-55 that the size of the $K2_{inclined}$ facet increases with time, indicating that other facets are etching relatively faster (consistent with the substantial increase of the under-etch rate curve in Figure 6-13 around $\delta \approx 35°$). Notice in Figure 6-55 the evolution with time of the roughness of the $P_{inclined}$ facet: from a rather smooth surface at 25min, the surface roughness increases, coincidentally with the emergence of $K2_{inclined}$ facet.

c) Si{110} 19wt.% TMAH, $\delta = 64.5°$

Figure 6-57 shows the evolution with time of the under-etch profile at deviation angle $\delta \approx 64.5°$. The under-etch profile (illustrated in Figure 6-56-(b)) is composed of a P-based vertical facet, $P_{vertical}$ (top-most facet) and a K-based inclined facet $K2_{inclined}$ (lower facet). Figure 6-56-(a) shows the ideal under-etch profile constructed from the canonical curve in Figure 6-26. Note that the crystal-feature-based model predicts that only the $P_{vertical}$ facet should appear as part of the under-etched surface. However, the relative etch rate of the $K2_{inclined}$.facet is close enough such that, in the case of an acceleration of the bottom surface etching rate, it is very probable to appear as shown in Figure 6-57.

It is observed in Figure 6-57 that the $P_{vertical}$ surface is composed of steps (a fast etch plane) propagating along flat {111} sub-facets. It is observed that the step spacing as well as the step height both increase with time.

In Figure 6-57, the various cross-sectional micrographs show that the $K2_{inclined}$ facet increases in size between 25min and 5h, which is consistent with the variations with time of the effective inclination angle $\alpha_{effective}$ in Figure 6-14. The variations of the size of the $K2_{inclined}$ facet may be due to simultaneous variations: acceleration of the etch rate of the $P_{vertical}$ facet, etch rate deceleration of the $K2_{inclined}$, etch rate acceleration of the bottom surface.

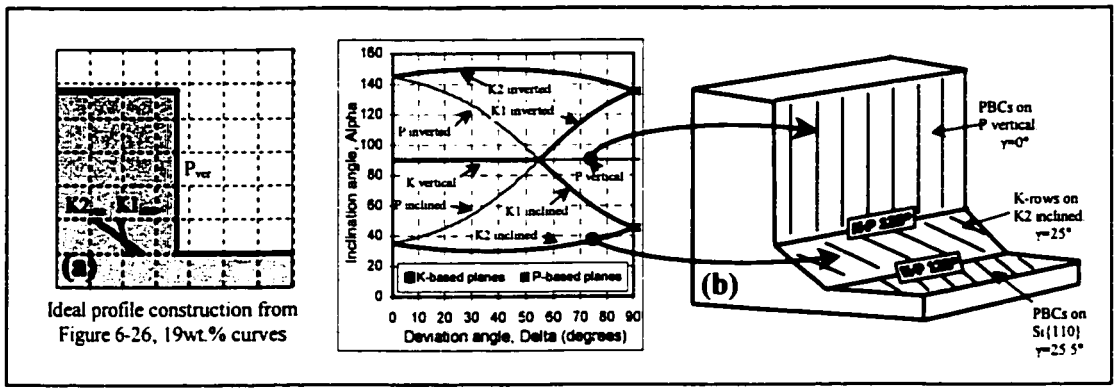

Figure 6-56: (a) Ideal profile construction; (b) Correspondence between under-etch facets at δ=64.5° and ideal inclination angles.

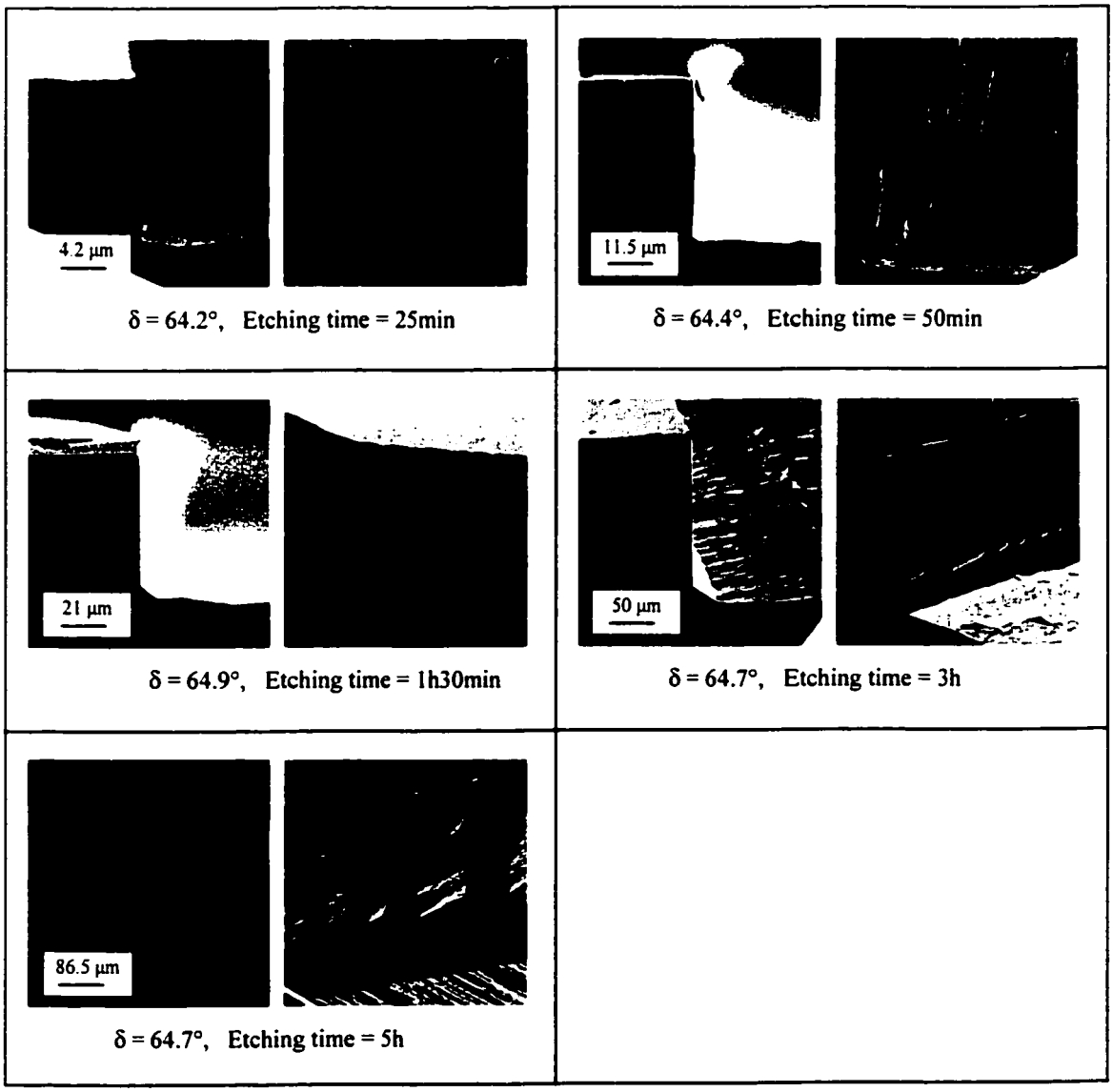

Figure 6-57 : Evolution with time of the under-etch profile at deviation angle δ≈64.5° in Si{110} 19wt%

d) Si{110} 19wt.% TMAH, $\delta = 81°$

Figure 6-59 shows the evolution with time of the under-etch profile at deviation angle $\delta \approx 81°$.The under-etch profile (illustrated in Figure 6-58-(b)) is composed of three facets: the top-most facet is a P-based vertical facet $P_{vertical}$, the two other facets $K1_{inclined}$ and $K2_{inclined}$ have a very close inclination angle α (about 45°) that makes them difficult to distinguish. The size of $K1_{inclined}$ is about half the size of the $K2_{inclined}$. Figure 6-58-(a) shows the ideal under-etch profile constructed from the canonical curve in Figure 6-26, which validates the experimental results of Figure 6-59.

Notice for the 3h side-view micrograph, the localized imperfection of the crystal which helps to identify the location of the junction between $K1_{inclined}$ and $K2_{inclined}$, and the direction of K-rows on the two K-based facets.

It is observed in Figure 6-59 that the size of the $P_{vertical}$ facet decreases with time, which implies that its etch rate increases with time at a faster rate (relatively) than the other facets. This is consistent with the under-etch rate acceleration observed in Figure 6-13 for $\delta \approx 81°$.

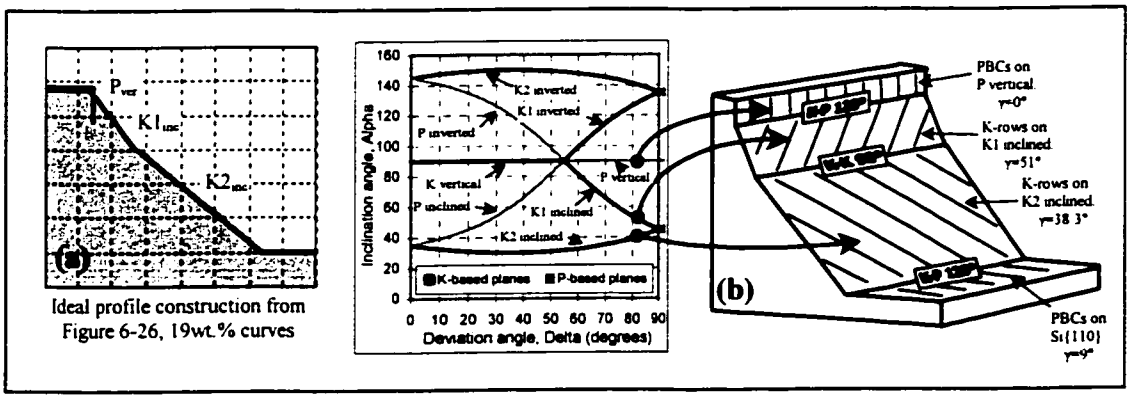

Figure 6-58 : (a) Ideal profile construction; (b) Correspondence between under-etch facets at $\delta = 81°$ and ideal inclination angles.

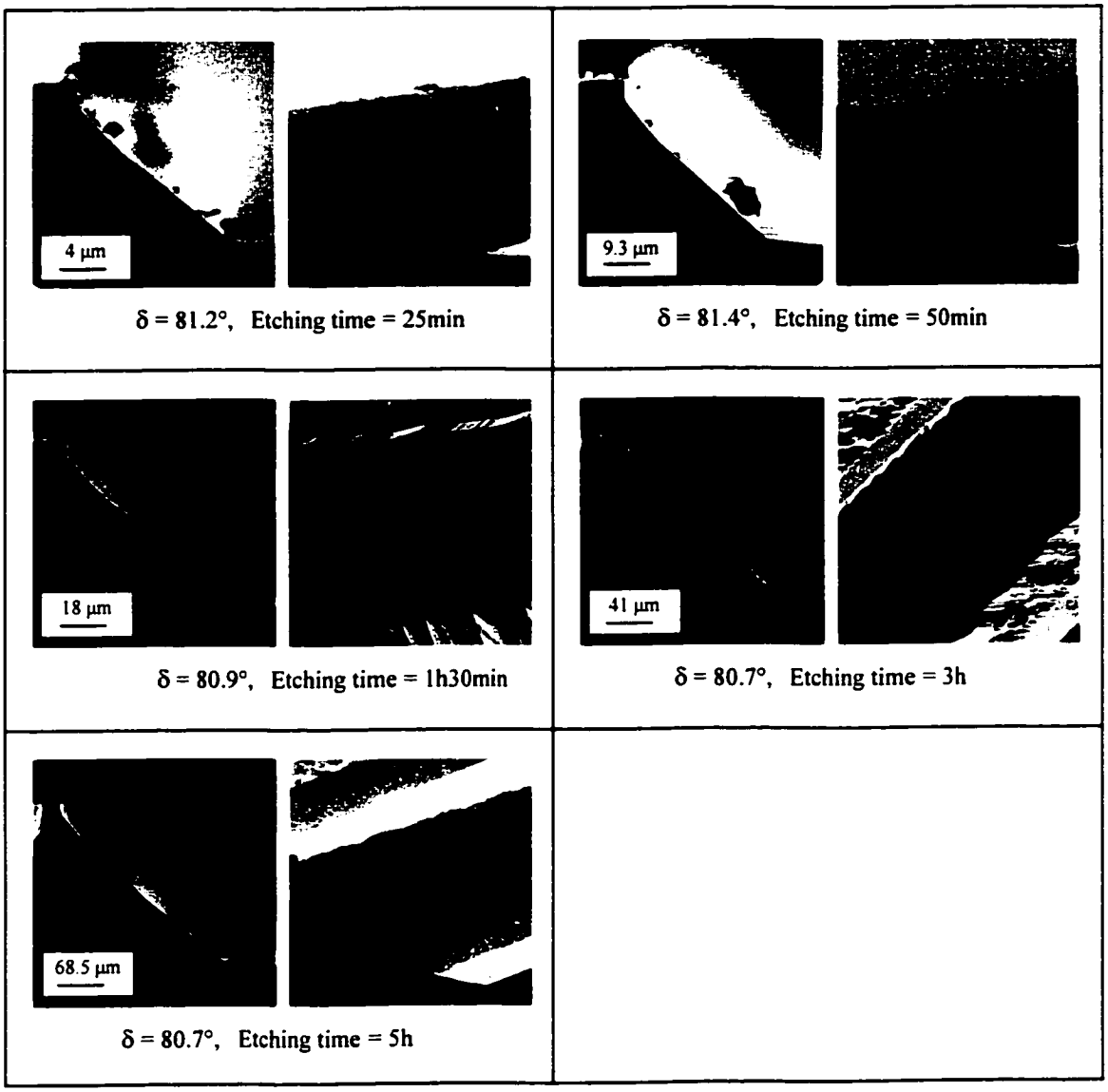

Figure 6-59 : Evolution with time of the under-etch profile at deviation angle δ≈81° in Si{110} 19wt%

6.4 Contributions

In Chapter 6, optical microscope measurements on Si{100} and Si{110} for 25wt.% and 19wt.% TMAH were conducted, and SEM micrographs were taken at strategic locations. Along with the measurements and SEMs, 1h30min etching samples were used to extract canonical etch rate curves of P-based and K-based series:

- The canonical curves were compared between the two concentrations and it was found the K-based series etch rate has increased more than P-based series as the concentration went from 25wt.% to 19wt%, consistent with the general trends found in previous work by other researchers [2,6].
- The canonical curves were used to construct ideal under-etch profiles for the comparison with experimental under-etch profiles.

The results of combined optical measurements and SEM micrographs include:

- Si{100} 25wt% TMAH
  - The under-etch rate and the bottom surface etch rate are approximately constant with time.
  - The effective inclination angle varies substantially with time for δ close to 0°.
  - Evidence of etch rate variation with time of the $P_{inclined}$ series is presented.
  - Substantial-sized inverted planes are observed having a constant relative size compared to inclined facets.

- Si{110} 25wt% TMAH
  - The under-etch rate is found to not vary significantly with time, however it is found to deviate form the crystal-feature-based etching model at specific locations: at $\delta \approx 39°$ (acceleration) and at $\delta \approx 70°$ (deceleration).
  - The bottom surface etch rate varies with the mask-edge angle.
  - The {110} bottom surface roughness does not change dramatically with time.
  - The bottom surface roughness of cavities is almost unchanged with time.

- Si{100} 19wt%
  - The under-etch rate and effective inclination angle are found to vary substantially with time in a particular range of deviation angle around $\delta=21°$, corresponding to the appearance of a rough near-vertical facet.
  - inverted planes smaller than in 25wt% are observed at the same deviation angles as in 25wt%.
  - Evidence of etch rate variation with time of the $P_{inclined}$ series at $\delta=5°$ is presented.

- for Si{110} 19wt.% TMAH
  - The under-etch rate is found to vary substantially with time (acceleration) in a particular range of deviation angle around δ=35°. The variations coincide with the appearance of the $K2_{inclined}$ facet.
  - The bottom surface etch rate increases substantially with time. It also varies as the mask-edge is deviated.
  - The bottom surface roughness increases with time with the appearance of protruding structures extending perpendicular to the direction of PBCs.
  - The presence of trenches on the {110} bottom surface is observed. These trenches propagate over time toward the center of the cavity.

In general, there are significant variations with time, of underetch rates, facet profiles, roughness and cavity-bottom etch rates, indicating clearly that the crystal-feature-based model does not hold over time.

7 Further Analysis of the Experimental Data

This chapter further analyzes the experimental results of Chapter 6. The analysis is constructed by comparison with the etching model (Chapter 3) and with the analysis of interaction between chains (Chapter 4).

In Chapter 6, we have presented the evolution with time of under-etch rates and under-etch profiles at particular deviation angles (δ). The various results demonstrate that many facets do experience an etch rate variation and a roughness change with time. In Chapter 7, these anomalies are explored in more depth, including more SEM pictures of nearby or related locations, and hypothesizing them to be due to boundary effects occurring at facet junctions.

This Chapter begins with a graphical summary of Chapter 6, then the K-K 90° and K-P 120° connections between chains are studied to explain most of the observed boundary effects.

7.1 Graphical review of Chapter 6

Figure 7-1 and Figure 7-2 summarize graphically the results of Chapter 6 for both the optical measurements and SEM observations for Si{100} and Si{110}, respectively. The following abbreviations are utilized in Figure 7-1 and Figure 7-2 to clarify the effects that are suggested to occur with time:

ΔUER :	variation of the etch rate of the top-most facet.
aux :	auxiliary facet experiencing a size or etch rate variation.
inv :	appearance of inverted planes
bot :	variation of the cavity bottom etch rate.
acc :	acceleration, the facet etch rate increase with time or is faster than expected.
dec :	deceleration, the facet etch rate slows down or etches slower than expected.

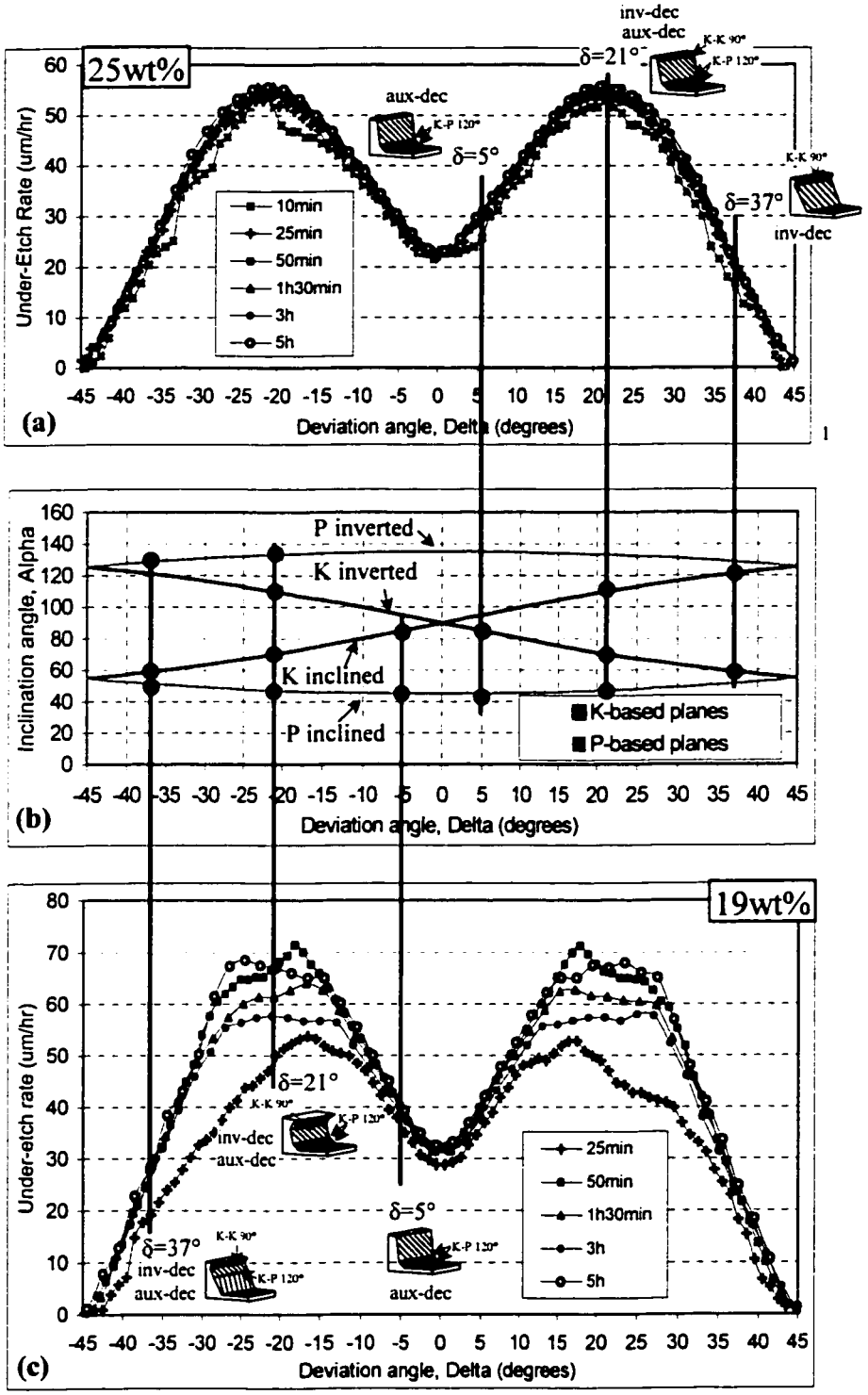

Figure 7-1: (a) Si{100} 25%, under-etch rate curve evolution with time; (b) appearing facets at specific locations; (c) Si{100} 19%, under-etch rate curve evolution with time.

[1] **ΔUER** : variation of the ER of the top-most facet.
inv : appearance of inverted planes
acc : acceleration dec :deceleration.
aux : auxiliary facet ER variation
bot : variation of the cavity bottom ER

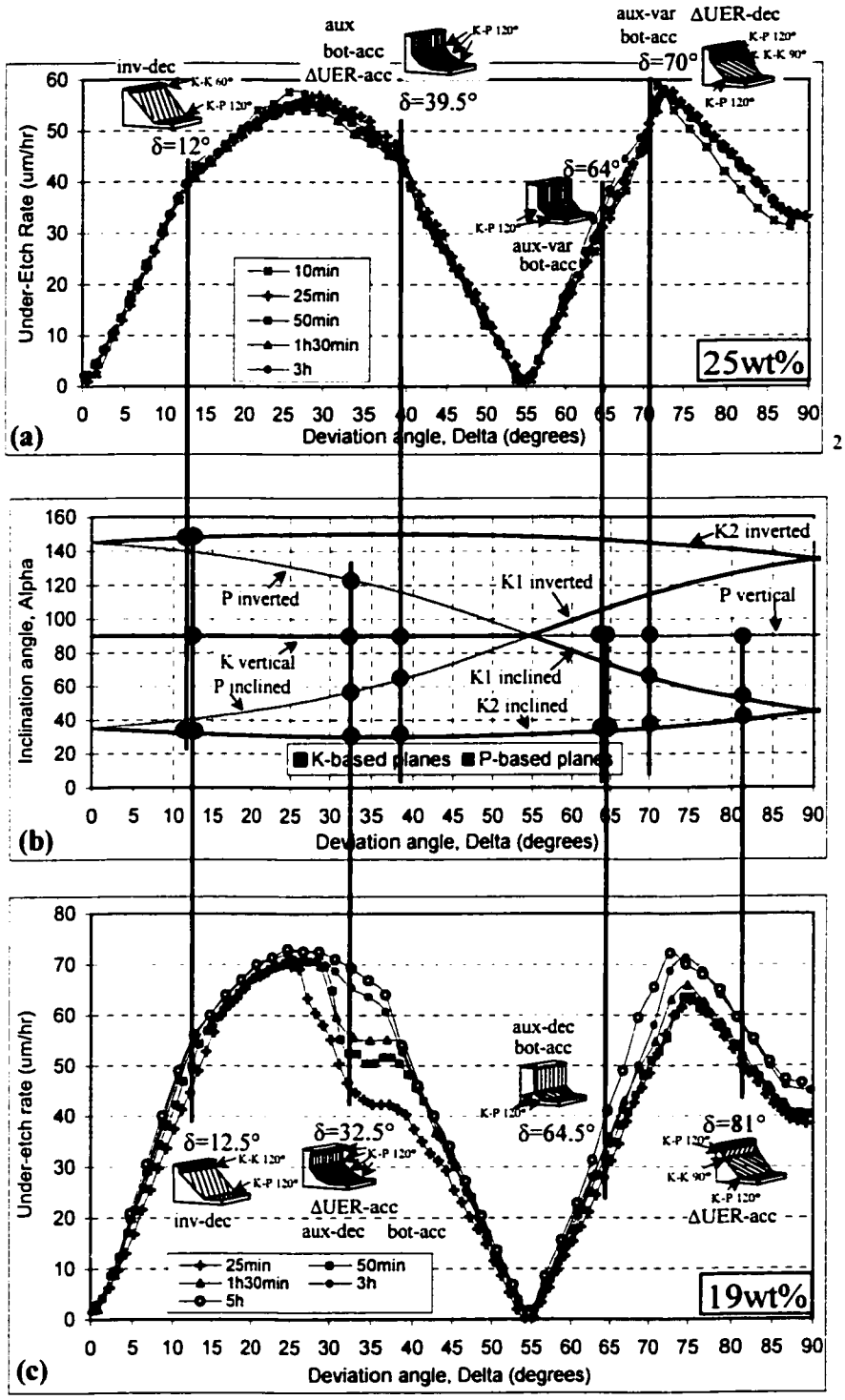

Figure 7-2: (a) Si{110} 25%, under-etch rate curve evolution with time; (b) appearing facets at specific locations; (c) Si{110} 19%, under-etch rate curve evolution with time.

[2] **ΔUER** : variation of the ER of the top-most facet.
inv : appearance of inverted planes
acc : acceleration dec :deceleration.
aux : auxiliary facet ER variation
bot : variation of the cavity bottom ER

7.2 Experimental Analysis of the interactions between chains

The two summary graphs presented in Figure 7-1 and Figure 7-2 show that most junctions between two K-based facets occur with chains connected K-K 90°, whereas most junctions between a K-based facet and a P-based facet occur with chains connected K-P 120°. As a result, these two particular connections between chain are studied in detail this section.

7.2.1 K-K-90°

- K-K 90° is the abbreviation of the connection between two K-rows (each on a different facet of the under-etched surface) at an angle ψ=90°. K-K 90° is one of the seven possible connections between chains that can occur on Si{100} and Si{110} (Figure 4-8). Note that the connection K-K 90° is symmetric, that is, it should affect identically both K-based facets at their junction. Figure 7-3 shows schematic and SEM views involving the K-K 90° connection between chains.

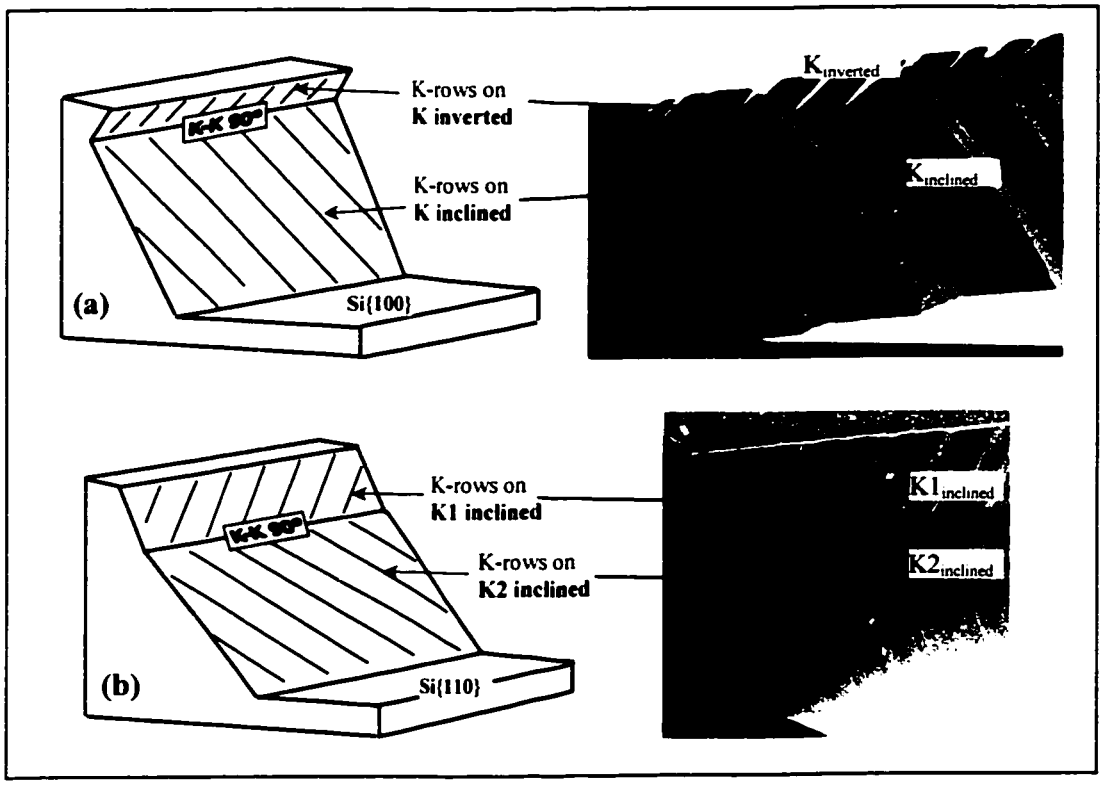

Figure 7-3 : Schematic and SEM views involving the K-K 90° connection between chains : (a) on Si{100} between $K_{inclined}$ and $K_{inverted}$; (b) on Si{110} between $K1_{inclined}$ and $K2_{inclined}$

The connection K-K 90° occurs on under-etched surfaces for both silicon orientations:

- On Si{100}, between the pair of facets $K_{inclined}$ and $K_{inverted}$ (Figure 7-3-(a)). A crystallographic reconstruction of this pair of facet is shown in Figure 4-9. This situation where $K_{inclined}$ and $K_{inverted}$ both are present occurs on Si{100} at deviation angles (δ) ranging from 15° to 43°.
- On Si{110}, between $K1_{inclined}$ and $K2_{inclined}$ (Figure 7-3-(b)). A crystallographic reconstruction of these two inclined facets is shown in Figure 4-12. This situation where $K_{inclined}$ and $K_{inverted}$ both are present occurs on Si{100} at deviation angles (δ) ranging from 70° to 90°.

a) Study of the interaction between $K_{inclined}$ and $K_{inverted}$ on Si{100}

The etching simulations performed in Chapter 4 (Section 4.3) support the hypothesis that inverted facets may be explained by boundary effects. Indeed, by having stable atoms at the junction between inclined and inverted planes and by stopping the propagation of zipping of chains at the junction, the simulations generated inverted planes that stabilize at a realistic relative size (compared to the inclined facets). Because the K-K 90° connection give birth to inverted planes, one can make the hypothesis that atoms at the junction of the K-rows connected by K-K 90° are stable or blocked, i.e. the zipping of chains does not propagate across the junction.

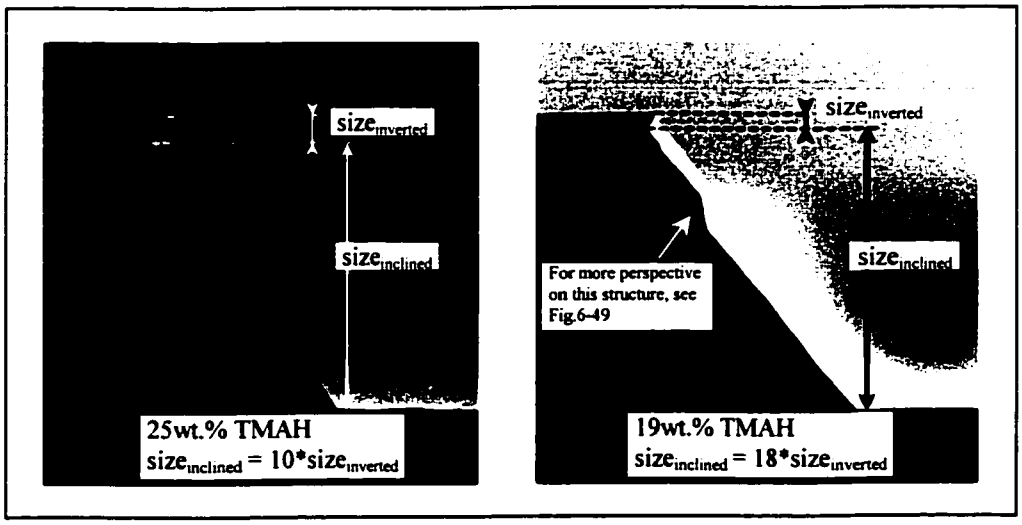

Figure 7-4 : Comparison of inverted plane sizes on Si{100} at δ=37° on 25wt.% and 19wt.% TMAH after 5h etching .

The simulations also show that varying the nucleation probability (Pn) has an effect on the size of inverted planes (Figure 4-23). The reconstructed canonical curves in Figure 6-26 show that the etching rate of both P-based and K-based series is higher in 19wt.% than in 25wt%. One can then make the hypothesis that $Pn_{19wt\%} > Pn_{25wt.\%}$ and surmise (by looking at Figure 6-26), for a given deviation angle (δ), that inverted planes in 19wt% should be smaller than in 25wt.%. This result predicted by the etching simulation is verified experimentally. Figure 7-4 shows two SEM micrographs (involving an inverted facet) at δ=37° on 25wt.% and 19wt.% after 5h etching. It is observed in Figure 7-4 that in 19wt.% the $K_{inverted}$ facet is 18 times smaller than the $K_{inclined}$, whereas in 25wt.% the $K_{inverted}$ is only 10 times smaller than the $K_{inclined}$ facet.

b) Study of the interaction between $K1_{inclined}$ and $K2_{inclined}$ on Si{110}

Figure 7-5 shows a top-view optical micrograph of an etched spoke (5h etching) on Si{110} with the right edge at deviation angle δ= 82° and the left edge at δ= 84°. Two inclined K-based facets ($K1_{inclined}$ and $K2_{inclined}$) are observed on the edges of the spoke for the two deviation angles. On each K-based facet in Figure 7-5, the orientation of K-rows is clearly seen. The orientation of K-rows is consistent with the crystallographic reconstruction of Figure 4-12. The fact that the visible lines (K-rows) on the facets are continuous through the junction suggests that these two facets are interacting.

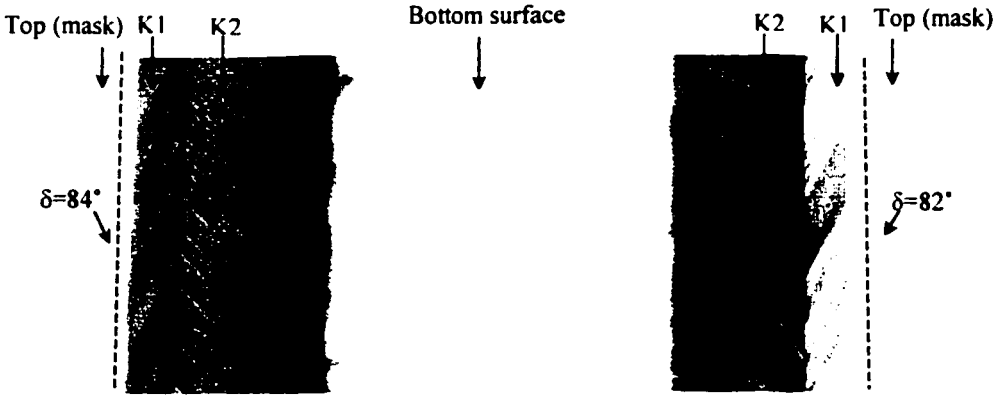

Figure 7-5 :Top view micrograph of the K-based inclined under-etch facets at δ=82° and δ=84° on Si{110} etched for 5h in 25wt.% TMAH

Figure 7-6-(a) shows a side-view micrograph at the left side (δ=84°) of the spoke of Figure 7-5. The inclination angles of each K-based facet is in accordance with the ideal inclination angles of Figure 3-21. Close inspection of the junction between the two facets is presented in Figure 7-6-(b), and show that the zipping lines (aligned parallel to the orientation of K-rows) are continuous across the facets boundary supporting the interaction hypothesis between $K1_{inlined}$ and $K2_{inclined}$ facets.

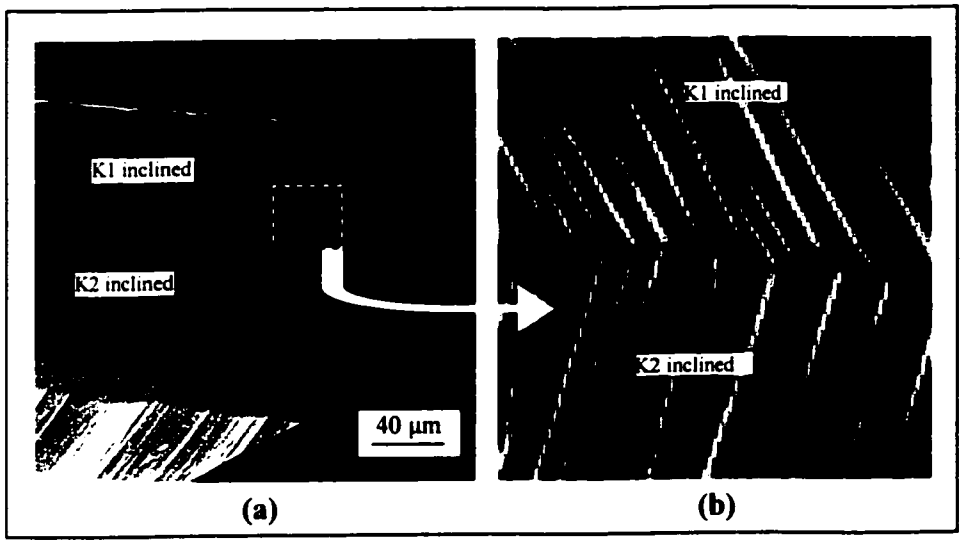

Figure 7-6 : (a) SEM side views of K1 and K2 inclined planes at δ=84° on Si{110} etched for 5h in 25wt.% TMAH. (b) Zoom of the junction between K1 and K2 showing the orientation of the K-rows on the facets and a possible interaction between these K-rows.

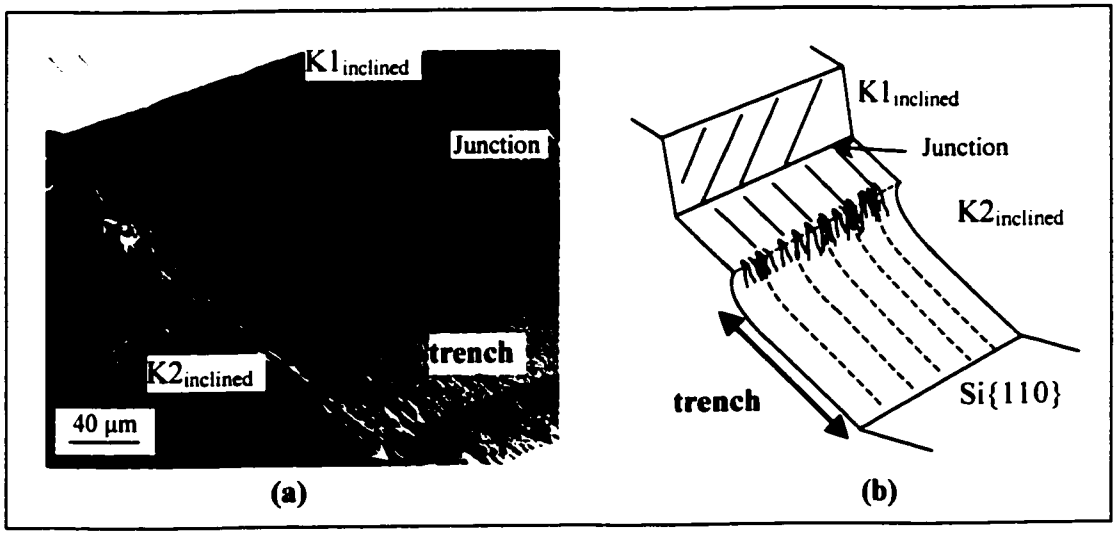

Figure 7-7 : (a) SEM side views of K1 and K2 inclined planes at δ=77.5° on Si{110} etched for 3h in 25wt.% TMAH; (b) Schematic view of (a)

Figure 7-7 shows other SEM pictures of $K1_{inclined}$ and $K2_{inclined}$ (at δ=77.5° for 3h etching). Close inspection of the junction between the two facets shows that the $K2_{inclined}$ plane etches with the formation of a trench from its lower boundary (see Figure 7-7). The trench is becoming wider by zipping of K-rows towards the junction with $K1_{inclined}$. Since evidently the trench area is etched more rapidly than the area next to the junction with $K1_{inclined}$, it is reasonable to surmise that the K-K 90° junction does not zip as much as the trench does.

Figure 7-8 shows the ideal etch rates of $K1_{inclined}$ and $K2_{inclined}$ imported from Figure 6-26 for the purpose of comparing the etch rates of the two planes at common deviation angles. Appendix IV shows all other P-based and K-based series etch rates (Figure IV-2). It is observed in Figure 7-8 for deviation angles greater than 70° (corresponding to the range of δ where $K1_{inclined}$ and $K2_{inclined}$ have a common boundary) that $K1_{inclined}$ etches slightly faster than $K2_{inclined}$ but the two K-based planes tend toward the same etch rate as the deviation angle approaches 90°. At δ=84° where visible lines across the boundary between the two facets are observed (Figure 7-6-(b)), $K1_{inclined}$ and $K2_{inclined}$ have almost the same etch rate so that it may explain why no clear variation with time of etch rates for these two planes has been observed.

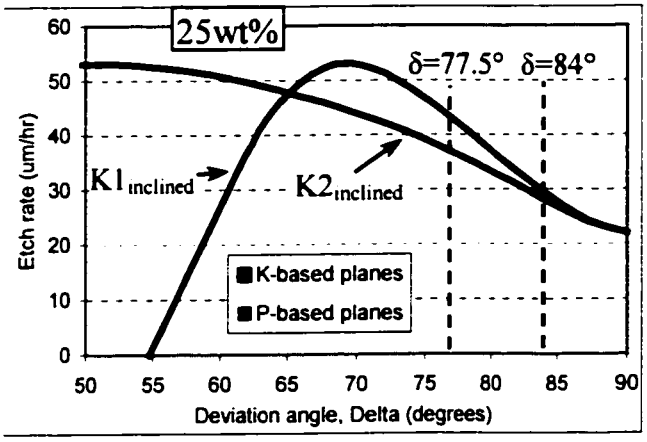

Figure 7-8 : $K1_{inclined}$ and $K2_{inclined}$ ideal etching rates in 25wt% TMAH (constructed from the 25wt% canonical curves of Figure 6-26).

7.2.2 K-P-120°

K-P 120° is the abbreviation representing the connection between a K-row and a PBC (each on a different facet of the under-etch) at an angle ψ=120°. K-P 120° is the most frequently-observed connection between chains that can occur on Si{100} and Si{110} (most small schematic views in Figure 7-1 and Figure 7-2 involve a K-P 120° connection). Note that the connection K-P 120° is asymmetric, that is, the zipping direction (whether the zipping propagates from PBC to K-row or from K-row to PBC) should be considered when describing the connection K-P 120°. Below in this section, P-to-K 120° will refer to a zipping propagating from the PBC to the K-row, whereas K-to-P 120° will refer to a zipping propagating from the K-row to the PBC. Figure 7-9 shows schematic and SEM views involving the K-P 120° connection between chains. The connection K-P 120° occurs on both silicon orientations:

- On Si{100}, simultaneously between $K_{inclined}$ and $P_{inclined}$, and between $P_{inclined}$ and the {100} bottom surface (see Figure 7-9-(a)). A crystallographic reconstruction of these three planes is shown in Figure 4-10. This situation where the $P_{inclined}$ is present may occur on Si{100} for all deviation angles (as it is the case for 19wt.% TMAH).
- On Si{110}, for δ<54.74°: between $K_{vertical}$ and $P_{inclined}$, between $P_{inclined}$ and $K2_{inclined}$, and finally between $K2_{inclined}$ and the {110} bottom surface (see Figure 7-9-(b)). A crystallographic reconstruction of these four planes is shown in Figure 4-11.
- On Si{110}, for δ>54.74°: between $P_{vertical}$ and $K1_{inclined}$ (see Figure 7-9-(c)), or between $P_{vertical}$ and $K2_{inclined}$ (see Figure 7-9-(d)), depending whether $K1_{inclined}$ has appeared between $P_{vertical}$ and $K2_{inclined}$.

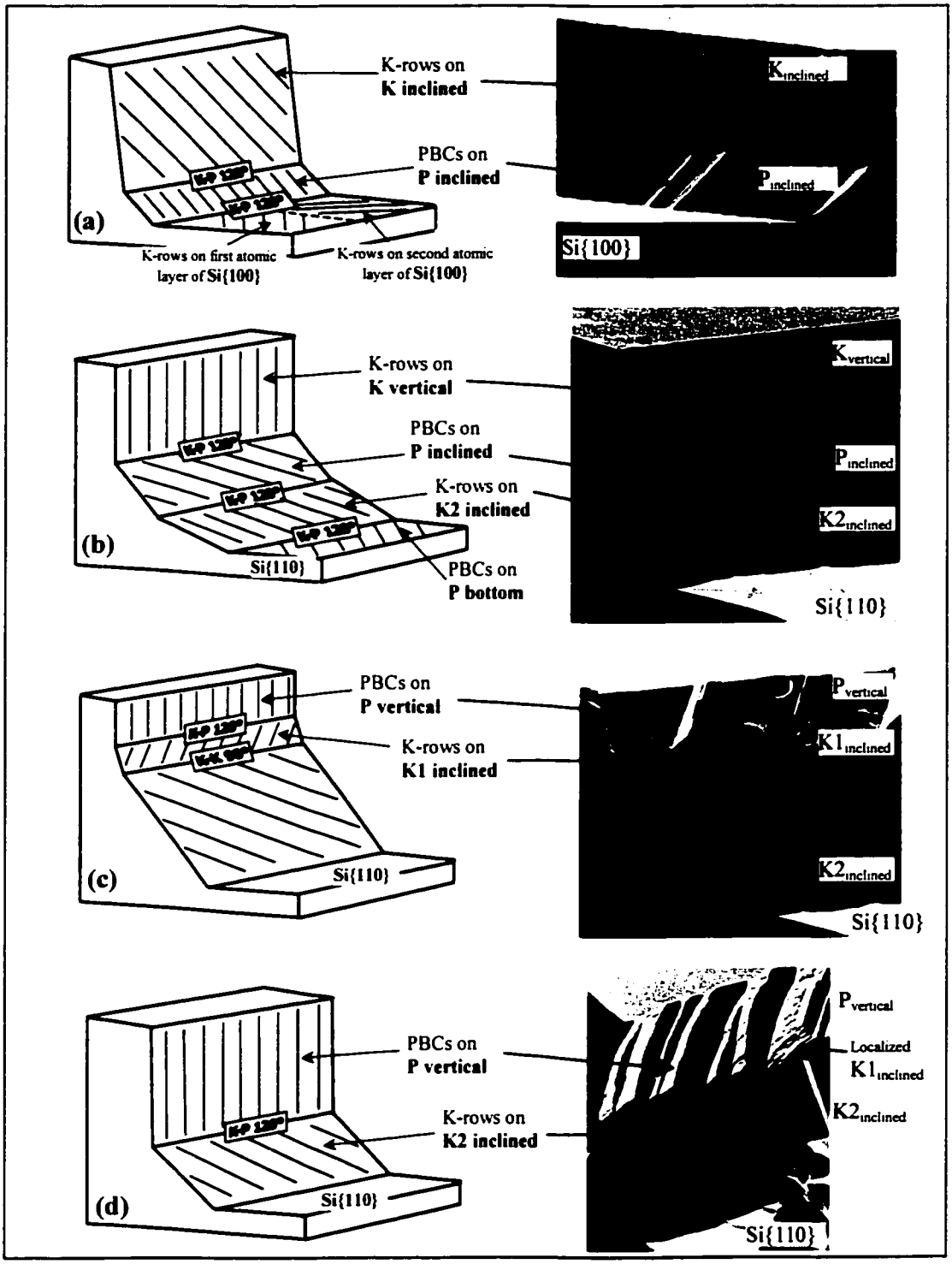

Figure 7-9 : Schematic and SEM views involving the K-P 120° connection between chains : **(a)** on Si{100} between $K_{inclined}$ and $P_{inclined}$, and between $P_{inclined}$ and the {100} bottom surface; **(b)** on Si{110} between $K_{vertical}$ and $P_{inclined}$, between $P_{inclined}$ and $K2_{inclined}$, and finally between $K2_{inclined}$ and the {110} bottom surface; **(c)** on Si{110} between $P_{vertical}$ and $K1_{inclined}$; **(d)** on Si{110} between $P_{vertical}$ and $K2_{inclined}$.

a) Study of the configuration where $P_{inclined}$ is present between $K_{inclined}$ and K_{bottom} on Si{100}

On Si{100}, for both 25wt.% and 19wt.% concentrations, SEM views show a P-based inclined facet appearing for deviation angles less than 30° (Figure 7-10-(a)), whereas the ideal canonical curves of Figure 6-26 predict that it should not appear at all. One concludes that the etching rate of the P-based plane, in the configuration where it is present between a $K_{inclined}$ facet and the bottom {100} surface, is decreased substantially. The fact that the Si{100} bottom surface is composed of K-rows extending alternatively in perpendicular directions (see Figure 7-10-(b)), may explain why the junction between $P_{inclined}$ and the bottom surface would not be a source of nucleation and contribute to lower the etching rate of the $P_{inclined}$ facet.

It is observed in Figure 7-10-(a) and for other deviation angles close to $\delta=0°$ that the roughness of the $P_{inclined}$ plane is changed dramatically with the appearance of sharp features aligned parallel to the direction of PBCs, as illustrated in Figure 7-10-(b). A possible explanation to this phenomenon is the formation of stable PBCs which would protect the etching of other nearby PBCs and induce the formation of localized {111} planes or near-{111} micro-surfaces, as illustrated in Figure 7-10-(c).

Figure 7-11 shows Si{100} ideal etch rates of $P_{inclined}$ and $K_{inclined}$ in 25wt% and 19wt.% (these curves are reconstructed from the canonical curves of Figure 6-26). It is observed in Figure 7-11 that the etching rate of the $K_{inclined}$ is lower than that of $P_{inclined}$ for all deviation angles in the case of 25wt% TMAH (left graph), and for deviation angles below 10° for 19wt% TMAH (right graph). As a result, one can hypothesize, for these deviation angles, that the $K_{inclined}$ facet does not induce zipping in the PBCs on the $P_{inclined}$ facet. Microscopically, it would mean either that the K-to-P 120° connection is blocked or that the K-to-P 120° connection zips but that there are few PBCs on the $P_{inclined}$ facet that are connected to K-rows of the $K_{inclined}$ facet.

It is suggested that the $P_{inclined}$ facet etches in this configuration independently from the other adjacent planes, and experiences a "size effect" whenever its size allows the formation of stable PBCs that modify the surface roughness and decrease the etching rate of the $P_{inclined}$ facet.

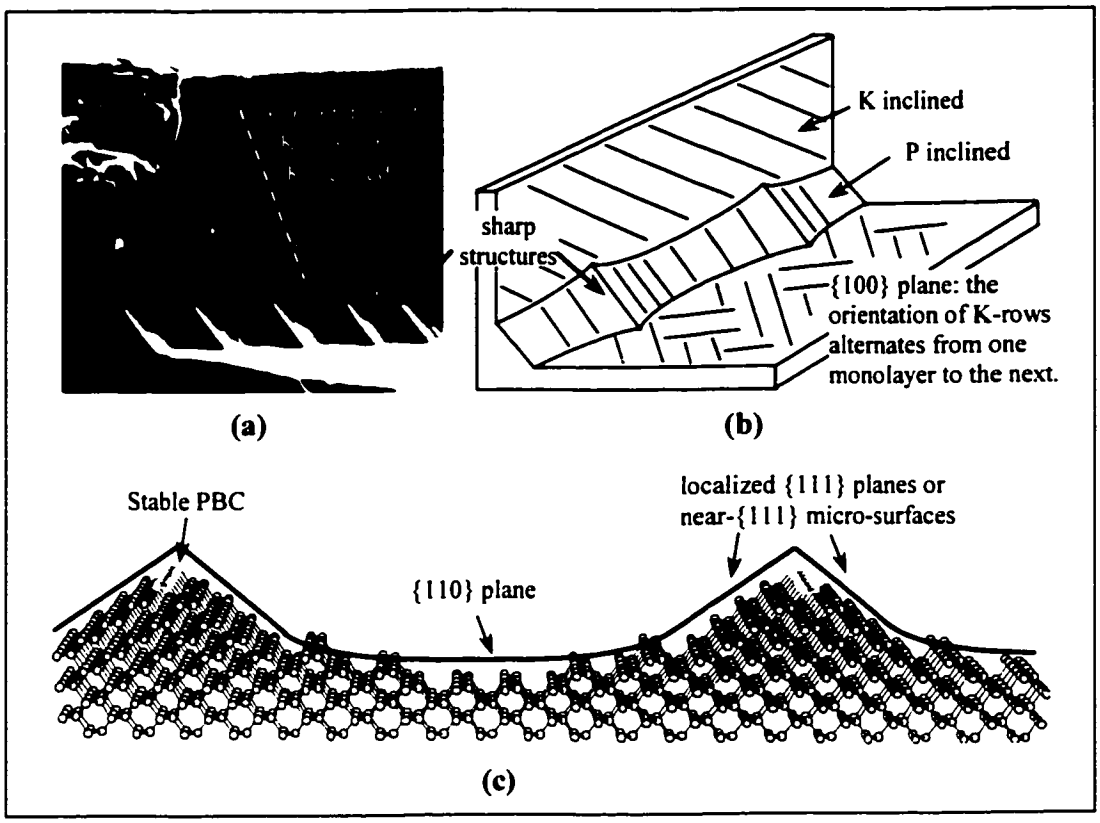

Figure 7-10 : (a) SEM micrograph of a cross section involving a rough $P_{inclined}$ plane; (b) schematic representation of figure-a; (c) cross section crystallographic reconstruction of the $P_{inclined}$ facet illustrating the formation of the {111} localized planes.

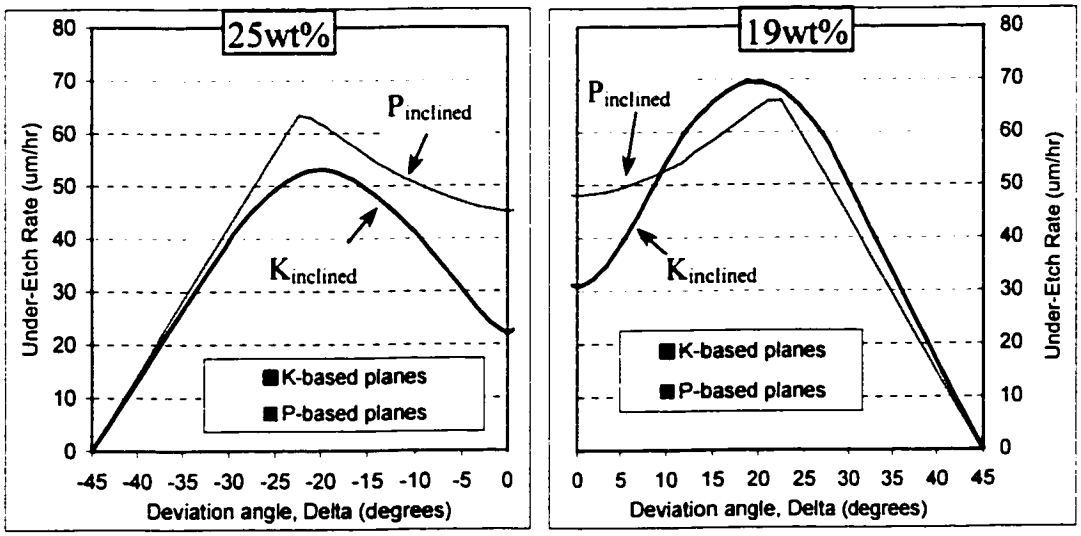

Figure 7-11 : 25wt% and 19wt% ideal etch rate of $P_{inclined}$ and $K_{inclined}$ series on Si{100}(constructed from the canonical curves of Figure 6-26).

b) Effects of $P_{inclined}$ on $K_{vertical}$ on Si{110}

The configuration where the $P_{inclined}$ facet is suspected to have an effect on $K_{vertical}$ occurs on Si{110}25wt.% at δ=39.5° (see Figure 6-37 for SEM pictures). The ideal etch rate construction of Figure 7-12 around δ=39.5° shows than the $P_{inclined}$ facet etches faster than the $K_{vertical}$ facet. UER measurements around the same deviation angle (Figure 6-38) have shown that the $K_{vertical}$ plane has been accelerated. It is suggested, according to Figure 7-12, that this acceleration is due to an interaction with the $P_{inclined}$ facet.

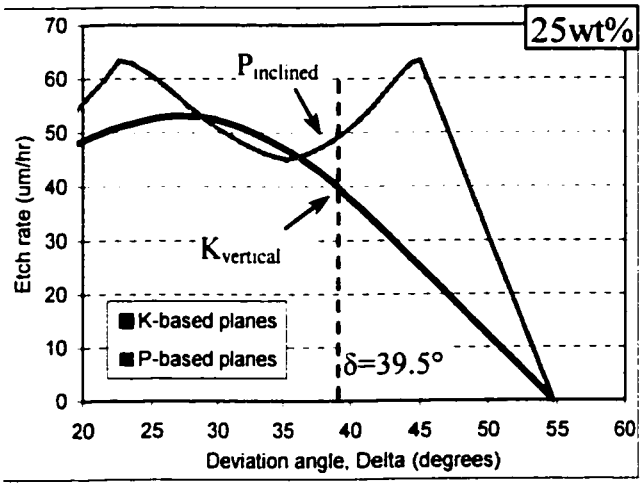

Figure 7-12 : $P_{inclined}$ and $K_{vertical}$ ideal etching rates around δ=39.5° in 25wt.% TMAH (constructed from the 25wt.% canonical curves of Figure 6-26).

Figure 7-13 shows two SEM micrographs where a dramatic roughness change of the surface of the $K_{vertical}$ facet occurs from one spoke to the other around the same deviation angle δ =39.5°. For both SEM pictures of Figure 7-13, the change of roughness (from a surface with a gentle waviness to a multifaceted surface) coincides with the disappearance of the $P_{inclined}$ facet. This result supports the hypothesis that the $P_{inclined}$ has an effect on the $K_{vertical}$. Figure 7-14 shows two SEM micrographs where nucleations from the junction between the mask and the $K_{vertical}$ are suggested to cause a "peeling" process that propagates with time along the $K_{vertical}$ facet [40]. The presence of such a peeling process supports the hypothesis that the $K_{vertical}$ would accelerate around δ=39.5°. In light of these various observations ($P_{inclined}$ faster than $K_{vertical}$, roughness change, peeling process), the mechanism of interaction of $P_{inclined}$ with the $K_{vertical}$ is suggested to be the following:

- the presence of a $P_{inclined}$ with a faster etch rate at the low boundary of the $K_{vertical}$ affects the surface roughness of the $K_{vertical}$ (makes it smooth as in Figure 7-13-(a) at δ=39.5°, at the junction it would be then zipping from P to K: P-to-K 120°).

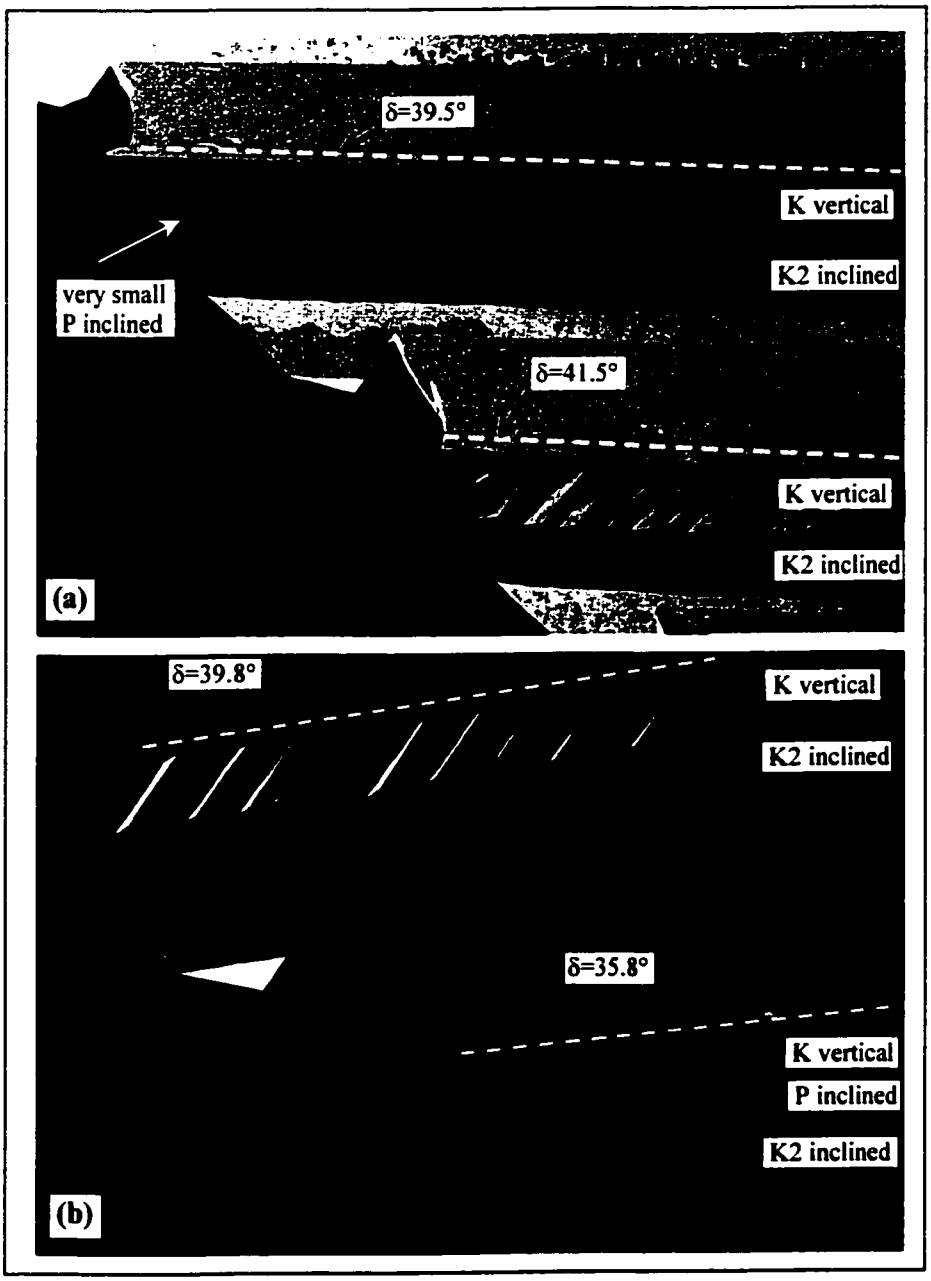

Figure 7-13 : Roughness dramatic change with small variations of δ in Si{110} etched in 25wt.% TMAH: (a) after 3h of etching, (b) after 5h of etching.

- the smoother $K_{vertical}$ facet (not multifaceted as in Figure 7-13-(a) at δ=41.5°) induces nucleations at the junction with the mask.
- the nucleations give birth to a "peeling" process that propagates down along the $K_{vertical}$ facet.
- as a result, the $K_{vertical}$ facet etch rate is increased, as seen in the UER curves.

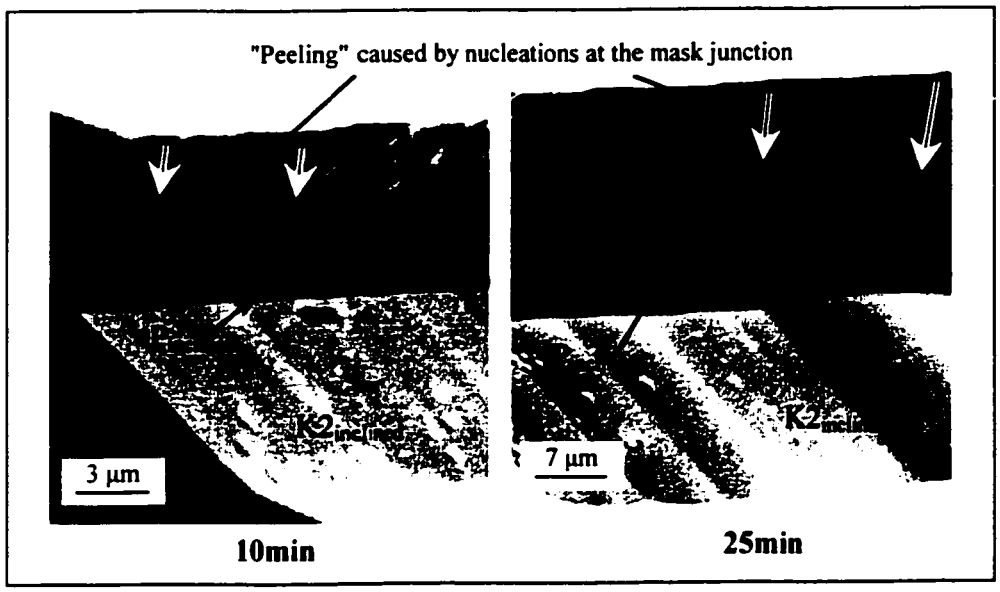

Figure 7-14 : Nucleations originating at the junction between the mask and the $K_{vertical}$ (images repeated from Figure 6-37, Si{110} δ=39.5°).

c) Effects of $K2_{inclined}$ on $P_{inclined}$ on Si{110}

The configuration where the $K2_{inclined}$ facet is suspected to have an effect on $P_{inclined}$ occurs on Si{110}19wt.% at deviation angle around δ=32.5° (see Figure 6-55 for SEMs). The ideal etch rate construction of Figure 7-15 around δ=32.5° shows that the $K2_{inclined}$ facet etches faster than the $P_{inclined}$ facet for $\delta > 30°$. Optical measurements (Figure 6-13) and SEM micrographs (Figure 6-55) around δ=32.5° have shown that the $P_{inclined}$ plane has been accelerated with the subsequent appearance of the $K2_{inclined}$. Figure 7-16 repeats some figures of Figure 6-55 to show the surface roughness evolution with time of the $P_{inclined}$ facet. Indeed, nucleations originating at the junction between the $P_{inclined}$ facet and the $K2_{inclined}$ facet seem to induce an auxiliary etching that propagates upward on the $P_{inclined}$ surface, accelerating the overall etching rate of the $P_{inclined}$ facet. In this case one can hypothesize that the *K-P 120°* connection allows the zipping of K-rows to propagate into zipping of PBCs. .

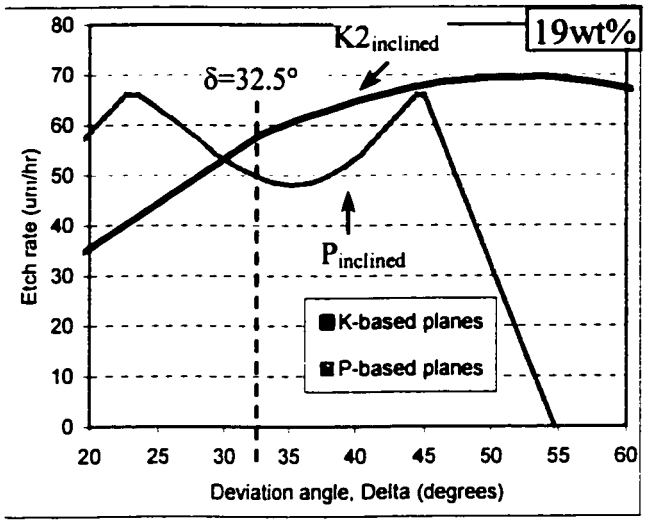

Figure 7-15 : $P_{inclined}$ and $K2_{inclined}$ ideal etching rates around δ=32.5° in 19wt.% TMAH (constructed from the 19wt.% canonical curves of Figure 6-26).

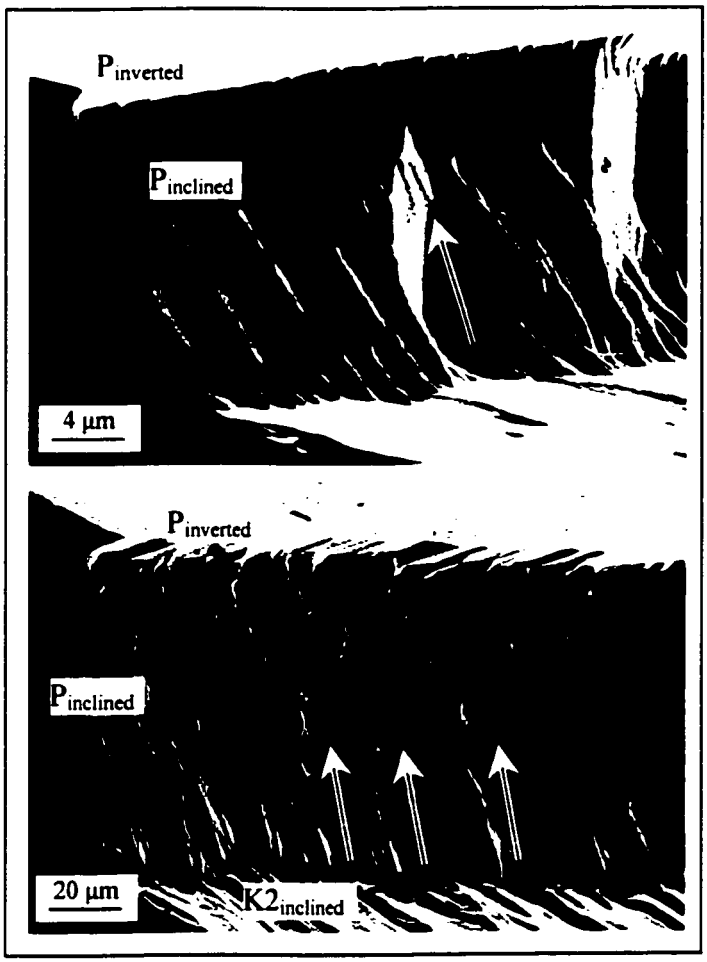

Figure 7-16 : Acceleration of the etch rate of the $P_{inclined}$ due to a boundary effect caused by the presence of $K2_{inclined}$ (images repeated from Figure 6-55, Si{110} δ=32.5°).

d) Effects of $P_{inclined}$ and P_{bottom} on $K2_{inclined}$ on Si{110}

Figure 7-17 shows a side-view and a cross-section view (SEM) micrographs at δ=37.5° on Si{110} 25wt.% after 3h of etching. It is observed in Figure 7-17 that the $K2_{inclined}$ facet has a particular roughness consisting of a gentle waviness at each of its boundaries (junction between $P_{inclined}$ and $K2_{inclined}$, and junction between $K2_{inclined}$ and bottom {110} surface). This gentle surface variations are very similar to the waviness observed on $K_{vertical}$ at δ=39.5° (same section, part (b), Figure 7-14) suggested to be induced by nucleations at the mask junction. Therefore, it is suspected here also, at δ=37.5°, that the $K2_{inclined}$ facet interacts simultaneously with the $P_{inclined}$ facet and the {110} bottom surface. In supporting this hypothesis of interactions, the cross-section view of Figure 7-17 shows that the $K2_{inclined}$ plane may be visualized as two sub-facets, each having its own inclination angle slightly shallower or steeper than the overall K2 inclination angle. Notice the surface roughness of middle part of the $K2_{inclined}$ facet that is suggested to be a sort of interference between zipping chains (K-rows) propagating from the upper boundary of $K2_{inclined}$ with zipping chains (K-rows) from the lower boundary of $K2_{inclined}$. As a result, one can make the hypothesis that microscopically the P-to-K 120° connection allows the zipping of K-rows to propagate into a zipping of PBCs.

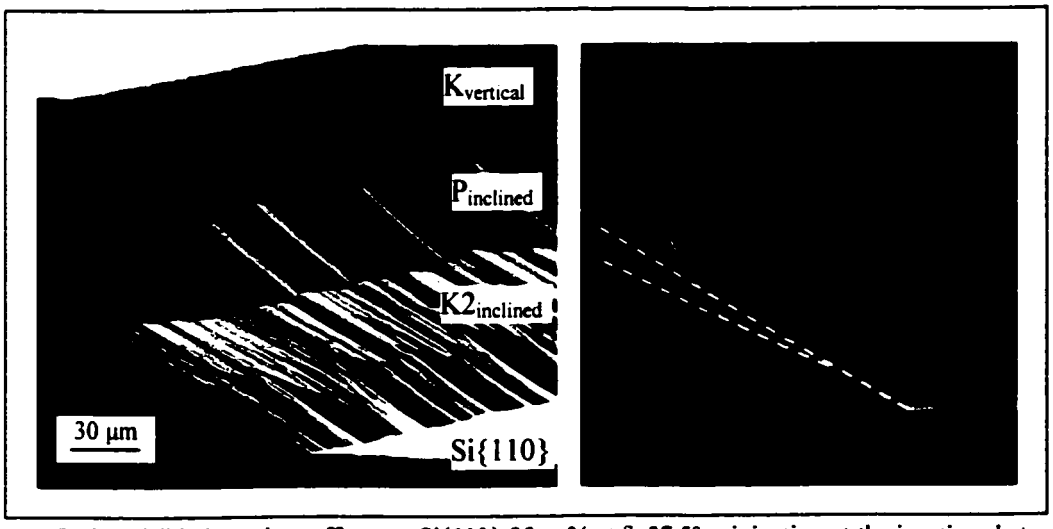

Figure 7-17 : Visible boundary effects on Si{110} 25wt.% at δ=37.5° originating at the junctions between $P_{inclined}$ and $K2_{inclined}$ and between $K2_{inclined}$ and the cavity bottom surface {110}. The interactions at boundaries induce an etch propagation along the $K2_{inclined}$ facet.

Figure 7-18 shows the ideal etch rate construction around δ=37.5° of the $P_{inclined}$, $K2_{inclined}$ and {110} bottom surface. It is observed in Figure 7-18 that the three curves are close one to each other at δ=37.5°. The fact that $P_{inclined}$ and the bottom surface are etching approximately at the same rate explains why the effects induced on each side of the $K2_{inclined}$facet are very similar.

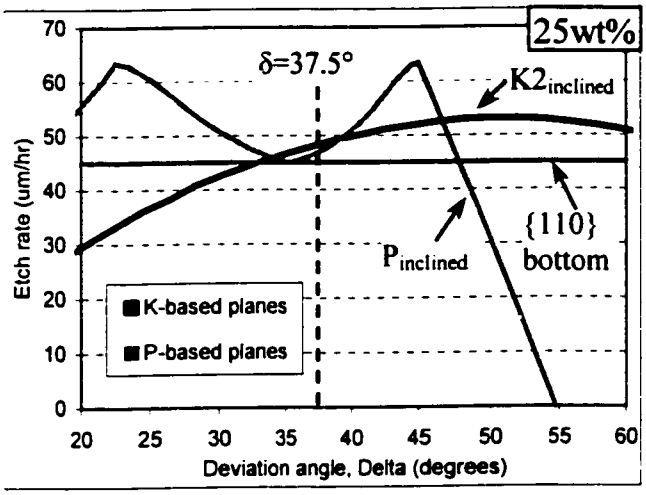

Figure 7-18 : $P_{inclined}$, $K2_{inclined}$, and Si{110} bottom surface ideal etching rates around δ=37.5° in 25wt.% TMAH (constructed from the 25wt.% canonical curves of Figure 6-26).

e) Effects of $K1_{inclined}$ on $P_{vertical}$

The configuration where the $K1_{inclined}$ facet is suspected to have an effect on $P_{vertical}$ occurs on Si{110}19wt.% at δ=70° (see Figure 6-42 for SEM pictures). The ideal etch rate construction of Figure 7-19 around δ=70° shows that the $K1_{inclined}$ facet and the $P_{vertical}$ facet have, according to the ideal model, identical etch rates. UER measurements around the same deviation angle δ=70° (Figure 6-43) have shown that the $P_{vertical}$ plane etch rate decreased as compared to the ideal model. It was remarked in Figure 6-43, that the decrease of the etch rate of the $P_{inclined}$ facet coincides with the appearance of the $K1_{inclined}$. In summary, the $P_{inclined}$ facet etch rate decreases after the appearance of a $K1_{inclined}$ facet which has approximately the same etching rate.

This result is similar to the case (a) of this section 7.2.2, where a decrease of the etch rate of a P-based facet is observed in close proximity to a K-based facet. A possible common explanation (for case (a) and case(e)) of such a decrease of the etch rate for the P-based plane is the *small size* of the P-based plane: it is suggested that the P-based facet etches in

this configuration independently from the other adjacent planes, and experiences a "size effect" whenever its size is smaller than a certain critical value.

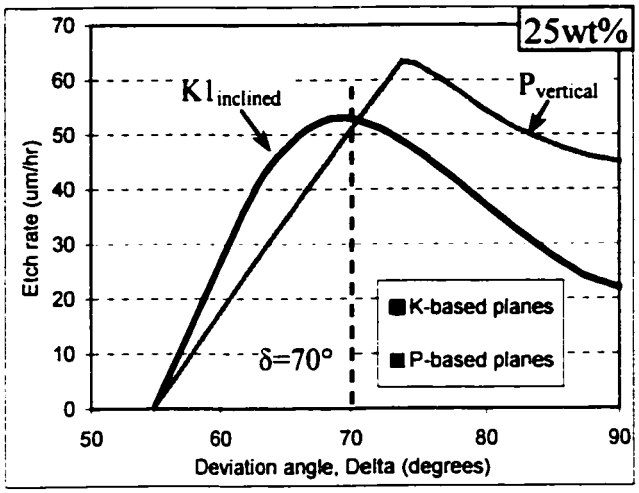

Figure 7-19 : $P_{vertical}$ and $K1_{inclined}$ ideal etching rates around δ=70° in 25wt.% TMAH (constructed from the 25wt.% canonical curves of Figure 6-26).

f) Effects of $K2_{inclined}$ on Si{110} bottom surface

In Chapter 6, it was observed that the etching rate (or etched depth) of the cavity bottom surface of the {110} silicon orientation for both concentrations was very dependent on the angle of the mask-edge (δ) (Figure 6-7 for Si{110} 25wt%, Figure 6-15 for Si{110} 19wt.%). By looking at the cross-sections of spokes using SEM, it was observed that the $K2_{inclined}$ facet was always the lowest facet of the under-etch at all deviation angles (δ), except for a range of δ around 54.74° where a vertical {111} facet composes the under-etch. As a result, one may suggest the hypothesis that the $K2_{inclined}$ facet may be responsible for accelerating the {110} surface at the bottom of the cavity. To test this hypothesis, the etch rates of the $K2_{inclined}$ (ideal etch rate imported from the K-based canonical curve of Figure 6-26) and the {110} bottom surface (experimental) are plotted in the same graph for 25wt% in Figure 7-20 and for 19wt.% in Figure 7-21. A dashed area has been drawn on the plots to show in each graph the range of δ where the $K2_{inclined}$ facet does not appear as the lowest facet. Also included in the plot is the ideal etch rate of the {110} surface which would occur if no boundary effects were present.

It is observed in Figure 7-20 (25wt.%) that the experimental etch rate curve of the {110} bottom surface is relatively constant in the ranges of δ where the $K2_{inclined}$ etch rate curve

is lower. However in the range of (δ) where the $K2_{inclined}$ etch rate curve is higher, the {110} bottom surface etching rate increases accordingly.

It is also observed in Figure 7-21 (19wt%) that the experimental etch rate curve of the {110} bottom surface also increases for the ranges of δ where the $K2_{inclined}$ etch rate curve is higher. Notice that the maximum of the {110} bottom etch rate does not quite coincide with the maximum of the $K2_{inclined}$ curve but still coincides with the disappearance of the $K2_{inclined}$ facet.

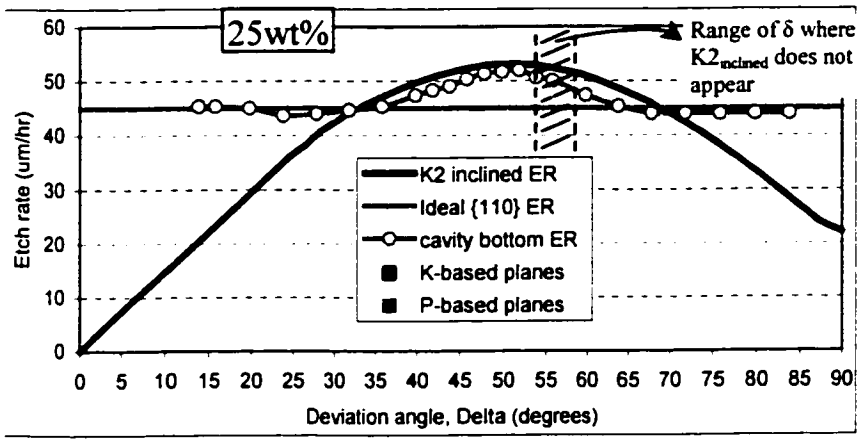

Figure 7-20 : Correlation between $K2_{inclined}$ ideal etching rate and the measured etching rate of the cavity bottom surface as a function of δ in 25wt.% TMAH.

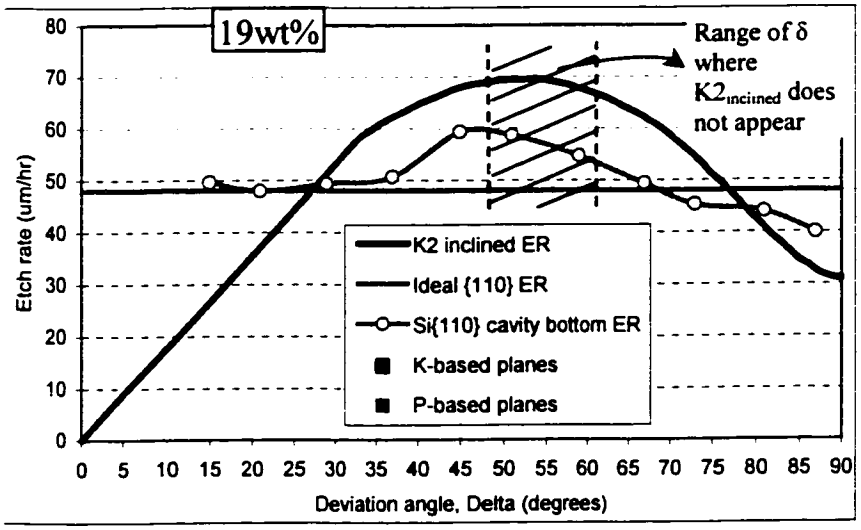

Figure 7-21 : Correlation between $K2_{inclined}$ ideal etching rate and the measured etching rate of the cavity bottom surface as a function of δ in 19 wt.% TMAH.

7.2.3 K-K 60° and K-K 120°

K-K 60° and K-K 120° connections appear on Si{110} at δ around 12°. Figure 7-22-(a) shows a schematic perspective view of a spoke where the cavity {110} bottom surface has disappeared (see Figure 7-22-(c)). The K-K 60° connection occurs between $K2_{inclined}$ facet and its symmetrically inverted facet $K2_{inverted}$. The inverted facets induced in a K-K 60° configuration are very small (see Figures 6-34, 6-35) as compared to the size of the inverted planes induced in a K-K 90° configuration. Therefore, one can make the hypothesis that atoms at the junction of a K-K 60° connection are less stable than the atoms at the junction of a K-K 90° configuration.

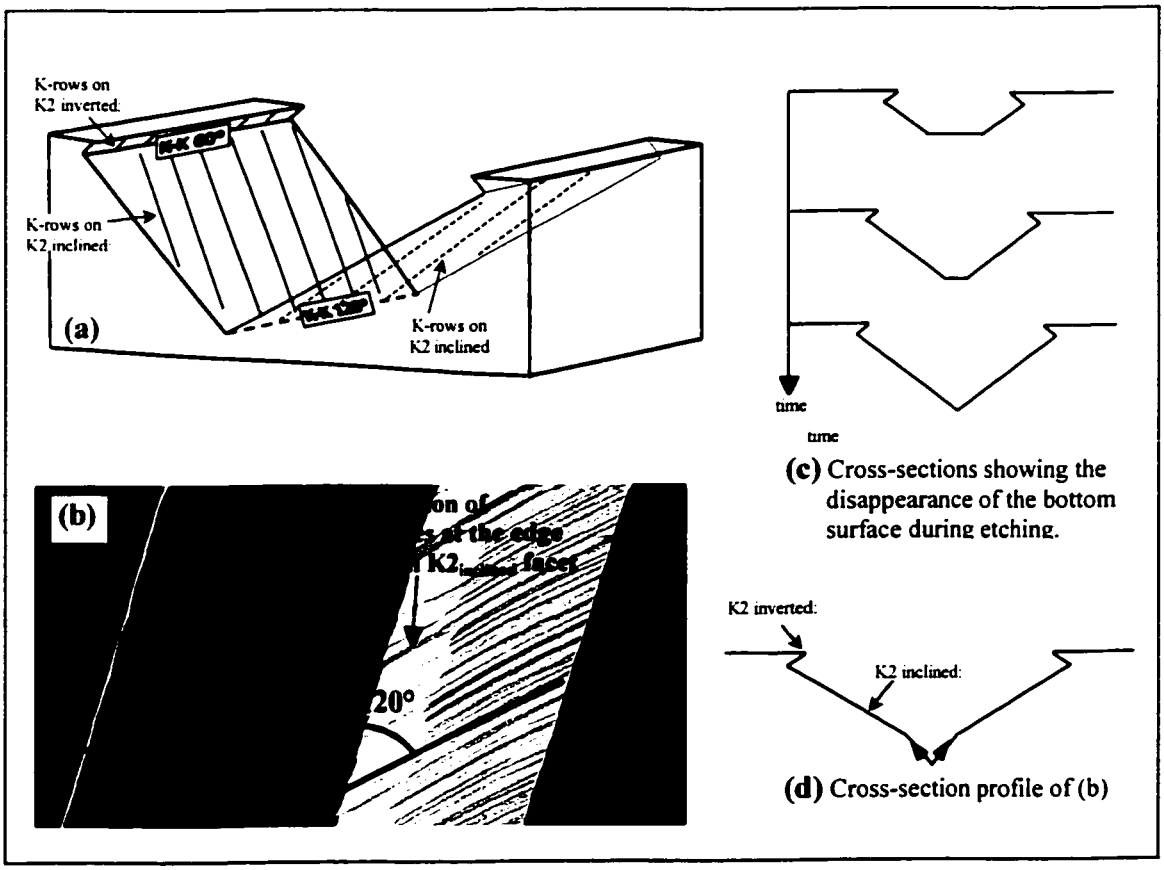

Figure 7-22 : (a) Side view schematic showing the connections between K-rows K-K 60° and K-K 120°; (b) Top view SEM micrograph at δ=11.9° on Si{110} 25wt.% etched for 5h (repeated from Figure 6-34); (c) mechanism of disappearance of the cavity bottom surface; (d) cross-section profile of SEM-(b).

Figure 7-22-(b) shows a top view SEM micrograph at δ=11.9° on Si{110} 25wt.% etched for 5h. The large facets are $K2_{inclined}$ facets, while the small inverted planes $K2_{inverted}$ are the top-most facets. It is observed in Figure 7-22-(b) that the surface roughness of each of

the $K2_{inclined}$ facets is modified near the junction between the two $K2_{inclined}$ facets: the visible lines aligned parallel to the K-rows are replaced in the bottom part of the $K2_{inclined}$ facets by smoother zones (possibly two new sub-facets) which appear to originate at the junction between the two inclined facets and propagate upward on the facets (Figure 7-22-(d)). The fact that this zone is formed may imply that the atoms at the junction of a K-K 120° connection do not have a lower removal probability (may have a higher removal probability) than the adjacent atoms.

7.3 Contributions

Chapter 7 presents further analysis of the experimental data. After a graphical summary of the experimental results of Chapter 6, the analysis supported by additional SEM pictures is organized mainly around two types of connections between steps (chains) on adjacent facets: K-K 90° and K-P 120°. It was found that:

- K-K 90° induces inverted planes on Si{100} around δ=37°.
- For long etching times (3h, 5h) on Si{110}, for δ>75°, visible lines in the configuration K-K 90° are observed. However no substantial etch rate variation is noticed.
- K-P 120° is found to induce many etch rate variations; either accelerations or decelerations.:
  - It is suggested that decelerations of P-based facets in close proximity to K-based facets occur in the configurations where the P-based facet is small, and is suspected to be caused by size effects rather than by interactions at boundaries.
  - In the case of accelerations, it is suggested that when a P-based facet is in close proximity to a K-based facet, the fastest of the two planes accelerates the other.
  - For similar etching rates, it is suggested P-based and K-based facets can accelerate mutually.
- Evidence of substantial roughness change from one spoke to the other is shown. It is suggested to be due to the disappearance of the $P_{inclined}$ facet.
- Auxiliary etching is shown to originate at the mask-$K_{vertical}$ junction at δ=37° on Si{110}, 25wt%.
- The bottom surface dependence on deviation angle is suggested to be partly due to interactions with the $K2_{inclined}$ facet.

These observations support the hypothesis that the anomalies (departures from the ideal crystal-feature-based model) are due to effects related to the boundaries between facets. Specifically, they point to the potential importance of propagation (or lack thereof) of chains (PBC's or kink-rows), across facet boundaries.

8 Conclusion

8.1 Overview

Most under-etched surface facets are defined by either PBCs or kink-rows. Indeed, the shapes of under-etch curves can be understood based on this assumption. However, same-index planes do not always etch at the same rates. The differences may be due to interactions between facets, operating at or through the boundaries of the facets. Altered facet etch rates, inverted facets, the formation of trenches, and etch depth variations, may all be partly explained by facet boundary effects.

8.2 Contributions

Building on the foundation of previous work by A. Pandy et al [8], where the step-based model was introduced and the theoretical dependence of the rotation angle θ on the deviation angle δ was developed, for P-based and K-based planes for both Si{100} and Si{110}, Chapter 3 further develops and presents the ideal crystal-feature-based model, particularly tailored to support and assist the experimental study of Si{100} and Si{110}:

- A method is developed to analyze typical under-etch data (under-etch rate and detailed facet inclination angles), to estimate a canonical crystal-feature-based curve for a given etchant at a given concentration.
- Based on the canonical curve, a model is developed to predict the details of the under-etch profile (relative sizes of the facet sizes), as a function of mask-edge deviation angle.

Chapter 4 further develops ideal crystal-based theoretical concepts to support the hypothesis of interactions between planes. These developments consist of a compendium of possible facet interactions during under-etch experiments on {100} and {110} silicon:

- The angle of orientation (γ) of steps on P-based and K-based facets is defined and visualized.

- The direction of propagation of steps for P-based and K-based facets is studied and schematically presented.
- The angle of interaction (ψ) between chains on adjacent facets is studied and summarized.
- The seven possible connections between chains on adjacent facets are identified and visually diagrammed for Si{100} and Si{110}.
- A Matlab simulation is developed to test the effects of boundaries on the etching of a single chain (PBC or K-row) depending on boundary conditions.
- A rudimentary simulation of inverted planes is developed. The C^{++} implementation of this simulation program is developed by graduate students in partial fulfillment for the course ELEC6251 [37], in collaboration with this author.

In Chapter 5, the experimental procedures for etching wagon-wheel patterned silicon samples are presented. Besides routine sample preparation and etching experiments, there are two particular contributions.:

- Two etching masks were designed to enable wagon-wheel etching experiments on Si{100} and Si{110} for up to six hours of etching, including patterns for measuring the misalignment of the mask within better than 0.5°.
- It is shown that stirring during anisotropic etching of silicon in TMAH gives much more reproducible results, both on a single sample, and over time.

In Chapter 6, optical microscope measurements on Si{100} and Si{110} for 25wt.% and 19wt.% TMAH were conducted, and SEM micrographs were taken at strategic locations. Along with the measurements and SEMs, 1h30min etching samples were used to extract canonical etch rate curves of P-based and K-based series:

- The canonical curves were compared between the two concentrations and it was found the K-based series etch rate has increased more than P-based series as the concentration went from 25wt.% to 19wt%, consistent with the general trends found in previous work by other researchers [2,6].

- The canonical curves were used to construct ideal under-etch profiles for the comparison with experimental under-etch profiles.

The results of combined optical measurements and SEM micrographs include:

- Si{100} 25wt% TMAH
  - The under-etch rate and the bottom surface etch rate are approximately constant with time.
  - The effective inclination angle varies substantially with time for δ close to 0°.
  - Evidence of etch rate variation with time of the $P_{inclined}$ series is presented.
  - Substantial-sized inverted planes are observed having a constant relative size compared to inclined facets.

- Si{110} 25wt% TMAH
  - The under-etch rate is found to not vary significantly with time, however it is found to deviate form the ideal etching model at specific locations: at $\delta \approx 39°$ (acceleration) and at $\delta \approx 70°$ (deceleration).
  - The bottom surface etch rate varies with the mask-edge angle.
  - The {110} bottom surface roughness does not change dramatically with time.
  - The bottom surface roughness of cavities is almost unchanged with time.

- Si{100} 19wt%
  - The under-etch rate and effective inclination angle are found to vary substantially with time in a particular range of deviation angle around δ=21°, corresponding to the appearance of a rough near-vertical facet.
  - inverted planes smaller than in 25wt% are observed at the same deviation angles as in 25wt%.
  - Evidence of etch rate variation with time of the $P_{inclined}$ series at δ=5° is presented.

- for Si{110} 19wt.% TMAH
  - The under-etch rate is found to vary substantially with time (acceleration) in a particular range of deviation angle around δ=35°. The variations coincide with the appearance of the $K2_{inclined}$ facet.
  - The bottom surface etch rate increases substantially with time. It also varies as the mask-edge is deviated.
  - The bottom surface roughness increases with time with the appearance of protruding structures extending perpendicular to the direction of PBCs.
  - The presence of trenches on the {110} bottom surface is observed. These trenches propagate over time toward the center of the cavity.

In general, there are significant variations with time, of underetch rates, facet profiles, roughness and cavity-bottom etch rates, indicating clearly that the ideal crystal-feature-based model does not hold over time.

Chapter 7 presents further analysis of the experimental data. After a graphical summary of the experimental results of Chapter 6, the analysis supported by additional SEMs is organized mainly around two types of connections between steps (chains) on adjacent facets: K-K 90° and K-P 120°. It was found that:

- K-K 90° induces inverted planes on Si{100} around δ=37°.
- For long etching times (3h, 5h) on Si{110}, for δ>75°, visible lines in the configuration K-K 90° are observed. However no substantial etch rate variation is noticed.
- K-P 120° is found to induce many etch rate variations; either accelerations or decelerations.:
  - It is suggested that decelerations of P-based facets in close proximity to K-based facets occur in the configurations where the P-based facet is small, and is suspected to be caused by size effects rather than by interactions at boundaries.
  - In the case of accelerations, it is suggested that when a P-based facet is in close proximity to a K-based facet, the fastest of the two planes accelerates the other.
  - For similar etching rates, it is suggested P-based and K-based facets can accelerate mutually.
- Evidence of substantial roughness change from on spoke to the other is shown. It is suggested to be due to the disappearance of the $P_{inclined}$ facet.
- Auxiliary etching is shown to originate at the mask-$K_{vertical}$ junction at δ=37° on Si{110}, 25wt%.
- The bottom surface dependence on deviation angle is suggested to be partly due to interactions with the $K2_{inclined}$facet.

These observations support the hypothesis that the anomalies (departures from the ideal crystal-feature-based model) are due to effects related to the boundaries between facets. Specifically, they point to the potential importance of propagation (or lack thereof) of chains (PBC's or kink-rows), across facet boundaries.

8.3 Suggestions for future work

A systematic study of boundary effects is necessary for a better control of real experiments of anisotropic etching of silicon. More experiments focusing on the interaction between facets with the combination of etching simulations and high resolution microscopy (such as AFM and SEM) could help:

- Determine for each of the seven possible connections between chains: which are the blocked connections, which are the zipping connections? in what extend the etching rate of interacting facets is modified?
- Determine if the step movement relationship between two facets influences the interaction between two facets.
- Determine how much the etch rate of a plane is affected by the size of the facet: size effects.
- Determine the effects of concentration and temperature on the various removal probabilities: nucleation probabilities, zipping probabilities, and removal probabilities of atoms at the junction between two interacting facets.
- Determine if the auxiliary facets that are created following an interaction between facets are "fast-etch facets" or "slow-etch facets".
- Explore the use of boundary effects in controlling micro-step formation on etched facets.
- Investigate the effect of depositing a nitride mask instead of an oxide mask: For example, would it give similar results at the deviation angles δ where nucleations from the mask edge are suspected to occur (example at $\delta = 39.5°$ on Si{110} 25wt%)?
- Explore the effect of surfactants on boundary effects and micro-step morphology.
- Explore and understand the effect of semi-permeable particles [41] on step dynamics, and on the appearance or disappearance of intermediate facets. (Understanding the effect of semi-permeable particles on boundary effects.)

<u>Other research topics not related to boundary effects</u>

- Explore how the crystal-feature-based etching model, with boundary effects, could be useful in modelling convex configurations.

- Estimate the P-based and K-based canonical etch rate curves for other concentrations.
- Investigate the relationship between {110} surface roughness change and variation in etch rate.
- Investigate if ultrasonic agitation give similar results than heavy stirring.

Application to further development of software simulation packages

The theory and findings that are presented in this thesis could participate in developing more accurate simulation of anisotropically etched structures in silicon. As a suggestion, the simulation programs could include boundary effects and structural defects in silicon (like stacking faults and dislocations [41]) superimposed to the crystal-feature based model. This would allow more precise simulation of concave and convex structures, and more accurate prediction of surface roughness and micro-steps on etched surfaces.

Appendix I : Orientation of specific crystallographic planes

- **Si{100}** : the top surface is oriented (001).

P-inclined (011) → (hkk) →(111)

	(011)	(199)	(166)	(155)	(144)	(133)	(255)	(122)	(233)	(344)	(111)
θ	35,26	30,77	28,54	27,21	25,24	22,00	19,47	15,79	10,03	7,33	0,00
α	45,00	45,18	45,39	45,56	45,87	46,51	47,12	48,19	50,24	51,34	54,74
δ	0,00	6,34	9,46	11,31	14,04	18,43	21,80	26,57	33,69	36,87	45,00

P-inverted (01 -1) → (hk -k) → (11 -1)

	(01 -1)	(19 -9)	(16 -6)	(15 -5)	(14 -4)	(13 -3)	(25 -5)	(12 -2)	(23 -3)	(34 -4)	(11 -1)
θ	35,26	30,77	28,54	27,21	25,24	22,00	19,47	15,79	10,03	7,33	0,00
α	135,00	134,82	134,61	134,44	134,13	133,49	132,88	131,81	129,76	128,66	125,26
δ	0,00	6,34	9,46	11,31	14,04	18,43	21,80	26,57	33,69	36,87	45,00

K-inclined (010) → (hkh) → (111)

	(010)	(191)	(161)	(151)	(141)	(131)	(252)	(121)	(232)	(343)	(111)
θ	54,74	45,81	41,47	38,94	35,26	29,50	25,24	19,47	11,42	8,05	0,00
α	90,00	83,70	80,66	78,90	76,37	72,45	69,63	65,91	60,98	59,04	54,74
δ	0,00	6,34	9,46	11,31	14,04	18,43	21,80	26,57	33,69	36,87	45,00

K-inverted (010) → (hk -h) → (11 -1)

	(010)	(19 -1)	(16 -1)	(15 -1)	(14 -1)	(13 -1)	(25 -2)	(12 -1)	(23 -2)	(34 -3)	(111)
θ	54,74	45,81	41,47	38,94	35,26	29,50	25,24	19,47	11,42	8,05	0,00
α	90,00	96,30	99,34	101,10	103,63	107,55	110,37	114,09	119,02	120,96	125,26
δ	0,00	6,34	9,46	11,31	14,04	18,43	21,80	26,57	33,69	36,87	45,00

- **Si{110}** : the top surface is oriented (011)

P-inclined (111) → (khk) → (101) → (k -hk) → (1 -11)

	(111)	(212)	(313)	(414)	(515)	(101)	(4 -14)	(3 -13)	(2 -12)	(1 -11)
θ	0,00	15,79	22,00	25,24	27,21	35,26	25,24	22,00	15,79	0,00
α	35,26	45,00	49,54	52,01	53,55	60,00	68,33	71,07	76,37	90,00
δ	0,00	19,47	25,24	27,94	29,50	35,26	41,47	43,31	46,69	54,74

P-inverted (1 -1 -1)→(k-k -h)→(1 -10)→(k -kh)→(1 -11)

	(1 -1 -1)	(2 -2 -1)	(3 -3 -1)	(4 -4 -1)	(5 -5 -1)	(1 -10)	(4 -41)	(3 -31)	(2 -21)	(1 -11)
θ	0,00	15,79	22,00	25,24	27,21	35,26	25,24	22,00	15,79	0,00
α	144,74	135,00	130,46	127,99	126,45	120,00	111,67	108,93	103,63	90,00
δ	0,00	19,47	25,24	27,94	29,50	35,26	41,47	43,31	46,69	54,74

P-vertical (1 -1 1) → (h -kk) → (0 -1 1)

	(1 -1 1)	(4 -5 5)	(3 -4 4)	(2 -3 3)	(3 -5 5)	(1 -2 2)	(1 -3 3)	(1 -4 4)	(0 -1 1)
θ	0,00	5,77	7,33	10,02	12,27	15,79	22,00	25,24	35,26
α	90,00	90,00	90,00	90,00	90,00	90,00	90,00	90,00	90,00
δ	54,74	60,51	62,07	64,76	67,01	70,53	76,74	79,98	90,00

K2-inclined (111) → (hhk) → (001)

	(111)	(445)	(334)	(223)	(335)	(447)	(112)	(225)	(338)
θ	0,00	6,21	8,05	11,42	14,42	15,79	19,47	25,24	26,80
α	35,26	32,55	31,91	30,96	30,38	30,20	30,00	30,50	30,8
δ	0,00	10,02	13,26	19,47	25,24	27,94	35,26	46,68	49,68
	(113)	(114)	(115)	(116)	(11 10)	(001)			
θ	29,50	35,26	38,94	41,47	46,69	54,74			
α	31,48	33,56	35,26	36,59	39,63	45,00			
δ	54,74	63,43	70,53	74,21	81,95	90,00			

K2-inverted (1 -1 -1) → (h -k -h) → (0 -1 0)

	(1 -1 -1)	(4 -5 -4)	(3 -4 -3)	(2 -3 -2)	(3 -5 -3)	(4 -7 -4)	(1 -2 -1)	(2 -5 -2)	(3 -8 -3)
θ	0,00	6,21	8,05	11,42	14,42	15,79	19,47	25,24	26,80
α	144,74	147,45	148,09	149,04	149,62	149,80	150,00	149,50	149,2
δ	0,00	10,02	13,26	19,47	25,24	27,94	35,26	46,68	49,68
	(1 -3 -1)	(1 -4 -1)	(1 -5 -1)	(1 -6 -1)	(1 -10 -1)	(0 -1 0)			
θ	29,50	35,26	38,94	41,47	46,69	54,74			
α	148,52	146,44	144,74	143,41	140,37	135,00			
δ	54,74	63,43	70,53	74,21	81,95	90,00			

K-vertical (100) → (k -hh) → (1 -1 1)

	(100)	(5 -1 1)	(4 -1 1)	(3 -1 1)	(2 -1 1)	(5 -3 3)	(3 -2 2)	(4 -3 3)	(5 -4 4)	(1 -1 1)
θ	54,74	38,94	35,26	29,50	19,47	14,42	11,42	8,05	6,21	0,00
α	90,00	90,00	90,00	90,00	90,00	90,00	90,00	90,00	90,00	90,00
δ	0,00	15,80	19,48	25,74	35,26	40,31	43,32	46,69	48,53	54,74

K1-inclined (1 -1 1) → (h -hk) → (001)

	(1 -1 1)	(2 -2 3)	(1 -1 2)	(1 -1 3)	(1 -1 4)	(1 -1 6)	(001)
θ	0,00	11,42	19,47	29,50	35,26	41,47	54,74
α	90,00	80,12	73,22	64,76	60,00	55,00	45,00
δ	54,74	60,51	64,76	70,53	74,21	78,58	90,00

K1-inverted (1 -1 1) → (h -kh) → (0 -1 0)

	(1 -1 1)	(2 -3 2)	(1 -2 1)	(1 -3 1)	(1 -4 1)	(1 -6 1)	(0-1 0)
θ	0,00	11,42	19,47	29,50	35,26	41,47	54,74
α	90,00	99,88	106,78	115,24	120,00	125,00	135,00
δ	54,74	60,51	64,76	70,53	74,21	78,58	90,00

Appendix II : Calculation of the angle (γ)

Assume Si110 wafer. The top surface is (011). For a given P-based plane described by δ and α, the objective is to find the angle γ between the PBCs and the vector $\vec{v}$ (see figure1).

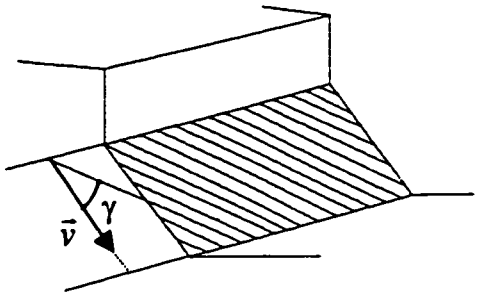

Illustration of γ

- The first step is to get $\vec{u}$:

$\vec{w} = [0\bar{1}1] + x \cdot [100]$ where

$$x = \sqrt{2} \cdot \tan(90 - \delta) = \frac{\sqrt{2}}{\tan(\delta)}$$

$$\vec{w} = \begin{pmatrix} \sqrt{2}/\tan(\delta) \\ -1 \\ 1 \end{pmatrix}$$

$$\vec{u} = \frac{\vec{w}}{\|\vec{w}\|} = \frac{1}{\sqrt{2.\tan^{-2}(\delta)+2}} \begin{pmatrix} \sqrt{2}/\tan(\delta) \\ -1 \\ 1 \end{pmatrix}$$

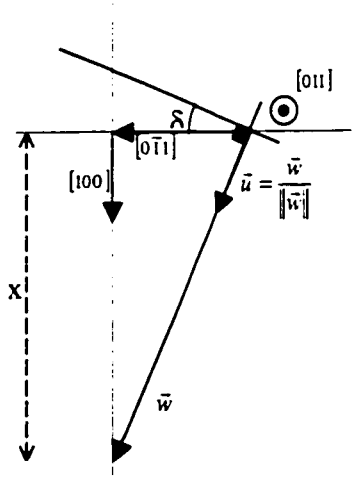

Top view

- Second step is to get $\vec{v}$

$\vec{v} = [0\bar{1}\bar{1}] + y \cdot \vec{u}$

where $y = \sqrt{2} \cdot \tan(90 - \alpha) = \sqrt{2}/\tan(\alpha)$

hence, $\vec{v} = [0\bar{1}\bar{1}] + \sqrt{2}/\tan(\alpha) \cdot \vec{u}$

- The last step is to get γ :

A vector aligned with the PBCs is needed.

Example: case of P-inclined :

PBCs' direction : $[10\bar{1}]$, so $\boxed{\gamma = A\cos\left(\frac{\vec{v} \cdot [10\bar{1}]}{\|\vec{v}\| \cdot \sqrt{2}}\right)}$

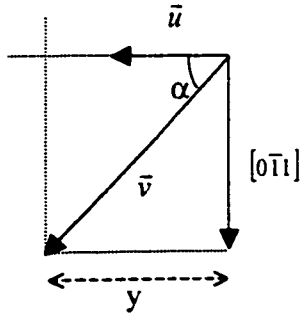

Side view

Appendix III : Inverted planes simulation

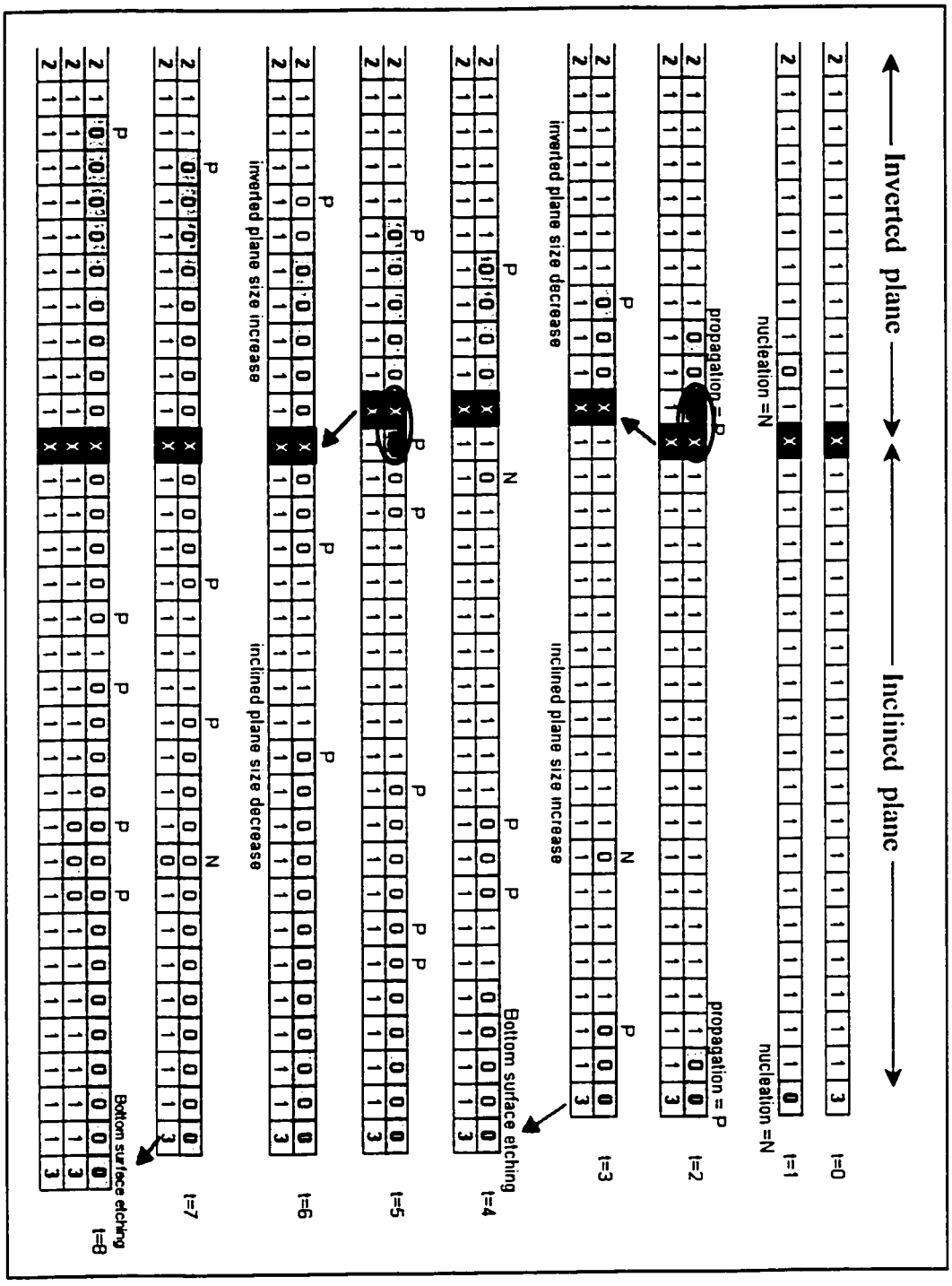

Figure III-1 : Example of etching simulation of an inverted plane.

Appendix IV : Si{110} ideal under-etch rate and etch rate reconstructions

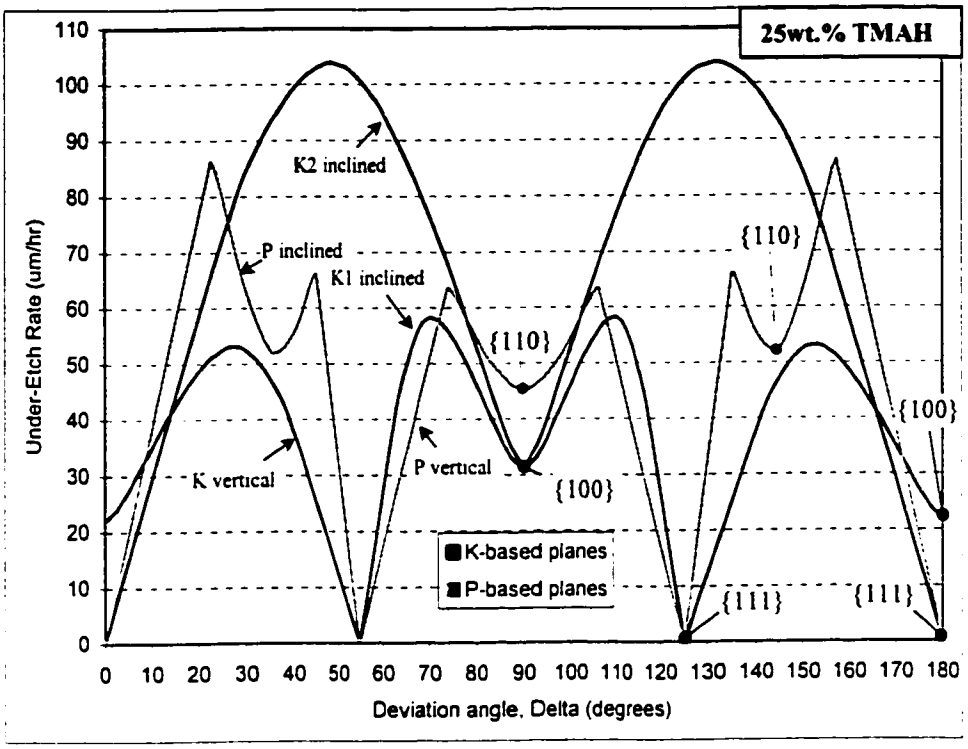

Figure IV-1 : Si{110} 25wt.% ideal under-etch rate construction of P-based and K-based series from canonical curves of Figure 6-26.

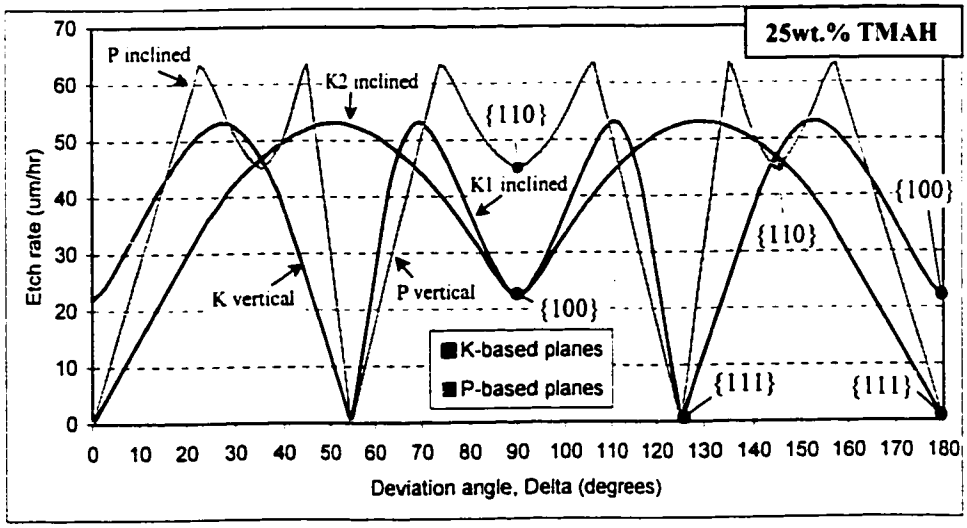

Figure IV-2 : Si{110} 25wt% ideal etch rate construction of P-based and K-based series from canonical curves of Figure 6-26.

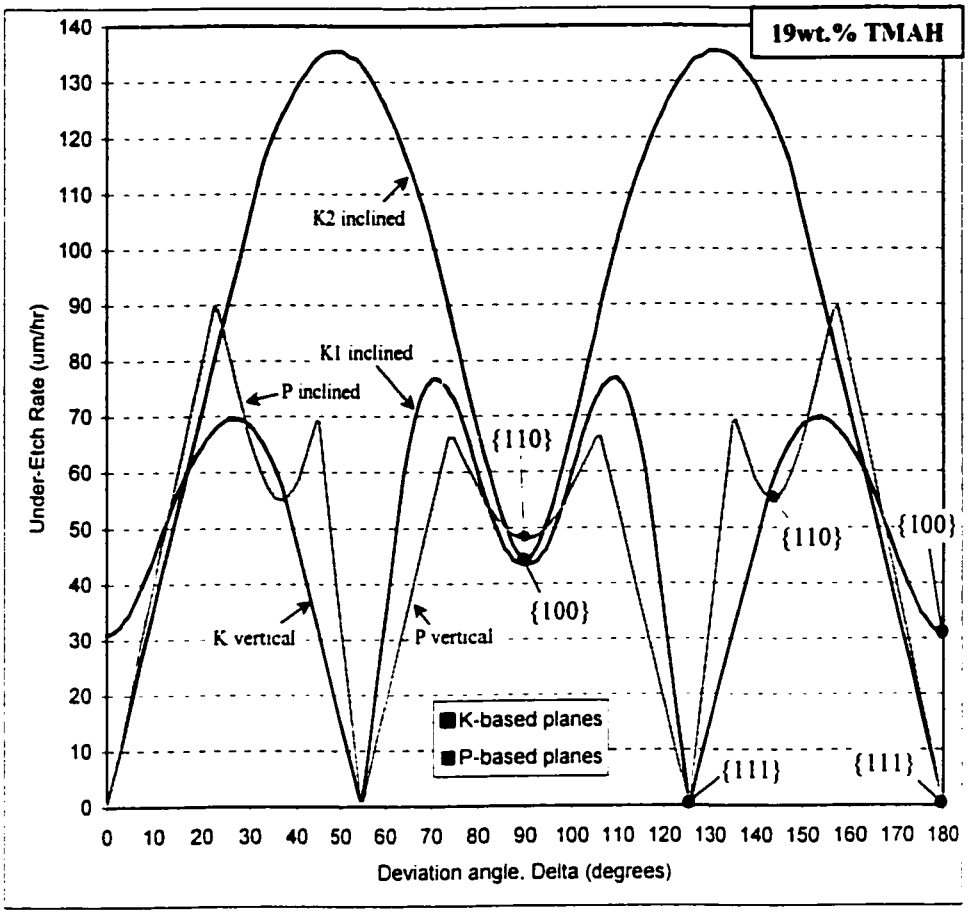

Figure IV-3 : Si{110} 19wt% Ideal under-etch rate construction of P-based and K-based series from canonical curves of Figure 6-26.

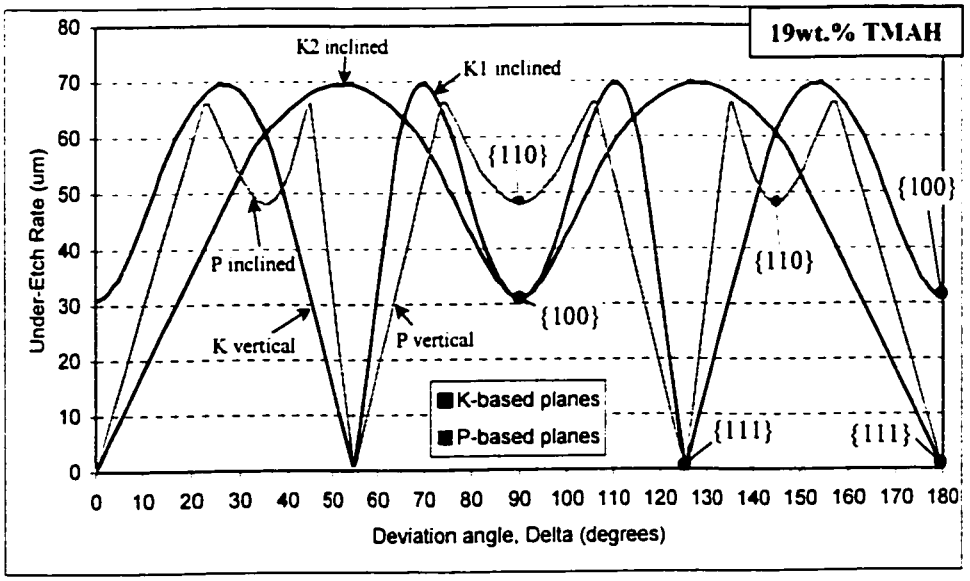

Figure IV-4 : Si{110} 19wt% ideal etch rate construction of P-based and K-based series from canonical curves of Figure 6-26.

References

[1] M. Madou, "Fundamentals of Microfabrication", CRC press, ISBN: 0-8493-9451-1.

[2] O. Tabata, "Anisotropic etching of silicon in TMAH solutions", *Sensors and Materials*, Vol. 13, No. 5 (2001) p. 271-283.

[3] M. Asano, T. Cho, and H. Muraoka, "Application of chlorine in semiconductor technology", *Electrochem. Soc. Extended Abstracts,* (1976) p.911.

[4] U. Schnakenberg, W. Benecke, and P. Lange, *Proc. of 6th Int. Conf. Solid-State Sensors and Actuators,* 24 (1991).

[5] O. Tabata, R. Asahi, H. Funabashi, and S. Sugiyama, *Tec. Dig. of Int. Conf. on Solid-State Sensors and Actuators,* 811 (1991).

[6] M. Shikida, K. Sato, K. Tokoro, and D. Uchikawa: Comparison of Anisotropic Etching Properties between KOH and TMAH Solutions, *Proc of IEEE Int. MEMS-99 Conf.* (Orlando, 17. 21. Jan. 1999), 315-320.

[7] K. Sato, D. Uchikawa, M. Shikida, "Change in orientation-dependent etching properties of single-crystal silicon caused by a surfactant added to TMAH", *Sensors and Materials*, Vol. 13, No. 5 (2001) p. 285-291.

[8] A. Pandy, "Experimental Investigations of Anisotropic etching of silicon in TMAH", Master of Applied Science Thesis in the Department of Electrical and Computer Engineering, Concordia University, Montreal, Canada (2002).

[9] L. M. Landsberger, A. Pandy, and M. Kahrizi, "Silicon etch anisotropy in TMAH: experimental and modelling observations", *Sensors and Materials,* 13, 5, (2001), p.293-300.

[10] O. Tabata, "Anisotropy and selectivity control of TMAH", *MEMS'98* (1998) p. 229-233.

[11] O. Tabata, M. Yashima, T. Yoshioka, K. Sato, "Effect of potassium ion on anisotropy of TMAH", *10th Int. Conf. on Solid-State Sensors and Actuators*, (1999) p. 542.

[12] M. Sekimura, "Anisotropic etching of surfactant-added TMAH solution", *Proc. MEMS'99* (1999) p. 650.

[13] Zubel, I. Barycla, K. Kotowska, M. Kramkowska, "Silicon anisotropic etching in alkaline solutions IV : The effect of organic and inorganic agents on silicon anisotropic etching process", *Sensors and Actuators*, A87, (2001), p. 163-171.

[14] Merlos , M. Acero, M. H. Bao, J. Bausells and J. Esteve, "TMAH/IPA anisotropic etching characteristics", *Sensors and Actuators*, A37-38 (1993) 737-743.

[15] A. Pandy, L. M. Landsberger, B. Nikpour, M. Paranjape, M. Kahrizi, "Experimental investigation of high Si/Al selectivity during anisotropic etching in TMAH", *J. Vac. Sci. Technol.* A16(2) (1998) p.868-872.

[16] O. Tabata, "pH-controlled TMAH etchants for silicon micromachining", *Sensors and Actuators*, A53 (1996) p.335-339.

[17] G. Yan, P. C. H. Chan, I. Hsing, R. K. Sharma, J. K. O. Sin, Y. Wang, "An improved TMAH Si-etching solution without attacking exposed aluminum", *Sensors and Actuators*, A89 (2001) p.135-141.

[18] S.R. Lee, D. Babic, "Investigation of AL selectivity in Si-doped TMAH by Raman spectroscopy", *J. Electrochem. Soc.* 146 (1999) 4213-4218.

[19] J. Tsaur, C. Du, C. Lee, "Investigation of TMAH for front -side bulk micromachining process from manufacturing aspect", *Sensors and Actuators*, A92 (2001) p.375-383.

[20] H. Seidel, L. Csepregi, A. Heuberger, H. Baumgartel, "Anisotropic Etching of Crystalline Silicon in Alkaline Solutions I. Orientation Dependence and Behavior of Passivation Layers", *J. Electrochem. Soc.*, Vol. 137, No. 11 (1990) p.3612-3626.

[21] E. Steinsland, M. Nese, A. Hanneborg, R. W. Bernstein, F. Meringdal, H. Sandmo, and G. Kittilsland, "Boron etch-stop in TMAH solutions", Sensors and Actuators, A54, (1996), 728-732.

[22] C. M. A. Ashruf, P. J. French, P. M. M. C. Bressers, P. M. Sarro, and J. J. Kelly, "A new contactless electrochemical etch-stop based on a gold/silicon/TMAH galvanic cell", *Sensors and Actuators*, A66 (1998)P.284-291.

[23] H.A. Waggener and J.V. Dalton, "Control of silicon etch rates in hot alkaline solutions by externally applied potentials," *Electrochem. Soc. Ext. Abstr.*, 72-2 (1972) 5817.

[24] P. J. French, M. Nagao, M. Esashi, "Electrochemical etch-stop in TMAH without externally applied bias", *Sensors and A ctuators,* A56 (1996) p.279-280.

[25] A.Tashtoush, L.M.Landsberger, A.Essalik, M.Kahrizi, M.Paranjape, J.F.Currie, and A.Pandy, "Experimental Characterization of the Si/Al/TMAH System," *J. Electrochem. Soc.*, Vol. 148(7), C456-C460, 2001.

[26] U. Schnakenberg, W. Benecke, P. Lange, "TMAHW etchants for silicon micromachining", *6th Int. Conf. Solid-State Sensors and Actuators, Tranducers'91*, p. 815-818.

[27] N. F. Raley, F. Sugiyama, and T. Van Duzer, "(100) silicon etch-rate dependence on boron concentration in EDP solutions", *J. Electrochem. Soc.*, 131, 161-171, (1984).

[28] P. Allongue, V. Kieling, H. Gerischer, "Etching of silicon in NaOH solutions. Part I : in situ STM investigation of Si(111)", *J. Electrochem. Soc.*, 140 (1993) 1009-1016

[29] M. A. Hines, "Understanding the evolution of silicon surface morphology during aqueous etching", *Sensors and Materials,* 13 (5), (2001), p.247-258.

[30] F.C. Frank, "On the kinematic theory of crystal growth and dissolution processes", in "*Growth and perfection of crystals*", John Wiley, New York, (1958), p411

[31] A.A. Chernov, "Applications of the method of characteristics to the theory of the growth forms of crystals", Soc. Phys. Crystallogr., 8, (1963), 63

[32] J. van Suchtelen, K. Sato, E. van Veenendaal, A.J. Nijdam, J.G.E. Gardeniers, W.J.P. van Enckevort, M. Elwenspoek,"Simulation of anisotropic wet-chemical etching using a physical model" *Sensors and Actuators A,* 84, 2000, 324.

[33] J. van Suchtelen, A.J. Nijdam, E. van Veenendaal, "The velocity source concept", *J. Crystal Growth,* 198-199, 1999, 17.

[34] A.Pandy, L.M.Landsberger, and M.Kahrizi, *Can. J. Elec. & Comp. Eng.*, 25, p.19 (2000).

[35] R.A. Wind, M.A. Hines, *Surf. Sci.* 460, 21 (2000).

[36] P. Jakob, Y. J. Chabal, *J. Chem. Phys.* 95, 2897 (1991).

[37] H. Jaffery, I. Malik, "Silicon etching simulation of inverted planes", ELEC6251 project report, Department of Electrical and Computer Engineering, Concordia University, Montreal, Canada (May 2002).

[38] A.C. Gracias, A. N. Rios, I. A. Maia, J. R. Senna, "Real-time, in-situ microscopic observation of silicon etching in KOH", *Rev. Bras. Aplic. Vacuo*, 19, (2000), p.27.

[39] J. Chen, L. Liu, Z. Li, Q. Jiang, "Study of anisotropic etching of (100) Si with ultrasonic agitation", *Sensors and Actuators*, A, 3168 (2002) p.1-5.

[40] A.J. Nijdam, J.G.E. Gardeniers, J.W. Berenschot, E. van Veenendaal, J. van Suchtelen, M. Elwenspoek, "Influence of the angle between etched (near) Si{111} surfaces and the substrate orientation on the underetch rate during anisotropic wet-chemical etching of silicon", J. Micromech. Microeng. 11 (2001) 499-503

[41] A.J. Nijdam, E. van Veenendaal, H.M. Cuppen, J. van Suchtelen, M.L. Reed, J.G.E. Gardeniers, W.J.P. van Enckevort, E. Vlieg, M. Elwenspoek, "Formation and stabilisation of pyramidal etch hillocks on silicon {100} in anisotropic etchants: experiments and Monte Carlo simulation", *J. of Applied Physics* 89 (2001) 4113